
Estimating Molecular Weights of Organometallics in Solution with Diffusion NMR Techniques

Dissertation

zur

Erlangung des mathematisch-naturwissenschaftlichen Doktorgrades

„Doctor rerum naturalium“

der Georg-August-Universität Göttingen

im Promotionsprogramm Chemie

der Georg-August University School of Science (GAUSS)

vorgelegt von

Sebastian Bachmann

aus Goslar

Göttingen, 2017

Betreuungsausschuss:

Prof. Dr. Dietmar Stalke, Institut für Anorganische Chemie

Dr. Michael John, Institut für Organische und Biomolekulare Chemie

Mitglieder der Prüfungskommission:

Referent: Prof. Dr. Dietmar Stalke, Institut für Anorganische Chemie

Korreferent: Prof. Dr. Konrad Koszinowski, Institut für Organische und Biomolekulare Chemie

weitere Mitglieder der Prüfungskommission:

Dr. Michael John, Institut für Organische und Biomolekulare Chemie

Prof. Dr. Ricardo Mata, Institut für Physikalische Chemie

Prof. Dr. Inke Siewert, Institut für Anorganische Chemie

Jun.-Prof. Dr. Selvan Demir, Institut für Anorganische Chemie

Tag der mündlichen Prüfung: 01.03.2017

für Anna Kristina

There is no real ending. It's just the place where you stop the story.

Frank Herbert

TABLE OF CONTENTS

ABBREVIATIONS	vii
1 INTRODUCTION	1
1.1 Organometallic Chemistry	1
1.1.1 Lithiumorganics	1
1.1.1.1 Relationship of Structure and Reactivity	2
1.1.1.2 Solvent-Separated Ion Pairs (SSIPs)	3
1.1.2 Alkali Metal Cyclopentadienides (CpMs)	4
1.1.2.1 A Short Historical Background	4
1.1.2.2 Practical Applications	4
1.1.2.3 Properties and Bonding	5
1.1.2.4 Aggregation of CpMs in the Solid State and in Solution	6
1.2 Nuclear Magnetic Resonance (NMR) Spectroscopy	8
1.2.1.1 Heteronuclear <i>Overhauser</i> Enhancement Spectroscopy (HOESY)	9
1.2.2 Overview of Diffusion NMR	10
1.2.2.1 Calculating Diffusion Coefficients	11
1.2.2.2 Advances in Diffusion NMR	12
1.2.2.3 Diffusion-Ordered Spectroscopy (DOSY)	12
1.2.3 Molecular Sizes and Weights from Diffusion Coefficients	13
1.2.3.1 <i>MW</i> Estimation Using Power Law Approaches	15
1.3 Scope of this Thesis	19
2 RESULTS AND DISCUSSION	21
2.1 Improving the External Calibration Curve (ECC)-DOSY- <i>MW</i> Estimation Methodology	21
2.1.1 New External Calibration Curves for Various Solvents	21
2.1.1.1 Merged External Calibration Curves	23
2.1.1.2 Shape-Optimized External Calibration Curves	28
2.1.2 Molecule Categorization	33
2.1.3 Theoretical Error Analysis	36
2.1.4 Heavy Atoms in the ECC-DOSY- <i>MW</i> Estimation	38
2.1.5 <i>MW</i> Estimation Software	41
2.2 Structure Elucidation of Alkali Metal Cyclopentadienide Derivatives <i>via</i> Diffusion NMR	44
2.2.1 Solution State Structures of Alkali Metal Cyclopentadienides (CpMs) in Different Solvents	44
2.2.1.1 Solution State Structures of CpMs in THF- <i>d</i> ₈	44
2.2.1.2 Solution State Structures of CpMs in ammonia and DMSO- <i>d</i> ₆	49
2.2.2 Solution State Structures of Methylated Alkali Metal Cyclopentadienides in THF- <i>d</i> ₈	53
2.2.2.1 Solution State Structure of MeCpLi in THF- <i>d</i> ₈	54
2.2.2.2 Solution State Structures of Cp*Ms in THF- <i>d</i> ₈	54
2.3 Combined Studies Involving Diffusion NMR to Solve Structural Ambiguities	56
2.3.1 Solution State Structures of Alkyl <i>Grignard</i> Reagents in THF- <i>d</i> ₈	56
2.3.1.1 External Calibration Curves for Rod-Like (RL) Molecules	59
2.3.1.2 <i>MW</i> Estimation of Alkyl <i>Grignard</i> Reagents from Diffusion Data	61

2.3.1.3	Solution State Structures of the “ <i>Turbo</i> ”-Grignard Analogues	63
2.3.2	Anion and Solvent Coordination Elucidated <i>via</i> DOSY	65
2.3.2.1	Coordination of Different Anions to an N-Heterocyclic Carbene in CD ₂ Cl ₂	66
2.3.2.2	Solvent-Anion Exchange of an Acridine-Based System in DMF- <i>d</i> ₇	68
2.3.2.3	Solvation of a Heterocyclic Substituted Methanide in C ₆ D ₆	72
3	SUMMARY & OUTLOOK	76
4	EXPERIMENTAL PART	81
4.1	Techniques and Experiments	81
4.1.1	Handling of Air- and Moisture-Sensitive Compounds	81
4.1.2	NMR Techniques and Experiments	81
4.1.3	DOSY Sample Preparation and Evaluation	82
4.1.4	Computation of Principal Moments of Inertia	83
4.1.5	Programming in Java	83
4.2	Syntheses and Characterizations	84
4.2.1	Syntheses and Characterizations of CpMs (M = Li, Na, K, Rb, Cs)	84
4.2.1.1	Synthesis and Characterization of CpLi	84
4.2.1.2	Synthesis and Characterization of CpNa	86
4.2.1.3	Synthesis and Characterization of CpK	87
4.2.1.4	Synthesis and Characterization of CpRb	88
4.2.1.5	Synthesis and Characterization of CpCs	89
4.2.2	Synthesis and Characterization of MeCpLi	90
4.2.2.1	Synthesis and Characterization of MeCpLi	90
4.2.3	Syntheses and Characterizations of Cp [*] M (M = Li, K, Cs)	91
4.2.3.1	Synthesis of Cp [*] Li	91
4.2.3.2	Synthesis and Characterization of Cp [*] K	91
4.2.3.3	Characterization of Cp [*] Cs	92
4.2.4	Characterizations of RMgCl (R = Et, <i>i</i> Pr, <i>n</i> Bu, <i>n</i> Hex, <i>n</i> Oct, <i>n</i> Dec)	93
4.2.4.1	Characterization of EtMgCl	93
4.2.4.2	Characterization of <i>i</i> PrMgCl	93
4.2.4.3	Characterization of <i>n</i> BuMgCl	94
4.2.4.4	Characterization of <i>n</i> HexMgCl	94
4.2.4.5	Characterization of <i>n</i> OctMgCl	94
4.2.4.6	Characterization of <i>n</i> DecMgCl	95
4.2.5	Characterization of <i>n</i> BuMgBr	95
4.2.5.1	Characterization of <i>n</i> BuMgBr	95
4.2.6	Characterizations of [<i>n</i> BuMgX · LiX] (X = Cl, Br)	96
4.2.6.1	Characterization of [<i>n</i> BuMgCl · LiCl]	96
4.2.6.2	Characterization of [<i>n</i> BuMgBr · LiBr]	96
4.2.7	Characterizations of [MX ₂ {(Me ₂ NCH ₂) ₂ Acr}] (MX ₂ = ZnBr(DMF), CdBr ₂)	97
4.2.7.1	Characterization of [ZnBr(DMF){(Me ₂ NCH ₂) ₂ Acr}]	97
4.2.7.2	Characterization of [CdBr ₂ {(Me ₂ NCH ₂) ₂ Acr}]	98
5	APPENDIX	99

6 REFERENCES	144
DANKSAGUNG	154
CURRICULUM VITAE	156

ABBREVIATIONS

1-PhN	1-phenylnaphthalene
2-PhP	2-phenylpyridine
9-MA	9-methylanthracene
Ac	acetyl
Acr	acridine
Adam	adamantane
av.	average
Batyl	batylalcohol
BEN	benzene
BINAP	2,2'-bis(diphenylphosphino)-1,1'-binaphthyl
Bn	benzyl
BPP-LDE	bipolar pulse pairs with longitudinal-eddy-current-delay
CIP	contact ion pair
COE	cyclooctene
cor.	correlated
COSY	correlation spectroscopy
Cp/Cp ⁻	cyclopentadiene/cyclopentadienide
Cp [*] /Cp ^{*-}	pentamethylcyclopentadiene/pentamethylcyclopentadienide
CpM	alkali metal cyclopentadienide
CS	compact spheres/compact spherical
Cycl	cyclohexane- <i>d</i> ₁₂
dev.	deviation(s)
DIPA	di- <i>iso</i> -propylamine
DHBP	3,4-dihydrobenzophenanthrene
DMF	dimethylformamide
DMSO	dimethylsulfoxide
DOSY	diffusion-ordered spectroscopy
DPA	diphenylacetylene
DPS	diphenylsulfoxide
ds	dummy scans
DSE	dissipated spheres and ellipsoids
D-STE	double-stimulated-echo
ECC	external calibration curve
ED	expanded discs
ESI	electrospray-ionization
Et	ethyl
Et ₂ O	diethyl ether
GUI	graphical user interface
HOESY	heteronuclear <i>Overhauser</i> enhancement spectroscopy

Abbreviations

HMBC	heteronuclear multiple bond correlation
HMDS	hexamethyldisilazane
HMPA	hexamethylphosphoramide
HSQC	heteronuclear single quantum correlation
ICC	internal calibration curve
<i>i</i> Pr	<i>iso</i> -propyl
IPr	1,3-bis(2,6-diisopropylphenyl)imidazol-2-yliden
<i>i</i> Pr ₂ O	di- <i>iso</i> -propylether
IR	infrared
JVM	Java virtual machine
LIFDI	liquid injection field desorption ionization
MAO	methylaluminoxane
MAS	magic angle spinning
max.	maximum
Me	methyl
MeCp/MeCp ⁻	methylcyclopentadiene/methylcyclopentadienide
Mp	melting point
MS	mass spectrometry
MTBE	methyl- <i>tert</i> -butylether
<i>MW</i>	molecular weight
<i>n</i> Bu	<i>n</i> -butyl
<i>n</i> Dec	<i>n</i> -decyl
NHC	<i>N</i> -heterocyclic carbene
<i>n</i> Hex	<i>n</i> -hexyl
<i>n</i> Oct	<i>n</i> -octyl
<i>n</i> Pen	<i>n</i> -pentyl
<i>n</i> Pr	<i>n</i> -propyl
NMR	nuclear magnetic resonance
NOE	nuclear <i>Overhauser</i> effect
NOESY	nuclear <i>Overhauser</i> enhancement spectroscopy
OTf	triflate
PFG-SE	pulsed-field gradient spin-echo
PFG-STE	pulsed-field gradient stimulated-echo
Ph	phenyl
PMDETA	<i>N,N,N',N'',N'''</i> -pentamethyldiethylenetriamine
R	residue
RINMR	rapid injection nuclear magnetic resonance
RL	rod-like
SSIP	solvent-separated ion pair
TBACl	tetrabutylammoniumchloride
TBDBS	<i>tert</i> -butyldiphenylsilyl
<i>s</i> Bu	<i>sec</i> -butyl

Abbreviations

<i>t</i> Bu	<i>tert</i> -butyl
TDE	1-tetradecene
TMB	2,2,3,3-tetramethylbutane
TMEDA	<i>N,N,N',N'</i> -tetramethylethylene-1,2-diamine
TMP	2,2,6,6-tetramethylpiperidide
THF	tetrahydrofurane
TOF	time of flight
Tol	toluene
TPhN	1,2,3,4-tetraphenylnaphthalene
UCC	universal calibration curve
UV	ultraviolet
VIS	visible

Parts of this Ph.D. thesis have been published separately:

[1] A. Visscher, **S. Bachmann**, C. Schnegelsberg, T. Teuteberg, R. A. Mata, D. Stalke, „Highly selective and sensitive fluorescence detection of Zn²⁺ and Cd²⁺ ions by using an acridine sensor“, *Dalton Trans.* **2016**, 45, 5689-5699.

[2] **S. Bachmann**, R. Neufeld, M. Dzemski, D. Stalke, „New external calibration curves (ECCs) for the estimation of molecular weights in various common NMR solvents.“, *Chem. Eur. J.* **2016**, 22, 8462-8465.

[3] C. Schnegelsberg, **S. Bachmann**, M. Kolter, T. Auth, M. John, D. Stalke, K. Koszinowski, „Association and dissociation of Grignard reagents RMgCl and their turbo variant RMgCl·LiCl“, *Chem. Eur. J.* **2016**, 22, 7752-7762.

[4] **S. Bachmann**, B. Gernert, D. Stalke, „Solution structures of alkali metal cyclopentadienides in THF estimated by ECC-DOSY NMR-spectroscopy (incl. software)“, *Chem. Commun.* **2016**, 52, 12861-12864.

Other publications related to this thesis are in preparation:

[5] A. Kreyenschmidt, **S. Bachmann**, T. Niklas, D. Stalke, „Molecular Weight Prediction of Molecules incorporating Heavier Elements using a Correction Factor for ECC-DOSY“, in preparation.

[6] **S. Bachmann**, T. Niklas, M. John, D. Stalke “Structure elucidation of s-Block organometallics with diffusion NMR”, in preparation.

1 INTRODUCTION

1.1 Organometallic Chemistry

Many *Nobel Prizes* have been awarded for the distinct subfield of organometallic chemistry, e.g. to *Fischer* and *Wilkinson* in 1973 for their work on metallocenes or to *Chauvin*, *Grubbs* and *Schrock* in 2005 for metal-catalyzed olefin metathesis. This shows the continuous importance of the field and it is therefore not surprising that organometallics, characterized by more or less polar bonds between $M^{\delta+}$ (metal) and $C^{\delta-}$ (carbon), have an innumerable amount of applications, e.g. in catalysis or as single molecular magnets.^[7] Organometallic precursor materials incorporate mostly alkali or alkaline earth metals. The understanding of such precursors will be the main focus of this thesis.

1.1.1 Lithiumorganics

Lithiumorganics have been of interest for many years as they possess extraordinary reactivities.^[8] Concerning this work, they resemble ideal case studies to explain basic aggregational patterns. The first lithiumorganic was reported back in 1917 by *Schlenk* and *Holtz*^[9] who synthesized methyllithium (MeLi) by transmetalation of dimethylmercury with elemental lithium. Since then the field has become much more diverse and lithiumorganics are nowadays available for a variety of applications, e.g. in pharmaceutical or polymer syntheses.^[10] In many cases they are formulated in chemical equations as RLi, indicating just a simple monomeric aggregate. However, it could already be shown over 50 years ago by *Dietrich*^[11] with the publication of the tetrameric aggregation of ethyllithium in the solid state ($[EtLi]_4$) that this view is too short-sighted. Most lithiumorganics favor forming oligomeric structures in the form of hexamers (e.g. $[nBuLi]_6$ ^[12]; $[iPrLi]_6$ ^[13]) or tetramers (e.g. $[MeLi]_4$ ^[14]; $[EtLi]_4$ ^[11]), depending not only on electrostatics but more importantly on differing organic residues and their respective steric demand. These aggregational motifs can in many cases be disaggregated to dimers (e.g. $[nBuLi(TMEDA)]_2$ ^[15]; $[tBuLi(Et_2O)]_2$ ^[12]) or even monomers (e.g. $[PhLi(PMDETA)]$ ^[16]) by the addition of neutral *Lewis* bases which supposedly mirror conditions present in solution during syntheses (see Figure 1-1). The principles defining these (dis)aggregational processes have already been reviewed in literature^[17] and shall not be discussed further herein.

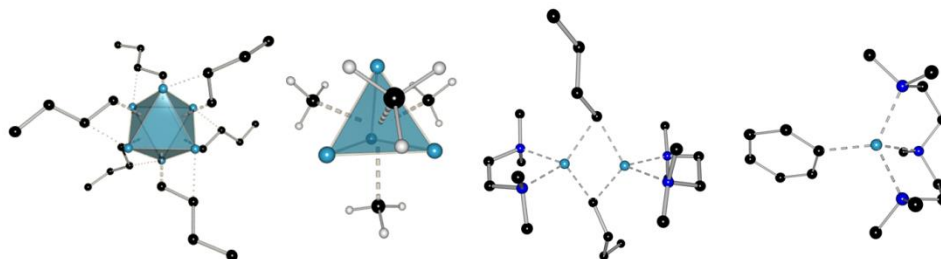
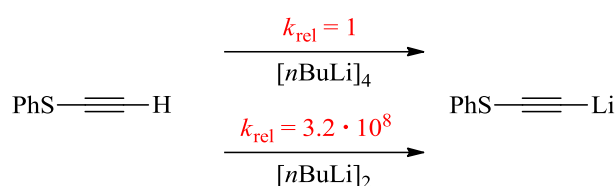


Figure 1-1: Aggregational motifs of lithiumorganics (from left to right: hexameric $[nBuLi]_6$ ^[12], tetrameric $[MeLi]_4$ ^[14], dimeric $[nBuLi(TMEDA)]_2$ ^[15] and monomeric $[PhLi(PMDETA)]$ ^[16]). Structures were reproduced from the data available in the cited references.

1.1.1.1 Relationship of Structure and Reactivity

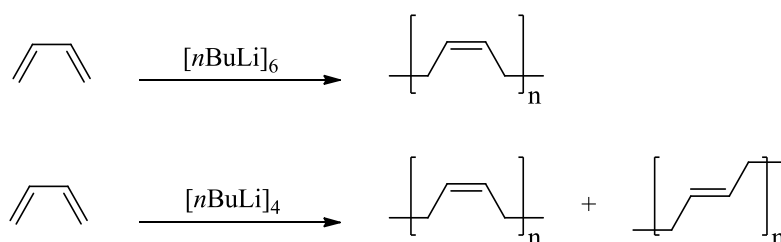
Determination of solid and solution state structures is immensely important to establish a structure-reactivity relationship. As a rule of thumb, lower aggregates of lithiumorganics (e.g. dimers; monomers) are more reactive than higher aggregates (e.g. hexamers; tetramers). This can be underlined by investigations of BuLi: In a recent study, *Reich et al.*^[18] found with the help of rapid injection NMR (RINMR)^[19] that dimeric *n*BuLi reacts $3.2 \cdot 10^8$ times faster with (phenylthio)-acetylene than its tetrameric aggregate (see Scheme 1-1). A few decades earlier, the same reactivity trend could already be observed towards other reactants by *McGarrity et al.*,^[20] even though exact relative reactivity rates were not determined.



Scheme 1-1: Lithiations of (phenylthio)acetylene with different *n*BuLi aggregates show an increased reactivity for the dimeric species compared to the tetrameric *n*BuLi.^[18]

Ogle et al.^[21] used the same technique to examine different BuLi isomers and derived relative reactivities towards the initiation of the polymerization reaction of styrene in THF. They concluded that the order of reactivity for the isomers is *s*BuLi > *t*BuLi > *n*BuLi for this observed reaction, whereas in hydrocarbon solvents it is *s*BuLi > *n*BuLi > *t*BuLi. These reactivity differences are also closely related to the aggregational states of the BuLi isomers. Theoretical calculations of the same study revealed a reactivity trend of $[\textit{nBuLi}]_1 > [\textit{sBuLi}]_1 > [\textit{tBuLi}]_1 > [\textit{nBuLi}]_2$, where the subscripts 1 and 2 refer to the monomeric and dimeric forms, respectively.^[21] All those findings point towards higher reactivities for smaller BuLi aggregates, as was assumed beforehand.

The inherent decrease in selectivity, when going to lower aggregational states, is mentioned by *Ebewele*:^[22] In an anionic polymerization reaction of 1,3-butadiene in unpolar solvents with *n*BuLi as initiator a high content of *cis*-1,4-polybutadiene is produced, whereas in more polar solvents the content of the *cis*-1,4-polymer decreases significantly which results in a *cis*-1,4- / *trans*-1,4-polybutadiene mixture (see Scheme 1-2).



Scheme 1-2: Polymerization reactions of 1,3-butadiene with different *n*BuLi aggregates show a lower selectivity of these reactions for the smaller tetrameric *n*BuLi aggregate, when compared to hexameric *n*BuLi.^[22]

However, this rule also has its exceptions: In 2003 *Zhao* and *Collum*^[23] could show for an enolization reaction of 2-methylcyclohexanone with LiHMDS that a dimer-based mechanism using Et₃N as co-solvent can lead to a faster reaction than the monomer-based mechanism with the co-solvent THF. *Collum*^[24] argued even earlier that the acceleration of organolithium reactions with strongly donating solvents is not altogether logical since strong solvation, high reactivity and lower aggregates are not necessarily, mutually dependent. There are other examples to support him, e.g. *Klumpp et al.*^[25] showed that some “secondary alkyl lithium dimers” [...] “are less reactive towards ethylene than their tetramer counterparts”. Even though the rule holds true for *n*BuLi, these counterexamples show that it is best to fully understand the solvation as well as aggregation of organometallics to access final reactivities.

1.1.1.2 Solvent-Separated Ion Pairs (SSIPs)

While all the structures mentioned in the sections above fall within the confines of the class of contact ion pairs (CIPs), there is another important aggregational motif in organometallic chemistry: Charged solvent-separated ion pairs (SSIPs).^[26] The term SSIP is generic and can be used for lithiumorganics, e.g. for [Li(THF)_n][C(SiCH₃)₃] reported by *Reich et al.*,^[27] or even when no lithium atoms at all are involved. If both, the anionic and cationic particles, contain lithium, they are known as lithium lithiates (e.g. [Li(THF)₄][Li(C(SiMe₃)₃)₂]).^[28] SSIPs are often even more reactive and therefore more unstable than their CIP counterparts and it is thus not surprising that the first crystal structure displaying this aggregation was not obtained before 1983: By then *Eaborn* and *Smith et al.*^[28] crystallized [Li(THF)₄][Li(C(SiMe₃)₃)₂] from THF solution. Since then, many other crystal structures of alkali or alkaline earth metal SSIPs have been published.^[29] Furthermore, they were studied extensively in solution.^[27a, 30] From all of these studies it can be concluded that SSIPs are formed and retained by strongly donating solvents with a high dielectric constant (see Table 1-1), such as HMPA, DMSO or in some cases even THF.

Table 1-1: Dielectric constants (ϵ) of a selection of solvents.

Solvent	CH ₂ Cl ₂ ^a	C ₆ H ₁₂ ^a	C ₆ H ₆ ^a	CHCl ₃ ^a	THF	HMPA	DMF	DMSO	H ₂ O
ϵ ^[31]	1.6	2.0	2.3	4.8	7.5	31	38	47	79

a) These solvents do not normally lead to SSIP structures.

Moreover, it is important that SSIPs can occur simultaneously with CIPs in solution. The aforementioned [Li(THF)_n][C(SiCH₃)₃] was shown to coexist in an equilibrium with the lithium lithiate [Li(THF)_n][Li(C(SiCH₃)₃)₂] and the CIP [LiC(SiCH₃)₃].^[27a] Additionally, lithium lithiates are also often called triple ions, because their anionic building block consists of a combination of three distinct ions (e.g. [Li(C(SiMe₃)₃)₂]⁻ consists of two C(SiMe₃)₃⁻ and one Li⁺). This portfolio of SSIPs could recently be extended towards the so-called pentuple ion, named by the same principle.^[29q, 32] In conclusion, most organometallic structures can be classified as either SSIPs or CIPs and their reactivities also depend in many cases on these basic aggregational concepts.

1.1.2 Alkali Metal Cyclopentadienides (CpMs)

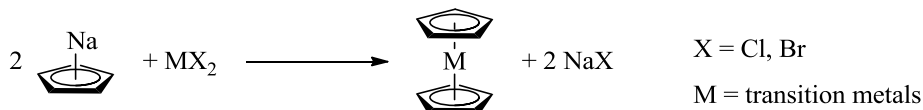
Another important class of compounds in organometallic chemistry are alkali metal cyclopentadienides (CpMs) and their derivatives which have been reviewed in literature^[33] extensively.

1.1.2.1 A Short Historical Background

A historical landmark of cyclopentadienide chemistry is the synthesis and structure determination of bis(cyclopentadienyl)iron(II), commonly known as ferrocene, which expedited the organometallic chemistry of the transition metals.^[34] However, ferrocene was discovered over half a century later than sodium cyclopentadienide (CpNa) which was already synthesized *in situ* by *Thiele*^[35] in 1900, even though he was not able to isolate it. However, a year later *Thiele*^[36] was able to synthesize and isolate potassium cyclopentadienide (CpK) which was the first purely isolated organometallic compound featuring an alkali metal. This all took place shortly after the isolation of cyclopentadiene itself which is achieved by the reversible *Diels-Alder* dimerization reaction of dicyclopentadiene (DCp), even though this reaction behavior was puzzling at those times.^[37] A few years after the discovery of ferrocene, *Fischer et al.*^[38] and *Ziegler et al.*^[39] independently isolated pure CpNa from xylene solution which made CpMs more accessible. Both studies point out that this had not been possible for *Thiele* due to his choice of solvent (benzene) and its lower boiling point.

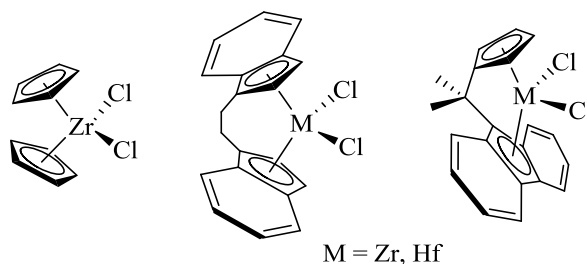
1.1.2.2 Practical Applications

CpMs are highly relevant precursors for a variety of different sandwich or half-sandwich d-block organometallics which can be synthesized through either transmetalation or salt elimination (see Scheme 1-3).^[40]



Scheme 1-3: General synthesis of transition metal metallocenes using CpNa as starting material.^[41]

Such metallocenes, whereas it is debateable, if the term includes only sandwich or also half-sandwich complexes,^[33e] and their derivatives can be used in the catalysis of polymerization reactions of alkenes. Especially the polymerization of propene by homogeneous *Kaminsky*-catalysts is of major importance in this regard. These were discovered in 1980 by *Kaminsky et al.*^[42] and consist of zirconium, hafnium or titanium sandwich complexes which may also contain bigger ligand systems based on indenides or fluorenydes (see Scheme 1-4) in combination with methylaluminoxane (MAO).^[43]



Scheme 1-4: Small selection of metallocene-type *Kaminsky*-catalysts which can be used for polymerization reactions.^[43c]

Different catalysts lead selectively to *a*-, syndio- or isotactic polymers and can be up to 100 times as effective as their close relatives, the *Ziegler-Natta* catalysts.^[43c] There are also many other syntheses, wherein complexes incorporating the cyclopentadienide ligand are of use, e.g. the synthesis of isoindolones^[44] or of fullerene-ferrocene-hybrids.^[45] Recently, *Cramer et al.*^[46] have also been using chiral cyclopentadienide ligands for asymmetric C-H functionalization. Additionally, there are some metallocene dihalides which exhibit anti-tumor properties, although none have proceeded far in clinical trials.^[47]

1.1.2.3 Properties and Bonding

CpMs are very salt-like which can be underlined by their high melting points and low volatilities.^[33d, 48] Due to this it is not surprising that their solubility in hydrocarbons and ethers (except THF) are quite poor which made structure elucidation, especially crystal structure determination of the donor-free compounds, challenging.

Some first analytical results concerning the bonding of CpMs have been gathered in the 60s and 70s by IR^[49] and NMR measurements^[50] which indicated that the metal cation and Cp⁻ are π -bonded along its fivefold axis (η^5 -coordination) in solution. Those findings already showed that the σ -bonded complex of CpLi, i.e. 2-lithio-cyclopentadiene, is unlikely which has also been confirmed by simple *ab initio* calculations (RHF/6-31 + G*) that result in a 49.3 kcal/mol difference in favor of the η^5 - π -bonded complex.^[33e] In principle, the alkali metal could be attached to the Cp⁻ at several positions, ranging from η^1 - to η^5 -coordination. However, the hapticity of CpLi was analyzed by means of a theoretical haptotropic search which again emphasized the preference of the η^5 -coordination motif (see Figure 1-2).^[33e]

Still, *Harder*^[33e] suggests that minor deviations from a perfect η^5 -coordination are common due to the rather flat minimum of the energy curve. The importance of electrostatics on the bonding between alkali metal and cyclopentadienide was explained in an extensive theoretical study by *Rayon* and *Frenking*^[51] in 2002.

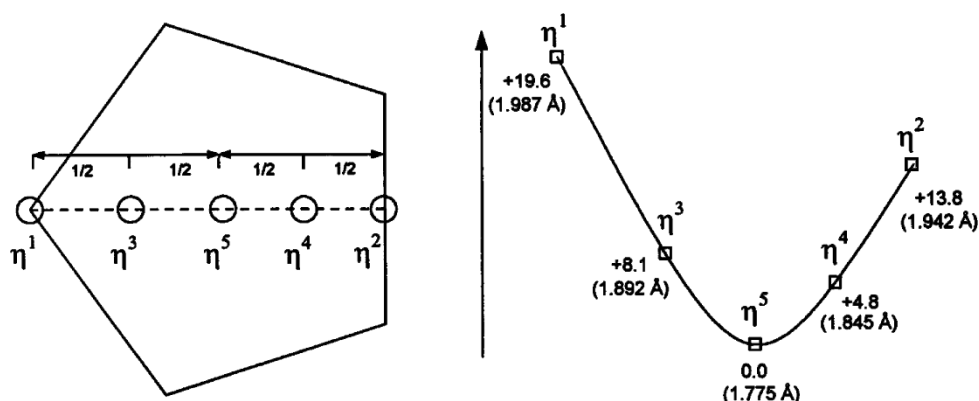


Figure 1-2: Results of a haptotropic search of CpLi (MP2/6-31 + G*). With decreasing hapticity the energy and distance of lithium to Cp⁻ increase, while lithium is shifted over the Cp-plane. Reprinted from reference [33e]. Copyright © 1998 Elsevier.

1.1.2.4 Aggregation of CpMs in the Solid State and in Solution

The first crystal structure of an underivatized CpM was published in the late 70s by Wade *et al.*^[52] with [CpNa(TMEDA)]_∞ which features a polymeric CIP with attached donating Lewis bases. Over the years, other crystal structures of CpMs were presented that entailed similar donor-coordinated polymeric chains.^[53] Still, it was not until over 20 years later that structures of donor-free CpMs were published: By then Olbrich *et al.*^[54] used powder diffraction to provide the solid state structures of CpLi, CpNa and CpK. These molecules also form CIPs arranged into polymers that are linear and isomorphous for CpLi and CpNa, whereas for CpK and the higher homologues bent structures could be observed (see Figure 1-3; for CpRb there are ambivalent structures).^[54-55]

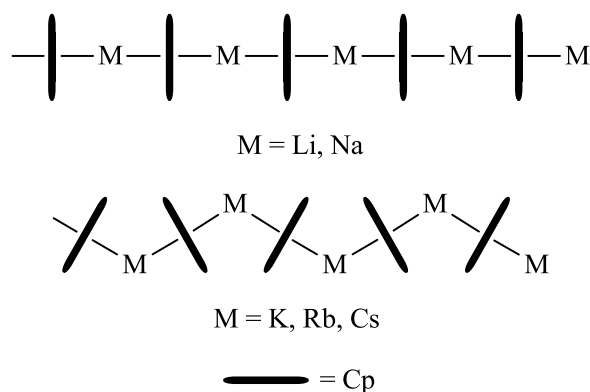


Figure 1-3: Donor-free aggregation of CpMs (also known for methyl- or silyl-substituted Cp-moieties, see literature mentioned above).

Polymeric donor-free structures are also known for the methylated derivatives (i.e. methylcyclopentadienides (CpMe) or pentamethylcyclopentadienides (Cp*)) and silyl-substituted Cp-systems.^[56] While silyl substituents stabilize the cyclopentadienide carbanion, alkyl groups have the opposite effect. Still, alkyl-substituted ring systems are widely used to fine-tune reactivities of the desired products or increase the steric demand.

In 1983, *Jutzi et al.*^[57] published the first single crystal structures featuring solvated monomeric aggregates $[(\text{Me}_3\text{Si})_3\text{CpLi}(\text{Base})]$ with Base = TMEDA, PMDETA or chinuclidin). They and others derivatized the cyclopentadienide with trimethylsilyl-substituents to increase its solubility.^[58] Today, many crystal structures are known with monomeric^a or polymeric aggregation, whilst containing additional donor bases (see Figure 1-4).^[52-53, 57-59] Monomeric aggregation is often achieved by crown ethers or other strongly donating tri-, bi- or monodentate ligands. While monomeric aggregates represent the complete disaggregation of the polymeric chain, in a few cases oligomers could also be observed.^[60] In 2011, two oligomeric structures of nonderivatized CpMs were reported by *Stalke et al.*^[290] who found dimeric $[(\text{CpLi})_2(\text{NH}_3)_3]$ and *Klett et al.*^[61] who reported tetrameric $[(\mu\text{-Cp})\text{Li}(\mu\text{-TMP})\text{Li}]_4$.

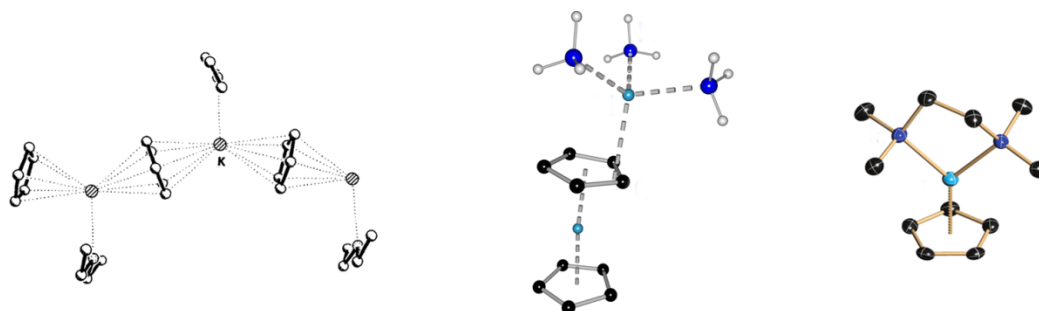


Figure 1-4: Selection of solid state structures of CpMs, illustrating different aggregational possibilities, when incorporating donating solvents. (from left to right: polymeric $[\text{CpK}(\text{Et}_2\text{O})]_\infty$ ^[53a], dimeric $[(\text{CpLi})_2(\text{NH}_3)_3]$ ^[290] and monomeric $[\text{CpLi}(\text{TMEDA})]$ ^[59n]) Structures were reprinted from references [53a], [59n] and [290]. Copyrights © 1996 Elsevier and © 2010, 2011 American Chemical Society.

Lastly, concerning CpM aggregational states, there are also charged species known (see Figure 1-5). The most interesting one is probably the smallest metallocene possible, the lithocene anion $[(\text{Cp}_2\text{Li})^-]$. It was first crystallized in 1994 by *Harder and Prosenic*^[62] as $[\text{Ph}_4\text{P}][\text{Cp}_2\text{Li}]$. A year later, *Mews et al.*^[63] were able to exchange the counter-ion for tris(dimethylamino)sulfonium $[(\text{Me}_2\text{N})_3\text{S}]^+$ and crystallized not only $[(\text{Me}_2\text{N})_3\text{S}][\text{Cp}_2\text{Li}]$, but also the sodium analogue (sodocene). *Harder et al.*^[64] reported another sodocene structure a year later $[(\text{Ph}_4\text{P}][\text{Cp}_2\text{Na}]$. Moreover, a silylated lithocene structure was published by *Westerhausen et al.*^[65] $[(\text{Li}(\text{THF})_4)[((\text{Me}_3\text{Si})_2\text{Cp})_2\text{Li}]$ which can also be classified as a lithium lithiate.

The possibility of the existence of lithocene in solution has been investigated as well. In 1990, *Paquette et al.*^[66] studied CpLi in THF *via* NMR spectroscopy and found out that there might exist an equilibrium between a monomeric CIP and the lithocene anion. In their study, they focused primarily on lithium isodicyclopentadienide and could prove for this the existence of a monomer-dimer equilibrium in THF at low temperatures (the dimer being a sandwich type aggregate).^[66] For CpLi they proposed a similar behavior, even though exchange rates seem to be much faster and they were not able to “tell whether the monomer-dimer equilibrium [...] is shifted to either side at room temperature”.^[66] In the same year, *Brandsma et al.*^[67] used cryoscopy to examine CpLi within

^a Monomeric CpM aggregates are in some cases called “piano stool” or half-sandwich complexes.

ammonia and proposed that CpLi does not form simple monomeric [CpLi] therein, whereas higher aggregates, including charged species, like lithocene, are likely. This is also hinted at by findings of *Stalke et al.*^[29o] who could show an involvement of lithocene type aggregates within a crystal structure (middle of Figure 1-4; [(CpLi)₂(NH₃)₃]) which was crystallized from ammonia and might be preserved in solution as well.

Stalke et al.^[29o] also crystallized another unprecedented aggregate utilizing a higher concentration of ammonia: A SSIP consisting of Cp⁻ anions with solvent-coordinated [Li(NH₃)₄]⁺ cations (see Figure 1-5). A handful of such SSIPs have been published over the years, but Cp⁻ anions could, in contrast to the above mentioned case, only be stabilized by sterically demanding cations.^[53b, 63] Aside from metallocene type structures, like the lithocene (a), cationic inverse sandwich complexes^[68] (b) as well as a caesocene triple-decker structure^[69] (c) were reported which conclude the range of charged species known for CpMs.

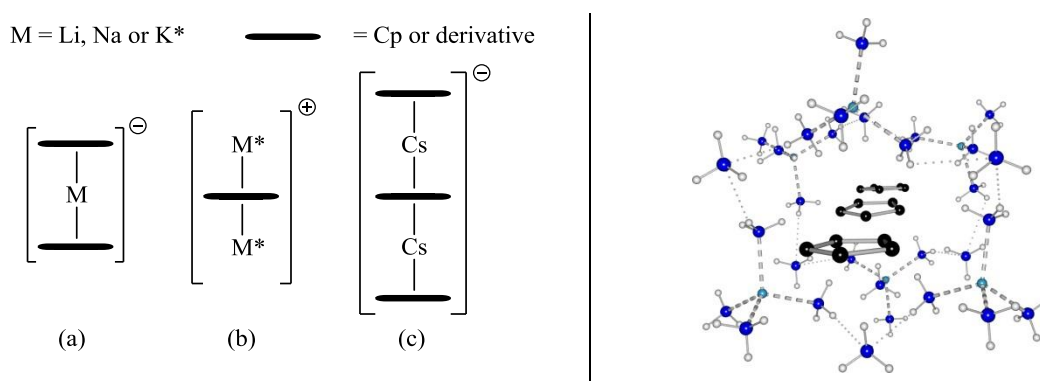


Figure 1-5: Selection of charged species known from crystal structure analysis (from left to right: metallocene-type sandwich complexes (a), inverse sandwich complexes (b), a caesocene triple-decker (c) (donating solvent molecules have been omitted for clarity) and an exemplary SSIP ([Li(NH₃)₄][Cp]). The SSIP structure (right) was reprinted from reference [29o]. Copyright © 2010 American Chemical Society.

1.2 Nuclear Magnetic Resonance (NMR) Spectroscopy

Even though most structures discussed above have been solved by single crystal or powder X-ray diffraction, and in recent years many advances were made in this field to improve structure determination of volatile, air- or moisture-sensitive compounds and the handling of crystals at lower temperatures, it is still only a first step towards understanding a molecule's reactivity.^[70] While a crystal structure can mostly be viewed as unambiguous, solution state structures are often complex equilibria of multiple co-existing aggregates. Since reactions are mostly carried out in solutions, it is therefore imperative to understand these equilibria and the individual aggregates thereof. While there are other methods available to observe and afterwards interpret the constitution of a molecule in solution (e.g. ultraviolet-visible (UV-VIS) or infrared (IR) spectroscopy, cryoscopy, ebulliometry), NMR spectroscopy has been on the rise in the last decades and can in many ways go beyond or be combined with other methodologies. Nowadays, advanced high-resolution NMR methods exist or are being developed which can be used to monitor reactions

or even determine a molecule's stereochemistry (e.g. by *Niklas et al.*^[71]). Furthermore, many other methods published in the last decades (e.g. correlation spectroscopy (COSY), heteronuclear single quantum correlation (HSQC), heteronuclear multiple bond correlation (HMBC) and many more) added to the NMR spectroscopist's repertoire. The basics and theoretical background of NMR spectroscopy as well as most routinely used 1D and 2D methods have been reviewed extensively in literature^[72] and will not be discussed in this work.^a

1.2.1.1 Heteronuclear *Overhauser* Enhancement Spectroscopy (HOESY)

Apart from routine experiments or diffusion NMR techniques which will be elucidated in the following sections, heteronuclear *Overhauser* enhancement spectroscopy (HOESY) is repeatedly utilized throughout this work. This type of experiment was introduced independently by *Levy et al.*^[73] and *Rinaldi*^[74] in 1983. It is derived from nuclear *Overhauser* enhancement spectroscopy (NOESY) which visualizes homonuclear dipole-dipole interactions through space using the nuclear *Overhauser* effect (NOE). The HOESY technique, in contrast to NOESY, aims at heteronuclear couplings and is nowadays often used in lithium chemistry to observe short ⁶Li-¹H or ⁷Li-¹H distances (up to 4 Å).^[75] This allows discrimination between different aggregational states (CIP vs. SSIP), since dipole-dipole interactions to solvents or ligandsystems can be interpreted. If used qualitatively, it is intuitive: If a crosspeak is observed, the coupling nuclei have to be in close proximity to each other. Furthermore, the higher the intensity of the crosspeak the closer are the nuclei, since the crosspeaks intensity is proportional to $\frac{1}{r^6}$. Hence, even quantitative distance calculations are possible.^[76]

Von Ragué Schleyer et al.^[75] were the first to use HOESY in organolithium chemistry.^[77] They showed that ⁶Li-¹H couplings can effortlessly be observed at natural abundance. This is possible since ⁶Li has the smallest quadrupolar moment known and behaves like a spin- $\frac{1}{2}$ nucleus (see Table 1-2).

Table 1-2: Quadrupole moments (Q) of alkali metal nuclei.

Nucleus	⁶ Li	⁷ Li	²³ Na	³⁹ K	³⁹ K	⁴¹ K	⁸⁵ Rb	⁸⁷ Rb	¹³³ Cs
Q ^[78] [fm ²]	-0.0808	-4.01	10.4	5.85	-7.3	7.11	27.6	13.35	-0.343

Interestingly enough, ⁷Li,¹H-HOESY experiments are also possible, even though its quadrupole moment is relatively large (see Table 1-2). ¹³³Cs,¹H-HOESY has also been applied in a few cases, but for it to be successful, T_1 relaxation times have to be higher than 0.1 s.^[79] For other alkali metals HOESY experiments are unknown, as their quadrupole moments are even larger (see Table 1-2) which enables quadrupolar relaxation and reduces the NOE needed to observe interactions through space.

^a Information on alkali metal NMR spectroscopy is given as deemed appropriate.

1.2.2 Overview of Diffusion NMR

Aside from the above-mentioned approaches, diffusion NMR experiments play a fundamental role in solving aggregational phenomena. Through such experiments diffusion coefficients (D) of molecules can be determined and afterwards correlated to their sizes or weights. The theoretical background as well as related experiments have been reviewed extensively in literature^[80] and shall only be discussed shortly herein. The basics of the methodology were already developed in the mid-1960s by *Stejskal* and *Tanner*^[81] who were looking for a way to reliably determine the self-diffusion coefficient of solutes. The result was the pulsed-field gradient spin-echo (PFG-SE^a) pulse sequence (see Figure 1-6).

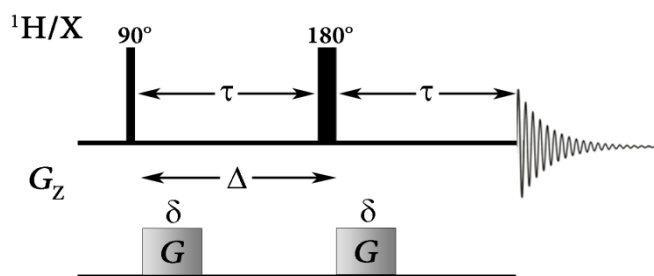


Figure 1-6: Pulse sequence of the PFG-SE experiment.^[81]

It incorporates the *Hahn* spin-echo sequence^[82] (consisting of a 90° and a 180° pulse) which is used to refocus the chemical shift evolution. This way, the detected signal is only attenuated by its spin-spin relaxation (T_2) during the experiment (2τ). Additionally, pulsed-field gradients are employed to encode the physical location of a spin. Molecules diffuse through random translational motion (*Brownian* motion) driven by the thermal energy of the system. This motion changes the physical location of a molecule (depending on its individual diffusion coefficient) and through the imposed field gradient also the local field it experiences. Due to this change in local field, magnetization is not completely refocused after the completion of the spin-echo sequence.

Varying the diffusion delay (time the molecule can diffuse; Δ), the length of the gradient pulses (δ) or their strength (G) enables the characterization and differentiation of diffusion rates (see Figure 1-7).^b

^a In literature sometimes PGSE.

^b Varying the gradient strength is preferred as longer diffusion times increase the loss of magnetization due to T_2 relaxation.

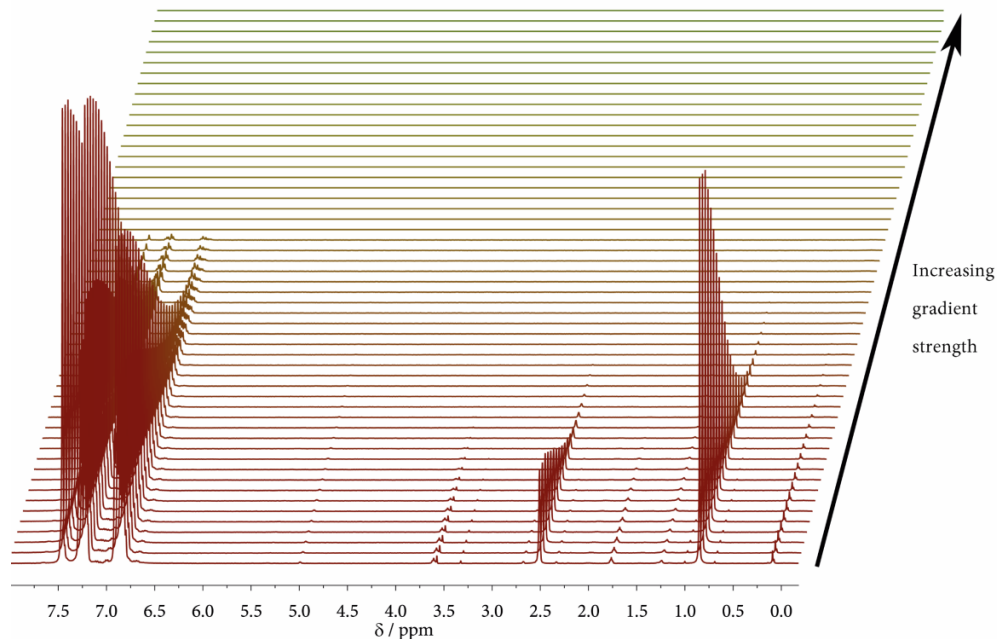


Figure 1-7: ^1H signal attenuation due to the continuous increase in gradient strength (G) in PFG-SE-based experiments.

1.2.2.1 Calculating Diffusion Coefficients

The signal intensity after a PFG-SE experiment (I_G) can be expressed by the *Stejskal-Tanner* equation (1-1) and is thereby correlated directly to the desired diffusion coefficient.

$$I_G = I_0 \exp\left(-\frac{2\tau}{T_2}\right) \exp\left(-(\gamma\delta G)^2 D \left(\Delta - \frac{\delta}{3}\right)\right) \quad (1-1)$$

Here I_0 represents the signal intensity recorded after the first 90° pulse before the application of the field gradient and spin echo, while G is the gradient strength, D the diffusion coefficient, γ the gyromagnetic ratio of the observed nuclei, T_2 the transverse relaxation rate constant and τ , δ and Δ delays that are shown in Figure 1-6.

Variation of G leads to a *Gaussian* decay profile for I_G that can be fitted according to equation (1-1).^a The signal attenuation should be neither too fast nor too slow as to consider all recorded points and get information as reliable as possible (see Figure 1-8).

Other possibilities to determine diffusion coefficients are to plot I_G against G^2 which results in an exponential profile or $\ln(I_G)$ against G^2 which can be fitted linearly. These options are also available in modern software applications, e.g. Topspin 3.1. To obtain the diffusion coefficients of individual components of a mixture, their resonances should be clearly separated.^b If, however, multiple signals overlap, the signal attenuation is comprised of a multiexponential decay.

^a Note that $k = \exp\left(-\frac{2\tau}{T_2}\right)$ is usually kept constant and vanishes as $I_0^* = I_0 \cdot k$.

^b Baseline distortions should also be avoided for a precise signal intensity acquisition.

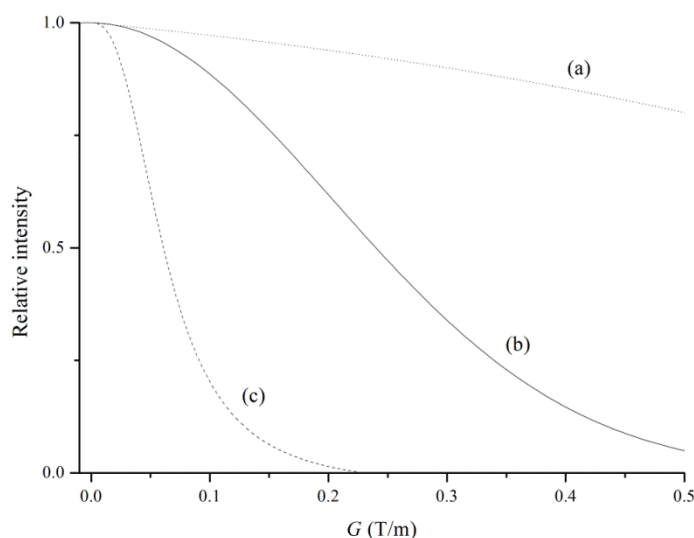


Figure 1-8: Qualitative *Gaussian* signal intensity decay profiles (I_G vs. G). Signal attenuation should not be too slow (a) or too fast (c). In an optimal decay profile (b) all points can contribute to the determination of D .^[80c]

1.2.2.2 Advances in Diffusion NMR

Modern NMR spectrometers are usually equipped with probe heads with the capability to generate pulsed-field gradients, and therefore diffusion NMR has become routinely accessible. Furthermore, there are improved pulse sequences available (e.g. pulsed field gradient stimulated-echo (PFG-STE)^[83], bipolar pulse pairs with longitudinal-eddy-current-delay (BPP-LED)^[84] or double-stimulated-echo (D-STE)^[85]) that reduce experimental times, magnetization loss through relaxation, spectral (eddy-current^a) distortions or the effect of convection.

Another technique that is gaining popularity and works well in combination with various NMR techniques is called pure-shift NMR.^[86] This technique entails homo nuclear decoupling and thus reduces signal overlap which is crucial for diffusion NMR. In 2014, *Maddaluno and Oulyadi et al.*^[87] showed the effectiveness of the combination of the two techniques (diffusion and pure-shift NMR) on model *n*BuLi aggregates in THF.

1.2.2.3 Diffusion-Ordered Spectroscopy (DOSY)

While 1D NMR experiments provide chemical shifts (δ) and scalar homo- or heteronuclear coupling constants (J) as basic and resilient parameters to judge a sample's composition, it was the introduction of a 2nd dimension which enabled easier access to their relations. In 1992, *Johnson and Morris*^[88] introduced a new representation for diffusion experiments which was a (pseudo) 2D arrangement they named diffusion-ordered spectroscopy (DOSY). Using DOSY, different components within a mixture are visually separated by their diffusion coefficients which are still

^a Swirling (eddy) currents are produced during rapid changes in the magnetic field (e.g. gradients) induced in conducting materials (mostly any metallic component in the surrounding NMR spectrometer).

being correlated to their chemical shift information (see Figure 1-9). The methodology has gained huge popularity since its publication and is frequently called “*NMR chromatography*”.^[89]

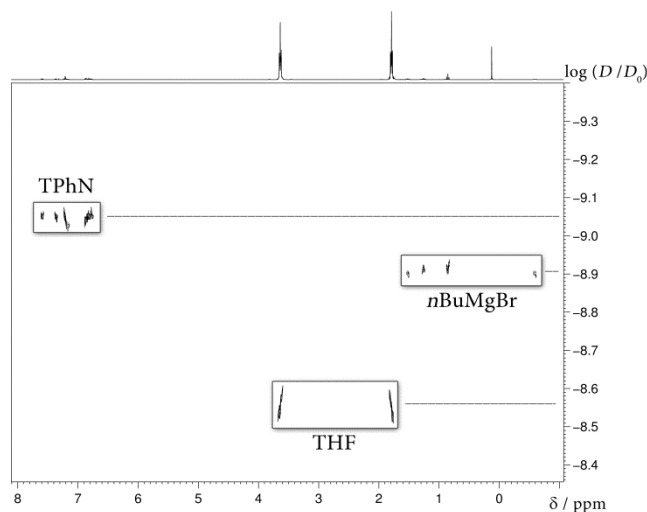


Figure 1-9: Pseudo 2D ¹H-DOSY spectrum of *n*-butylmagnesium bromide (*n*BuMgBr) and the internal reference 1,2,3,4-tetraphenyl-naphthalene (TPhN) in THF-*d*₈. Signals corresponding to the same compound have the same diffusion coefficient and appear in the same row of the spectrum. ($D_0 = 1 \text{ m}^2/\text{s}$)

In organometallic chemistry, DOSY has been used in the last few decades to analyze a number of transition metal complexes.^[90] Additionally, the work of *Williard et al.*^[91] should be emphasized, as they have been focusing heavily on lithiumorganics (e.g. they proved the tetramer-dimer equilibrium of *n*BuLi in THF using DOSY). These studies also focused heavily on heteronuclear DOSY experiments. Even though heteronuclei often suffer from lower sensitivities, due to their higher chemical shift ranges (e.g. for ¹³C) their employment can reduce signal overlap. Moreover, such DOSY analyses can be used to prove coordination behavior (e.g. for ⁷Li). However, it does not work for nuclei with short T_2 relaxation times.

Recent developments expand the DOSY methodology towards the 3rd dimension to correlate more vital information to the diffusivity of aggregates.^[85, 92]

1.2.3 Molecular Sizes and Weights from Diffusion Coefficients

A key interest of chemists lies within the correlation of self-diffusion coefficients (D) to molecular sizes or weights to deduce either aggregational states or interpret other diffusion phenomena (e.g. host-guest interactions).^[93] The relationship of the diffusion coefficients to the size of a molecule can most easily be shown by the *Stokes-Einstein* equation (1-2):^[94]

$$D = \frac{k_b T}{6\pi\eta r_s} \quad (1-2)$$

^a Chromatography is usually used for diffusion experiments supported by stationary phases.

Here, r_s represents the *Stokes*-radius which is the radius of a hard sphere that diffuses at the same rate as the observed solute. k_b is the *Boltzmann* constant, T the absolute temperature and η the solvent viscosity at the respective temperature.

However, this equation is only valid for spherical molecules that are much larger than the solvent. While it may be acceptable to make size estimations in a qualitative way, further steps have to be taken to receive more quantitative results, especially for molecules that match or fall below the size of the solvent. Early on, it was proposed to change the frictional coefficient (denominator) “ $6\pi\eta r_s$ ” (stick-boundary condition) to “ $4\pi\eta r_s$ ” (slip-boundary condition).^[94] Later, it was argued that instead of a fixed value, a correctional factor (c) should be introduced that depends on the ratio of the radii of solvent (r_{solv}) and solute (r_s). Additionally, a second correctional term (f_s) needs to be added to take differing solute geometries/shapes into account. The combination of both correctional factors leads to equation (1-3).

$$D = \frac{k_b T}{c(r_{\text{solv}}, r_s) \cdot f_s(a, b) \cdot \pi\eta r_s} \quad (1-3)$$

Multiple attempts to express c as function of r_{solv}/r_s resulted in equation (1-4) by *Gierer* and *Wirtz*,^[95] attained by microfrictional theory, and equation (1-5) by *Chen* and *Chen*^[96] who used a semi-empirical approach. Both equations result in a numerical factor of 6 for bigger solutes, while *Chen*'s approach reaches this value faster (see Figure 1-10). Still, they drastically improve the model for solutes that have a similar size as the solvent.

$$c = \frac{6}{1.5 \cdot \left(\frac{r_{\text{solv}}}{r_s}\right) + \frac{1}{1 + \left(\frac{r_{\text{solv}}}{r_s}\right)}} \quad (1-4)$$

$$c = \frac{6}{1 + 0.695 \cdot \left(\frac{r_{\text{solv}}}{r_s}\right)^{2.234}} \quad (1-5)$$

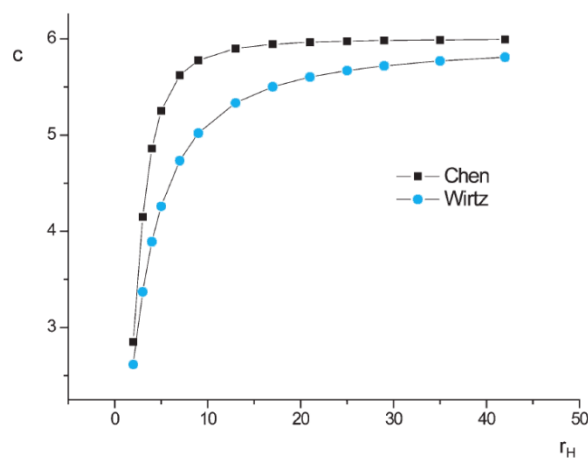


Figure 1-10: Comparison of the approaches of *Wirtz*^[95] and *Chen*^[96] on the correctional factor c correlated with a change in hydrodynamic radius (size of the solute). Adapted from reference [80d]. Copyright © 2008 The Royal Society of Chemistry.

The shape correctional factor f_s can be based on early results of Perrin.^[97] He differentiated prolate and oblate ellipsoid molecules depending on the ratio of their minor (b) and major (a) semiaxes (see Figure 1-11).

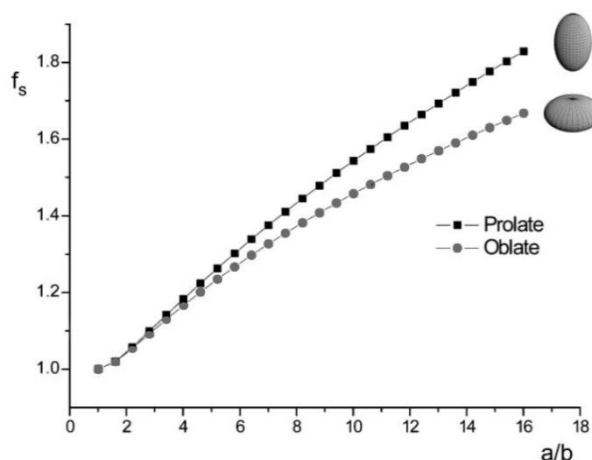


Figure 1-11: Dependence of the shape correctional factor f_s for prolate and oblate ellipsoid molecules. Adapted from reference [80d]. Copyright © 2008 The Royal Society of Chemistry.

In 2013, Morris *et al.*^[98] improved the aforementioned *Stokes-Einstein* based equations. They used the effective solvent density (ρ_{eff}) instead of solvent radii and were able to drastically increase the average (av.) accuracy (up to about 15%) of the calculated hydrodynamic radii (r_H), especially in regard to small molecules.

These calculated molecular sizes in form of r_s or r_H need to be compared to other theoretically or experimentally accessible radii, e.g. *van-der-Waals* radii (r_{vdW}) or radii obtained from X-ray crystallography ($r_{\text{X-ray}}$). While r_{vdW} are in good agreement with r_s for very spherical molecules, they completely fail for molecules with any inlets or cavities. Since r_{vdW} are based on the assumption that molecules are made up of perfect spheres, they naturally represent the lower limit of radii. In contrast, radii obtained by X-ray crystallography are larger than r_s and correlate best for non-spherical molecules incorporating inlets.^[80d] In light of these facts, it is essential to know what type of molecule and aggregation is to be interpreted and what kind of information is already available for it, so that the right conclusions are drawn from calculated hydrodynamic radii or other information based on these.

1.2.3.1 MW Estimation Using Power Law Approaches

There are several formulae to estimate molecular weights (MW s) from the aforementioned radii. However, these incorporate at least the same shortcomings and errors as the radii themselves since they are all based on the *Stokes-Einstein* equation. Recently, an empirical power law has become the center of attention for the correlation of measured diffusion coefficients to MW s (see equation (1-6)).

$$D \propto MW^{-\alpha} \quad (1-6)$$

In this correlation, α is a parameter that incorporates molecular properties and that is also often referred^[99] to as the *Flory* exponent. That is because *Flory*^[100] established a similar relation for polymers and proteins in the 1950s. A *Flory* exponent of $\alpha = 1$ is achieved for completely linear molecules, while a *Flory* exponent of $\alpha = 1/3$ is related to objects or molecules that completely fill up all available space. Therefore, this exponent is a measure for molecular compactness amongst others. While, like in the case of *Flory*, power laws were and are mostly used for larger molecules (e.g. for polymers^[99, 101], hollow clusters^[102] or biomolecules^[103]), *Crutchfield* and *Harris*^[104] could show in 2007 that even for small molecules a greatly improved accuracy can be accomplished compared to *Stokes-Einstein* approaches. Since diffusion measurements themselves and therefore absolute diffusion coefficients are strongly influenced by temperature, viscosity, concentration and instrument specific variables (e.g. gradient strength), there was need for a complimentary technique. *Harris et al.*^[104] chose to relate diffusion coefficients of analytes to those of internal references which they believed are “conveniently present in common NMR solvents”, like tetramethylsilane (TMS) or water. The av. deviation of estimated *MW*s using this method was according to *Harris et al.* only 11% (maximum deviations were 35%), while the lowest average deviation of the *Stokes-Einstein* based estimations was 15% (*Morris*^[98] approach). The independence of viscosity for such relations (see equation (1-7)) could already be shown earlier.^[105]

$$D_{\text{rel,ref}} = \frac{D_{\text{ref}}}{D_x} \quad (1-7)$$

Here D_{ref} is the diffusion coefficient of an internal reference and D_x of an analyte x . *Dobson et al.*^[105a] termed this ratio relative diffusivity ($D_{\text{rel,ref}}$). *Harris et al.*^[104] used this relation to obtain relative diffusivity vs. *MW* calibration curves in CDCl_3 and D_2O . They also showed that those relative diffusivities are widely constant in various solvents (variations of up to 25%). However, through their calibration curves they also showed that differentiating solvent environments is vital (see Figure 1-12).

Another approach to estimate *MW*s from diffusion coefficients was introduced by *Williard et al.*^[106] They used at least three different internal references (see Figure 1-13) with known *MW*s to establish internal calibration curves (ICCs). Because these references as well as the analytes were in the same sample, they were exposed to the same temperature, viscosity, etc. which made their diffusion coefficients mutually comparable. Using a logarithmic form of the power law (see equation (1-8)) they were able to estimate *MW*s of the remaining solutes using a linear fit of a plot of logarithmic diffusion coefficients against logarithmic molecular weights.

$$\log(D) = \log(K) - \alpha \cdot \log(MW) \quad (1-8)$$

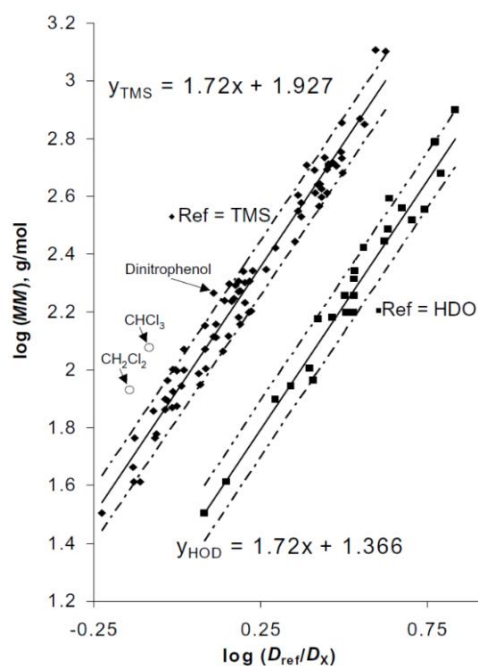


Figure 1-12: Calibration curves of a multitude of references in CDCl_3 (diamonds) and D_2O (squares) using their logarithmic relative diffusivities and molecular weights. Reprinted from reference [104]. Copyright © 2007 Elsevier.

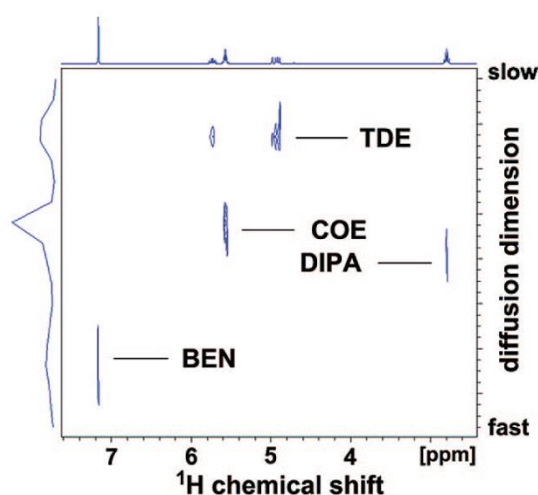


Figure 1-13: ^1H -DOSY spectrum showcasing several internal references (1-tetracene (TDE); cyclooctene (COE) and benzene (BEN)). These can later be used to form an ICC and estimate the MW s of other solutes (in this case of diisopropylamide (DIPA)). Reprinted from reference [106b]. Copyright © 2009 American Chemical Society.

This ICC methodology was used extensively to estimate MW s of a multitude of compounds (e.g. organometallics) and deduce their solution state structures.^[107] Moreover, *Williard et al.*^[108] were able to extend the methodology towards heteronuclei. There are still a few setbacks with this technique that are on the one hand related to the needed reference count (a minimum of three) and the limited applicability (an ICC is only viable for a single NMR sample and experiment). Furthermore, this technique is in the same accuracy region as *Harris'* normalization approach.

Very recently, our group was able to develop a new method on the basis of this ICC technique of *Williard*.^[109] As was already mentioned, *Williard's* method required a multitude of different

references present in an NMR sample which produces a number of complications, since the references needed to possess certain properties. They needed to be inert, should not produce signal overlap or interact in any way with other solutes, especially not with the analytes. They should also be well soluble and have a good *MW* distribution so that the subsequent *MW* estimation is based on a wide range of *MWs*. It is difficult to accommodate all these criteria, since especially signal overlap is a prevalent problem. Normalizing diffusion coefficients similar to *Harris'* approach proved to be the easiest way to produce comparability, while only utilizing a single reference. Such normalized diffusion coefficients can be arranged in the same way as in ICCs by simply plotting them logarithmically against known logarithmic *MWs* (see Figure 1-14, left).

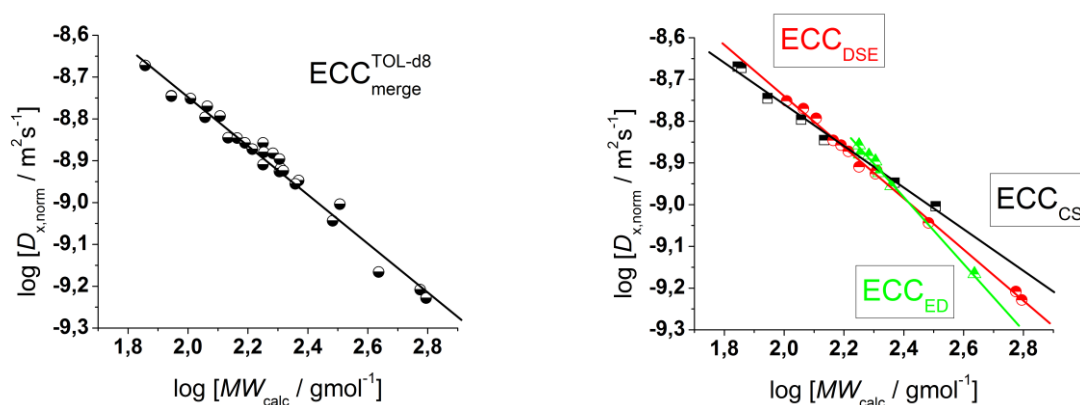


Figure 1-14: External calibration curves (ECCs) of several references in toluene. Molecules with very high or very low *MW* deviate in some cases more strongly from an averaged ECC (left). This can be improved by using separate ECCs based on molecular shape (right). Reprinted from reference [109a]. Copyright © 2015 The Royal Society of Chemistry.

Since all diffusion coefficients were normalized, they also did not need to be measured at the same time, but rather in different samples and experiments which made it possible to establish a wider, more extensive *MW* distribution. The resulting logarithmic plots were named external calibration curves (ECCs).

It was already mentioned for the *Stokes-Einstein* approaches that deriving molecular sizes or masses from diffusion coefficients is tightly related to their shapes. Therefore, the accuracy of the ECC method was further increased by differentiating between molecular shapes (see Figure 1-14, right).^[109a] This was done by semi-empirically dividing the compounds used for calibration into three categories (the categorization process will be explained in more detail in section 2.1): Compact spheres (CS), dissipated spheres and ellipsoids (DSE) or expanded discs (ED) (see Figure 1-15). After this categorization, *MWs* could be estimated with the resulting ECCs with a maximum deviation of 9% in until now two solvents (THF-*d*₈ and toluene-*d*₈) which was deemed an immense improvement compared to averaged ECCs.^a Using this method, our group was able to solve the solution structures of lithium diisopropylamide^[110] as well as several *Hauser* bases.^[111] Moreover, the methodology has already been adopted by other groups: *Mulvey et al.*^[112]

^a Deviations of the average ECCs were not given in reference [109].

investigated alkali metal and alkali metal magnesiate amido systems, Wang and Pedersen *et al.*^[113] glycosylation intermediates and O'Hara *et al.*^[114] alkali metal hexamethyldisilazides using ECCs.

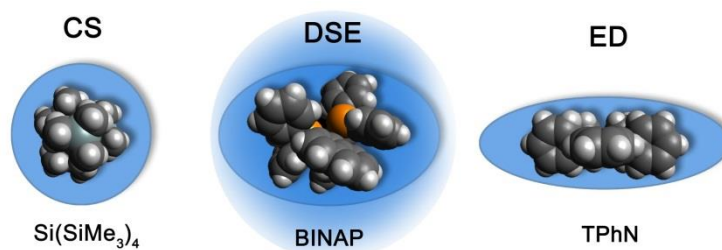


Figure 1-15: Different molecular shapes defined for ECC-DOSY: Compact spheres (CS), dissipated spheres and ellipsoids (DSE) and expanded discs (ED). Reprinted from reference [109a]. Copyright © 2015 The Royal Society of Chemistry.

Even though all the herein-presented *MW* estimations from diffusion data may never be as precise as mass spectrometry, it was proven that they hold great value for the structure determination in solution.

1.3 Scope of this Thesis

It is the aim of this thesis to improve and apply the recently developed ECC-DOSY-*MW* estimation methodology which can aid in a more straightforward solution of occurring ambiguities related to equilibria in solution *via* NMR spectroscopy. This is important since aggregates within these equilibria may determine the result of a reaction.

In the first part of this work, the ECC-DOSY-*MW* estimation methodology itself is reviewed, improved and extended to assure an easy and robust application. In particular, the limited applicability is addressed, since ECCs were only available for THF-*d*₈ and toluene-*d*₈. Therefore, creating new external calibration curves for other solvent environments is a key element of this work (see Figure 1-16 (left)). Furthermore, most of the research regarding ECCs has been solely empirical; a theoretical calculation of the limits of the ECC-*MW* estimation as well as a theoretical approach towards the categorization of model compounds according to their shapes is pursued.

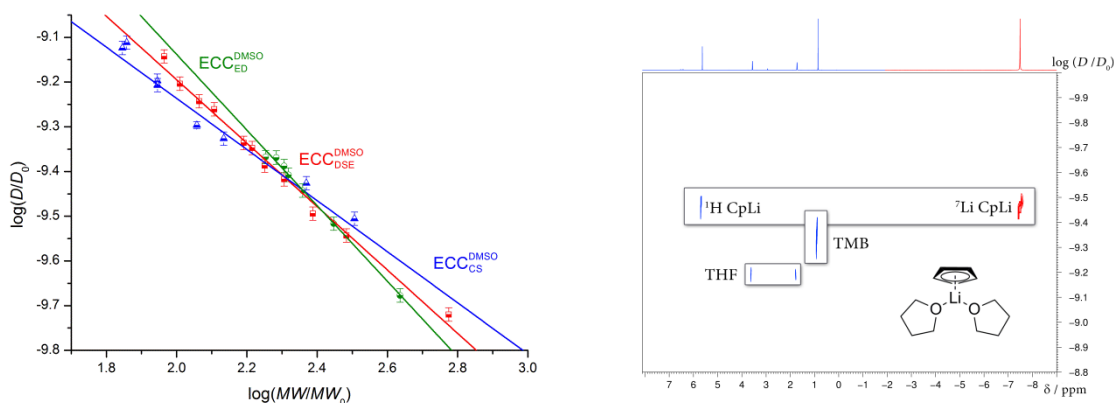


Figure 1-16: Illustrations of the advancement and application of the ECC-DOSY methodology presented in this work.

The second section features the application of the ECC methodology towards alkali metal cyclopentadienide derivatives in different solvents (see Figure 1-16 (right)). Prior to this work they have been characterized extensively and different aggregational states have been established in the solid state (see section 1.1.2.4). These results can be compared to solution state structures deduced from ECC-DOSY. Moreover, *Paquette et al.*^[66] observed CpLi in THF and stated that they could not “*tell whether the monomer-dimer equilibrium [...] is shifted to either side at room temperature*”. This question is addressed in greater detail and exemplified *via* ECC-DOSY.

In the third and final part of this work, different ambiguities concerning various organometallic compounds shall be clarified using DOSY: Aside from several potential catalyst and sensor materials, for which simple characterization as well as identifying ion or solvent interactions are envisioned, especially alkyl *Grignard* systems are in the focus of this section. Here, solution state structures estimated by ECC-DOSY are compared to high-resolution ESI mass spectrometry results from the *Koszinowski* group, who found trimeric species of alkyl *Grignard* compounds which extend the classical *Schlenk* equilibrium.

2 RESULTS AND DISCUSSION

2.1 Improving the External Calibration Curve (ECC)-DOSY-MW Estimation Methodology

The external calibration curve (ECC) methodology was developed in our group^[109a] just recently and has already resulted in a multitude of important characterizations of organometallic molecules in solution using DOSY NMR.^[110-115] Some of the basics of the methodology have been discussed in section 1.2.3.1, however they will be extended in this chapter, if special considerations are required. Herein, measurements were mostly performed at 25 °C and low concentrations (15-25 mM), while the methodology was proven to be resilient towards changes in temperature from -75 °C to 100 °C and concentrations of up to 120 mM in THF^a and toluene.^[109a] However, there are other issues remaining which will be addressed in this chapter, i.e. the limited applicability in only two solvents, the empirical molecule categorization, the theoretical limitations of the ECCs and the MW prediction for molecules incorporating heavier atoms. Furthermore, the ECC methodology shall be made accessible for a wider scope of application by introducing a user-friendly software application.

2.1.1 New External Calibration Curves for Various Solvents^b

One of the major tasks for the improvement of the ECC methodology is the establishment of new calibration curves for different deuterated solvents. Up until now ECCs were available for THF-*d*₈ and toluene-*d*₈ only, however, there are other solvents frequently used in solution state NMR spectroscopy. In this work, the portfolio of ECCs will be extended towards chloroform-*d*₁ (CDCl₃), dichloromethane-*d*₂ (CD₂Cl₂), benzene-*d*₆ (C₆D₆), cyclohexane-*d*₁₂ (C₆D₁₂ or Cycl), dimethylsulfoxide-*d*₆ (DMSO-*d*₆), methanol-*d*₄ (CD₃OD) and acetonitrile-*d*₃ (CD₃CN). To establish new ECCs for these solvents, fixed logarithmic diffusion coefficients of specific internal references ($\log(D_{\text{ref,fix}})$) are needed for the normalization of other diffusion coefficients according to equation (2-1).

$$\log(D_{x,\text{norm}}) = \log(D_x) + (\log(D_{\text{ref,fix}}) - \log(D_{\text{ref}})) \quad (2-1)$$

These fixed diffusion coefficients ($D_{\text{ref,fix}}$) were generated by averaging the results from multiple separate DOSY measurements (at least five). The addition of one of these internal references to an

^a Note that for temperature-dependent measurements, solvent signals should not be used as internal reference. It was shown that at especially lower temperatures deviations of predicted MWs increase.^[109a]

^b Some results of this section have been published separately: S. Bachmann, R. Neufeld, M. Dzemski, D. Stalke, *Chem. Eur. J.* **2016**, *22*, 8462-8465.^[2]

NMR sample together with an analyte x and application of their measured (D_x and D_{ref}) and the fixed diffusion coefficient to equation (2-1) results in normalized diffusion coefficients ($D_{x,norm}$) of the analyte. All normalized diffusion coefficients correlated to the same fixed diffusion coefficient are then mutually comparable and therefore independent of temperature, viscosity and instrument-specific properties. This is especially useful for the comparison of measurements of different samples, as can be underlined by Figure 2-1.

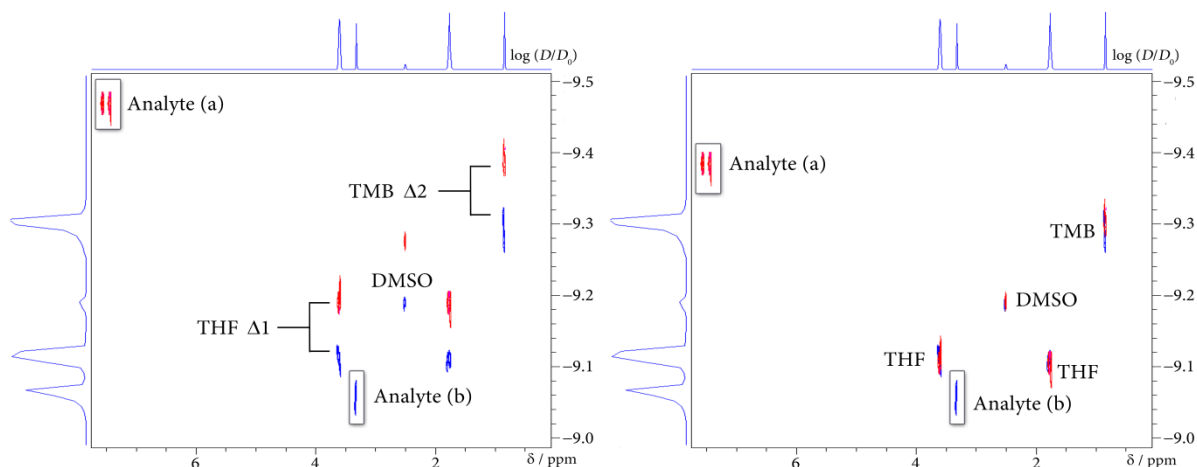


Figure 2-1: Superposition of two ^1H -DOSY NMR spectra of different samples measured at different instruments and temperatures (red and blue). Before normalization, the individual compounds (analyte (a) and (b)) of these samples are not comparable. Absolute diffusion coefficients of the same compounds (THF, TMB) are different, but differ by the same amount ($\Delta 1 = \Delta 2 \neq 0$; left). References can be locked on their fixed diffusion values; all other diffusion coefficients are normalized at the same time. The normalized diffusion coefficients are now mutually comparable. The same compounds (THF, TMB) receive identical values ($\Delta 1 = \Delta 2 = 0$; right). ($D_0 = 1 \text{ m}^2/\text{s}$)

For C_6D_{12} , CDCl_3 , CD_2Cl_2 and C_6D_6 adamantane (Adam) was used as internal reference which produces two signals at about 1.9 and 1.8 ppm. Since Adam was barely soluble in $\text{DMSO}-d_6$, CD_3OD and CD_3CN , 2,2,3,3-tetramethylbutane (TMB) was used instead. TMB produces a single singlet at about 0.85 ppm. Their logarithmic fixed diffusion coefficients are given in Table 2-1.

Table 2-1: $\log(D_{ref,fix})$ of internal references.

Solvent	Internal reference	$\log(D_{ref,fix})$
C_6D_6	Adam	-8.8025
C_6D_{12}	Adam	-9.0204
CD_2Cl_2	Adam	-8.7035
CDCl_3	Adam	-8.8155
CD_3CN	TMB	-8.5464
CD_3OD	TMB	-8.7737
$\text{DMSO}-d_6$	TMB	-9.2963

Several compounds were measured together with these internal references for each solvent and their diffusion coefficients were afterwards normalized according to equation (2-1). This way, these model compounds can be used as internal references themselves ($\log(D_{x,norm}) = \log(D_{ref,fix})$), as long as they are available in the respective normalized system. Hence, tables with normalized diffusion

values of up to 31 model compounds for each solvent are given in the appendix of this work (Table 5-5 (DMSO-*d*₆), Table 5-9 (C₆D₁₂), Table 5-11 (CDCl₃), Table 5-13 (CD₂Cl₂), Table 5-15 (C₆D₆), Table 5-17 (CD₃OD) and Table 5-19 (CD₃CN)). A small selection of these model compounds that can preferably be used as internal references and their respective normalized diffusion coefficients for each solvent are presented in Table 2-2.

Table 2-2: $\log(D_{x,\text{norm}}) = \log(D_{\text{ref,fix}})$ for a selection of model compounds that may be used as internal references.

Solvent	C ₆ D ₆	C ₆ D ₁₂	CDCl ₃	CD ₂ Cl ₂	CD ₃ CN	CD ₃ OD	DMSO- <i>d</i> ₆
Reference	$\log(D_{x,\text{norm}})$	$\log(D_{x,\text{norm}})$	$\log(D_{x,\text{norm}})$	$\log(D_{x,\text{norm}})$	$\log(D_{x,\text{norm}})$	$\log(D_{x,\text{norm}})$	$\log(D_{x,\text{norm}})$
1-PhN	-8.9085	-9.0418	-8.8925	-8.7860	-8.6612	-8.8796	-
DHBP	-8.9793	-9.1570	-8.9745	-8.8623	-8.7428	-8.9766	-9.5168
Adam	-8.8025	-9.0204	-8.8155	-8.7035	-8.5630	-8.8025	-9.3262
Anthracene	-8.8400	-8.9495	-8.8142	-8.6949	-8.5909	-8.8080	-
C₆D₆*	-8.6894	-	-	-	-	-	-
C₆D₁₂*	-	-8.8827	-	-	-	-	-
CDCl₃*	-	-	-8.6580	-	-	-	-
CD₂Cl₂*	-	-	-	-8.4982	-	-	-
CD₃CN*	-	-	-	-	-8.3784	-	-
CD₃OD*	-	-	-	-	-	-8.6926	-
Cyclopentane	-8.6276	-8.8091	-8.6510	-8.5514	-8.4072	-8.6247	-9.1238
DPA	-8.8749	-8.9949	-8.8589	-8.7536	-8.6259	-8.8541	-9.3869
DMSO-<i>d</i>₆*	-	-	-	-	-	-	-9.1787
Indene	-8.7533	-8.8679	-8.7482	-8.6462	-8.5183	-8.7204	-9.2429
Naphthalene	-8.7650	-8.8697	-8.7453	-8.6439	-8.5290	-8.7382	-9.2609
Pyrene	-8.8698	-8.9830	-8.8431	-8.7386	-8.6302	-8.8571	-9.3876
Si(SiMe₃)₄	-8.9698	-9.1839	-8.9689	-8.8717	-8.7317	-9.0128	-9.5058
TPhN	-9.1408	-9.3471	-9.1166	-9.0069	-8.8750	-9.1068	-9.6772
TMB	-8.7771	-8.9783	-8.7889	-8.6789	-8.5464	-8.7737	-9.2963
TMS	-8.7144	-8.8781	-8.7237	-8.6252	-8.4916	-8.7222	-9.2037
Toluene	-8.6900	-8.7966	-8.6864	-8.5687	-8.4630	-8.6650	-9.1423
*residual solvent signal							

Residual solvent signals are also included in Table 2-2. Still, for these solvents as well as for any other compound that is to be used as internal reference, it must be kept in mind that they should not interact with other solutes or cause signal overlap in the final spectrum, as that can influence the results which leads to the wrong conclusions.

2.1.1.1 Merged External Calibration Curves

After the normalization process, *Williard's* approach^[106a] (see section 1.2.3.1 for a short summary) of plotting logarithmic diffusion coefficients ($\log(D_{x,\text{norm}})$) against logarithmic molecular weights ($\log(MW_{\text{calc}})$) can be employed to receive a linear dependence. A linear fit (calibration curve) provides the parameters $\log(K)$ (intercept) and $-\alpha$ (slope) which can afterwards be used in formulae (2-2) and (2-3) to estimate MWs (MW_{det}).

$$\log(D_{x,\text{norm}}) = \log(K) - \alpha \cdot \log(MW_{\text{det}}) \quad (2-2)$$

$$\Rightarrow MW_{\text{det}} = 10^{\left(\frac{-\log(D_{x,\text{norm}}) + \log(K)}{\alpha}\right)} \quad (2-3)$$

In this work, the normalized diffusion values of model compounds are obtained from many separate measurements with only one internal reference, as mentioned before. Therefore, the corresponding calibration curves are called external calibration curves (ECCs), in contrast to the internal calibration curves (ICCs) of *Williard* who measured all references and analytes at the same time. This makes a wider range of model compounds accessible (e.g. concerning *MW* distribution). In this work, small molecules with *MW*s ranging from 70 to 600 g/mol were used. *MW*s of analytes with diffusion coefficients corresponding to *MW*s inside the given appropriate range can safely be predicted.^a If these ECCs incorporate all measured model compounds without any discrimination, they are called “merged” calibration curves (two examples are shown in Figure 2-2; the complete set of merged ECCs for all solvents is given in the appendix: Figure 5-1 (DMSO); Figure 5-2 (C₆D₁₂); Figure 5-3 (CDCl₃); Figure 5-4 (CD₂Cl₂); Figure 5-5 (C₆D₆); Figure 5-6 (CD₃OD) and Figure 5-7 (CD₃CN)).

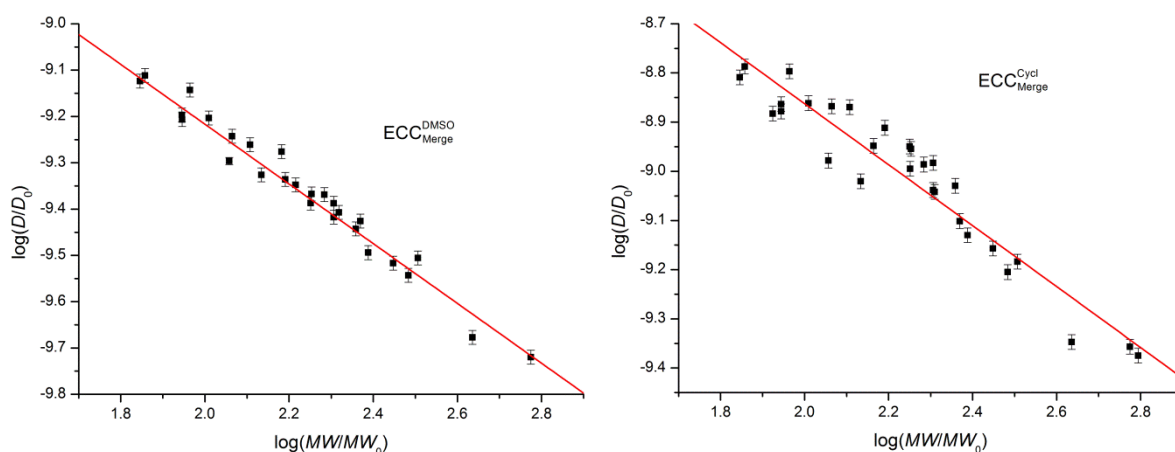


Figure 2-2: Merged ECCs for DMSO-*d*₆ and cyclohexane-*d*₁₂ (Cycl). For some solvents (e.g. DMSO) the deviations are rather small, while in other cases (e.g. Cycl) some molecules deviate heavily. ($D_0 = 1 \text{ m}^2/\text{s}$; $MW_0 = 1 \text{ g/mol}$)

The ECC parameters ($\log(K)$, $-\alpha$ and their errors) of these merged ECCs are given in Table 2-3 for all solvents. In the original publication,^[109a] the approach towards merged ECCs was different (see comments in section 2.1.1.2) which required the repetition with normalized diffusion coefficients given in literature.^[109a] The resulting ECC parameters for THF-*d*₈ and toluene-*d*₈ have also been listed in Table 2-3. At this point it should be noted that three significant digits were used for the ECC parameters as more would overstate the accuracy of the method. This is why some of the estimated *MW*s of organometallic compounds that are discussed in the following chapters are differing slightly from literature.^[2-3, 109a] To estimate the suitability of ECCs for *MW* predictions, *MW*s were back-calculated for all model compounds (MW_{det}) and compared with their true molecular weights (MW_{calc}). Av. and maximum (max.) deviations (dev.; MW_{dif}) of these estimated *MW*s are also listed in Table 2-3. These deviations were calculated with equation (2-4).^{[2, 109a], b}

^a The corresponding diffusion coefficient range is different for each solvent.

^b The formula $MW_{\text{dif}} = \left(1 - \frac{MW_{\text{det}}}{MW_{\text{calc}}}\right)$ used in literature^[2, 109] leads to different deviations, if an estimated MW_{det} is lighter or heavier by the same amount than MW_{calc} , since MW_{dif} is calculated relative to 1.

$$MW_{\text{dif}} = \left(\frac{MW_{\text{calc}} - MW_{\text{det}}}{MW_{\text{det}}} \right) \cdot 100\% \quad (2-4)$$

Table 2-3: ECC parameters and their errors, av. and max. deviations of back-calculated MW s and cor. R^2 values of merged calibration curves for all solvents available for the ECC method.

Solvent	$\log(K)$	$\Delta\log(K)$	$-\alpha$	$\Delta\alpha$	av. dev.	max. dev.	cor. R^2
DMSO- d_6	-7.93	0.0535	-0.644	0.0241	$\pm 7\%$	$\pm 20\%$	0.96
C_6D_{12}	-7.62	0.0831	-0.620	0.0369	$\pm 15\%$	$\pm 29\%$	0.91
$CDCl_3$	-7.67	0.0537	-0.532	0.0239	$\pm 11\%$	$\pm 26\%$	0.94
CD_2Cl_2	-7.55	0.0487	-0.535	0.0215	$\pm 10\%$	$\pm 23\%$	0.96
C_6D_6	-7.58	0.0380	-0.572	0.0172	$\pm 8\%$	$\pm 20\%$	0.97
CD_3OD	-7.51	0.0555	-0.600	0.0247	$\pm 9\%$	$\pm 22\%$	0.96
CD_3CN	-7.38	0.0456	-0.553	0.0204	$\pm 8\%$	$\pm 19\%$	0.96
THF- d_8	-7.60	0.0407	-0.553	0.0180	$\pm 7\%$	$\pm 18\%$	0.97
Toluene- d_8	-7.59	0.0389	-0.579	0.0172	$\pm 7\%$	$\pm 18\%$	0.98

Merged ECCs produce av. deviations of 7-15% and max. deviations of 18-29%. This is impressive, since all model compounds were considered and no structural differentiation has been done *a priori*.^a This accuracy enables the verification or falsification of a wide range of aggregates, e.g. a monomeric aggregate can easily be distinguished from dimeric aggregates (this is usually the case, since massive co-aggregation of solvent molecules (solvation) would be necessary to close the MW gap). Additionally, correlated (cor.) R^2 values which indicate how good the variation of the points is explained by the fit are given for all merged ECCs. The closer cor. R^2 values are to 1, the better the fit. The cor. R^2 values fit in most cases the tendencies of deviations of back-calculated MW s for the different ECCs.

The normalization process for the preparation of the ECCs is similar to the method used by *Harris et al.*^[104] (a short summary of their method can be found in section 1.2.3.1) who employed relative diffusivities ($D_{\text{ref,rel}}$). For the ECC methodology, the relative diffusivities are referenced to fixed diffusion coefficients ($D_{\text{ref,fix}}$) of internal references as shown in equation (2-5).

$$\Rightarrow D_{x,\text{norm}} = \frac{D_x}{D_{\text{ref}}} \cdot D_{\text{ref,fix}} = \frac{1}{D_{\text{ref,rel}}} \cdot D_{\text{ref,fix}} \quad (2-5)$$

Harris et al.^[104] reported similar relative error limits (11% av. dev. and 35% max. dev.; MW distribution of 2 to 1280 g/mol) compared to the merged ECCs which indicates that this normalization is conclusive and transferable. Unfortunately, *Harris et al.* did not explicitly list their used references or individual diffusion coefficients which hampers the direct comparison between their calibration curve in $CDCl_3$ and the merged ECC of this work. However, *Harris et al.*^[104] plotted $\log(D_{\text{ref,rel}})$ vs. $\log(MW_{\text{calc}})$ which was fitted linearly. This could be repeated with diffusion coefficients measured herein for $CDCl_3$ (see Figure 2-3).

^a Model compounds with elevated molar *van-der-Waals* density were excluded (MD_w ; will be explained in section 2.1.4). Note that $Si(OMe)_4$ was removed for this reason and therefore resulting ECCs and conclusions thereof may differ compared to reference [2] (for further information see at the end of section 2.1.1.2).

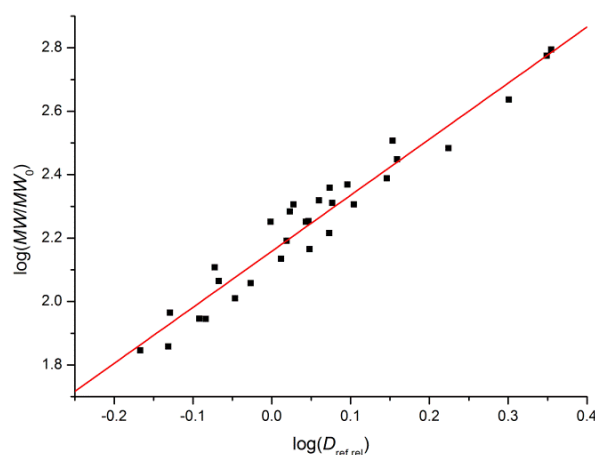


Figure 2-3: Plot of $\log(D_{\text{ref,rel}})$ vs. $\log(MW_{\text{calc}})$ of measurements in CDCl_3 . The cor. R^2 (0.94) value remains identical in comparison to the conventional plot. ($MW_0 = 1 \text{ g/mol}$)

The linear fit parameters of the plot with the data of this work (slope: 1.77; intercept: 2.16) differ slightly compared to those reported by *Harris et al.*^[104] (slope: 1.72; intercept: 1.93). This is probably due to the different pool of substances utilized by *Harris et al.* compared to this work. Since the compounds were not given by *Harris et al.*,^[104] this could not be investigated.

The usefulness of the normalization process and advantage of the introduction of a standardized system can be further illustrated by the following example. *Wang and Pedersen et al.*^[113] investigated glycosylation intermediates incorporating fluorinated counter ions that are soluble in dichloromethane (CD_2Cl_2). These are a result of the use of fluorinated catalysts, e.g. $[\text{BF}_3 \cdot \text{Et}_2\text{O}]$ or $[\text{TMSOTf}]$. They decided to prepare their own ECCs, to account for specific features of these compounds. One model compound *Wang and Pedersen et al.* used was diethylether (Et_2O). To enable cross-referencing, Et_2O ($\log(D_{\text{x,norm}}) = -8.5724$) was also measured for this work and normalized according to equation (2-1) in CD_2Cl_2 . This way, all normalized diffusion coefficients of *Wang and Pedersen et al.* (see Supporting Information of reference^[113]) could be converted to the herein used internal standard by repeatedly applying formula (2-1) (A complete list of all diffusion coefficients is given in the appendix: Table 5-25). Figure 2-4 depicts the resulting ECC of *Wang and Pedersen et al.* converted into the herein used system (red) together with the merged ECC in CD_2Cl_2 (black) for comparison. It is immediately obvious that these two shown calibration curves cannot simply be combined. Their slopes are substantially different: $-\alpha(\text{ECC}_{\text{merge}}) = -0.535$; $-\alpha(\text{ECC}_{\text{Wang/Pedersen}}) = -0.220$.

This could be due to the used references of *Wang and Pedersen et al.*, however, after careful evaluation this assumption can be dismissed: While Et_2O (marked in Figure 2-4) would be in a reasonable region for the herein presented merged ECC, the other references that were meant to resemble their investigated aggregates exhibit irregularities. These molecules display mainly an increasingly elevated molar *van-der-Waals* density (MD_W ; **A-C** shown in Scheme 2-1) which rises continuously along their calibration curve (for 5 of the 6 molecules; see Table 5-25) and effectively

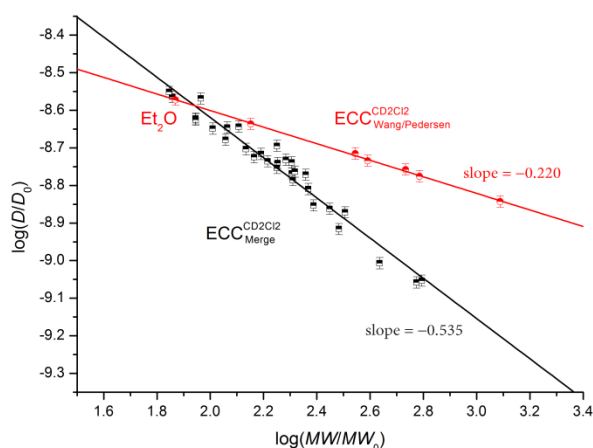
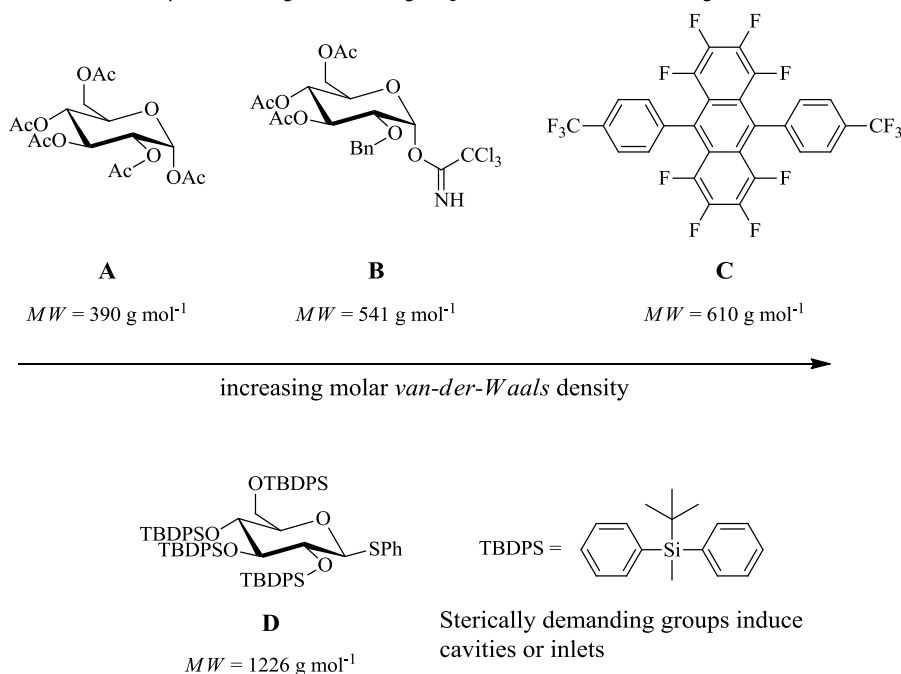


Figure 2-4: Merged ECC for CD_2Cl_2 (black) and ECC of Wang and Pedersen *et al.*^[113] (red) converted into the herein used normalized system. Wang and Pedersen *et al.* used references that produce irregularities, i.e. due to increasing molar *van-der-Waals*-densities or sterically demanding functional groups. ($D_0 = 1 \text{ m}^2/\text{s}$; $MW_0 = 1 \text{ g/mol}$)



Scheme 2-1: Selection of utilized references of Wang and Pedersen *et al.*^[113] References A-C show increasing levels of *van-der-Waals* densities, whereas the substituents of reference D induce substantial inlets and cavities.

induces underestimation of MW s which would explain their raised diffusion coefficients (MD_W will be discussed in more detail in section 2.1.4). However, their last utilized reference (D shown in Scheme 2-1) has no elevated *van-der-Waals* density and even possesses enormous cavities and inlets, induced by sterically demanding substituents which would more likely have an opposite effect and lead to an overestimation of MW s. Even without this reference, their slope ($-\alpha(\text{ECC}_{\text{Wang/Pedersen}}) = -0.220$) does not fit the assumption for a Flory-coefficient ($0.33 \leq \alpha \leq 1$). Hence, it is probable that there has been an error in their measurement, e.g. due to convection.^a While it is unfortunate that these ECCs cannot be combined, it could be made apparent that the normalization process can help detect irregularities.

^a Wang and Pedersen *et al.*^[113] utilized the pulse sequence ledbpgp2s and measured at $-55 \text{ }^\circ\text{C}$.

2.1.1.2 Shape-Optimized External Calibration Curves

The shape dependency of D is also the main reason for the elevated max. deviations of merged ECCs. These result mostly from individual model compounds with distinct molecular shapes. Alas, theoretical calculations of diffusion coefficients are currently not precise enough to complement experimental findings (at least for small molecules).^[116] Advanced theoretical means achieved by rising computational power may in the future make shape-related discrepancies predictable.

Such geometry-related effects on diffusion experiments were already acknowledged with the correctional factor (f_s) of Perrin^[97] for Stokes-Einstein approaches (see section 1.2.3.1), however neither by Harris nor by Williard for their power-law based methods. Therefore, to further improve the accuracy of ECCs, the pool of model compounds was semi-empirically divided into one of the following categories of molecular shapes: Compact spheres (CS), dissipated spheres and ellipsoids (DSE) and expanded discs (ED).^[109a] Compact spherical molecules are highly symmetric (e.g. T_d , O_h) and densely packed (e.g. tetramethylsilane (TMS) or Adam). However, most model compounds are not ideally spherical, but rather ellipsoidal (e.g. tetramethoxypropane or diphenylsulfoxide (DPS)) or incorporate small cavities/inlets or dative bonds. These are grouped in the DSE category. Moreover, small aromatic molecules like toluene are included, since expanded discs do not seem to behave significantly different before $MWs > 170$ g/mol. Above 170 g/mol, larger expanded discs may also be differentiated (e.g. anthracene or pyrene). A complete list of all model compounds and their individual categorization is given in the appendix (Table 5-1).^b

Shape-optimized ECCs (using the given procedure) were then created after this geometrical categorization (see Figure 2-5).

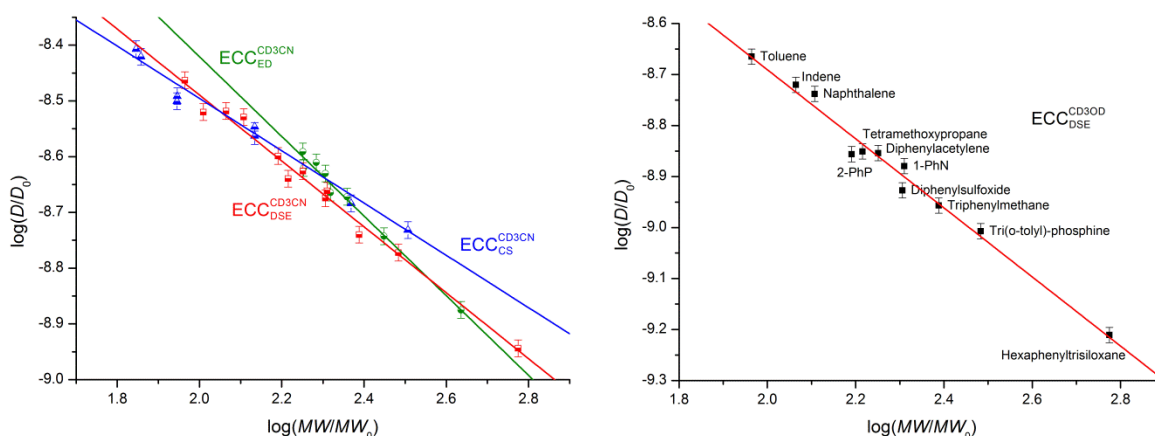


Figure 2-5: Shape-optimized ECCs: Semi-empirical differentiation of molecular shapes leads to three distinct categories: Compact spheres (CS), dissipated spheres and ellipsoids (DSE) and expanded discs (ED). Such categorization is shown for CD_3CN (left). The individual shape-optimized ECCs show increased accuracy compared to raw merged ECCs, e.g. shape-optimized ECC for DSE molecules in CD_3OD (right). ($D_0 = 1 \text{ m}^2/\text{s}$; $MW_0 = 1 \text{ g/mol}$)

^a A fourth molecular shape will be introduced and discussed in section 2.3.1.

^b There are some borderline molecules, but there are also clear systematic trends.

The complete set of shape-optimized ECCs for all solvents is given in the appendix (Figure 5-1 (DMSO); Figure 5-2 (C_6D_{12}); Figure 5-3 ($CDCl_3$); Figure 5-4 (CD_2Cl_2); Figure 5-5 (C_6D_6); Figure 5-6 (CD_3OD) and Figure 5-7 (CD_3CN)). For most organometallic molecules, the calibration curves for dissipated spheres and ellipsoids (DSE) have been proven to be the best choice for *MW* estimation.^[109-112] Further calibration curves (CS, ED) are suited to discuss molecules with well-defined shapes.

This categorization led to an immense increase in accuracy of back-calculated *MWs* of the model compounds. However, for shape-optimized ECCs to be applied, the molecular shape of an analyte needs to be known *a priori*. This is usually a delicate situation and in some cases, where it is not possible to conclude the “right” molecular shape, universal merged ECCs should instead be utilized. In the original work,^[109a] such merged ECCs were obtained by averaging the ECC parameters of the three shape-optimized ECCs to equally weigh the shapes. However, it is most probably not suitable, since the shape-optimized ECCs may be biased, e.g. through the categorization of borderline molecules (other approaches towards categorization are discussed in section 2.1.2). Therefore, merged ECCs reported in this work were simply obtained by utilizing all model compounds and weighing them evenly, as explained before. However, if any evidence towards the constitution of an aggregate in solution exists or a reasonable guess can be made, shape-optimized ECCs are still useful.

For C_6D_6 , $CDCl_3$, CD_2Cl_2 , CD_3CN and CD_3OD calibration curves for the three molecular shapes (ED, CS, and DSE) could be assembled. Their ECC parameters as well as av. and max. deviations and cor. R^2 values are given in Table 2-4. Furthermore, av. and max. deviations recalculated *via* equation (2-4) and errors of the ECC parameters are listed for THF- d_8 and toluene- d_8 , as these were not listed in the original publication.^[109a] Additionally, the same information is given in Table 2-4 for the ED and DSE calibration curves of DMSO- d_6 and cyclohexane- d_{12} (problems with the CS calibration curves are discussed later).

The av. deviations of these ECCs vary between 1 and 10%, while max. deviations stray substantially more (3 to 22%). A realistic av. deviation of about 5% can be proposed for these ECCs; anything better should be viewed skeptically. Still, these error limits mark a substantial improvement (around 5 to 15%) compared to the merged ECCs. The very pronounced max. deviations are still caused by some specific borderline molecules in many of the ECCs: Naphthalene and toluene diffuse a little faster than anticipated for the DSE shape which could be due to their planarity, like for most ED molecules. However, they are essentially too small to be considered for the ED shape, as they would produce even more elevated deviations for the ED ECCs. Also, some oxygen-containing molecules like diisopropylether and tetramethoxypropane tend to diffuse slower than expected; maybe some intermolecular interactions (e.g. with the solvent) cause this behavior. This however, could not be confirmed, yet.

Table 2-4: ECC parameters and their errors, av. and max. deviations of back-calculated MWs and cor. R^2 values of shape-optimized calibration curves (CS, DSE and ED) for $CDCl_3$, CD_2Cl_2 , C_6D_6 , CD_3OD , CD_3CN , THF- d_8 and toluene- d_8 . The same information is given for shape-optimized calibration curves (DSE and ED) for DMSO- d_6 and C_6D_{12} .

	$\log(K)$	$\Delta\log(K)$	$-\alpha$	$\Delta\alpha$	av. dev.	max. dev.	cor. R^2
Solvent: $CDCl_3$							
CS	-7.84	0.0487	-0.457	0.0231	$\pm 6\%$	$\pm 18\%$	0.98
DSE	-7.59	0.0694	-0.572	0.0302	$\pm 10\%$	$\pm 22\%$	0.97
ED	-7.13	0.133	-0.753	0.0565	$\pm 4\%$	$\pm 10\%$	0.96
Solvent: CD_2Cl_2							
CS	-7.70	0.0354	-0.469	0.0169	$\pm 4\%$	$\pm 7\%$	0.99
DSE	-7.46	0.0484	-0.577	0.0210	$\pm 5\%$	$\pm 14\%$	0.98
ED	-6.98	0.113	-0.767	0.0480	$\pm 3\%$	$\pm 9\%$	0.97
Solvent: C_6D_6							
CS	-7.75	0.0545	-0.494	0.0260	$\pm 7\%$	$\pm 17\%$	0.98
DSE	-7.47	0.0284	-0.622	0.0124	$\pm 3\%$	$\pm 8\%$	0.99
ED	-7.06	0.0861	-0.787	0.0365	$\pm 3\%$	$\pm 6\%$	0.99
Solvent: CD_3OD							
CS	-7.64	0.0809	-0.539	0.0383	$\pm 5\%$	$\pm 13\%$	0.96
DSE	-7.34	0.0677	-0.677	0.0296	$\pm 5\%$	$\pm 11\%$	0.98
ED	-7.08	0.0530	-0.773	0.0223	$\pm 2\%$	$\pm 3\%$	1.00
Solvent: CD_3CN							
CS	-7.55	0.0677	-0.469	0.0320	$\pm 9\%$	$\pm 17\%$	0.97
DSE	-7.31	0.0491	-0.591	0.0217	$\pm 4\%$	$\pm 13\%$	0.99
ED	-6.99	0.0871	-0.714	0.0369	$\pm 3\%$	$\pm 7\%$	0.98
Solvent: THF-d_8							
CS	-7.74	0.0397	-0.494	0.0187	$\pm 2\%$	$\pm 4\%$	0.99
DSE	-7.54	0.0285	-0.582	0.0124	$\pm 4\%$	$\pm 8\%$	0.99
ED	-7.12	0.0449	-0.752	0.0191	$\pm 1\%$	$\pm 3\%$	1.00
Solvent: Toluene-d_8							
CS	-7.76	0.0469	-0.502	0.0224	$\pm 6\%$	$\pm 10\%$	0.99
DSE	-7.51	0.0246	-0.613	0.0106	$\pm 3\%$	$\pm 7\%$	1.00
ED	-7.10	0.0717	-0.784	0.0306	$\pm 2\%$	$\pm 4\%$	0.99
Solvent: DMSO-d_6							
DSE	-7.78	0.0487	-0.709	0.0215	$\pm 3\%$	$\pm 10\%$	0.99
ED	-7.45	0.0660	-0.846	0.0278	$\pm 2\%$	$\pm 4\%$	0.99
Solvent: C_6D_{12}							
DSE	-7.41	0.0643	-0.707	0.0279	$\pm 5\%$	$\pm 17\%$	0.98
ED	-6.59	0.109	-1.04	0.0461	$\pm 1\%$	$\pm 5\%$	0.99

It was already explained that the slope ($-\alpha$) is a measure of molecular compactness, which is also reflected in the shape-optimized ECCs. The ECCs for CS compounds have comparably the lowest α values, while they increase over DSE to ED as the molecules get more two-dimensional.

The parameters for shape-optimized calibration curves of CS compounds of DMSO- d_6 and cyclohexane- d_{12} are deliberately left out, since these ECCs displayed atypical deviations. Linear fitting of the CS-type references resulted in a significantly reduced quality of the fit (cor. $R^2 = 0.88$

for C_6D_{12} and cor. $R^2 = 0.92$ for DMSO- d_6). To exclude aggregation phenomena, two CS references, $Si(SiMe_3)_4$ and TMS, were measured at different concentrations which resulted in almost identical diffusion coefficients (e.g. $\log(D_{x,norm})(Si(SiMe_3)_4, 2.9 \text{ mM}) = -9.4867$, $\log(D_{x,norm})(Si(SiMe_3)_4, 17.5 \text{ mM}) = -9.4921$, $\Delta\log(D_{x,norm})(Si(SiMe_3)_4, 2.9 \text{ mM}/17.5 \text{ mM}) = 0.0054$). More likely, the polarity of the solvents causes these deviations in diffusion (note that cyclohexane has no dipole moment, whereas DMSO adopts $3.96 \text{ D}^{[117]}$). Still, grouping polar (e.g. THF $1.75 \text{ D}^{[117]}$, $N(SiMe_3)_3$ $0.51 \text{ D}^{[118]}$) and nonpolar (e.g. TMB, TMS) compact spheres together did not result in a classification, in which all references fitted the corresponding ECCs. Furthermore, the slope of these ECCs should be inverted for DMSO and cyclohexane, if polarity was the only responsible property. Measurements have also been performed in dry DMSO to exclude interactions with water. This also did not alter the findings significantly.

In a separate publication,^[2] we divided CS compounds into purely hydrocarbon (PCS; e.g. TMB, Adam) and non-hydrocarbon (NCS; e.g. MTBE, $Si(SiMe_3)_4$) compounds which resulted in a clear increase in accuracy (see reference [2] for deviations, normalized diffusion coefficients and plots). However, different effects of hydrocarbon and non-hydrocarbon compounds on diffusion are questionable and this problem was therefore investigated in more detail since publication: Both solvents in question display an increased viscosity (DMSO: $2.24 \text{ mPa} \cdot \text{s}$; cyclohexane: $1.0 \text{ mPa} \cdot \text{s}$ (at $20 \text{ }^\circ\text{C}$))^[119] compared to other solvents (e.g. chloroform: $0.57 \text{ mPa} \cdot \text{s}$; methanol: $0.59 \text{ mPa} \cdot \text{s}$ (at $20 \text{ }^\circ\text{C}$)).^[119] This can be further underlined by comparison of absolute diffusion coefficients (before normalization; the complete list of diffusion coefficients for all references and solvents is given in the appendix: Table 5-3) which were significantly lower for DMSO and cyclohexane within the defined measurement setup than for other solvents. Hence, to investigate, if changes in viscosity were the cause for the aberrant behavior of CS compounds in these solvents, temperature-dependent measurements were performed exemplary for DMSO- d_6 .^a Upon heating, the normalized diffusion coefficients did not change significantly (see Figure 2-6 (left); the complete set of data for the measurements at different temperatures in DMSO is given in the appendix: Table 5-6; cooling was not an option ($mp(\text{DMSO-}d_6) = 20.2 \text{ }^\circ\text{C}$; $mp(C_6D_{12}) = 7 \text{ }^\circ\text{C}$)^[78]). The logarithmic diffusion coefficients stayed mostly within the assumed error interval (0.015; see section 2.1.3). With this data, calibration curves were obtained for all investigated temperatures ($25 \text{ }^\circ\text{C}$, $30 \text{ }^\circ\text{C}$, $40 \text{ }^\circ\text{C}$, $50 \text{ }^\circ\text{C}$ and $60 \text{ }^\circ\text{C}$; the complete set of parameters for these ECCs is given in the appendix: Table 5-7). As shown in Figure 2-6 (right), cor. R^2 values vary slightly, but independent of temperature changes which was generally presumed for ECCs and can therefore be confirmed (note that TMB was excluded for these ECCs, as it was used as internal reference). While it cannot be dismissed that viscosity plays a role in the determination of diffusion coefficients, it obviously does not explain the elevated deviations in this case.

^aNote that DMSO was used without being dried beforehand and therefore will accommodate varying quantities of water, which could potentially slightly alter the overall viscosities.

Finally, a closer look at the utilized references revealed a problem: A single reference ($\text{Si}(\text{OMe})_4$) displayed an increased *van-der-Waals* density (further illustrated in section 2.1.4). After removal of

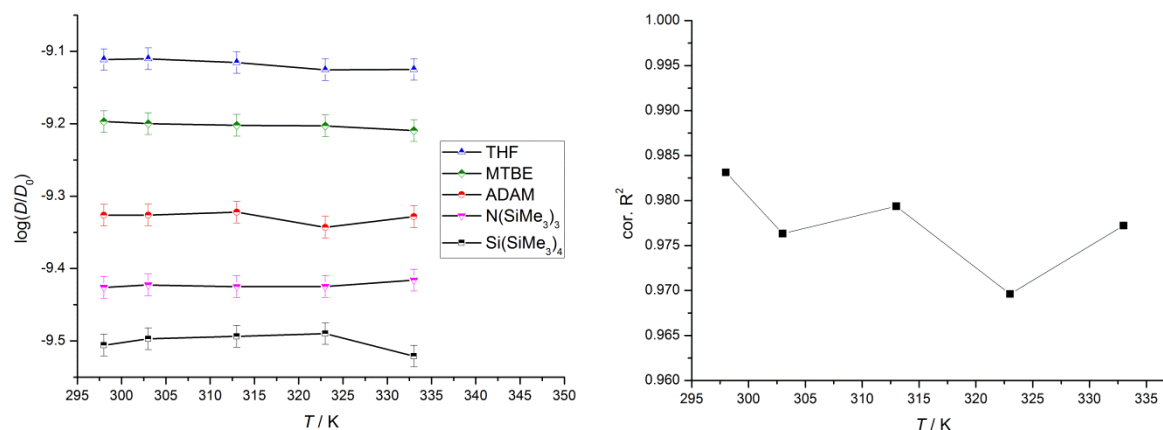


Figure 2-6: Temperature dependence of normalized diffusion coefficients of a selection of CS model compounds in $\text{DMSO-}d_6$ (left; 25 °C to 60 °C). Most diffusion coefficients only deviate within the assumed error interval. $\text{Cor. } R^2$ values of the corresponding ECCs vary independently of temperature (right). ($D_0 = 1 \text{ m}^2/\text{s}$)

this reference,^a the linear fits of compact spherical compounds in $\text{DMSO-}d_6$ and cyclohexane- d_{12} displayed substantially improved accuracies and $\text{cor. } R^2$ values (see Table 2-5). While it should be mentioned that the fit qualities are still a little worse compared to other solvents, the need to differentiate between PCS and NCS compounds in DMSO and cyclohexane has essentially been negated.

Table 2-5: ECC parameters and their errors, av. and max. deviations of back-calculated MW s and $\text{cor. } R^2$ values of shape-optimized calibration curves (CS) for $\text{DMSO-}d_6$ and C_6D_{12} .

	$\log(K)$	$\Delta\log(K)$	$-\alpha$	$\Delta\alpha$	av. dev.	max. dev.	$\text{cor. } R^2$
Solvent: $\text{DMSO-}d_6$							
CS	-8.09	0.106	-0.572	0.0508	$\pm 8\%$	$\pm 18\%$	0.95
Solvent: C_6D_{12}							
CS	-7.76	0.0877	-0.572	0.0422	$\pm 8\%$	$\pm 15\%$	0.96

In conclusion, the empirical categorization in terms of molecular shapes should be applied with caution. Even though accuracies increase and the correlation between shape and diffusion coefficient is scientifically valid; the categorization itself as well as conclusions thereof can in some cases be prone to bias. It was demonstrated that even a single unsuited reference can alter the findings significantly. Hence, an increase in reference count may help avert this problem in the future, while other approaches towards categorization may also improve the entire methodology and enable prevention of unnecessary bias.

^a Resulting from its increased *van-der-Waals* density, $\text{Si}(\text{OMe})_4$ was removed from all ECCs herein.

2.1.2 Molecule Categorization

The categorization of model compounds has been a huge improvement of the ECC methodology (see section 2.1.1.2). Still, as already mentioned, this categorization process lacks clear criteria and includes bias. A misplaced or unsuited reference may have negative consequences, as illustrated in the previous section. Hence, to optimize this categorization process, parameters need to be utilized that are accessible theoretically or experimentally and furthermore related to the individual molecular shape. There are many possibilities for such shape-related parameters, i.e. molecular sizes and relations obtained from crystal structure analysis or theoretical calculations.^a

In this thesis, the approach of calculating principal moments of inertia (I_{xx} , I_{yy} , I_{zz}) of the different model compounds was pursued. Since diffusion experiments were performed in isotropic environments, the molecules can rotate freely (molecular tumbling). This rotation is largely determined by the mass and size of the particle as well as its interactions with the solvent.^b Hence, principle moments of inertia should be able to express these criteria and delimit molecular shapes. For example, toluene is flat but comparably small (and light) and can therefore rotate faster than larger, similarly flat compounds. It was previously categorized as DSE instead of ED which might therefore be recognizable utilizing principal moments of inertia. The principal moments of inertia are the elements of the principal inertia matrix (\mathbf{I}) (2-6), for which $0 \neq I_{xx} \leq I_{yy} \leq I_{zz}$ applies.

$$\mathbf{I} = \begin{bmatrix} I_{xx} & 0 & 0 \\ 0 & I_{yy} & 0 \\ 0 & 0 & I_{zz} \end{bmatrix} \quad (2-6)$$

The matrix elements can also be used to calculate the relative shape anisotropy κ^2 , as shown in formula (2-7):^[121]

$$\kappa^2 = 1 - \frac{3(I_{xx}I_{yy} + I_{xx}I_{zz} + I_{yy}I_{zz})}{(I_{xx} + I_{yy} + I_{zz})^2} \quad (2-7)$$

This relative shape anisotropy κ^2 is always between zero and one. If it is zero, all points are spherically symmetrically distributed and if it is one, they are all located on a line. Hence, this is a good parameter to discuss molecular shapes, especially to differentiate linear from spherical molecules.

Principal moments of inertia were calculated for all model compounds utilizing the program PMIFST^[122] with force-field (MMFF94) optimized structures (see Figure 2-7) which produce reasonably good geometries to give a proof of concept.

^a Nowadays, very elaborate parameters can be calculated, e.g. by employing spherical harmonics.^[120]

^b For high concentrations, even solute-solute interactions may have to be considered.

From these principal moments, relative shape anisotropies κ^2 were calculated according to equation (2-7). The complete set of principal moments of inertia as well as their relations and shape anisotropies are given in the appendix (see Table 5-2). In Table 2-6 a limited selection is shown.

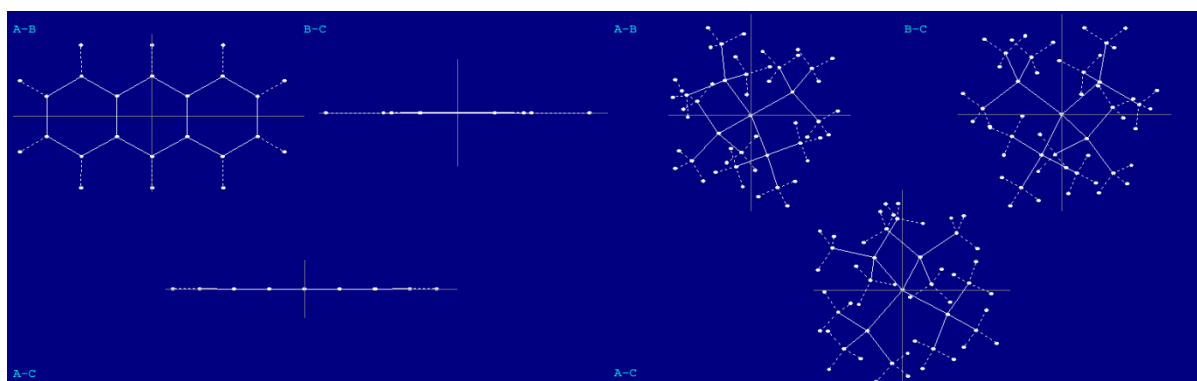


Figure 2-7: Principal axes defined by PMIFST for the calculation of principal moments of inertia of anthracene (left) and $\text{Si}(\text{SiMe}_3)_4$ (right).

Table 2-6: Principal moments of inertia calculated with PMIFST^[122] for geometry optimized (MMFF94) structures of model compounds used in ECCs. The relative shape anisotropy κ^2 is also listed for each model compound.

Compound	I_{xx} [$\text{u}\text{\AA}^2$]	I_{yy} [$\text{u}\text{\AA}^2$]	I_{zz} [$\text{u}\text{\AA}^2$]	$\sim I_{xx} : I_{yy} : I_{zz}$	$\kappa^2 \cdot 100\%$
1,3-Indanedione	301	408	707	1 : 1 : 2	6.6
2-PhP	173	905	1053	1 : 5 : 6	14.7
9-MA	356	1133	1485	1 : 3 : 4	11.3
Anthracene	230	1113	1343	1 : 5 : 6	14.4
Benzene	89	89	177	1 : 1 : 2	6.1
DHBP	1146	1890	2716	1 : 2 : 2	5.6
Cyclopentane	76	76	132	1 : 1 : 3	3.9
DPS	426	1217	1425	1 : 3 : 3	8.9
Hexaphenyltrisiloxane	6123	7683	8920	1 : 1 : 1	1.1
<i>i</i>Pr₂O	122	326	370	1 : 3 : 3	7.9
Naphthalene	160	409	568	1 : 3 : 4	9.8
N(SiMe₃)₃	893	893	1311	1 : 1 : 1	1.8
Pyrene	490	904	1394	1 : 2 : 3	7.9
Si(SiMe₃)₄	1914	1914	1914	1 : 1 : 1	0
TPhN	2876	4349	6524	1 : 2 : 2	5.4
THF	70	72	126	1 : 1 : 2	4.2
TMB	219	510	515	1 : 2 : 2	5.6
TMS	162	162	162	1 : 1 : 1	0
Toluene	92	199	288	1 : 2 : 3	8.6
Triphenylene	990	990	1980	1 : 1 : 2	6.3

Two attempts were made to categorize the model compounds utilizing the calculated data: First, model compounds were grouped together that exhibited similar ratios of their principal moments of inertia ($I_{xx} : I_{yy} : I_{zz}$) which resulted in three categories: Molecules with the same or similar principal moments for all directions ($I_{xx} \approx I_{yy} \approx I_{zz}$) and molecules with the same or similar principal moments for two directions ($I_{xx} < I_{yy} \approx I_{zz}$ and $I_{xx} \approx I_{yy} < I_{zz}$). Some model compounds fit the expectations, e.g. TMS and $\text{Si}(\text{SiMe}_3)_4$ display $I_{xx} \approx I_{yy} \approx I_{zz}$ and are therefore to be classified as spherical. Others may not be as easily classifiable with this approach, e.g. hexamethyldisilazane which also has similar principal moments in all three dimensions, but was previously assumed to be a dissipated sphere. Additionally, these molecules were categorized depending on their relative

shape anisotropies ($\kappa^2 \cdot 100\%$) which were differentiated once again into three categories: Molecules displaying anisotropies of 0-5%, 5-10% and more than 10%. While these shape anisotropies are helpful in differentiating linear from spherical compounds, the minute differences of the model compounds herein were not as easily distinguishable utilizing this parameter. The findings are presented exemplarily for benzene- d_6 in Figure 2-8.

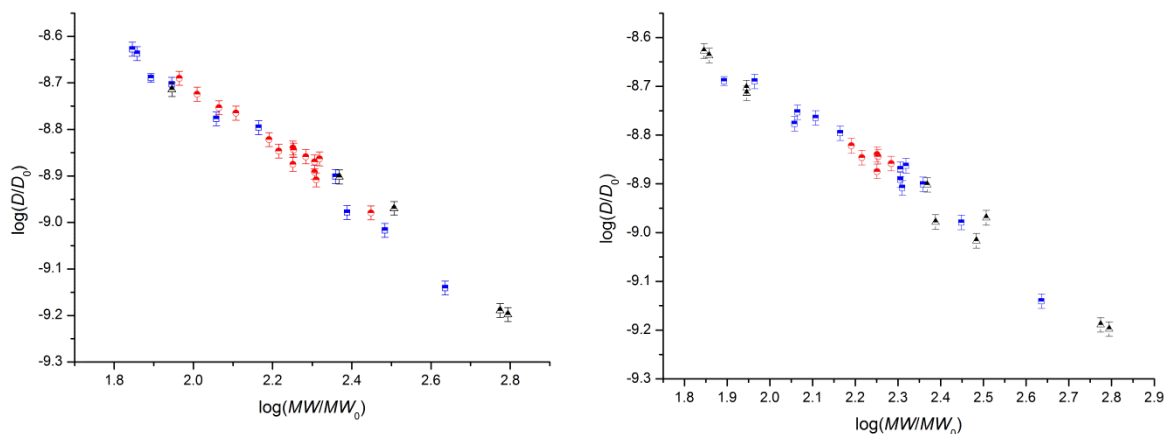


Figure 2-8: Categorization attempts using principle moments of inertia of all model compounds for benzene- d_6 . On the left, molecules are divided by the relations of their principle moments of inertia (black = $I_{xx} \approx I_{yy} \approx I_{zz}$; red = $I_{xx} \approx I_{yy} \neq I_{zz}$; blue = $I_{xx} \neq I_{yy} \approx I_{zz}$). On the right, the same molecules are categorized by their relative shape anisotropies κ^2 (black = 0-5%; red = 5-10% and blue = 10%+). ($D_0 = 1 \text{ m}^2/\text{s}$; $MW_0 = 1 \text{ g/mol}$)

Linear fits of these categorization attempts led to cor. R^2 values similar to merged ECCs (e.g. for compounds with $I_{xx} \approx I_{yy} \approx I_{zz}$: cor. $R^2 = 0.97$; worst for compounds with $\kappa^2 = 5\text{-}10\%$: cor. $R^2 = 0.31$). The best result was received for compounds with $\kappa^2 = 0\text{-}5\%$ (cor. $R^2 = 0.98$) which shows that at least a differentiation into spherical and linear compounds seems feasible using shape anisotropies. This could also help to establish better merged ECCs by simply ruling out the very spherical or very linear molecules. However, the categorization attempts would overall, according to the cor. R^2 values, not result in a more accurate MW estimation. This is unfortunate, since the goal of a straightforward categorization procedure could not be accomplished using this route.

It was also difficult to find suitable limits for the categorization of molecules utilizing not only the ratios of principal moments of inertia, but also their absolute values, e.g. THF and cyclopentane have principal moments that behave like $I_{xx} \approx I_{yy} \neq I_{zz}$, however, the absolute principal moments are also very small. The observed diffusion coefficients of these molecules were reduced and they were therefore previously empirically categorized as CS compounds, for which $I_{xx} \approx I_{yy} \approx I_{zz}$ would be assumed. Hence, in the future, a differentiation utilizing absolute principal moments of inertia may be worthwhile, since these incorporate the size of the solute and therefore enable a more accurate classification, e.g. naphthalene has ratios of principal moments similar to anthracene, whereas their absolute values are only half. However, this approach would most certainly require careful evaluation for every compound, therefore also further complicate a desired simple categorization process. Such individual differentiations may also be aided by the calculation of the gyration tensor (\mathbf{S}) (2-8) which is purely geometry-based, i.e. it only depends on the angles and bond lengths of the

investigated molecule. Also, the gyration tensor should be very similar to the inertia tensor in the absence of very heavy elements. The elements of this gyration tensor can be used to calculate the asphericity b and the acylindricity c shown in formulae (2-9) and (2-10), respectively which can be further criteria for a more elaborate categorization.

$$\mathbf{S} = \begin{bmatrix} S_{xx} & 0 & 0 \\ 0 & S_{yy} & 0 \\ 0 & 0 & S_{zz} \end{bmatrix} \quad (2-8)$$

$$b = S_{zz} - \frac{1}{2}(S_{xx} + S_{yy}) \quad (2-9)$$

$$c = S_{yy} - S_{xx} \quad (2-10)$$

2.1.3 Theoretical Error Analysis^a

Deviations of back-calculated MW s correspond to an empirical error limit of the ECCs, but cannot replace a theoretical error calculation. So far, this subject has scarcely been touched in preceding studies. Equation (2-11) incorporates all parameters to predict MW_{det} :

$$MW_{\text{det}} = \left(\frac{D_x D_{\text{ref,fix}}}{D_{\text{ref}} K} \right)^{-\frac{1}{\alpha}} \quad (2-11)$$

The diffusion coefficients (D_x , $D_{\text{ref,fix}}$ and D_{ref}) used therein are clearly error-prone as well as the linear fit parameters $-\alpha$ and K of the ECCs. Error propagation of formula (2-11) resulted in equations (2-12) and (2-13) for the calculation of the maximum error of the predicted MW_{det} (ΔMW_{det}) and the relative error ($\Delta MW_{\text{det,rel}}$), respectively:

$$\Delta MW_{\text{det}} = \sqrt{\left(\frac{MW_{\text{det}}}{D_{\text{ref}} \alpha} \cdot \Delta D_{\text{ref}} \right)^2 + \left(\frac{MW_{\text{det}}}{K \alpha} \cdot \Delta K \right)^2 + \left(-\frac{MW_{\text{det}}}{D_x \alpha} \cdot \Delta D_x \right)^2 + \left(-\frac{MW_{\text{det}}}{D_{\text{ref,fix}} \alpha} \cdot \Delta D_{\text{ref,fix}} \right)^2 + \left(-\frac{MW_{\text{det}} \log \left(\frac{D_x D_{\text{ref,fix}}}{D_{\text{ref}} K} \right)}{\alpha^2} \cdot \Delta \alpha \right)^2} \quad (2-12)$$

$$\Delta MW_{\text{det,rel}} = \frac{\Delta MW_{\text{det}}}{MW_{\text{det}}} \cdot 100\% \quad (2-13)$$

The errors for the linear fit parameters ($\Delta \alpha$ and $\Delta \log(K)$) are listed further above (Table 2-3, Table 2-4 and Table 2-5). These errors are taken from the least-squares fitting procedure as implemented in the program Origin Pro 8.5G. Errors for the diffusion coefficients were estimated from multiple DOSY measurements which resulted in a maximum variation of $\log(D)$ values of about 0.0075. $\Delta \log(D)$ was defined as twice this deviation (0.015) and ΔD were calculated relatively using equation (2-14) for analytes and internal references (ΔK was calculated likewise).

^a The theoretical error analysis was not featured, but first presented in: S. Bachmann, B. Gernert, D. Stalke, *Chem. Commun.* **2016**, 52, 12861-12864.^[4]

$$\Delta D = D \left(\frac{\Delta \log(D)}{\log(D)} \right) \cdot 100\% \quad (2-14)$$

However, this leads to smaller relative errors for smaller diffusion coefficients, i.e. smaller aggregates. Still, there is only a difference of about 1% in the final errors which seems to be negligible. The average errors for all ECCs are given in Table 2-7.

Table 2-7: Average relative theoretical errors ($\Delta MW_{\text{det,rel}}$) for all solvents and merged as well as shape-optimized ECCs.

	$\Delta MW_{\text{det,rel}}$	$\Delta MW_{\text{det,rel}}$	$\Delta MW_{\text{det,rel}}$	$\Delta MW_{\text{det,rel}}$
Solvent	Merged	DSE	ED	CS
CDCl₃	±10%	±12%	±18%	±10%
CD₂Cl₂	±9%	±8%	±15%	±8%
C₆D₆	±7%	±5%	±11%	±11%
CD₃OD	±9%	±10%	±7%	±15%
CD₃CN	±8%	±9%	±12%	±15%
THF-<i>d</i>₈	±7%	±5%	±6%	±8%
Toluene-<i>d</i>₈	±7%	±4%	±9%	±9%
DMSO-<i>d</i>₆	±8%	±7%	±8%	±19%
C₆D₁₂	±13%	±9%	±11%	±15%

The complete set of all individual, calculated $\Delta MW_{\text{det,rel}}$ for all references and solvents is given in the appendix (Table 5-22 (merged ECCs); Table 5-23 (shape-optimized ECCs)).

The theoretical errors (ΔMW_{det}) are mostly influenced by the errors of the linear fit parameters themselves ($\Delta \log(K)$ and $\Delta \alpha$). Their contributions make up about 99% of the final error. The limitation of the technique is therefore closely related to the quality and validity of the ECCs, i.e. the validity of the power-law. Still, the presented theoretical errors seem to be an adequate measure of how accurate the MW prediction can effectively be. Essentially, this would be 4 to 19% which matches the previously discussed empirical deviations attained from back-calculated MWs .

For the merged ECCs the theoretical limitations are mostly exceeded by their previously discussed empirical max. deviations (e.g. for DMSO-*d*₆: max. dev. (merge) = ±20%, $\Delta MW_{\text{det,rel}}$ (merge) = ±8%). This is on the one hand encouraging, as the methodology is not overstating the data, but on the other hand a clear indication that there is room for improvement. Such improvements have been attempted by introducing the categorization of compounds in relation to their shape (see section 2.1.1.2). The theoretical errors of the resulting shape-optimized ECCs are comparable to those of merged ECCs, while their empirical deviations are substantially diminished. Empirical deviations are in some cases even better than the theoretical limitations. Hence, an over-interpretation of the data is a possibility and in such cases, theoretical limitations should be taken into account instead of the empirical deviations. Furthermore, the theoretical error calculation can be an indicator towards the overall quality of ECCs, e.g. the high theoretical error for the CS ECC of DMSO-*d*₆ shows that the categorization might in this case still be improved.

2.1.4 Heavy Atoms in the ECC-DOSY-*MW* Estimation

There is another issue which is of great importance for the interpretation of results obtained from ECC-DOSY: Molecular sizes (volumes) can mostly be correlated proportionally to molecular weights (see Figure 2-9). This works well, if only hydrocarbons with an occasional heavier atom are compared. But, there are some cases where the increase in size is no longer correlated to the increase in weight. For example, deuterium atoms are roughly the same size as hydrogen atoms, whereas their weights are doubled. Thus, in the ECC-*MW* estimation deuterated and hydrogenated molecules cannot be distinguished, since their diffusion coefficients are almost the same in solution as these are mainly dependent on their quasi-identical molecular sizes. For this reason, all hypothetical aggregates herein are only proposed to be coordinated by hydrogenated donors, even though in deuterated solvents this does not have to be the case.

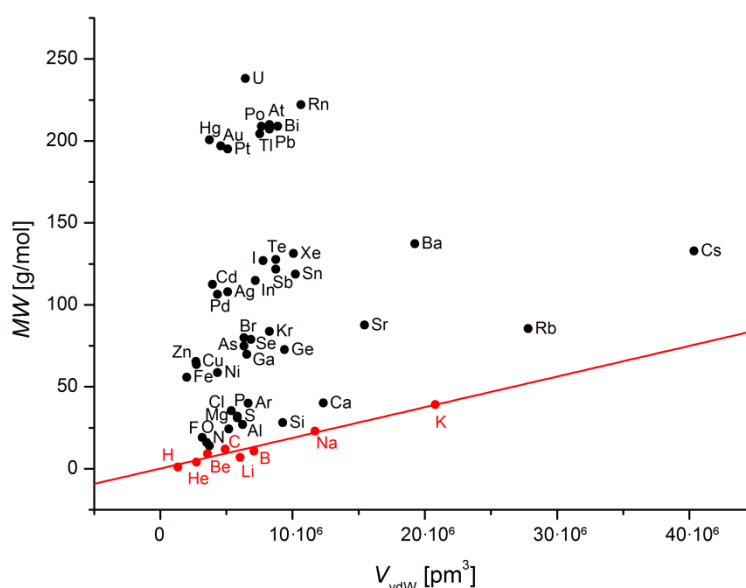


Figure 2-9: Plot of the molecular weight (*MW*) of atoms against their *van-der-Waals* volumes ($V_{\text{vdw}} = \frac{4}{3}\pi r_{\text{vdw}}^3$). The red line demonstrates for which elements (also marked red) a linear dependence can be assumed for the ECCs herein. Other elements (e.g. heavier halides like Br or transition metals like Cd) deviate strongly.

This is problematic for heavier elements (e.g. transition metals or higher halides) which invoke the same problem. The diffusion coefficients of molecules incorporating such elements are normally higher than that of molecules of the same mass, but without heavier elements and their molecular weights would be underestimated. The influence of these elements gets weaker as the molecules get larger, e.g. a bromine atom has a heavier impact on falsifying diffusion coefficients of a small molecule, since the effect depends on the bromine's percentage of the overall mass. One way to compensate for this is to establish specialized calibration curves with molecules that incorporate the same heavy elements or other similar irregularities as was done by Wang and Pedersen *et al.*^[113],^a However, it is only viable if certain molecular properties are known *a priori*, e.g. the number of

^a Calculations of MD_w for their used molecules can be found in the appendix (see Table 5-25).

heavy atoms. Still, utilizing this procedure of specialized ECCs is valid. However, by recognizing these problems beforehand they can be circumnavigated or used to improve the whole methodology. Our group could previously show that such irregularities can be recognized by simply calculating the so-called molar *van-der-Waals* density (MD_W ; see equation (2-15)) of proposed aggregates or utilized references.^[109]

$$MD_W = \frac{MW}{\sum V_{vdW}} = \frac{MW}{\sum_{i=1}^n \frac{4}{3}\pi r_{vdW,i}^3} \quad (2-15)$$

If MD_W values are between 4.2 and $5.9 \cdot 10^{29}$ g/(mol·m³), MW s can be safely predicted by the ECCs given herein, as the corresponding aggregates do either not contain any heavy elements or their effects are negated by the fact that the molecules are of considerable size.

The sum of the *van-der-Waals* volumes of all individual atoms (V_{vdW}) of a molecule is the denominator, when calculating MD_W . *Van-der-Waals* volumes of a selection of elements are given in Table 2-8.

Table 2-8: *Van-der-Waals* volumes (V_{vdW}) of a selection of elements in increasing order. *Van-der-Waals* radii (r_{vdW}) were taken from references [123].

Element	H	Zn	F	O	N	Cd	C	Mg	Cl	P	S
V_{vdW} [m³ · 10⁻³⁰]	5.6	11.3	13.3	14.7	15.6	16.5	20.6	21.7	22.5	24.4	24.4
Element	Li	Br	B	Si	Na	K	Rb	Cs			
V_{vdW} [m³ · 10⁻³⁰]	25.3	26.5	29.7	38.8	49.0	87.1	116.5	169.0			

To exclude related discrepancies, MD_W were calculated for all herein proposed aggregates as well as model compounds (see Table 5-24). All molecules that inhibit higher MD_W were dismissed in the preparation of ECCs (e.g. $CDCl_3$, DMSO or $Si(OMe)_4$).

MD_W enabled other options to correct corresponding deviations within the MW estimation process aside from establishing the aforementioned specialized ECCs, i.e. deviations of MW s or diffusion coefficients can simply be correlated to the respective molar *van-der-Waals* densities of molecules that inhibit heavier atoms to generate a correctional factor. This was first explained by *Neufeld*.^[109b] The estimated MW s of molecules with elevated MD_W were corrected to what they should have been for the merged ECCs depending on their diffusion coefficients. The ratio of these corrected and the uncorrected MW s (correction factor) was plotted against the respective molecule's MD_W which resulted in a seemingly linear dependency that could be fitted accordingly. However, due to the limited reference count, this result was ultimately not very reliable.

Therefore, the following results were produced in cooperation with *Kreyenschmidt*^[124] with a master thesis (for more detailed information see reference ^[124]):^a To cure the lack of limited references, 60 different mono- or multibrominated and -iodated molecules were measured that also exhibited

^a Manuscript in preparation.^[5]

elevated MD_W . With this data, a similar approach to that of *Neufeld* was chosen, i.e. to correct diffusion coefficients and plot the ratio of the normalized uncorrected and corrected diffusion coefficients against the MD_W . Instead of obtaining the previously anticipated linear dependence a non-linear correlation became apparent due to the increased reference count and could be fitted adequately (see equation (2-16); see Figure 2-10). This was done for THF- d_8 and benzene- d_6 . Unfortunately, the additional parameters (a , k and xc) are only identified from distribution and do not have any physical basis, yet.

$$X_{cor} = \frac{\log(D_{merge})}{\log(D_{x,norm})} = \frac{a}{(1 + e^{(-k(MD_W - xc))})} \quad (2-16)$$

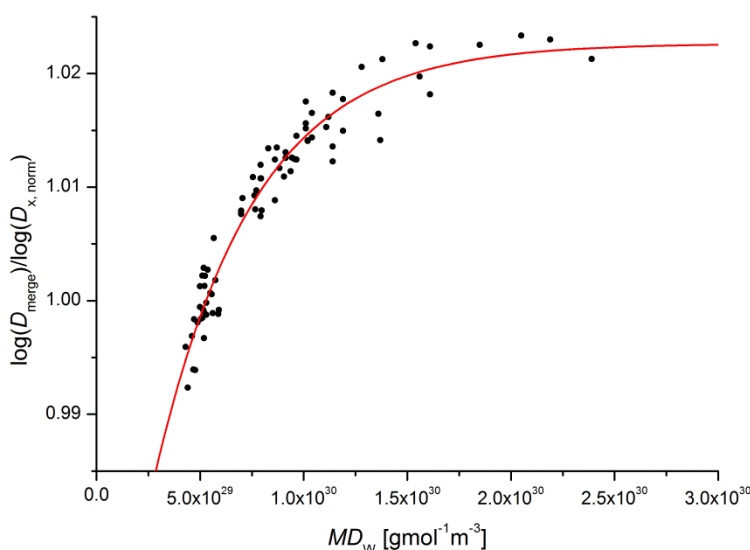


Figure 2-10: Non-linear fit of a plot of $\log(D_{merge})/\log(D_{x,norm})$ against MD_W in THF- d_8 .

Here, D_{merge} are the corrected diffusion coefficients assumed for aggregates of the same MW without heavy atoms on the corresponding merged ECC. The correctional factor (X_{cor}) seems to approach a limiting value with increasing MD_W . While there need to be further investigation into this behavior, it can be noted that molecules that display high MD_W are comparably small with high heavy atom content, e.g. $MD_W(\text{CHBr}_3) = 2.39 \cdot 10^{30} \text{ g}/(\text{mol} \cdot \text{m}^3)$; $MD_W(\text{SiHBr}_3) = 2.17 \cdot 10^{30} \text{ g}/(\text{mol} \cdot \text{m}^3)$; $MD_W(\text{C}_2\text{H}_4\text{I}_2) = 2.19 \cdot 10^{30} \text{ g}/(\text{mol} \cdot \text{m}^3)$.

Using the parameters of the fit curves (THF- d_8 : $a = 1.023 \pm 0.001$, $k = (2.156 \pm 0.188) \cdot 10^{-30}$, $xc = (-1.228 \pm 0.137) \cdot 10^{30}$; benzene- d_6 : $a = 1.028 \pm 0.001$, $k = (1.799 \pm 0.155) \cdot 10^{-30}$, $xc = (-1.495 \pm 0.155) \cdot 10^{30}$) the normalized diffusion coefficients of compounds with elevated MD_W can be corrected in dependence of their MD_W by simply multiplying them with their individual correction factor X_{cor} . While the correction factor seems to have a narrow range ($0.99 < X_{cor} < 1.025$), the correction does in almost all cases exceed the theoretical variation of diffusion coefficients (0.015).

Afterwards, the corrected diffusion coefficients can be used in a classical ECC-DOSY- MW estimation with merged calibration curves of the respective solvents. Note that the fit curve

parameters have to be improved at the same time as the merged ECCs are improved, since they are closely related. Using this technique, MW s were calculated with highly improved accuracy for molecules with a MD_W of $5.6 \cdot 10^{29}$ to $2.4 \cdot 10^{30}$ g/(mol·m³). Unfortunately, just using this approach, a better MW prediction of molecules that do not have elevated MD_W was not achieved and therefore this procedure does not need to be applied in such cases. Furthermore, due to the incorporation of this additional empirical fit to the methodology, the theoretical errors would certainly rise and it is therefore doubtful that a MW estimation should be any better than 10 to 20% as is reflected by the maximum empirical deviations (THF- d_8 : av. dev. = $\pm 6\%$; max. dev. = $\pm 23\%$; benzene- d_6 : av. dev. = $\pm 4\%$; max. dev. = $\pm 13\%$).

2.1.5 MW Estimation Software^a

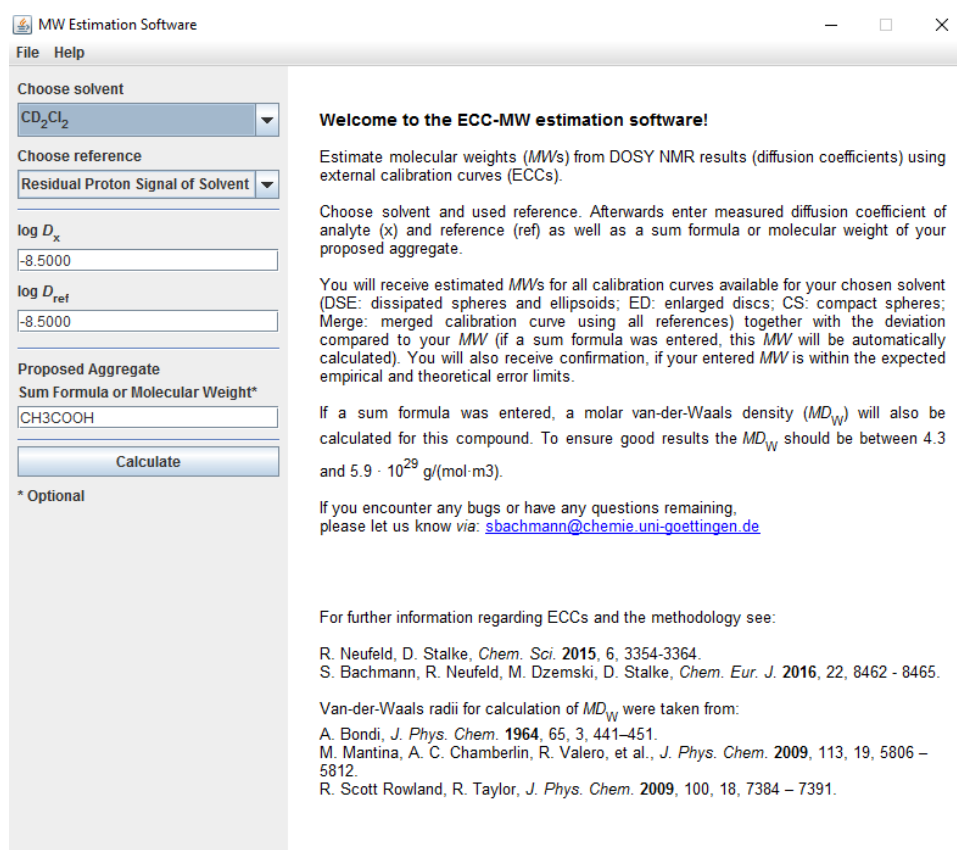


Figure 2-11: Screenshot of the starting screen displaying the welcoming message of the ECC- MW estimation software along with its general graphical user interface (GUI).

To address a larger number of researchers, an easy to use yet comprehensive software was programmed that incorporates state-of-the-art approaches towards ECCs. The software will be continuously updated. Everything that is discussed in this section is related to version 1.0. The

^a Some results of this section have been published separately: S. Bachmann, B. Gernert, D. Stalke, *Chem. Commun.* **2016**, 52, 12861-12864.^[4]

newest version is always available for download on: <http://www.stalke.chemie.uni-goettingen.de/mwestimation/>

On startup, the software recognizes the user's system setting and is displayed in the according language (the default setting is English, while German is also available). The idea behind the program is to simplify the MW estimation process and guide the user to ultimately estimate MW s systematically and precisely. Therefore, a welcoming message familiarizes the user with the required input and the methodology itself (see Figure 2-11).

Within the main graphical user interface (GUI), the user is asked to choose the used solvent and internal reference and insert logarithmic measured diffusion coefficients of the analyte ($\log(D_x)$) and the internal reference ($\log(D_{ref})$). In the options, the input can be changed towards the non-logarithmic form of the diffusion coefficients. Furthermore, users can input an MW_{calc} or a sum formula of hypothetical aggregates. If a sum formula is entered, MW_{calc} and MD_W will be automatically calculated. The user will receive verification, if the MD_W is within a reasonable range.

With the entered diffusion values, MW_{det} will be calculated and displayed for every available ECC of the chosen solvent. MW_{calc} will be compared to these MW_{det} s i.e. MW_{dif} will be calculated and displayed. Furthermore, confirmation will be given if the calculated MW_{dif} is within the empirical and/or theoretical error limit of the respective ECC (see Figure 2-12). The error limits may also be displayed numerically. Additionally, there is an option to change the theoretical errors of the individual diffusion coefficients.

MW Estimation Software

File Help

Choose solvent: CD_2Cl_2

Choose reference: Residual Proton Signal of Solvent

$\log D_x$: -8.5000

$\log D_{ref}$: -8.5000

Proposed Aggregate: CH3COOH

Sum Formula or Molecular Weight*

* Optional

Solvent = CD_2Cl_2

Reference = Residual Proton Signal of Solvent

$\log D_{x, norm} = -8.4982$ g/mol

$MW_{calc} = 60$ g/mol

ECC	MW_{det}	MW_{dif}	Within expected error interval	
			Emperical	Theoretical
CS	50 g/mol	20 %		
Merge	59 g/mol	2 %	✓	✓
DSE	63 g/mol	-5 %	✓	✓
ED	95 g/mol	-37 %		

$MD_w = 6.47 \cdot 10^{29}$ g/(mol · m³) not okay

Date: Fri Dec 02 13:18:25 CET 2016

Figure 2-12: Screenshot of a MW estimation. The left-hand side shows the chosen and entered parameters, while the right-hand side shows results, i.e. the normalized diffusion coefficient, the calculated MW_{calc} from the entered sum formula, the calculated MW_{det} for every available ECC for the chosen solvent, MW_{dif} for each ECC, respectively, confirmations if MW_{dif} is within the theoretical and/or empirical error range, date and time of the estimation and finally a molar *van-der-Waals* density for the entered sum formula.

The chosen and entered data will automatically be saved upon closing the program. Furthermore, manually saving and loading this data is an option. Results may also be copied, printed or simply reproduced from saved data to facilitate publication. Within the software a library is given (in form of several .json files) that can easily be changed and new calibration curves as well as references can be added. Moreover, previous ECCs can easily be adapted to new findings.

In the future, further improvements towards the software are envisioned, i.e. correction of diffusion coefficients in relation to MD_w (for information on this and MD_w see section 2.1.4).

2.2 Structure Elucidation of Alkali Metal Cyclopentadienide Derivatives *via* Diffusion NMR

In the previous chapter, the ECC methodology was reviewed and improvements were made to elevate the degree of reliance. In this chapter, this methodology will be utilized to elucidate the solution state structures of alkali metal cyclopentadienides (CpMs) and their derivatives (MeCpMs and Cp^{*}Ms). As was described in section 1.1.2, these heavily used organometallic building blocks have been thoroughly investigated in the solid state and were reviewed in many articles.^[33] However, information on solution state structures is scarce. Hence, further evidence is needed to finally clarify persistent ambiguities.

2.2.1 Solution State Structures of Alkali Metal Cyclopentadienides (CpMs) in Different Solvents^a

Alkali metal cyclopentadienides (CpLi, CpNa, CpK, CpRb and CpCs) were synthesized according to literature procedures or in slightly adapted one-step syntheses. These syntheses will not be discussed any further in the main part of this work, but are listed for completeness in section 4.2.1. CpMs were then analyzed fully by 1D and 2D NMR experiments in different solvent environments.

2.2.1.1 Solution State Structures of CpMs in THF-*d*₈

In the solid state CpMs arrange into polymeric chains and can be disaggregated into monomers by donating solvents (for further information see section 1.1.2). These structures are mostly contact ion pairs (CIPs) and provide the basis on which solution structures have to be judged. CpMs have very poor solubilities in hydrocarbons and ethers. THF is the only solvent that provides reasonable concentrations and was therefore chosen for solution state structure analysis. The effects of more strongly donating solvents, i.e. ammonia and DMSO, on the solution state structures of CpMs will be discussed in a subsequent section.

In THF-*d*₈, the ¹H and ¹³C NMR spectra of all CpMs show only a single resonance. The signal tends to be shifted towards higher field when descending Group 1 (see Figure 2-13). ⁷Li ($\delta = -7.75$ ppm) for CpLi and ¹³³Cs resonances ($\delta = -240.1$ ppm) for CpCs were found to be in accordance with literature.^[125] The ²³Na resonance of CpNa ($\delta = -28$ to -31 ppm) is shifted towards lower field in solution compared to solid state magic angle spinning (MAS) NMR findings for a mixture of CpNa/[CpNa(THF)] and can be shifted even lower upon cooling.^[59m]

^a Some results of this section have been published separately: S. Bachmann, B. Gernert, D. Stalke, *Chem. Commun.* **2016**, 52, 12861-12864.^[4]

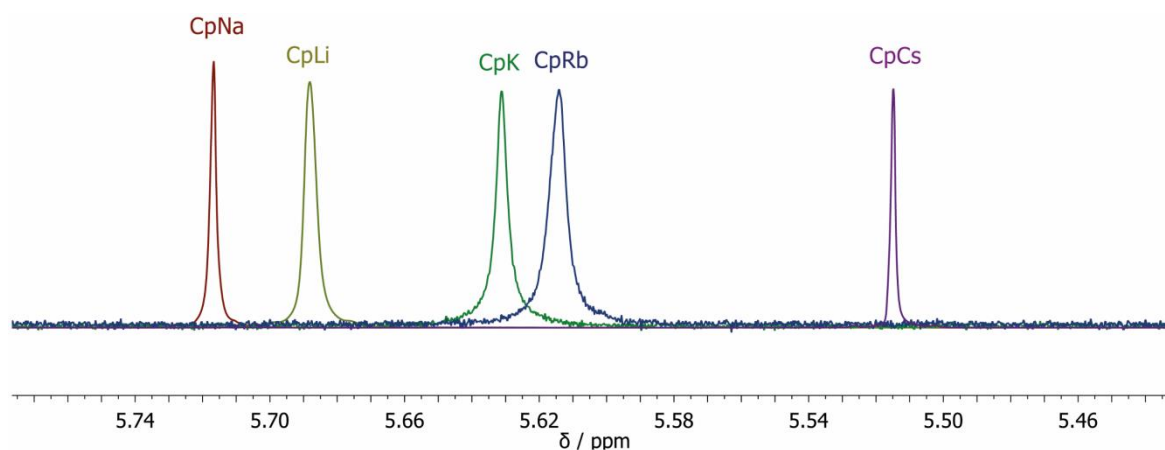


Figure 2-13: Superposition of ^1H NMR spectra of CpLi, CpNa, CpK, CpRb and CpCs (15 mM solutions, except for CpK and CpRb which were barely soluble) in $\text{THF-}d_8$ at 25 °C. A shift towards higher field can be observed for larger alkali metals (exception CpNa).

It should be stated that all of these chemical shifts for the alkali metals are quite abnormal for organometallic compounds (e.g. normally the chemical shifts of caesiumorganics range from $\delta = 250$ to -60 ppm).^[126] One reason for these unique shifts is the fact that the alkali metals are situated above the π -plane of the aromatic five-membered cyclopentadienide which provides additional shielding to the metal nuclei. However, such ring currents should only provide a maximum of 10 ppm of shielding independent of observed nucleus.

A similar downfield shift as observed upon cooling for the ^{23}Na resonance of CpNa was also noticed for the ^7Li NMR signal of CpLi and is further accompanied by broadening (see Figure 2-14).

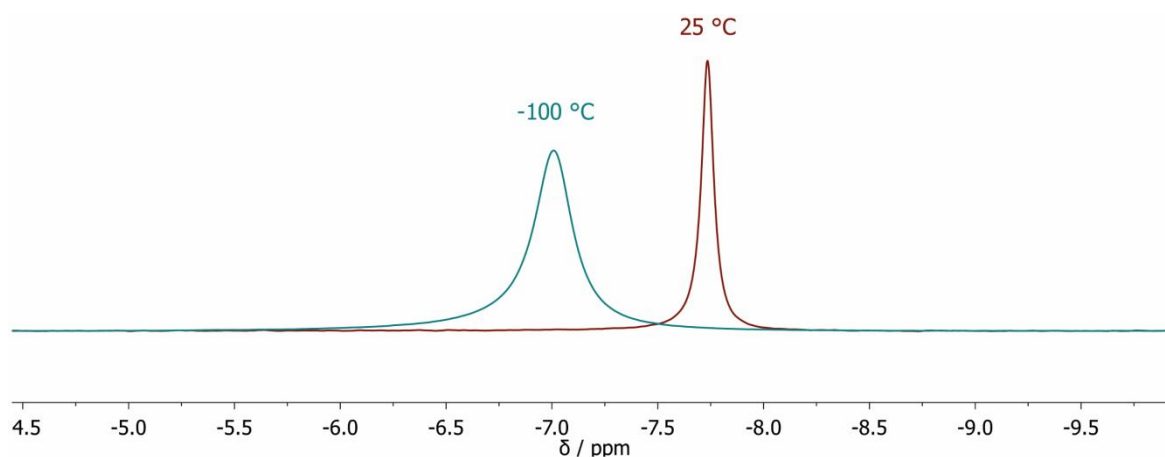


Figure 2-14: Superposition of ^7Li NMR spectra of different samples of CpLi at ambient temperature (red) and -100 °C (cyan). Broadening and shifting of the resonance are clearly observable.

In 1990, *Paquette et al.* already reported this behavior.^[66] They investigated a closely related compound to CpLi, namely lithium isodicyclopentadienide, and could provide evidence for a fast exchange process between a monomeric and a “sandwich” dimeric species. In the same study, they also investigated CpLi and concluded a similar behavior, based on the splitting of the ^6Li NMR signal at lower temperatures (splitting was first observed at -107 °C). Still, they could not “tell

whether the monomer-dimer equilibrium of CpLi “is shifted to either side at room temperature”. In this work, CpLi was cooled to $-100\text{ }^{\circ}\text{C}$. However, measurements showed no splitting (see Figure 2-14) and at about $-105\text{ }^{\circ}\text{C}$ CpLi precipitated completely. Its behavior could therefore not be studied further.

Aside from these 1D spectra that provide chemical shift information, DOSY NMR spectroscopy was used to estimate MW s utilizing the ECC methodology. The ECCs for dissipated spheres and ellipsoids (DSE) were found to be quite accurate for determining the MW s of organometallic reagents.^[109a] Therefore, all MW s of CpMs in THF- d_8 were estimated *via* the DSE-ECC. For comparison, MW s were also estimated using the merged ECC. The mandatory molar *van-der-Waals* density calculations have also been done and the complete set of data is given in the appendix (see Table 5-39). However, for all aggregates proposed herein errors due to higher MD_W can be excluded. The estimated MW_{det} were compared to MW_{calc} of likely monomeric $[\text{CpM}(\text{THF})_x]$ and dimeric aggregates $[(\text{CpM})_2(\text{THF})_x]$ with $x = 0-4$, $M = \text{Li, Na, K, Rb, Cs}$ (see Table 2-9; the complete set of data is given in the appendix: Table 5-26 (CpLi); Table 5-28 (CpNa); Table 5-30 (CpK); Table 5-32 (CpRb); Table 5-34 (CpCs)).

Table 2-9: ECC^{THF} (DSE and merged) were used to predict MW_{det} of CpMs in THF- d_8 . The accuracy of the ECC^{THF} (DSE) is in the range of $MW_{\text{dif}} = \pm 8\%$ and of the ECC^{THF} (merged) in the range of $MW_{\text{dif}} = \pm 18\%$. Theoretical errors as discussed in section 2.1.3 are given as standard deviations for all estimated MW s. All results in this table are from measurements at $25\text{ }^{\circ}\text{C}$. MW_{dif} are given for some exemplary aggregates.

	[CpM(THF) ₂]		[CpM(THF) ₃]	[(CpM) ₂ (THF) ₄]	
	MW_{det} (merged)[g/mol]	MW_{det} (DSE)[g/mol]	MW_{dif} (DSE) [%]	MW_{dif} (DSE) [%]	MW_{dif} (DSE) [%]
CpLi	225 ± 17	218 ± 11	-1	32	98
CpNa	310 ± 25	295 ± 16	-21	3	57
CpK	354 ± 30	335 ± 18	-26	-4	48
CpRb	309 ± 25	294 ± 16	0	25	100
CpCs	1864 ± 198	1624 ± 111	-	-	-

The results fit best for monomeric aggregates with different quantities of coordinated THF per alkali metal (except for CpCs); hence, these are proposed to be the most populated species for CpMs in THF solution (see Figure 2-15). Just considering the MW_{det} of dimeric aggregates, without or with a minimum of coordinated THF, they would also be an option, e.g. $MW_{\text{dif}}(\text{DSE}; [(\text{CpLi})_2(\text{THF})]) = -1\%$ (the complete set of data for the other CpMs is given in the appendix). However, such dimeric aggregates are more unlikely. They do not only presume a very low coordination number, but, e.g. for $[(\text{CpLi})_2(\text{THF})]$ it is also difficult to imagine a bonding situation where only one lithium resonance would be observable at lower temperatures, even with fast exchange. Metallocene-type aggregates e.g. $[\text{Cp}_2\text{M}(\text{THF})_x]^-$ cannot be differentiated from $[\text{CpM}(\text{THF})_{x+1}]$, because $MW(\text{THF}) \approx MW(\text{Cp})$. Therefore, the question of existing metallocene-type species in solution cannot be irrevocably answered by the ECC technique.

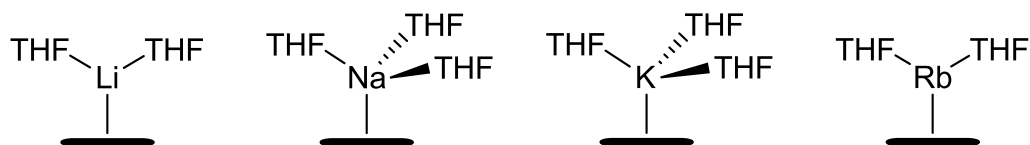


Figure 2-15: Proposed monomeric aggregates of CpLi, CpNa, CpK and CpRb in THF solution.

For CpLi the predominant monomeric aggregate seems to be coordinated by only two THF molecules. This molecule is stable over a large temperature range. If normalized $\log(D_{x,\text{norm}})$ are compared, there is almost a perfect fit for all measured temperatures: $\log(D_{x,\text{norm}})(\text{CpLi}, 50\text{ }^\circ\text{C}) = -8.886$; $\log(D_{x,\text{norm}})(\text{CpLi}, 25\text{ }^\circ\text{C}) = -8.901$; $\log(D_{x,\text{norm}})(\text{CpLi}, -50\text{ }^\circ\text{C}) = -8.905$; $\log(D_{x,\text{norm}})(\text{CpLi}, -80\text{ }^\circ\text{C}) = -8.909$; $\Delta\log(D_{x,\text{norm}})(\text{CpLi}, 50/-80\text{ }^\circ\text{C}) = 0.023$. Furthermore, the formation of CIPs can be deduced from the identical $\log(D_{x,\text{norm}})$ values from the ^7Li - and ^1H -DOSY NMR spectra (see Figure 2-16 and Table 5-26 in the appendix).

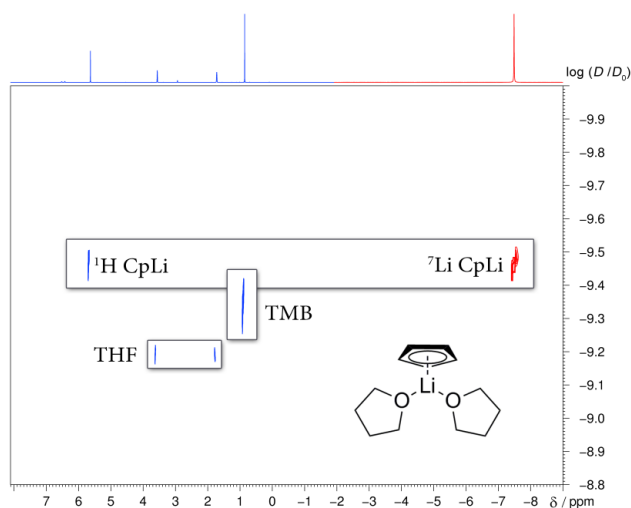


Figure 2-16: Superposition of ^1H - (blue) and ^7Li -DOSY (red) NMR spectra of CpLi in $\text{THF-}d_8$ at $-50\text{ }^\circ\text{C}$. Since only 15 mM solutions of CpLi were used, not all THF is coordinated to CpLi and the diffusion coefficients are averaged with free THF. ($D_0 = 1\text{ m}^2/\text{s}$)

For CpNa and CpK the coordination by 3 THF molecules is preferred with a slightly bigger MW_{dif} for CpK. Cooling CpNa to $-50\text{ }^\circ\text{C}$ resulted in almost identical diffusion coefficients as were observed at $25\text{ }^\circ\text{C}$ ($\log(D_{x,\text{norm}})(\text{CpNa}, 25\text{ }^\circ\text{C}) = -8.978$; $\log(D_{x,\text{norm}})(\text{CpNa}, -50\text{ }^\circ\text{C}) = -8.971$; $\Delta\log(D_{x,\text{norm}})(\text{CpNa}, 25/-50\text{ }^\circ\text{C}) = 0.007$). It was previously proposed that the mono-solvated $[\text{CpNa}(\text{THF})]$ is a possible aggregate in the solid state which could not be confirmed for solution.^[59m] Cooling led to precipitation of CpK, CpRb and CpCs, therefore no further insight into thermal dependence could be gained for either of them.

Interestingly, the normalized diffusion coefficient of CpRb ($\log(D_{x,\text{norm}})(\text{CpRb}, 25\text{ }^\circ\text{C}) = -8.9770$) is elevated in comparison to CpK ($\log(D_{x,\text{norm}})(\text{CpK}, 25\text{ }^\circ\text{C}) = -9.0098$). Hence, CpRb seems to be coordinated by only 2 THF molecules at $25\text{ }^\circ\text{C}$. In literature, a coordination polymer of CpRb is known which crystallized with two THF molecules attached to the metal.^[127] This provides

plausibility to the disaggregation in solution by breaking one of the two Cp–Rb bonds. This atypical trimeric coordination of Rb in solution is supposedly due to the fading donor capacity of THF towards increasingly soft *Lewis* acidic cations. This can be underlined by alkali metal/ammonia binding energies ($\Delta E(M^+-NH_3) = 170.3$ (Li); 117.2 (Na); 82.0 (K); 71.1 (Rb); 61.9 (Cs) kJmol^{-1}).^[128] These correspond with recently observed structures for hexamethyldisilazides crystallized from liquid ammonia.^[115] The same analogous trend can be assumed for $\Delta E(M^+-THF)$, as the heavier alkali metal Cp compounds tend to form coordination polymers instead of taking on more coordinated solvent molecules. Rb seems to be the borderline case of not adding solvent molecules and not coordinating additional cyclopentadienide ligands.

DOSY NMR spectroscopic measurements show that only CpCs forms oligomeric aggregates. As described above, such formations of coordination polymers are more prevalent among caesium than rubidium compounds. The observed aggregates display a $MW > 1500$ g/mol ($\log(D_{x,\text{norm}})(\text{CpCs}, 25^\circ\text{C}) = -9.407$) and stay intact after heating to 50°C ($\log(D_{x,\text{norm}})(\text{CpCs}, 50^\circ\text{C}) = -9.409$, $\Delta\log(D_{x,\text{norm}})(\text{CpCs}, 50/25^\circ\text{C}) = 0.002$). Hence, it seems that very specific species are formed and retained. To gather further insights into this behavior of CpCs in THF, it was crystallized from a saturated THF solution. While this crystallization was effortlessly achieved at slightly lowered temperatures (4°C) or even ambient temperature, the crystallized needles (see Figure 2-17) exhibited some limitations towards crystal structure analysis.



Figure 2-17: Needles of CpCs which were crystallized at ambient temperature in THF solution.

The crystals were sensitive towards air and moisture and furthermore displayed a phase transition upon cooling. After several attempts only a poor dataset could be acquired at -23°C . This data did not fulfill quality requirements for publication, since it displayed a modulated structure. Still, a polymeric setup with two coordinated THF molecules is indicated from the data which seems reasonable, as this has been previously observed for other related CpM structures.^[59k, 59m, 127] However, due to the low quality of the data, crystallographic parameters will not be discussed in this work.

In 1996, *Harder* and *Prosenc* could show the formation of a caesocene triple-decker.^[69] From this and the estimated MW , pentameric $[(\text{CpCs})_5(\text{THF})_{10}]$ ($MW_{\text{dif}}(\text{merged}) = -8\%$) or hexameric $[(\text{CpCs})_6(\text{THF})_{12}]$ ($MW_{\text{dif}}(\text{merged}) = 12\%$) cyclic structures can be envisioned for the solution state

structure of CpCs (see Figure 2-18), whereas other motifs (linear structures) with different amounts of THF or Cp are feasible, as well.

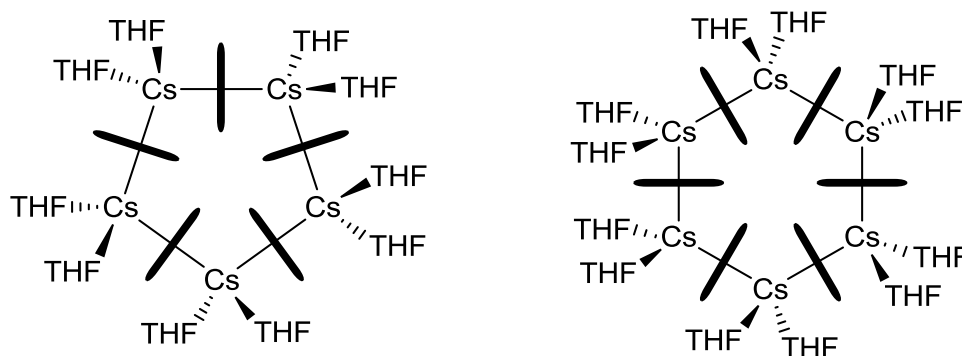


Figure 2-18: Proposed pentameric (left) and hexameric (right) cyclic aggregates of CpCs in THF solution.

The assumption of such cyclic structures can also be made, since high hapticities are known to prevail with soft *Lewis* acidic cations like Cs^+ .^[79b, 129] Also, similar hexameric structures have been observed in the solid state for bis(trimethylsilyl)cyclopentadienylthallium^[130] and pentamethylcyclopentadienylindium^[131]. Still, it needs to be emphasized that current ECCs are not optimized for accurate *MW* estimations of such aggregates, since reference compounds do not cover *MWs* > 600 g/mol, yet.

2.2.1.2 Solution State Structures of CpMs in ammonia and DMSO- d_6

In the last section, solution state structures of CpMs in THF have been presented after utilizing ECC-*MW* estimations. Analyzing their aggregation in other solvents, for which different aggregational motifs could be observed in the solid state, are of similar interest, as they present new opportunities of fine-tuning reactivities. Structures which were crystallized from ammonia, i.e. $[(\text{CpLi})_2(\text{NH}_3)_3]$ and $[\text{Li}(\text{NH}_3)_4][\text{Cp}]$, are especially fascinating, since they reveal on the one hand the formation of an SSIP containing naked Cp^- and on the other a lithocene-type structure which may be preserved in solution as well.^[290] Furthermore, these crystal structures show that different aggregational states may be achieved depending on ammonia concentrations.^[290]

It is reasonably difficult to control ammonia concentrations, since it is gaseous at ambient temperatures. Hence, the establishment of ECCs which are dependent on solvent viscosity would not be feasible. Still, CpLi was dissolved within pure ammonia (the procedure is given in section 4.2.1.1) in a sealed NMR tube with little amounts of toluene for referencing and measured at 25 °C. A chemical shift for the ^7Li NMR signal of $\delta = -0.59$ ppm was observed which is an immense difference compared to findings in THF ($\delta = -7.75$ ppm), while the resonances in the proton and carbon spectra only varied slightly from THF measurements (^1H : $\Delta\delta = 0.2$ ppm; ^{13}C : $\Delta\delta = 0.7$ ppm). As was already stated, the strong high field shift of the ^7Li signal in THF is a consequence of the η^5 -coordination of the alkali metal. Therefore, the difference in chemical shift

observed in ammonia is a clear indication that this coordination behavior has changed. Additionally, a coupling between ammonia and lithium could be observed in a ${}^7\text{Li}, {}^1\text{H}$ -HOESY experiment, while a similar coupling to the cyclopentadienide could not be found (see Figure 2-19). All this points towards the formation of SSIPs. A ${}^1\text{H}$ -DOSY spectrum was measured which did not provide any further insights (see Figure 5-9 in the appendix).^a

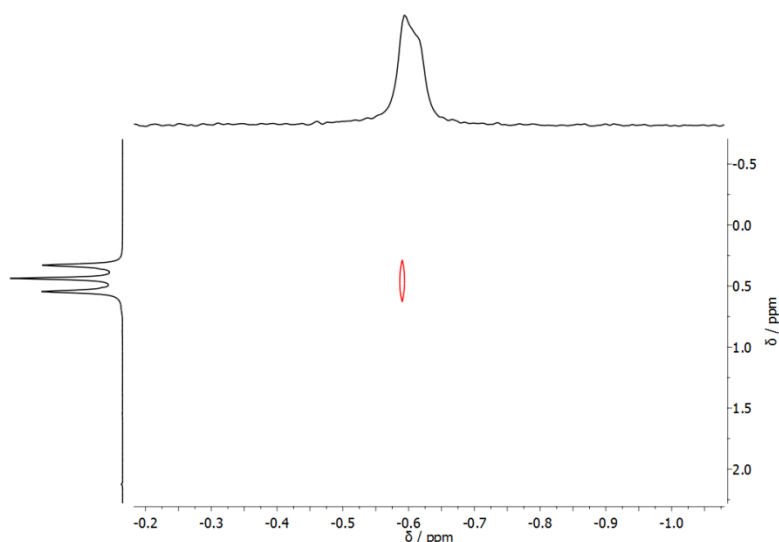


Figure 2-19: Excerpt from ${}^7\text{Li}, {}^1\text{H}$ -HOESY NMR spectrum of CpLi in ammonia at 25 °C. A coupling of ammonia and lithium is visible.

All CpMs were also fully characterized in DMSO- d_6 . Due to its comparably high dielectric constant ($\epsilon(\text{DMSO}) = 47$; see Table 1-1) and the availability of ECCs, DMSO presents an opportunity for the observation of SSIPs that are comparable to species presumed for ammonia. Chemical shifts obtained from proton and carbon spectra in DMSO were similar for all CpM reagents (${}^1\text{H}$: $\delta = 5.33$ to 5.41 ppm, ${}^{13}\text{C}$: $\delta = 103.0$ to 103.9 ppm). These spectra also show only one nucleus for the CpMs. This indicates that no decomposition into e.g. starting material^b took place, which might be possible if highly reactive SSIPs are formed. Chemical shifts observed for the alkali metals in DMSO were drastically shifted towards lower field compared to resonances observed in THF which is (same as before in ammonia) a good indication for an SSIP. The ${}^7\text{Li}$ resonance of CpLi ($\delta = -1.07$ ppm) is comparable to chemical shifts of solvated lithium-salts in DMSO shown in literature.^[132] The same is true for the ${}^{23}\text{Na}$ ($\delta = -1$ to -4 ppm) and ${}^{133}\text{Cs}$ resonances ($\delta = -14.7$ ppm) of CpNa and CpCs, respectively.

To further elucidate this behavior, DOSY and HOESY NMR experiments were employed: Similar to ammonia an NOE was observed between the solvent (DMSO) and lithium in a ${}^7\text{Li}, {}^1\text{H}$ -HOESY experiment of CpLi (see Figure 5-10 in the appendix), while no coupling to the cyclopentadienide was visible. The formation of SSIPs for DMSO can be further underlined by the differences of normalized diffusion coefficients received from ${}^1\text{H}$ - and ${}^7\text{Li}$ -DOSY NMR (see Figure 2-20; the

^a ${}^7\text{Li}$ -DOSY was not measured.

^b Dicyclopentadiene has multiple resonances and was measured in DMSO- d_6 for comparison.

complete set of data is given in the appendix: Table 5-27). Unfortunately, such a comparison was not possible for the other CpMs, since DOSY experiments of the other alkali metals could not be attained. Furthermore, HOESY spectra would be ineffective for the other alkali metals, as discussed in section 1.2.1.1. Still, these findings seem to confirm the formation of SSIPs at least for CpLi.

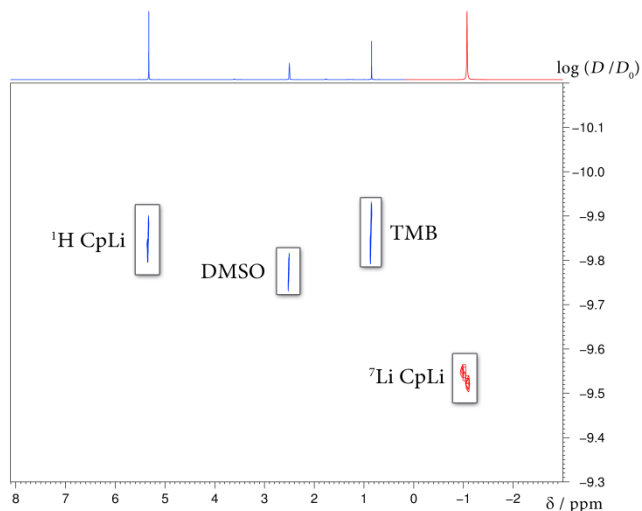


Figure 2-20: Superposition of ^1H - (blue) and ^7Li -DOSY NMR spectra (red) of CpLi in $\text{DMSO-}d_6$ at $25\text{ }^\circ\text{C}$. This superposition shows a clear discrepancy of the diffusion coefficients of the cyclopentadienide and lithium ions as expected for the formation of SSIPs. ($D_0 = 1\text{ m}^2/\text{s}$)

To transfer these indicative findings from CpLi to the other CpMs and further clarify the specific types of aggregates that are formed, normalized diffusion coefficients from ^1H -DOSY can be compared amongst each other and ECC- MW predictions can be employed. For all CpMs (except CpCs) almost identical values for the normalized diffusion coefficients (see Table 2-10) were measured. Hence, it can be rationalized that SSIPs are formed by CpNa, CpK and CpRb as well, since CIPs would result in differences of their diffusion coefficients of at least the contribution of the respective alkali metals and possibly differences in solvation.

Table 2-10: ECC^{DMSO} (DSE, ED and merged) were used to predict MW_{det} of CpMs in $\text{DMSO-}d_6$. The accuracy of the ECC^{DMSO} (DSE) is in the range of $MW_{\text{dif}} = \pm 10\%$, of the ECC^{DMSO} (ED) is in the range of $MW_{\text{dif}} = \pm 4\%$ and of the ECC^{DMSO} (merged) in the range of $MW_{\text{dif}} = \pm 20\%$. Theoretical errors as discussed in section 2.1.3 are given as standard deviations for all estimated MW s. All results in this table are from measurements at $25\text{ }^\circ\text{C}$. $\log(D_{x,\text{norm}})$ are also given for comparison.

	$\log(D_{x,\text{norm}})$	MW_{det} (merged) [g/mol]	MW_{det} (DSE) [g/mol]	MW_{det} (ED) [g/mol]
CpLi	-9.2763	123 ± 10	129 ± 8	144 ± 10
CpNa	-9.2733	122 ± 10	128 ± 6	143 ± 10
CpK	-9.2706	121 ± 9	127 ± 6	142 ± 10
CpRb	-9.2671	119 ± 9	125 ± 6	141 ± 10
CpCs	-9.3699	172 ± 15	175 ± 7	186 ± 15
(^7Li) CpLi	-8.9039	43 ± 3	49 ± 5	64 ± 4

ECC- MW predictions (see Table 2-10) show that the MW s of all the CpMs (except CpCs) for the merged ECC are about 120 g/mol (similar values are obtained for the DSE ECC; the complete set of

data is given in the appendix: Table 5-27 (CpLi); Table 5-29 (CpNa); Table 5-31 (CpK); Table 5-33 (CpRb); Table 5-35(CpCs)). Since the formation of SSIP-type aggregates seems confirmed by the findings of CpLi stated above, the estimated MW s pose the question of how exactly they aggregate. The estimated MW s could be interpreted directly and viewed as unambiguous like it was done previously for CpMs in THF solution. However, for THF reasonable aggregates could be presented, whereas the estimated MW s for DMSO are not that conclusive. If the assumption of complete SSIP formation was true, only Cp^- anions with a MW of 65 g/mol should be observed. This is obviously not the case, as the estimated MW s are nearly doubled.^a While these MW s would fit the starting material (dicyclopentadiene), decomposition can be disregarded, as well. Taking a step back from the SSIP assumption, the estimated MW s also exclude even most monomeric CIP structures with and without coordinated solvent, let alone dimeric or metallocene-like aggregates.^b

Hence, interpreting the predicted MW s directly does not result in any reasonable aggregates. Some approximation within the methodology may prohibit a reasonable analysis: In section 2.1.4 the influence of elevated *van-der-Waals* densities was discussed which can be mostly disregarded here, since Li, Na and K aggregates display normal MD_w . Note that some CIP structures produce elevated MD_w values for CpRb and CpCs ($MD_w([CpRb]) = 6.09 \cdot 10^{29} \text{ g}/(\text{mol} \cdot \text{m}^3)$; $MD_w([CpRb(\text{DMSO})]) = 6.33 \cdot 10^{29} \text{ g}/(\text{mol} \cdot \text{m}^3)$; $MD_w([CpCs]) = 6.60 \cdot 10^{29} \text{ g}/(\text{mol} \cdot \text{m}^3)$; $MD_w([CpCs(\text{DMSO})]) = 6.68 \cdot 10^{29} \text{ g}/(\text{mol} \cdot \text{m}^3)$). Another important aspect is that the whole methodology is based on measured self-diffusion coefficients. Any influence on the self-diffusion of the particles is therefore also accumulated within the estimated MW s. In the introduction, it was stated that the diffusion coefficients can display averaged values for multiple aggregates in an equilibrium which might be the case for CpMs in DMSO. Hence, temperature-dependent measurements were performed exemplary for CpNa (25 °C, 50 °C and 75 °C) which resulted in an increase of the diffusion coefficient ($\Delta \log(D_{x,\text{norm}})(\text{CpNa}, 75/25 \text{ °C}) = 0.027$) upon heating that exceeded significance (the complete set of data is given in the appendix: Table 5-29). This may be a hint for dynamic behavior, but unfortunately does not offer other new insights, as predicted MW s are still within a similar margin.

Other intermolecular effects can also affect self-diffusion: For ammonia, the comparison to the $[\text{Li}(\text{NH}_3)_4][\text{Cp}]$ structure was drawn. This solid state structure indicates the formation of a “two-dimensional net with tailored meshes bridged by hydrogen bonding to free lattice ammonia”^[290], thus forming channels, wherein the anionic cyclopentadienides are shielded by solvent molecules from the solvent-coordinated lithium cations (see Figure 2-21).

While the formation of such polar channels is questionable in an isotropic solution and no direct comparison to a crystal structure in DMSO can be made, since all attempts to crystallize CpMs

^a Note that estimated MW s fit for the ED-ECC $[\text{Cp}(\text{DMSO})]^-$ ($MW_{\text{calc}} = 143 \text{ g/mol}$).

^b They fit incidentally for [CpK] and [CpCs] which are deemed unlikely in the strongly coordinating solvent DMSO.

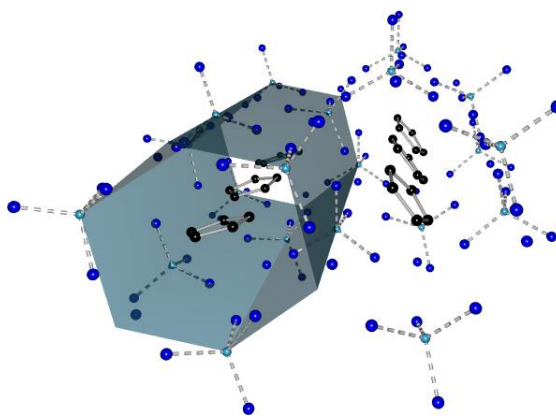


Figure 2-21: Polar channels for the accommodation of cyclopentadienide anions shown in the crystal structure of $[\text{Li}(\text{NH}_3)_4][\text{Cp}]$. Reprinted from reference [290]. Copyright © 2010 American Chemical Society.

from DMSO failed,^a the overall similar behavior to ammonia may hint to some (partial) association or formation of coordinative bonds as the reason for the observed elevated *MW*s of the cyclopentadienide. In future, conductivity or further temperature-dependent measurements of other CpMs might lead to a more conclusive explanation. However, in this case, the ECC methodology alone does not give clear results about the aggregation of CpMs. This nicely illustrates the methodology's current limits, as diffusion-influencing effects that are not cancelled due to referencing have to be considered and known *a priori* for a successful interpretation.

Lastly, CpCs will be discussed shortly, since it was the only CpM that displayed a significantly different diffusion coefficient in DMSO: Its estimated *MW* was about 170 g/mol. While, similar to CpLi and CpNa, the alkali metal shift of CpCs ($\delta(^{133}\text{Cs}) = -14.7$ ppm) was shifted substantially towards lower field compared to findings in THF ($\delta(^{133}\text{Cs}) = -240.1$ ppm), it is still significantly different to shifts observed for completely solvent-separated Cs^+ cations (caesium-salts) in DMSO presented in literature by *DeWitte et al.* ($\delta = 68$ ppm).^[133] *DeWitte et al.* also mention that Cs^+ ions are more likely to form CIPs than the other alkali metals.^[133] This is also indicated by the findings herein. The possible equilibrium, indicated by the temperature-dependent measurements of CpNa, might be pushed towards the CIP side for CpCs. Unfortunately, this behaviour cannot be further investigated, as cooling is not possible for DMSO

2.2.2 Solution State Structures of Methylated Alkali Metal Cyclopentadienides in THF-*d*₈

To further augment the acquired knowledge on aggregation and solvation as well as obtain additional information on the effects of methyl substituents on CpM aggregation, synthetically

^a Even attempts to diffuse nonpolar solvents (e.g. pentane) slowly into DMSO did not result in crystallization. After a few days the solution always turned dark in an argon glove box, indicating decomposition.

accessible^a mono- (MeCpM) and pentamethylated (Cp^{*}M) alkali metal cyclopentadienide reagents were analyzed by NMR (MeCpLi, Cp^{*}Li, Cp^{*}K and Cp^{*}Cs). The synthetic routes for these reagents were either already known in literature or simple one-step syntheses and will therefore not be discussed in the main part of this thesis (for further information see sections 4.2.2 and 4.2.3).

2.2.2.1 Solution State Structure of MeCpLi in THF-*d*₈

Neither in the solid state nor in solution has methylcyclopentadienyllithium (MeCpLi) been investigated intensely. Still, a single crystal structure of monomeric MeCpLi has been published by *Hammel et al.* in 1990 ([MeCpLi(TMEDA)]).^[59b] Since the solution state structures of THF aggregates could be successfully investigated for underivatized CpMs with ECC-DOSY-MW predictions, this should be repeated for MeCpLi and the pentamethylated compounds in the following section. MeCpLi was synthesized in good yields (90%) and was readily available for NMR spectroscopic analysis. Its ¹H and ¹³C NMR spectra as well as the ⁷Li resonance which was observed at -7.6 ppm indicate a single aggregate at 25 °C (see section 4.2.2). While multiplicities are comparable, the ¹H chemical shifts are a little different compared to literature.^[134]

ECC-DOSY NMR spectroscopy was also employed to investigate MeCpLi. The estimated $MW_{\text{det}}(\text{DSE})$ of 237 g/mol was compared to MW_{calc} of likely monomeric [MeCpLi(THF)_x] and dimeric aggregates [(MeCpLi)₂(THF)_x] with x = 0-4 (the complete set of data is given in the appendix: Table 5-36). This comparison indicates the clear preference of aggregation as [MeCpLi(THF)₂] ($MW_{\text{dif}}(\text{DSE}) = -3\%$) which is isostructural to species found for CpLi, i.e. [CpLi(THF)₂]. Interestingly, these solution state structures underline the preference of the coordination number three for such lithium aggregates.

2.2.2.2 Solution State Structures of Cp^{*}Ms in THF-*d*₈

The pentamethylated alkali metal cyclopentadienides (Cp^{*}Ms) have been more thoroughly investigated in the solid state than the monomethylated MeCpMs: Crystal structures are known that range from the polymeric form without coordinating solvent to monomeric aggregates featuring donating *Lewis* bases such as pyridine and crown ethers.^[56c, 56d, 56g, 59c, 59h, 59i] These structures closely resemble the solid state structures of underivatized CpM reagents (see introduction section 1.1.2.4). Pentamethylcyclopentadienyllithium (Cp^{*}Li), -potassium (Cp^{*}K) and -caesium (Cp^{*}Cs) were analyzed in this work. While Cp^{*}K and Cp^{*}Cs could be investigated straightforward

^a Freshly cut, not further activated, elemental sodium was not reactive enough to metalate MeCp or Cp^{*} (with otherwise the same reaction conditions as listed for MeCpLi in section 4.2.2). For further studies other sodium reagents (e.g. NaH or NaHMDS) should be utilized. Syntheses of the higher homologues of MeCpNa as well as of Cp^{*}K were not pursued.

in THF solution, alas, Cp*Li was not soluble. Hence, chemical shifts, normalized diffusion coefficients and estimated MW_{det} are only given for Cp*K and Cp*Cs in Table 2-11.

Table 2-11: Chemical shifts, normalized diffusion coefficients ($\log(D_{x,\text{norm}})$) and estimated MW_{det} of Cp*K and Cp*Cs. ECC^{THF} (DSE and merged) were used to predict MW_{det} in THF- d_8 . The accuracy of the ECC^{THF} (DSE) is in the range of $MW_{\text{dif}} = \pm 8\%$ and of the ECC^{THF} (merged) in the range of $MW_{\text{dif}} = \pm 18\%$. Theoretical errors as discussed in section 2.1.3 are given as standard deviations for all estimated MW_{det} s. All results in this table are from measurements at 25 °C.

	¹ H δ [ppm]	¹³ C{ ¹ H} δ [ppm]	$\log(D_{x,\text{norm}})$	MW_{det} (merged) [g/mol]	MW_{det} (DSE) [g/mol]
Cp*K	1.95 (s)	104.8, 11.4	-9.0393	401 ± 34	377 ± 21
Cp*Cs	1.85 (s)	108.0, 11.1	-9.1411	612 ± 56	564 ± 33

For both compounds, only a single signal set was observable (see Figure 2-22 exemplary for Cp*K).

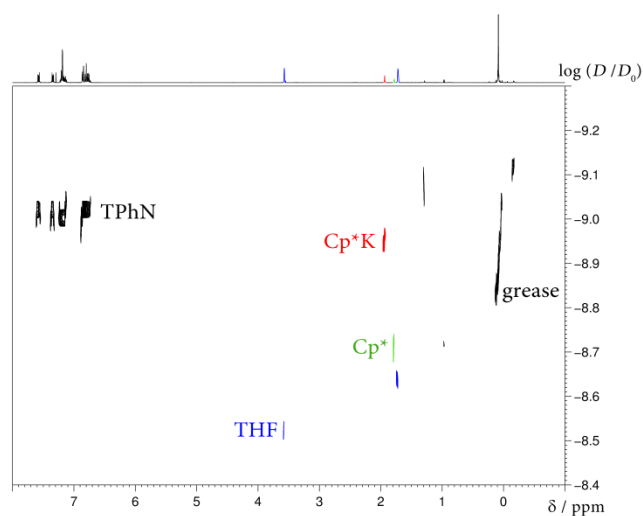


Figure 2-22: ¹H-DOSY spectrum of Cp*K in THF- d_8 at 25 °C. Since only 15 mM solutions of Cp*K were used, not all THF is coordinated to Cp*K and the diffusion coefficients are averaged with free THF. Residues of the starting material (pentamethylcyclopentadiene; Cp*) are also visible. ($D_0 = 1 \text{ m}^2/\text{s}$)

Since these compounds behaved like underivatized CpMs in the solid state, the same was anticipated for solution: Indeed, Cp*K displayed the same aggregation and solvation ($[\text{Cp}^*\text{K}(\text{THF})_3]$; $MW_{\text{dif}}(\text{DSE}) = 4\%$; the complete set of data is given in the appendix: Table 5-37) as CpK ($[\text{CpK}(\text{THF})_3]$). However, Cp*Cs did not reveal oligomeric aggregation, as previously observed for CpCs, but instead seems to be aggregated in a monomeric fashion as $[\text{Cp}^*\text{Cs}(\text{THF})_4]$ ($MW_{\text{dif}}(\text{DSE}) = -1\%$; the complete set of data is given in the appendix: Table 5-38). The Cp*Cs solution state structure indicates that the methyl groups prevent or hinder oligomeric aggregate formation, perhaps by introducing more steric demand. The increased coordination number of Cs that would be required for the predicted MW might be explained by the inclination of Cs to form higher coordination polymers, as was already explained for the CpCs compound.

These two examples show that further investigations are promising. Possibly, other solvents can be utilized to solvate Cp*Li. Moreover, temperature-dependent measurements might shed further light onto the aggregational behavior of all Cp*Ms as well as investigations through alkali metal

NMR. Additionally, the synthetic endeavors towards MeCpMs and Cp*Ms should be continued to compliment this work.

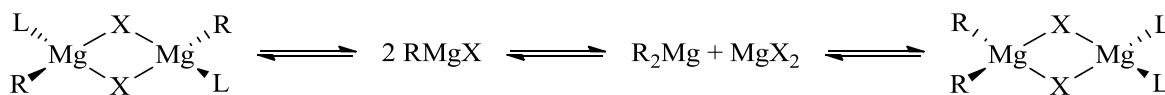
2.3 Combined Studies Involving Diffusion NMR to Solve Structural Ambiguities

In the previous chapter, the ECC methodology was utilized to determine the aggregation and solvation of CpMs and some of their methylated derivatives in different deuterated solvents. While these findings enable a closer look into s-block chemistry of Group 1, other organometallic reagents have so far not been discussed. However, with the acquired knowledge of the ECC-DOSY methodology, the transferability towards Group 2 or even transition metal organometallics is possible and has already been demonstrated in several studies.^[111-112] Hence, in this chapter the ECC methodology and DOSY itself will be utilized to investigate reagents which were provided by collaborators. Each section will contain a different research area which will be introduced shortly, while the chapter will mainly concern insights acquired through NMR.

2.3.1 Solution State Structures of Alkyl *Grignard* Reagents in THF-*d*₈^a

Prominent examples of Group 2 reagents are organomagnesium halides (RMgX; R = alkyl- or arylgroups; X = halides) which were first discovered in the year of 1900 by *Grignard* and are named accordingly *Grignard* reagents.^[135] Their applicability towards a multitude of reactants and the ability of carbon-carbon bond formation is widely utilized and has been reviewed and featured in literature extensively.^[136] Their use can be highlighted e.g. in the total synthesis of the natural antibiotic vancomycin.^[137]

Accordingly, structure elucidation of these strong nucleophiles has been of interest for a long time.^[138] They were investigated early on by *Schlenk* and *Schlenk*, who showed that they undergo a disproportionation into dialkyl- or diaryl-magnesium compounds (R₂Mg) and magnesium halides (MgX₂).^[139] Their complex solution behavior can be depicted with the so-called *Schlenk* equilibrium (see Scheme 2-2) which has since been refined by further studies, e.g. by *Ashby et al.* through NMR- and IR-spectroscopic investigations.^[140]

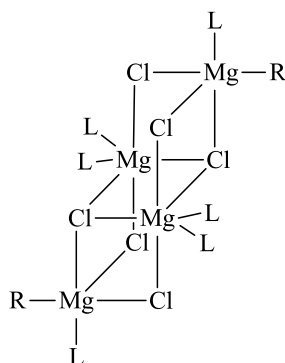


Scheme 2-2: *Schlenk* equilibrium of *Grignard* reagents, depicting the disproportionation and dimerization in solution. (L is a *Lewis* base or donating solvent, whereas R is an organic residue and X a halide)

^a Some results of this section have been published separately: C. Schnegelsberg, S. Bachmann, M. Kolter, T. Auth, M. John, D. Stalke, K. Koszinowski, *Chem. Eur. J.* **2016**, *22*, 7752-7762.^[3]

While this equilibrium is very fast and no signal separation can be observed at room temperature on the NMR timescale, it could still be shown that *Grignard* reagents are prone to form either monomeric or dimeric species. Their formation is highly dependent on the solvent, the analyte's concentration, temperature and the reagents themselves. While in Et₂O monomeric and dimeric species were observed simultaneously, in THF only monomeric species were found.^[140f] However, the disproportionation is more pronounced in THF leading to increased amounts of R₂Mg and MgX₂.

In the solid state, *Grignard* reagents crystallized from bulk RMgCl solutions (R = Me, *t*Bu, Ph, Bn) prefer forming a tetrameric open-cube that is depicted in Scheme 2-3.^[141]



Scheme 2-3: Observed solid state structure after crystallization of bulk *Grignard* reagents displaying an open-cube setup. This specific open-cube was crystallized from a THF solution of [*i*PrMgCl · LiCl] layered with Et₂O.^[141b]

Herein, conventional alkyl RMgX (R = Et, *n*Bu, *n*Hex, *n*Oct, *n*Dec, *i*Pr; X = Cl, Br) were investigated to elucidate their behavior in cooperation with the *Koszinowski* group. This study entailed a combination of electrospray-ionization (ESI) mass spectrometry (MS), electrical conductivity measurements, NMR spectroscopy and quantum chemical calculations. In this study, negative ion mode ESI mass spectrometry measurements of the different alkyl *Grignard* reagents in THF resulted in mainly trinuclear anionic species of the type [R_nMg₃Cl_{7-n}]⁻. An exemplary spectrum for *n*BuMgCl is shown in Figure 2-23. Those results stand in contrast to the classical *Schlenk* equilibrium and are most probably due to the increased analyte concentration in the charged droplets that are produced during the ESI process. The high selectivity for trinuclear anions is rooted in their close resemblance to the tetrameric open-cube solid state structures which could be further underlined by theoretical calculations. The subtraction of only a single [MgX]⁺ moiety leads to the corresponding trinuclear anion.^[3]

To further compliment the ESI-MS findings, NMR spectroscopy was used. Notably, magnesium amide bases or so-called *Hauser*-bases (R₂NMgX) which are closely related to *Grignard* reagents, have already been investigated *via* ECC-DOSY in our group.^[111] Hence, the solution state structures of alkyl *Grignard* reagents were investigated by the same technique in THF-*d*₈. For this study, 25 mM solutions of RMgX with equimolar amounts of the internal reference 1,2,3,4-tetraphenyl-naphthalene (TPhN) were prepared.

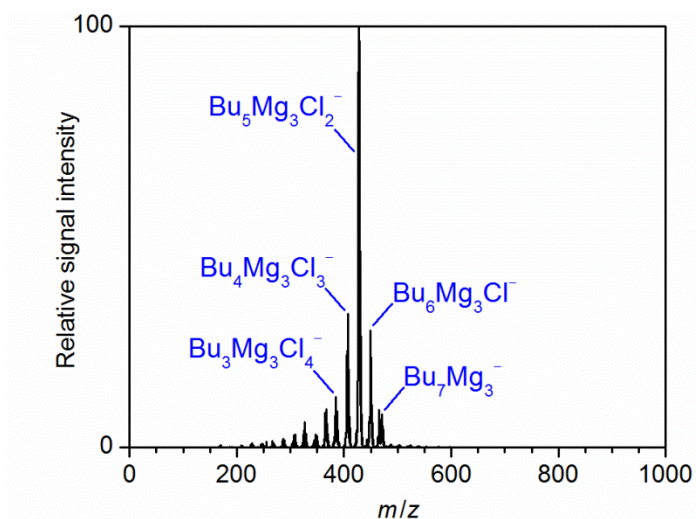


Figure 2-23: Negative ion-mode ESI mass spectrum of a 25 mM solution of *n*BuMgCl in THF.^[3]

The proton and carbon spectra of the alkyl *Grignard* systems showed the expected upfield-shifted signals of the methylene or methine groups at 25 °C, respectively, which were directly bound to the magnesium (see Figure 2-24).^a Furthermore, a second set of signals (marked red in Figure 2-24) revealed the presence of minimum amounts of possibly starting material RCl for all systems. Cooling to -50 °C did not result in additional signals.

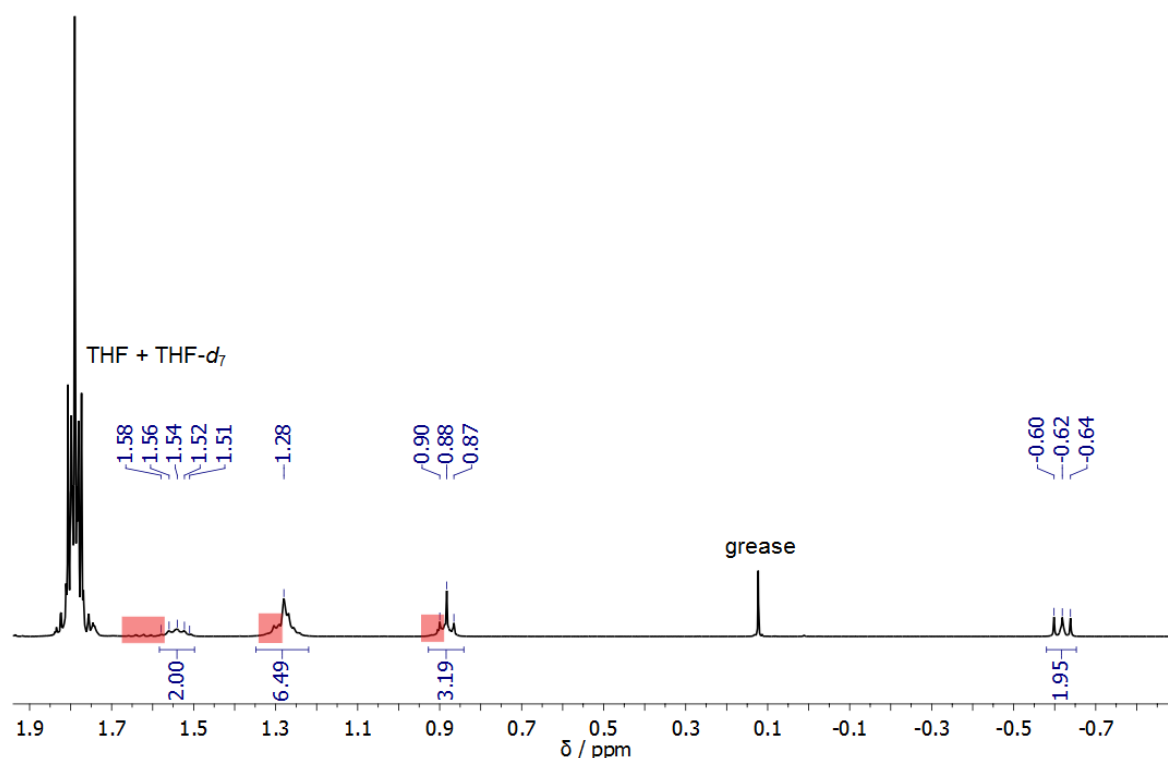


Figure 2-24: Excerpt from the ¹H NMR spectrum of *n*HexMgCl in THF-*d*₈ at 25 °C reveals a second set of signals (marked in red).

^a The complete set of 1D and DOSY NMR spectra is given in the Supporting Information of reference [3].

Additionally, ^1H -DOSY NMR was used to determine the aggregation of *Grignard* reagents. In the DOSY spectra only their diffusion coefficients were observable, whereas the signal intensity of RCl was too low to gather any related information. An exemplary ^1H -DOSY spectrum is shown in Figure 2-25.

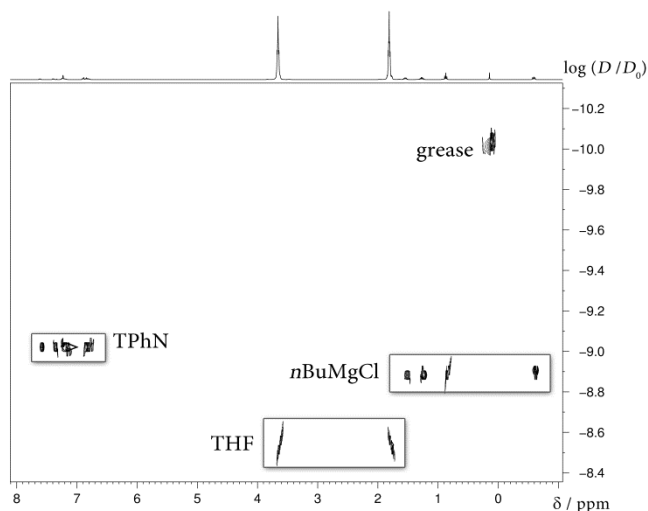


Figure 2-25: ^1H -DOSY spectrum of *n*BuMgCl with the internal reference TPhN in $\text{THF-}d_8$ at 25 °C. ($D_0 = 1 \text{ m}^2/\text{s}$)

2.3.1.1 External Calibration Curves for Rod-Like (RL) Molecules

While the calibration curves for dissipated spheres and ellipsoids (DSE) have been proven to be effective for the *MW* prediction of organometallic species before, in the case of the larger alkyl *Grignard* systems they would most certainly fail.^a The shapes of these reagents are dominated by the increasing lengths of the alkyl chains and cannot be described as spherical. Hence, references were sought that demonstrated a similar geometry to establish more specialized ECCs. References were mostly starting materials used in synthesis (e.g. 1-chlorohexane (*n*HexCl; $\text{CH}_3(\text{CH}_2)_4\text{CH}_2\text{Cl}$)) as well as other compounds incorporating long alkyl chains (e.g. batylalcohol (Batyl; $\text{CH}_3(\text{CH}_2)_{17}\text{OCH}_2\text{CH}(\text{OH})\text{CH}_2\text{OH}$)). The comparability and suitability of these references can be easily confirmed by the calculation of principal moments of inertia *I* and subsequently relative shape anisotropies κ^2 , as explained in section 2.1.2. While it was demonstrated that the calculation of these principal moments of inertia would overall not lead to a more straightforward molecule categorization, they can still be an adequate indicator to distinguish linear from more spherical molecules. Model compounds that were intended to represent rod-like (RL) molecules incorporating alkyl chains all display shape anisotropies of more than 20% which is considerably higher than values observed for other model compounds (see Table 2-12).^b

^a For small alkyl chains (EtMgCl) or more spherical systems (*i*PrMgCl) the DSE ECC is feasible.

^b Tetrabutylammoniumchloride (TBACl) was removed as model compound from the ECC for rod-like (RL) molecules, as it is more spherical than linear. Results based on the ECCs may differ slightly from literature.^[3]

Accordingly, utilizing the references listed in Table 2-12, an ECC for rod-like (RL) molecules, i.e. the alkyl *Grignard* systems, was established in THF- d_8 .

Table 2-12: Principal moments of inertia calculated with PMIFST^[122] for geometry optimized (MMFF94) structures of model compounds used in ECCs for rod-like aggregates. The relative shape anisotropy κ^2 is also listed for each model compound.

Compound	I_{xx} [$\text{u}\text{\AA}^2$]	I_{yy} [$\text{u}\text{\AA}^2$]	I_{zz} [$\text{u}\text{\AA}^2$]	$I_{xx} : I_{yy} : I_{zz}$	$\kappa^2 \cdot 100\%$
Batylalcohol	274	20730	20911	1 : 76 : 76	24.0
<i>n</i> DecCl	70	3349	3387	1 : 48 : 48	23.5
<i>n</i> HexCl	44	956	980	1 : 22 : 22	21.8
<i>n</i> OctCl	57	1916	1948	1 : 34 : 34	22.9

Since also brominated reagents with elevated MD_W (see section 2.1.4), i.e. *n*BuMgBr, were to be analyzed, another specialized ECC for rod-like molecules was established utilizing brominated references^a (RLBr; the complete set of normalized diffusion coefficients for RL and RLBr references is given in the appendix: Table 5-21). Note that only mono-brominated references can be described by the RLBr ECC. Figure 2-26 depicts these ECCs, whereas in Table 2-13 the corresponding ECC parameters as well as other quality factors, i.e. av. and max. deviations of back-calculated MW s and cor. R^2 values, are listed.

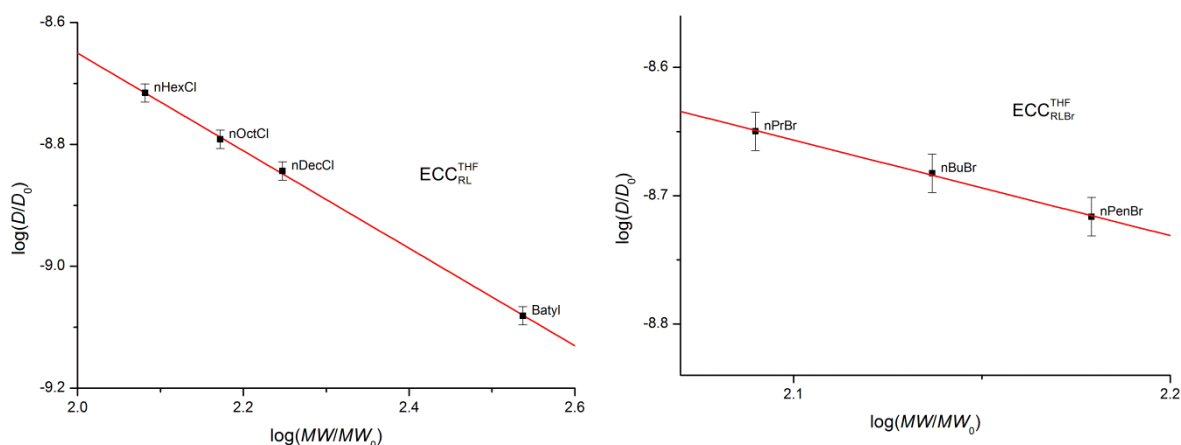


Figure 2-26: ECCs for rod-like (RL) (left) and brominated rod-like (RLBr) (right) compounds for THF- d_8 . ($D_0 = 1 \text{ m}^2/\text{s}$; $MW_0 = 1 \text{ g/mol}$)

The same information is given for specialized ECCs developed in the master thesis of *Kreyenschmidt* for mono- (Br) and di-brominated (Br_2) reagents.^{[124], b}

Since the reference count was quite limited for the RL and RLBr ECCs, theoretical errors are more feasible than empirical deviations. Theoretical errors are listed for the individual model compounds in Table 2-14. These were calculated according to the formulae described in section 2.1.3.

^a Principal moments of inertia were not calculated for brominated references.

^b Molecules of the Br and Br_2 ECCs are not differentiated by shape.

Table 2-13: ECC parameters and their errors, av. and max. deviations of back-calculated MW s and cor. R^2 values of shape-optimized calibration curves (RL and RLBr) as well as for specialized ECCs for mono- and di-brominated reagents (Br and Br₂)^[124] for THF- d_8 .

	$\log(K)$	$\Delta\log(K)$	$-\alpha$	$\Delta\alpha$	av. dev.	max. dev.	cor. R^2
Solvent: THF-d_8							
RL	-7.05	0.0277	-0.800	0.0122	±1%	±1%	1.00
RLBr	-7.09	0.0625	-0.745	0.0293	±1%	±1%	1.00
Br ^[124]	-7.12	0.0632	-0.728	0.0284	±4%	±15%	0.96
Br ₂ ^[124]	-6.80	0.0176	-0.834	0.0740	±6%	±18%	0.93

Table 2-14: Calculated relative theoretical errors ($\Delta MW_{\text{det,rel}}$) of used model compounds for RL and RLBr ECCs as well as average values.

Compound	RL	RLBr	Merge
	ΔMW [%]	ΔMW [%]	ΔMW [%]
Batylalcohol	4	-	9
<i>n</i> DecCl	3	-	7
<i>n</i> HexCl	3	-	7
<i>n</i> OctCl	3	-	7
<i>n</i> PrBr	-	8	6
<i>n</i> BuBr	-	9	6
<i>n</i> PenBr	-	9	7
Ø	3	9	7

The theoretical errors, at least of the RL ECC, are still questionably low. A deviation of up to 8% seems to be a realistic margin (same as for the DSE ECC in THF- d_8).

2.3.1.2 MW Estimation of Alkyl Grignard Reagents from Diffusion Data

Because the internal reference TPhN was added beforehand, normalized diffusion coefficients could be calculated for all alkyl Grignard reagents for MW predictions *via* ECCs.

Additionally, utilizing normalized diffusion coefficients, the concentration dependence could be investigated. A tenfold increase in concentration did not lead to a significant change of the normalized diffusion coefficients ($\log(D_{x,\text{norm}})(n\text{BuMgCl}, 25 \text{ mM}) = -8.9750$; $\log(D_{x,\text{norm}})(n\text{BuMgCl}, 250 \text{ mM}) = -8.9787$). Only at a concentration of 1 M of *n*BuMgCl did the increase in diffusion coefficient exceed theoretical error limits ($\log(D_{x,\text{norm}})(n\text{BuMgCl}, 1 \text{ M}) = -9.0072$). This could be an indication for the (partial) formation of higher aggregates, however, ECC-DOSY has not been rigorously tested for solutions with concentrations higher than 120 mM.^[109a] Hence, the concentration dependence seems negligible in THF at least for the low concentrations investigated herein.

Utilizing the ECCs for RL compounds, MW s were predicted for all measured alkyl Grignard systems. Furthermore, for comparison, MW s were estimated with merged and DSE ECCs. For *n*BuMgBr the RLBr ECC as well as the Br ECC provided by Kreyenschmidt^[124] and the correctional factor (X_{cor}) introduced in section 2.1.4 were utilized for the estimation of MW s. Results for chlorinated and brominated Grignard systems are listed in Table 2-15 and Table 2-16, respectively

(the complete set of data is given in the appendix: Table 5-40 (EtMgCl); Table 5-41 (*i*PrMgCl); Table 5-42 (*n*BuMgCl); Table 5-43 (*n*HexMgCl); Table 5-44 (*n*OctMgCl); Table 5-45 (*n*DecMgCl); Table 5-46 (*n*BuMgBr)).

Table 2-15: ECC^{THF} (RL, DSE and merged) were used to predict MW_{det} of RMgCl in THF-*d*₈. The accuracy of the ECC^{THF} (RL) is in the range of $\pm 8\%$ (see section 2.3.1.1), of the ECC^{THF} (DSE) in the range of $MW_{\text{dif}} = \pm 8\%$ and of the ECC^{THF} (merged) in the range of $MW_{\text{dif}} = \pm 18\%$. Theoretical errors, as discussed in section 2.1.3, are given as standard deviations for all estimated MW s. All results in this table are from measurements at 25 °C. MW_{dif} is given for monomeric [RMgCl(THF)₂] and dimeric [RMgCl(THF)₂]₂ for the RL ECC.

	[RMgCl(THF) ₂]		[RMgCl(THF) ₂] ₂		
	MW_{det} (merged) [g/mol]	MW_{det} (DSE) [g/mol]	MW_{det} (RL) [g/mol]	MW_{dif} (RL) [%]	MW_{dif} (RL) [%]
EtMgCl	261 ± 21	250 ± 13	228 ± 8	2	41
<i>i</i>PrMgCl	262 ± 21	251 ± 13	228 ± 8	8	53
<i>n</i>BuMgCl	307 ± 25	292 ± 15	255 ± 9	2	48
<i>n</i>HexMgCl	366 ± 31	345 ± 19	288 ± 11	0	51
<i>n</i>OctMgCl	405 ± 35	381 ± 21	317 ± 12	0	55
<i>n</i>DecMgCl	445 ± 39	417 ± 24	348 ± 14	-1	57

Table 2-16: ECC^{THF} (RLBr, Br) were used to predict MW_{det} of *n*BuMgBr in THF-*d*₈.^[124] The accuracy of the ECC^{THF} (RLBr) is in the range of $\Delta MW_{\text{det,rel}} = \pm 8\%$ (theoretical; see section 2.3.1.1) and of the ECC^{THF} (Br) is in the range of $MW_{\text{dif}} = \pm 15\%$.^[124] Theoretical errors, as discussed in section 2.1.3, are given as standard deviations for these estimated MW s. All results in this table are from measurements at 25 °C. MW_{dif} is given for monomeric [*n*BuMgBr(THF)₂] and dimeric [*n*BuMgBr(THF)₂]₂ for the RLBr ECC. Additionally, the correctional factor X_{cor} as discussed in section 2.1.4 has been utilized to calculate a MW ($MD_w([\textit{nBuMgBr}(\text{THF})_2]) = 6.59 \cdot 10^{29} \text{ g}/(\text{mol} \cdot \text{m}^3)$ was used).

	[<i>n</i> BuMgBr(THF) ₂]		[<i>n</i> BuMgBr(THF) ₂] ₂		
	MW_{det} (RLBr) [g/mol]	MW_{det} (Br) [g/mol]	MW_{det} (X_{cor}) [g/mol]	MW_{dif} (RLBr) [%]	MW_{dif} (RLBr) [%]
<i>n</i>BuMgBr	330 ± 33	343 ± 34	362 (merge)	-8	41

The mandatory molar *van-der-Waals* density calculations have also been done and the complete set of data is given in the appendix (see Table 5-47). Except for *n*BuMgBr, for all herein proposed aggregates errors due to higher MD_w can be excluded. The estimated MW_{det} were compared to hypothetical monomeric [RMgX(THF)₂] and dimeric [RMgX(THF)₂]₂ aggregates that are in accordance with the *Schlenk* equilibrium.

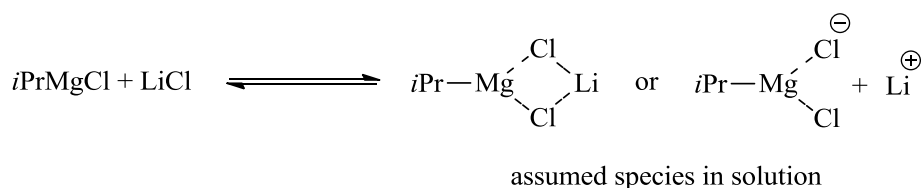
Estimated MW s show the clear preference for monomeric aggregation as [RMgX(THF)₂] of alkyl *Grignard* reagents in THF, which confirms the results and consensus reached in many other studies.^[136b, 140a-c, 140e-h] Since the diffusion coefficients may be averaged, it is difficult to say, if there are other monomeric species coexisting with proposed [RMgX(THF)₂] which is a possibility, as shown in the *Schlenk* equilibrium. However, trinuclear molecules which were observed in the ESI experiments or even dimeric aggregation can be disregarded or are extremely low populated. For *i*PrMgCl the ECC for RL molecules should not be utilized, as this molecule cannot be described as rod-like. However, calculations using the DSE-ECC led to similarly good results for monomeric

aggregation of $[i\text{PrMgCl}(\text{THF})_2]$ as for the other *Grignard* systems ($MW_{\text{diff}}(\text{DSE}) = -2\%$; see Table 5-41 in the appendix).

A special case in this investigation was $n\text{BuMgBr}$. Its proposed aggregates exhibit increased *van-der-Waals* densities (see Table 5-39 in the appendix). Therefore, specialized ECCs for brominated systems (RLBr and Br of *Kreyenschmidt*^[124]) were utilized to describe this aggregate. These produce almost identical *MW*s which fit best $[n\text{BuMgBr}(\text{THF})_2]$. Also, the correctional factor (X_{cor}) for molecules with increased MD_w was calculated according to the procedure described in section 2.1.4 ($X_{\text{cor}} = 1.005796$; with $MD_w([n\text{BuMgBr}(\text{THF})_2]) = 6.59 \cdot 10^{29} \text{ g}/(\text{mol}\cdot\text{m}^3)$) and applied which resulted in a slightly raised but similar *MW*. The increase in *MW* is reasonable, as no shape-optimization has been done and the corrected diffusion coefficient was applied to the merged ECC. However, if the corrected diffusion coefficient ($\log(D_{x,\text{norm,cor}})(n\text{BuMgBr}) = -9.0180$) is applied to the RL ECC, a *MW* of 288 g/mol is obtained, which fits even better the proposed $[n\text{BuMgBr}(\text{THF})_2]$.^a

2.3.1.3 Solution State Structures of the “Turbo”-Grignard Analogues^b

More recently, *Grignard* reagents were further advanced by *Knochel et al.* by the investigation of metal halides on their reactivity.^[142] The addition of metal halides, e.g. LiCl , led to an immense increase in reactivity, accompanied by an enhanced functional group tolerance. These reagents were accordingly named “turbo”-Grignards and have been largely utilized in different fields across academia and industry ever since.^[143] *Knochel et al.* proposed that this increased reactivity was a result of the formation of *ate* complexes (see Scheme 2-4). This proposal could be further substantiated by quantum chemical calculations. These also suggested the formation of solvent-separated ion pairs.^[144]



Scheme 2-4: $[i\text{PrMgCl} \cdot \text{LiCl}]$ species assumed to be present in solution (*ate* complexes).^[142a, 144] Coordinating solvent molecules are omitted for clarity.

Lerner et al. tried to crystallize “turbo”-Grignard compounds, i.e. $[i\text{PrMgCl} \cdot \text{LiCl}]$, but only found the open-cube analogue for RMgCl (see Scheme 2-3).^[141b] This indicates an exchange between conventional RMgX and the lithiated *ate* species. Since the conventional RMgX were investigated

^a While this approach seems feasible here, note that the correctional factor is based on the merged ECCs and therefore applying the corrected diffusion coefficients to other ECCs has not been proven, yet.

^b Some results of this section have been published separately: C. Schnegelsberg, S. Bachmann, M. Kolter, T. Auth, M. John, D. Stalke, K. Koszinowski, *Chem. Eur. J.* **2016**, *22*, 7752-7762.^[3]

in the previous section, description of the effect of LiX in solution on these aggregates would be an interesting addition. Hence, “turbo”-analogues were investigated by the same analytical methods (e.g. ESI-MS) as RMgX in cooperation with the *Koszinowski* group.^a As for NMR spectroscopy, the addition of one equivalent of LiCl to solutions of *n*BuMgCl did not change its ¹H or ¹³C spectra in any significant way. ⁷Li NMR displayed only a single resonance at $\delta = 0.28$ ppm, which is slightly different to the chemical shift of pure LiCl in THF ($\delta = 0.49$ ppm). However, ¹H-DOSY measurements resulted in significantly raised normalized diffusion coefficients for [*n*BuMgCl · LiCl] ($\log(D_{x,\text{norm}})([n\text{BuMgCl} \cdot \text{LiCl}]) = -9.0293$) compared to the conventional *n*BuMgCl ($\log(D_{x,\text{norm}})(n\text{BuMgCl}) = -8.9750$). This is consistent with findings from *Pöppler* concerning *i*PrMgCl · LiCl.^[32c] Hence, (partial) association of LiCl with the *Grignard* reagents can be concluded which is a confirmation of at least partial formation of the proposed *ate* complexes of *Knochel et al.* or neutral complexes shown in Scheme 2-4.^[142a, 144] The estimated *MW*s for RL, DSE and merge ECCs are shown in Table 2-17 for [*n*BuMgCl · LiCl] (the complete set of data is given in the appendix: Table 5-48).

Table 2-17: ECC^{THF} (RL, DSE and merged) were used to predict *MW*_{det} of [*n*BuMgCl · LiCl] in THF-*d*₈. The accuracy of the ECC^{THF} (RL) is in the range of $\pm 8\%$ (see section 2.3.1.1); of the ECC^{THF} (DSE) is in the range of $MW_{\text{dif}} = \pm 8\%$ and of the ECC^{THF} (merged) in the range of $MW_{\text{dif}} = \pm 18\%$. Theoretical errors, as discussed in section 2.1.3, are given as standard deviations for all estimated *MW*s. All results in this table are from measurements at 25 °C. *MW*_{dif} is given for monomeric [*n*BuMgCl(THF)₃ · LiCl] for the DSE ECC.

	[<i>n</i>BuMgCl(THF)₃ · LiCl] 376 g mol⁻¹			
	<i>MW</i> _{det} (RL) [g/mol]	<i>MW</i> _{det} (DSE) [g/mol]	<i>MW</i> _{det} (Merge) [g/mol]	<i>MW</i> _{dif} (DSE) [%]
[<i>n</i>BuMgCl · LiCl]	330 ± 11	362 ± 20	384 ± 33	4

Results from the RL ECC must be interpreted with caution, as the addition of LiCl to the structure would certainly result in a smaller influence of the alkyl chain to the overall shape of the solute compared to conventional RMgX. While the RL ECC results in an estimated *MW* that corresponds to [*n*BuMgCl(THF)₂ · LiCl] which has a slightly increased *MD*_w and is not in agreement with the coordination number four for either magnesium or lithium, the results of the DSE ECCs are more feasible. Hence, the solution state structure [*n*BuMgCl(THF)₃ · LiCl] is proposed, which fits the expectations.^b

The brominated *n*BuMgBr also exhibited elevated diffusion coefficients after addition of LiBr ($\log(D_{x,\text{norm}})([n\text{BuMgBr} \cdot \text{LiBr}]) = -8.9816$; $\log(D_{x,\text{norm}})(n\text{BuMgBr}) = -8.9660$) which indicates a (partial) association of the solutes. *MW*s were estimated with the specialized Br₂ ECC of *Kreyenschmidt*.^[124] Moreover, calculations with the correctional factor *X*_{cor} were made (*X*_{cor} =

^a For a detailed description of results from ESI-MS, electrical conductivity measurements and quantum chemical calculations consult reference [3].

^b ⁷Li-DOSY was not measured.

1.007461; presuming the formation of $[n\text{BuMgBr}(\text{THF})_3 \cdot \text{LiBr}]$ with $MD_W([n\text{BuMgBr}(\text{THF})_3 \cdot \text{LiBr}] = 7.07 \cdot 10^{29} \text{ g}/(\text{mol} \cdot \text{m}^3))$. Results are shown in Table 2-18 (the complete set of data is given in the appendix: Table 5-49).

Table 2-18: $\text{ECC}^{\text{THF}}(\text{Br}_2)$ was used to predict MW_{det} of $[n\text{BuMgBr} \cdot \text{LiBr}]$ in $\text{THF-}d_8$.^[124] The accuracy of the $\text{ECC}^{\text{THF}}(\text{Br}_2)$ is in the range of $MW_{\text{dif}} = \pm 18\%$.^[124] Theoretical errors, as discussed in section 2.1.3, are given as standard deviations for these estimated MW . All results in this table are from measurements at 25 °C. MW_{dif} is given for monomeric $[n\text{BuMgBr}(\text{THF})_3 \cdot \text{LiBr}]$ and $[n\text{BuMgBr}(\text{THF})_2 \cdot \text{LiBr}]$ for the Br_2 ECC. Additionally, the correctional factor X_{cor} as discussed in section 2.1.4 has been utilized to calculate a MW (MD_W of $[n\text{BuMgBr}(\text{THF})_3 \cdot \text{LiBr}]$ was used).

	$[n\text{BuMgBr}(\text{THF})_3 \cdot \text{LiBr}]$ 465 g mol ⁻¹		$[n\text{BuMgBr}(\text{THF})_2 \cdot \text{LiBr}]$ 392 g mol ⁻¹	
	MW_{det} (Br ₂) [g/mol]	MW_{det} (X_{cor}) [g/mol]	MW_{dif} (Br ₂) [%]	MW_{dif} (Br ₂) [%]
$[n\text{BuMgBr} \cdot \text{LiBr}]$	413 ± 96	412 (merge)	12	-5

These results point towards the formation of $[n\text{BuMgBr}(\text{THF})_3 \cdot \text{LiBr}]$ or $[n\text{BuMgBr}(\text{THF})_2 \cdot \text{LiBr}]$.^a However, for the Br_2 calibration curve as well as for the correctional factor, the assumption of the coordination of LiBr was already made *a priori*. Hence, these results should be weighted even more carefully than in the case of the chlorinated reagents. Furthermore, the exact solvation state is difficult to assign, as the errors of the ECCs and correctional factor exceed the deviations of the different species. It is always possible that the diffusion coefficients are averaged as some part of an equilibrium, however, as $[n\text{BuMgBr}(\text{THF})_3 \cdot \text{LiBr}]$ would invoke lithium's and magnesium's preferred coordination number four, it is more likely from a chemical point of view.

In conclusion, while the aggregation of these “turbo”-Grignard reagents cannot be described without uncertainty, the increase in diffusion coefficient upon addition of LiX salts corroborates the formation of *ate* complexes proposed by *Knochel et al.* in the past.^[142a, 144]

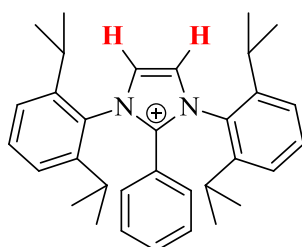
2.3.2 Anion and Solvent Coordination Elucidated *via* DOSY

The ECC technique is mostly restricted to hydrocarbons and less sensitive when considering transition metal complexes due to problems related to elevated MD_W or shape irregularities. However, DOSY and diffusion coefficient normalization in general are useful tools to investigate even such molecules. This will be demonstrated and discussed in this section while investigating the coordination of different anions to an *N*-heterocyclic carbene precursor. Additionally, the solvation of an acridine-based fluorophore and a heterocyclic substituted methanide and their metal complexes are elucidated by diffusion NMR techniques.

^a Note that no shape dependence can be discussed for the utilized ECC and correctional factor.

2.3.2.1 Coordination of Different Anions to an N-Heterocyclic Carbene in CD_2Cl_2 ^a

The synthesis of stable *N*-heterocyclic carbenes (NHCs),^[146] which are widely used as ligands in transition metal chemistry and can even be used as powerful organocatalysts, has been an important addition to modern organometallic chemistry. Their metal complexes frequently display enhanced catalytic activity, e.g. *Grubbs'* second generation catalyst for olefin metathesis.^[147] Recently, the synthesis of unconventional carbenes, i.e. mesoionic carbenes, has come to the focus of researchers, as such compounds have an even higher σ -donor strength.^[148] Hence, new synthetic approaches were made by *Reichmann* to widen the scope of such unconventional carbenes. He synthesized 1,3-bis(2,6-diisopropylphenyl)-2-(*o*-tolyl)-imidazolium (IPrPh⁺; Scheme 2-5) in our group as precursor in this pursuit. To enhance its solubility and this way optimize follow-up reactions the corresponding anions were varied, i.e. strongly coordinating halides (Br^- , I^-) and less coordinating fluorinated anions (BF_4^- , PF_6^- , OTf^-) were used.



Scheme 2-5: Structure of 1,3-bis(2,6-diisopropylphenyl)-2-(*o*-tolyl)-imidazolium (IPrPh⁺).

The variation of anions had a visible effect on the proton spectra of these compounds in CD_2Cl_2 , as the signal of the back-bone protons (marked red in Scheme 2-5) of IPrPh⁺ changed significantly ($\delta = 8.29$ ppm (Br^-); 8.07 ppm (I^-); 7.97 ppm (OTf^-); 7.88 ppm (BF_4^-); 7.76 ppm (PF_6^-)), while all other signals remained identical.^[145] *Reichmann* correlated this chemical shift difference to the acidity of the protons and proposed that the brominated species is most acidic, whereas the compound with PF_6^- is the least acidic.^[145] The assumption that the fluorinated anions would be less likely coordinated to the IPrPh⁺ could be dismissed by ^{19}F , ^1H -HOESY experiments which showed in all three cases couplings between the anions and the backbone protons of the precursor.^[145]

ECC-DOSY has then been utilized to further elucidate structural motifs: Adamantane (Adam) was used as internal reference and samples were prepared of each derivative in CD_2Cl_2 . *MWs* were estimated utilizing the DSE and merged ECCs, as the molecules can be described neither as flat nor purely spherical. Results are shown in Table 2-19 (the complete set of data is given in the appendix:

^a Some of the results have been published separately: S. O. Reichmann, *Unconventional Carbene-Donor Ligands for the Development of New Catalysts*, Ph. D. thesis, Göttingen, 2016.^[145] Furthermore, syntheses, NMR assignments and crystal structures of the individual reagents can be found there.

Table 5-51 ((IPrPh)Br); Table 5-52 ((IPrPh)I); Table 5-53 ((IPrPh)OTf); Table 5-54 ((IPrPh)BF₄); Table 5-55((IPrPh)PF₆)).

The predicted MW s were compared to MW_{calc} of species with and without coordinated anions and in all cases this comparison concludes the anion's coordination. Theoretical error ranges further disprove the possibility that some anions might not coordinate at all. Hence, these observations are in accordance with the ¹⁹F, ¹H-HOESY experiments.

Table 2-19: ECC^{CD₂Cl₂} (DSE and merged) were used to predict MW_{det} of (IPrPh)Br, (IPrPh)I, (IPrPh)OTf, (IPrPh)BF₄ and (IPrPh)PF₆ in CD₂Cl₂. The accuracy of the ECC^{CD₂Cl₂} (DSE) is in the range of $MW_{\text{dif}} = \pm 14\%$ and of the ECC^{CD₂Cl₂} (merged) in the range of $MW_{\text{dif}} = \pm 23\%$. Theoretical errors, as discussed in section 2.1.3, are given as standard deviations for all estimated MW s. All results in this table are from measurements at 25 °C. MW_{dif} is always given for (IPrPh)⁺ and the corresponding aggregate with the respective coordinated anion for the DSE ECC.

			IPrPh ⁺ 466 g/mol	
	MW_{det} (merged) [g/mol]	MW_{det} (DSE) [g/mol]	MW_{dif} (DSE) [%]	MW_{dif} (DSE) [%]
(IPrPh)Br	661 ± 75	590 ± 60	-21	-8
(IPrPh)I	614 ± 69	551 ± 55	-15	8
(IPrPh)OTf	629 ± 71	564 ± 57	-17	9
(IPrPh)BF₄	641 ± 73	573 ± 58	-19	-4
(IPrPh)PF₆	631 ± 71	565 ± 57	-18	8

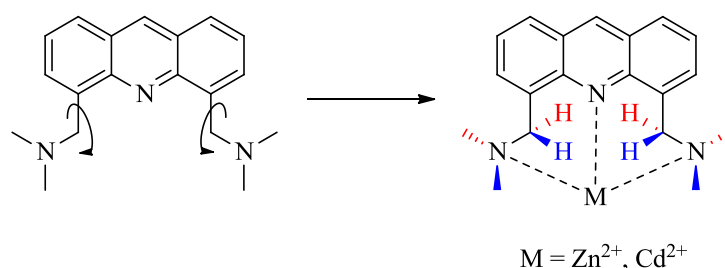
Still, taking a closer look at the predicted MW s, there are some questions remaining that should be discussed: These aggregates display almost identical normalized diffusion coefficients (e.g. $\log(D_{x,\text{norm}})((\text{IPrPh})\text{I}) = -9.0416$; $\log(D_{x,\text{norm}})((\text{IPrPh})\text{PF}_6) = -9.0480$). Hence, it is difficult to compare absolute values, as their differences mostly do not transcend error ranges. However, it should be possible to rationalize tendencies, if the anions had equal influence on the overall structure, i.e. coordinate equally strong. The decrease in diffusion coefficient should then be proportional to the increase of the *van-der-Waals* volumes of the anions. This does not seem to be the case, as the *van-der-Waals* volumes of the anions are related like $\text{Br}^- (2.65 \cdot 10^{-29} \text{ m}^3) > \text{I}^- (3.25 \cdot 10^{-29} \text{ m}^3) > \text{BF}_4^- (8.29 \cdot 10^{-29} \text{ m}^3) > \text{PF}_6^- (1.04 \cdot 10^{-28} \text{ m}^3) > \text{OTf}^- (1.29 \cdot 10^{-28} \text{ m}^3)$, whereas the diffusion coefficients and the resulting MW s are not (see Table 2-19). This could have several reasons: Either the anions do not have enough impact on the overall structure, and their differences are simply compensated by the error of the experiment, or the degree of coordination varies for each anion which therefore results in diffusion values that do not correlate directly with the anion's volumes. Whichever it is, cannot be unequivocally determined. Furthermore, elevated molecular densities (MD_w) can lead to the underestimation of some MW s. However, here this is only the case for the iodated reagent (the complete set of data is given in the appendix: Table 5-56).

Additionally, it must be noted that IPrPh⁺ has sterically demanding groups, i.e. *i*Pr and Ph, which can rotate and therefore exhibit increased hydrodynamic radii which is not covered by the existing power law variations. Hence, diffusion coefficients for all these molecules might be overestimated.

What degree of overestimation this would produce is difficult to predict. However, this should be comparable for all aggregates. In the future, possibly theoretical calculations may enlighten these observations.

2.3.2.2 Solvent-Anion Exchange of an Acridine-Based System in DMF- d_7 ^a

The detection and/or quantification of specific ions in solution, e.g. Zn^{2+} and Cd^{2+} in the human body, is highly relevant, as their concentration can be an important diagnostic tool or in other cases even their occurrence can have harmful effects.^[149] Hence, the synthesis of sensor molecules designed to fulfil that need is a rewarding goal. In our group *Visscher* recently synthesized an acridine-based fluorophore (4,5-bis-(*N,N*-dimethylaminemethylene)-acridine; see Scheme 2-6) which shows selective Zn^{2+} and Cd^{2+} ion binding together with a detectable fluorescence response.^[1, 150]



Scheme 2-6: Structure of 4,5-bis-(*N,N*-dimethylaminemethylene)-acridine) and its metal complexes. The possibility of rotation of the amines is hindered after metal coordination. Highlighted groups (red and blue) then lose their chemical equivalency.

In his work, *Visscher* was able to show that after metal binding the molecule fluoresces. He further characterized the ligand itself as well as the resulting Zn^{2+} and Cd^{2+} metal complexes with different analytical techniques (X-ray diffraction, ESI-TOF mass spectrometry, fluorescence spectroscopy). For a more detailed look at these results as well as a description of the synthesis of bis(*N,N*-dimethylaminemethylene)acridine see the corresponding publication.^[1, 150] Since it is important for a solution-based sensor to understand its solution state structure, the ligand system and the metal complexes were also investigated by NMR and the corresponding findings will be highlighted in this section. *Visscher* recorded proton spectra of the three compounds $(Me_2NCH_2)_2Acr$, $[ZnBr(DMF)((Me_2NCH_2)_2Acr)]^+$ and $[CdBr_2((Me_2NCH_2)_2Acr)]^b$ by dissolving their crystals in DMSO- d_6 . While the spectrum of the ligand showed the expected signal set, the resonances of the metal complexes were highly broadened at 25 °C (for $[CdBr_2((Me_2NCH_2)_2Acr)]$ only the non-aromatic signals were broadened). Due to this broadening a sensible DOSY analysis was impossible at this temperature. Therefore, in cooperation with *Visscher*, the solvent was changed to

^a Some results of this section have been published separately: A. Visscher, S. Bachmann, C. Schnegelsberg, T. Teuteberg, R. A. Mata, D. Stalke, *Dalton Trans.* **2016**, 45, 5689-5699.^[1]

^b Sum formulae from crystal structures, for further information see reference [1].

DMF- d_7 , which made a wider temperature range accessible (-61 to 151 °C). Even though signals were still broadened at 25 °C in this solvent, temperature-dependent NMR revealed at elevated temperatures (80 °C) one definite signal set for both metal complexes, which was similar, but shifted compared to the ligand (for NMR assignments see section 4.2.7). Cooling the samples led to a splitting of the signals of the diastereotopic methyl groups and methylene protons (marked red and blue in Scheme 2-6) below the coalescence temperature (about 30 °C for the Zn^{2+} complex and 40 °C for the Cd^{2+} complex; could be slightly different for methyl and methylene groups). This dynamic behavior explains their broadened resonances at ambient temperature. The temperature-dependent measurements (from 80 °C to -40 °C) are shown for the Cd^{2+} complex in Figure 2-27 and for the Zn^{2+} complex in Figure 2-29.

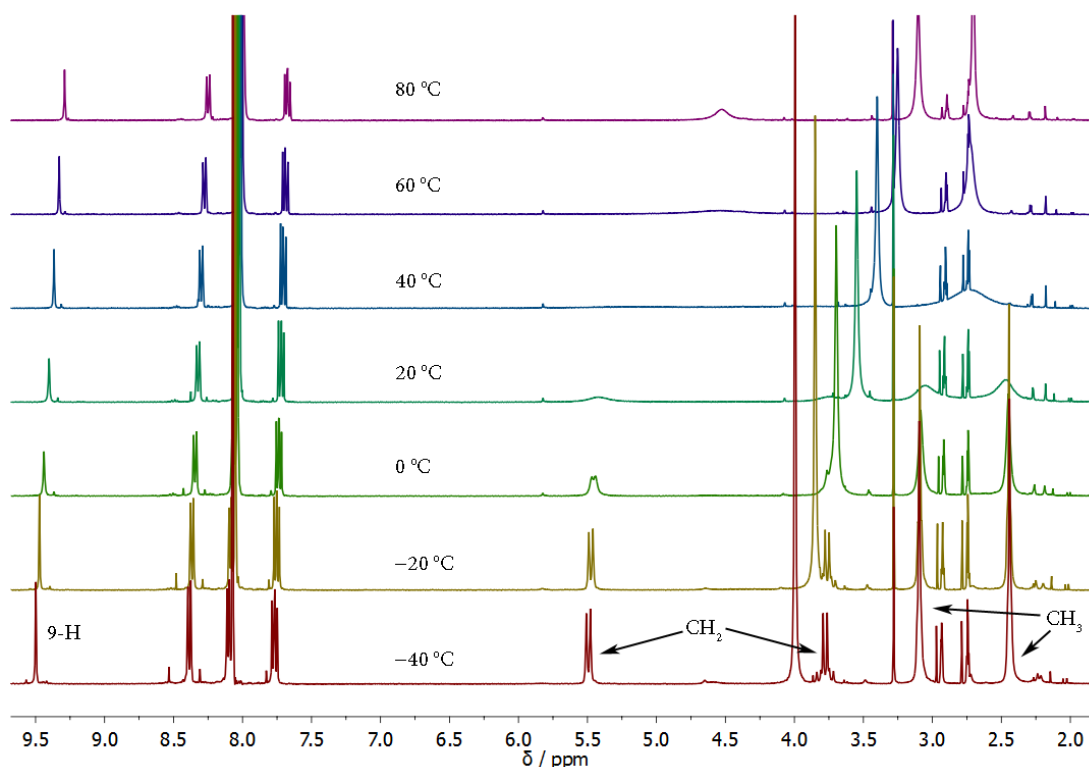


Figure 2-27: Temperature-dependent ^1H NMR spectra of $[\text{CdBr}_2((\text{Me}_2\text{NCH}_2)_2\text{Acr})]$ in $\text{DMF-}d_7$ from 80 °C to -40 °C. Coalescence temperature is at about 40 °C.

To fully ascertain the ligand binding, further experiments were conducted: For $[\text{CdBr}_2((\text{Me}_2\text{NCH}_2)_2\text{Acr})]$ couplings of the NMR-active ^{113}Cd nuclei to the methyl- and methylene-protons could be observed in a $^{113}\text{Cd},^1\text{H}$ -HMBC experiment at -30 °C (see Figure 2-28).

The chemical shift of ^{113}Cd was observed at $\delta = -345$ ppm (referenced to Me_2Cd). Only the coupling of one dihedral proton of each methylene group towards cadmium was visible, possibly due to an unfavourable angle of the related atoms which is important for the observation of vicinal couplings.^[151]

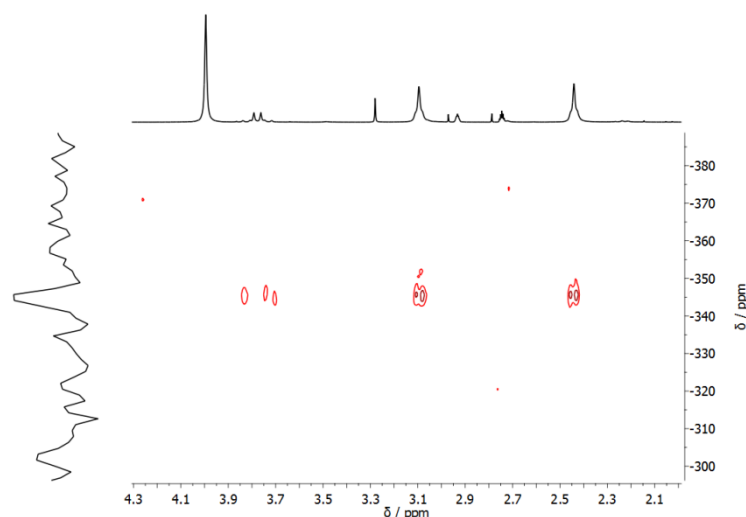


Figure 2-28: $^{113}\text{Cd},^1\text{H}$ -HMBC spectrum of $[\text{CdBr}_2((\text{Me}_2\text{NCH}_2)_2\text{Acr})]$ in $\text{DMF-}d_7$ at $-30\text{ }^\circ\text{C}$. Couplings of the ^{113}Cd nuclei to the methyl-groups and one methylene-group are visible.

Since the only NMR active nucleus for zinc (^{67}Zn) has low natural abundance (4.1%) and a large quadrupole moment, since it is a spin 5/2 nucleus, the observation of ^{15}N chemical shifts and couplings *via* $^{15}\text{N},^1\text{H}$ -HMBC experiments was the only feasible way to further attest its binding. A small but significant deshielding of $\delta = 8.6\text{ ppm}$ could be observed by comparison of the ^{15}N chemical shifts of the side-arm nitrogen of the free ligand and the metal complex.^[152] Also, for the Zn^{2+} complex the formation of additional species was observed at lower temperatures which explains why its aromatic signals are also broadened at ambient temperatures in contrast to the Cd^{2+} complex (see Figure 2-29).

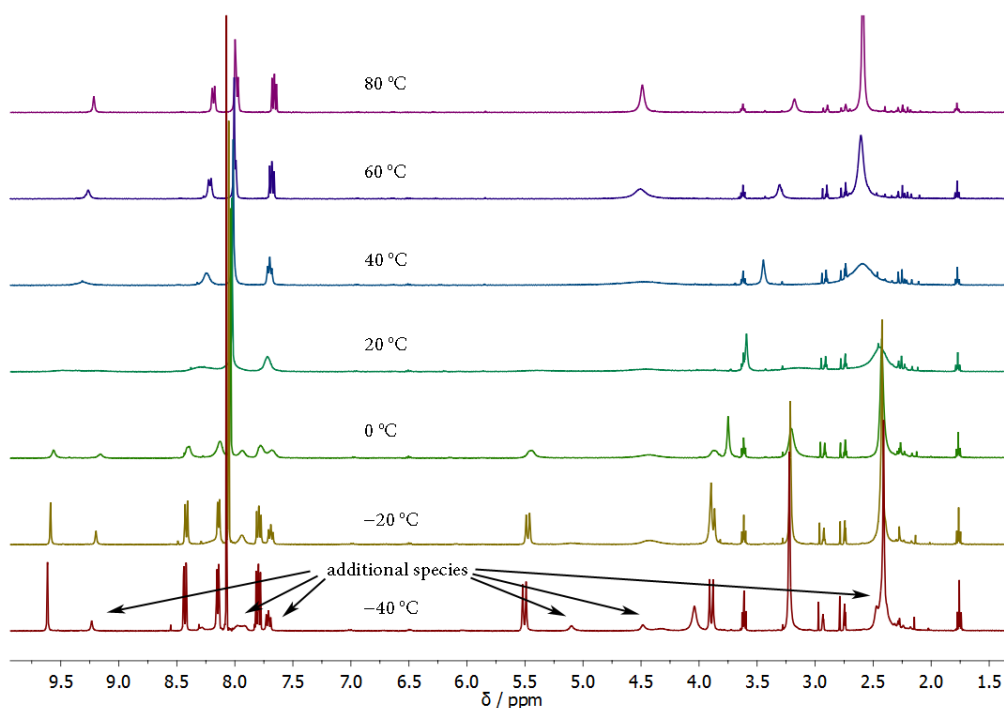


Figure 2-29: Temperature-dependent ^1H NMR spectra of $[\text{ZnBr}(\text{DMF})((\text{Me}_2\text{NCH}_2)_2\text{Acr})]^+$ in $\text{DMF-}d_7$ from $80\text{ }^\circ\text{C}$ to $-40\text{ }^\circ\text{C}$. Coalescence temperature is at about $30\text{ }^\circ\text{C}$. Additional species can be identified at lower temperatures (with an intensity maximum at about $-20\text{ }^\circ\text{C}$).

Since such species could not be observed at higher temperatures, they seem to originate from dynamical exchange processes that are slowed below the NMR timescale by cooling. A hint towards the origin of this exchange is given by the crystal structures of the metal complexes: While for $[\text{CdBr}_2((\text{Me}_2\text{NCH}_2)_2\text{Acr})]$ the Cd^{2+} is coordinated by two bromine atoms, in case of $[\text{ZnBr}(\text{DMF})((\text{Me}_2\text{NCH}_2)_2\text{Acr})]^+$ one of these bromines has been exchanged for a DMF molecule. The stronger binding of the Br^- anions towards Cd^{2+} can be explained by the HSAB theory, as Cd^{2+} is a softer metal than Zn^{2+} and hence more prone to bind the softer Br^- . Due to this observation from the solid state, it is reasonable to assume that such an exchange of bromine and solvent might also be the reason for the additional species observed at lower temperatures in the NMR spectra of the Zn^{2+} complex. Hence, to shift the corresponding equilibrium towards the brominated species, a solution of NaBr was added in excess (10 eq.) to the sample. This addition reduced the broadening of the aromatic signals at 25 °C. Furthermore, the ratio of signal intensities observed at lower temperatures for the different aggregates was reversed after the addition of NaBr (see Figure 2-30), indicating that the dominant species before has been $[\text{Zn}(\text{DMF})_2((\text{Me}_2\text{NCH}_2)_2\text{Acr})]^{2+}$.

A closer look at the methylene region of the spectrum reveals the possibility of altogether three distinct, coexisting species (**A**, **B**, **C**; see Figure 2-30), whereas for two of these species most signals seem to overlap. Since the signal intensity of **B** and **C** rose after the addition of the NaBr solution, it can be assumed that these signals belong to the brominated derivatives, probably $[\text{ZnBr}(\text{DMF})((\text{Me}_2\text{NCH}_2)_2\text{Acr})]^+$ and $[\text{ZnBr}_2((\text{Me}_2\text{NCH}_2)_2\text{Acr})]$.

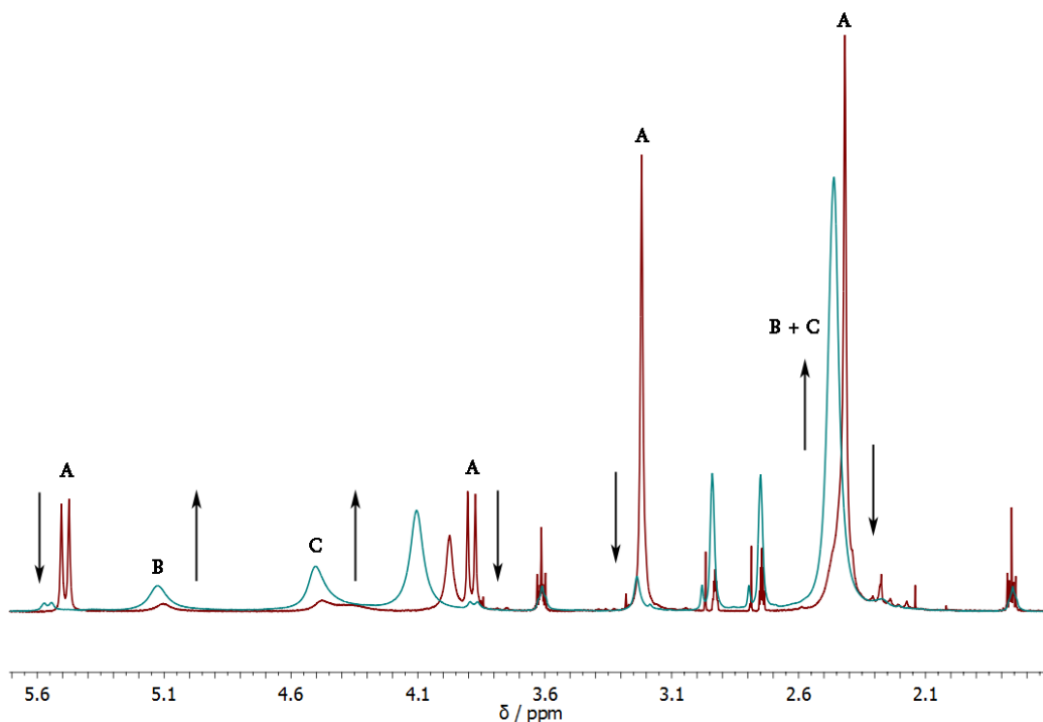


Figure 2-30: Excerpt from the superimposed ^1H NMR spectra of $[\text{ZnBr}(\text{DMF})((\text{Me}_2\text{NCH}_2)_2\text{Acr})]^+$ in $\text{DMF-}d_7$ at $-30\text{ }^\circ\text{C}$ before (red) and after the addition of 10 eq. NaBr (turquoise). The methylene region displays three sets of signals indicating three species (**A**, **B** and **C**). While the signal intensity of **A** decreases after the NaBr addition, it rises for **B/C**.

To confirm this suspicion ^1H -DOSY NMR was employed (see Figure 2-31).

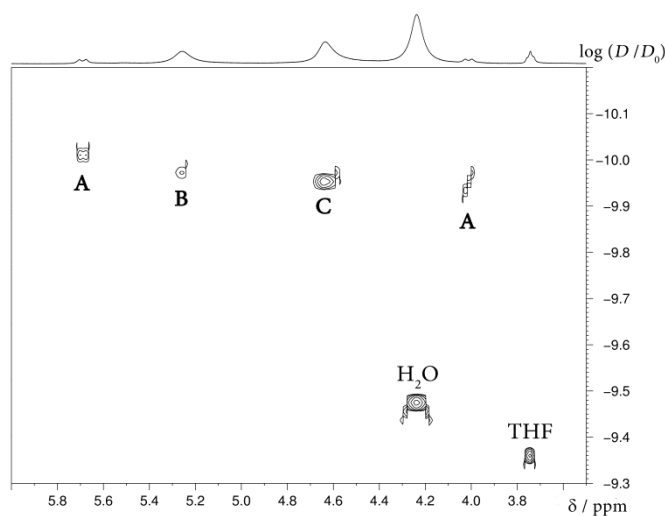


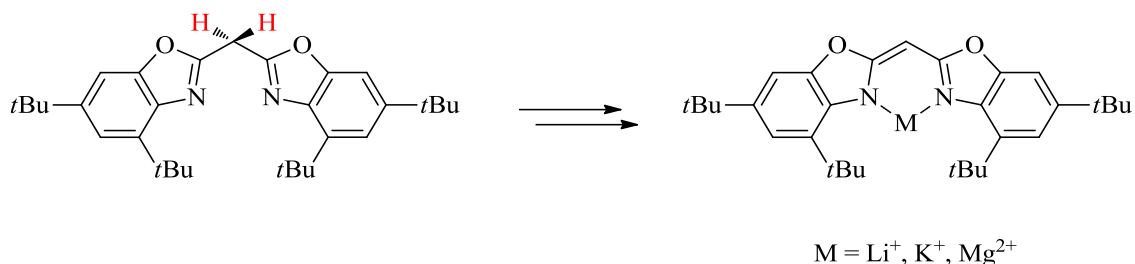
Figure 2-31: Excerpt from the ^1H -DOSY spectrum of $[\text{ZnBr}(\text{DMF})((\text{Me}_2\text{NCH}_2)_2\text{Acr})]^+$ in $\text{DMF-}d_7$ at $-30\text{ }^\circ\text{C}$ after the addition of 10 eq. NaBr . The three methylene-resonances display different diffusion coefficients which further underlines the formation of three species (A, B and C).^a ($D_0 = 1\text{ m}^2/\text{s}$)

Even though the diffusion coefficients of the different methylene signals vary only slightly, they match the tendency for size of the proposed solution state structures. Since the *van-der-Waals* volume of bromine is smaller than of DMF ($V_{\text{vdW}}(\text{Br}) = 2.74 \cdot 10^{-29}\text{ m}^3$; $V_{\text{vdW}}(\text{DMF}) = 13.1 \cdot 10^{-29}\text{ m}^3$) the largest species should be $[\text{Zn}(\text{DMF})_2((\text{Me}_2\text{NCH}_2)_2\text{Acr})]^{2+}$ which is in this case aggregate A, whereas $[\text{ZnBr}(\text{DMF})((\text{Me}_2\text{NCH}_2)_2\text{Acr})]^+$ and $[\text{ZnBr}_2((\text{Me}_2\text{NCH}_2)_2\text{Acr})]$ would be aggregates B and C, respectively. Unfortunately, no ECCs have been established for $\text{DMF-}d_7$ and therefore these findings cannot be used for *MW* predictions. However, the diffusion coefficients and the behavior of the signals after the addition of NaBr corroborate the assumptions.

2.3.2.3 Solvation of a Heterocyclic Substituted Methanide in C_6D_6

Another important aim of our group is the stabilization of low oxidation states of metals. To further foster this goal, different bisheterocyclomethanides which offer the potential to shield coordinated low-valent metal cations as well as some corresponding Group 13 metal complexes have been synthesized and characterized recently.^[153] These studies show that such ligand systems hold great potential for metal coordination and therefore offer promising opportunities for investigation. That in mind, *Köhne* synthesized the bis-(4,6-*tert*butyl-benzoxazol-2-yl)-methanide ligand $(4,6\text{-}t\text{Bu-NCOC}_6\text{H}_2)_2\text{CH}_2$; Scheme 2-7).

^a Since a high content of water was in the samples, we also tried varying this water content. This did not result in significant changes of any signals and therefore its influence can be dismissed. Elevated diffusion coefficient of water is possibly a result of hydrogen bonding.



Scheme 2-7: Structure of bis-(4,6-*tert*butyl-benzoxazol-2-yl)-methanide and its deprotonated and metalated form.

The ligand backbone can be deprotonated which enables the coordination of different metal cations by the two endocyclic nitrogen donor atoms, thus forming a six-membered ring system. This deprotonation is a good indication of a successful synthesis, as the resonance of the methanide ($\delta = 4.19$ ppm; marked red in Scheme 2-7) is shifted significantly in the ^1H NMR spectra of the metal complexes (e.g. for $[\text{Li}(4,6\text{-}t\text{Bu-NCOC}_6\text{H}_2)_2\text{CH}]$ $\delta = 5.59$ ppm; for $[\text{MgCl}_2(4,6\text{-}t\text{Bu-NCOC}_6\text{H}_2)_2\text{CH}]^-$ $\delta = 5.65$ ppm), while its integral halves. Furthermore, all other ligand signals (two doublets of the benzoxazole at $\delta = 7.39$ and 7.20 ppm as well as two singlets of the *t*Bu-groups at $\delta = 1.67$ and 1.23 ppm) shift slightly as well after metalation.

To fully characterize the resulting organometallic reagents ($[\text{Li}(4,6\text{-}t\text{Bu-NCOC}_6\text{H}_2)_2\text{CH}]$, $[\text{K}(4,6\text{-}t\text{Bu-NCOC}_6\text{H}_2)_2\text{CH}]$, $[\text{MgCl}_2(4,6\text{-}t\text{Bu-NCOC}_6\text{H}_2)_2\text{CH}]^-$ and $[\text{MgBr}_2(4,6\text{-}t\text{Bu-NCOC}_6\text{H}_2)_2\text{CH}]^-$) and understand their aggregation behavior, ECC-DOSY *MW*-estimations have been performed in cooperation with Köhne.^a All compounds have been analyzed in C_6D_6 with the internal reference TMB. Also, there were traces of THF remaining from synthesis in all samples. MW_{det} have been estimated with merged, DSE and ED ECCs. The ED ECC is in this instance helpful, as especially the protonated ligand can be described as flat rather than spherical. MW_{det} were then compared to monomeric aggregates featuring varying solvation, i.e. $[\text{M}(4,6\text{-}t\text{Bu-NCOC}_6\text{H}_2)_2\text{CH}(\text{THF})_x]$ with $x = 0\text{-}2$; $M = \text{Li}, \text{K}, \text{MgCl}_{2-x}; \text{MgBr}_{2-x}$.^b The protonated ligand has also been assumed to be monomeric, i.e. $(4,6\text{-}t\text{Bu-NCOC}_6\text{H}_2)_2\text{CH}_2$. Results are given in Table 2-20 for the most likely species (the complete set of data is given in the appendix: Table 5-57 ($(4,6\text{-}t\text{Bu-NCOC}_6\text{H}_2)_2\text{CH}_2$); Table 5-58 ($[\text{Li}(4,6\text{-}t\text{Bu-NCOC}_6\text{H}_2)_2\text{CH}]$); Table 5-59 ($[\text{K}(4,6\text{-}t\text{Bu-NCOC}_6\text{H}_2)_2\text{CH}]$); Table 5-60 ($[\text{MgCl}_2(4,6\text{-}t\text{Bu-NCOC}_6\text{H}_2)_2\text{CH}]^-$); Table 5-61 ($[\text{MgBr}_2(4,6\text{-}t\text{Bu-NCOC}_6\text{H}_2)_2\text{CH}]^-$)).

Note that the ECCs were only prepared for molecules with *MW*s of up to 600 g/mol and that some MW_{det} exceed this range. While it is straightforward that for these methanides always monomeric aggregation is preferred, the exact solvation state is in some cases not as easily determinable. For the alkali metal complexes everything points towards a threefold coordination incorporating a single THF molecule, i.e. $[\text{M}(4,6\text{-}t\text{Bu-NCOC}_6\text{H}_2)_2\text{CH}(\text{THF})]$ with $M = \text{Li}, \text{K}$. $[\text{K}(4,6\text{-}t\text{Bu-NCOC}_6\text{H}_2)_2\text{CH}]$ would also be a possibility, but is more unlikely. The preferred coordination

^a As this is an ongoing investigation for the Ph.D. thesis of Köhne, further information regarding syntheses and characterizations (e.g. individual NMR assignments and crystal structures) will not be given herein. Findings will be mentioned, if they help elucidate the solvation or aggregation state of the different molecules.

^b Dimeric aggregates can be excluded.

number of four for the alkali metals is either way not achieved, possibly due to the sterical hindrance provided by the ligand.

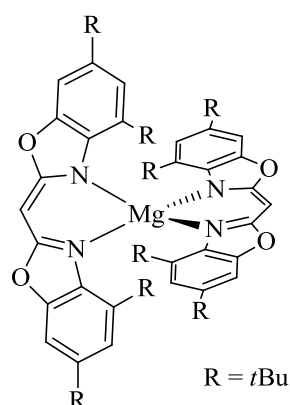
Table 2-20: ECC^{C6D6} (DSE, ED and merged) were used to predict MW_{det} of (4,6-*t*Bu-NCOC₆H₂)₂CH₂, [Li(4,6-*t*Bu-NCOC₆H₂)₂CH], [K(4,6-*t*Bu-NCOC₆H₂)₂CH], [MgCl₂(4,6-*t*Bu-NCOC₆H₂)₂CH] and [MgBr₂(4,6-*t*Bu-NCOC₆H₂)₂CH] in C₆D₆. The accuracy of the ECC^{C6D6} (DSE) is in the range of $MW_{dif} = \pm 8\%$, of the ECC^{C6D6} (ED) in the range of $MW_{dif} = \pm 6\%$ and of the ECC^{C6D6} (merged) in the range of $MW_{dif} = \pm 19\%$. Theoretical errors, as discussed in section 2.1.3, are given as standard deviations for all estimated MW s. All results in this table are from measurements at 25 °C. MW_{dif} is given for most likely monomeric aggregates for either DSE or ED ECCs.

Possible aggregate(s)	MW_{calc}	MW_{det}	MW_{det}	MW_{det}	MW_{dif}
	[g/mol]	(merged) [g/mol]	(DSE) [g/mol]	(ED) [g/mol]	[%]
(4,6- <i>t</i> Bu-NCOC ₆ H ₂) ₂ CH ₂	475	607 ± 51	545 ± 30	483 ± 61	-2 (ED)
[Li(4,6- <i>t</i> Bu-NCOC ₆ H ₂) ₂ CH(THF)]	553	643 ± 55	575 ± 32	503 ± 64	-4 (DSE)
[K(4,6- <i>t</i> Bu-NCOC ₆ H ₂) ₂ CH]	513	620 ± 52	556 ± 31	490 ± 62	-8 (DSE)
[K(4,6- <i>t</i> Bu-NCOC ₆ H ₂) ₂ CH(THF)]	585				5 (DSE)
[MgCl ₂ (4,6- <i>t</i> Bu-NCOC ₆ H ₂) ₂ CH] ⁻	569	685 ± 59	609 ± 34	527 ± 67	-7 (DSE)
[MgCl(4,6- <i>t</i> Bu-NCOC ₆ H ₂) ₂ CH(THF)]	606				-1 (DSE)
[Mg(4,6- <i>t</i> Bu-NCOC ₆ H ₂) ₂ CH(THF) ₂] ⁺	642				5 (DSE)
[MgBr(4,6- <i>t</i> Bu-NCOC ₆ H ₂) ₂ CH(THF)]	650	715 ± 62	634 ± 36	544 ± 70	3 (DSE)
[Mg(4,6- <i>t</i> Bu-NCOC ₆ H ₂) ₂ CH(THF) ₂] ⁺	642				1 (DSE)

For the magnesium compounds a coordination number of four was postulated leading to aggregates like [MgHal_{2-x}(4,6-*t*Bu-NCOC₆H₂)₂CH(THF)_x] with Hal = Cl, Br. However, the [MgBr₂(4,6-*t*Bu-NCOC₆H₂)₂CH]⁻ aggregate can be disregarded, since it displays elevated MD_W . All other possible aggregates shown in Table 2-20 do not (the complete set of MD_W calculations is given in the appendix: Table 5-63). Other than that, all listed magnesium aggregates seem based on the estimated MW s theoretically possible.

To elucidate the exact solvation of [MgCl₂(4,6-*t*Bu-NCOC₆H₂)₂CH]⁻, the normalized diffusion coefficient of THF in the measured sample was determined ($\log(D_{x,norm}) = -8.9318$) and compared with the normalized diffusion coefficient of separately measured free THF ($\log(D_{x,norm}) = -8.6371$) and the [MgCl₂(4,6-*t*Bu-NCOC₆H₂)₂CH(THF)_x]⁻ aggregate ($\log(D_{x,norm}) = -9.2020$). Integration showed that approximately 1.25 eq. THF were in the sample altogether. Out of this amount of THF, about 50% coordinated based on the elevated diffusion coefficients compared to the diffusion coefficient of a pure THF solution and to the diffusion coefficient of the metal complex. Another sample was prepared with approximately 2.75 eq. THF which showed that about 55% aided in the solvation of the metal complex. In both cases the number of coordinating THF molecules is between 0 and 2, as proposed by the ECC calculations. It seems to be a defined equilibrium, wherein possibly a chloride is exchanged by THF, whereas always about 50% of the available THF is involved. In the future, it might be interesting to further vary the THF concentration and see if a saturation is achieved after a certain amount. Also, the addition of e.g. NaCl may help direct the equilibrium towards the chlorinated species and thus provide further insights. Similar experiments can be envisioned for the brominated reagent.

Lastly, the stabilization of low oxidation states was the aim of the synthesis of these structures. Therefore, *Köhne* tried reducing the $[\text{MgCl}_2(4,6\text{-}t\text{Bu-NCO}_6\text{H}_2)_2\text{CH}]^-$ compound. The resulting reaction mixture was also investigated with ECC-DOSY and showed elevated diffusion coefficients for the resulting reagent, whereas other spectroscopic data (chemical shifts) did not vary significantly. The estimated *MW*s were 993 ± 90 g/mol for the merged ECC and 857 ± 50 g/mol for the DSE ECC. Both exceed 600 g/mol and it was therefore questionable how accurate an ECC-*MW* estimation could be. *Köhne* also investigated the molecule by the LIFDI-MS technique (LIFDI = liquid injection field desorption ionization) and could show that the aggregate is not the expected reduced species, but rather $[\text{Mg}((4,6\text{-}t\text{Bu-NCO}_6\text{H}_2)_2\text{CH})_2]$ (see Scheme 2-8) with a MW_{calc} of 972 g/mol.



Scheme 2-8: Structure of bis-(bis-(4,6-*tert*butyl-benzoxazol-2-yl)-methanide)-magnesium.

This aggregate corresponds well with the *MW* estimated by the merged ECC. While the synthesis of this aggregate was not the envisioned reduced species, it still was an important result to show the limits of the shape-optimized ECCs. These do not work, when the *MW* range of the model compounds is exceeded. However, the merged ECC seems to be reliable. Note that this is only a single result and the usability of the ECC *MW*-prediction for bigger aggregates needs to be investigated further to make a conclusion.

3 SUMMARY & OUTLOOK

The focus of this thesis has been the development and application of a high-resolution NMR spectroscopic diffusion-based technique, i.e. external calibration curve DOSY (ECC-DOSY), for molecular weight (MW) estimation of solutes. In the three parts of this thesis, it was not only possible to augment this technique by many important features, but also to explain and alleviate some of the pitfalls of the methodology as well as to unambiguously solve solution state structures of different organometallic reagents and precursor molecules.

In the first part of this thesis, the applicability of ECC-DOSY was severely improved by the addition of new ECCs for seven commonly used deuterated solvents, namely chloroform- d_1 , dichloromethane- d_2 , benzene- d_6 , dimethylsulfoxide- d_6 , cyclohexane- d_{12} , acetonitrile- d_3 and methanol- d_4 to enable MW predictions. Merged as well as three semi-empirically shape-optimized ECCs could be established for each solvent, utilizing the normalized diffusion coefficients of up to 31 model compounds with a MW -range of 70 to 600 g/mol. These normalized diffusion coefficients are the first step towards solvent-dependent normalized diffusion coefficient databases. The need for such databases or at least for the increase of the overall reference count could be shown in this work, as the misconception of a single unsuited reference has led for some solvents (DMSO and cyclohexane) to reduced fit qualities of their corresponding ECCs. Fortunately, this model compound ($\text{Si}(\text{OMe})_4$) could be identified after careful evaluation. Furthermore, not only the diversification of the overall references has to be improved, but also the empirical categorization process. Hence, a more theoretical approach to categorization was tested utilizing the calculation of principal moments of inertia. While this molecular property seems feasible to distinguish very spherical and linear molecules, the minute changes in molecular shape that most of the herein-used model compounds exhibited cannot be described reasonably well.

However, overall ECCs are shown to be very accurate even without any categorization. Empirical deviations of predicted MW_{det} compared to theoretical MW_{calc} did not exceed a maximum of 29% for the merged ECCs. Average deviations (and deviations of shape-optimized ECCs) are in most cases much better. To further underline the method's accuracy, theoretical error calculations were performed. In most cases, these corresponded well with the empirical deviations, however, in a few cases a possible underestimation of errors might be conceivable, if just the empirical deviations were considered. Additionally, the influence of molecular densities (MD_w) was discussed and in cooperation with *Kreyenschmidt* a method was developed which might prevent MD_w -related errors in the future, as it entails the application of a MD_w -based correctional factor X_{cor} to normalized diffusion coefficients.^[124] However, this approach has one setback, the need to predict the solution state structure of a solute *a priori*. All these improvements to the methodology are or will be implemented in a software application that hopefully widens the audience of ECC-DOSY. They are also shown schematically in Figure 3-1.

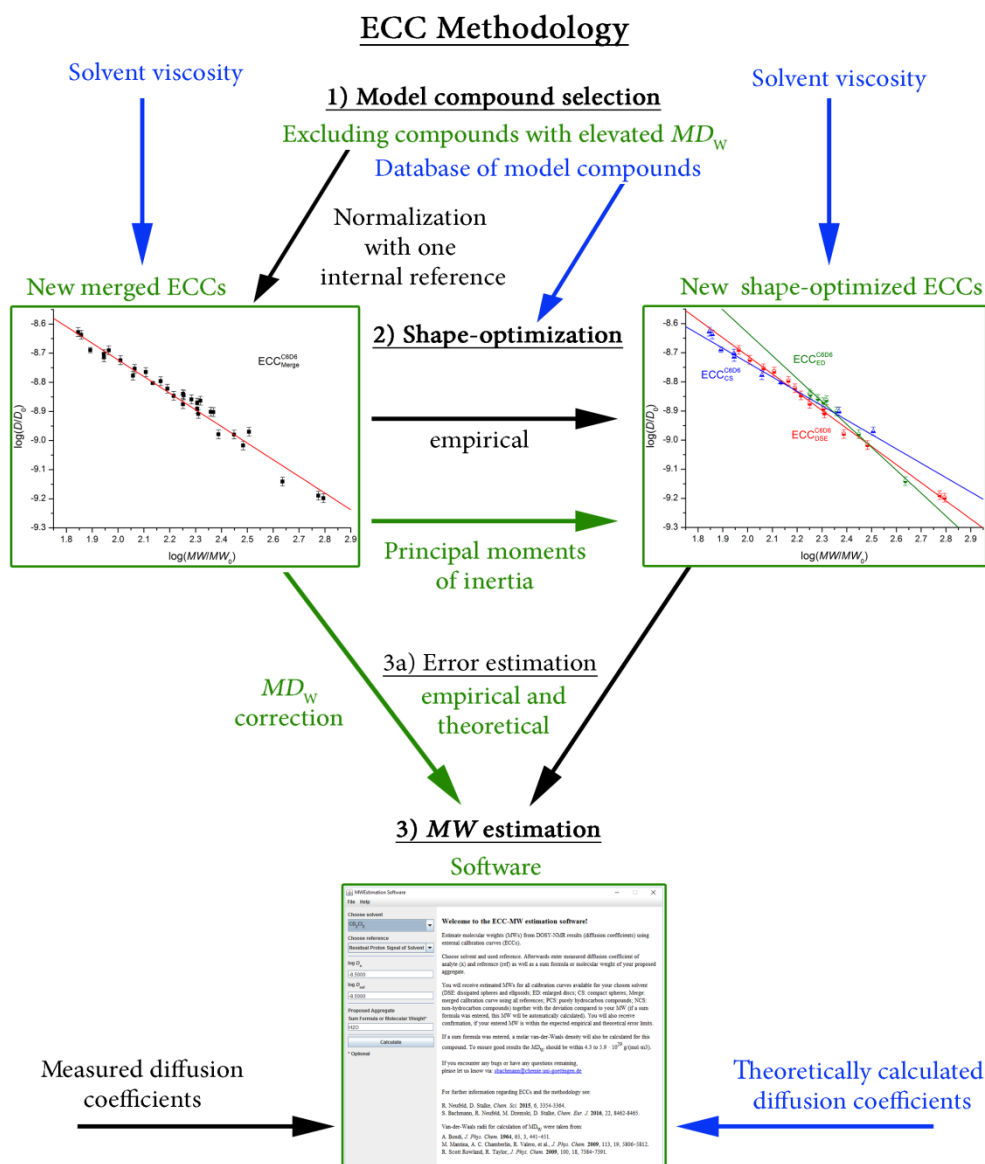


Figure 3-1: Schematic representation of the ECC-DOSY-MW estimation process. Highlighted green are improvements and implementations of this work, whereas blue objects are proposed additions for the future.

As of now, only measured diffusion coefficients are considered in the MW prediction, however, as calculation prowess improves, theoretically calculated diffusion coefficients might end up being an important addition. Furthermore, a so-called universal calibration curve (UCC) has surfaced very recently in the polymer community which incorporates solvent viscosity for MW estimations and hence eliminates the need to distinguish solvent environments.^[154] However, this method seemed to be less accurate for small molecules. Still, if solvent viscosity can be implemented into the ECC methodology in the future, it could streamline the entire process and with the data gathered in this work, it might also be possible to detect aberrations beyond viscosity-related effects. There are such aberrations, else all ECCs with the same references should not vary in their α parameters.

In the second part of this thesis, the applicability of ECC-DOSY was demonstrated on a widely-used group of organometallic precursors, i.e. alkali metal cyclopentadienides (CpMs, with $M = \text{Li, Na, K, Rb and Cs}$). These reagents were characterized in THF and DMSO. CpLi was also

investigated in ammonia solution. While in the solid state most of these reagents form polymeric chains, even in some cases with donating solvents (e.g. $[\text{CpNa}(\text{TMEDA})]_{\infty}$ ^[52]), the results gathered in this thesis suggest that in THF they are fully disaggregated into monomers. The same observation was made for some methylated cyclopentadienide derivatives (MeCpLi, Cp^{*}K and Cp^{*}Cs). Even at different temperatures these species stay intact. This was shown for CpLi which was investigated for a temperature range from 50 °C to -100 °C. The only exception was CpCs which displayed oligomeric aggregation in THF, forming an aggregate of $MW_{\text{det}} > 1500$ g/mol which goes far beyond the MW range of measured model compounds. With ECC estimations the degree of solvation could also be determined and the solution state structures of all CpMs depicted in Figure 3-2 show the best accordance of theoretical and experimental MW s.

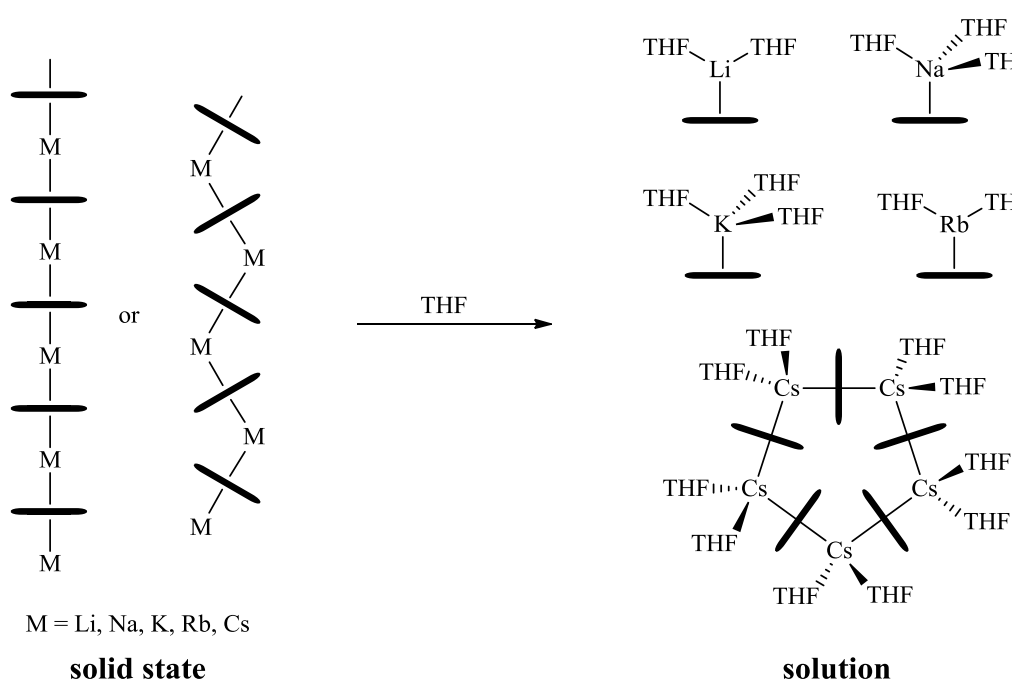
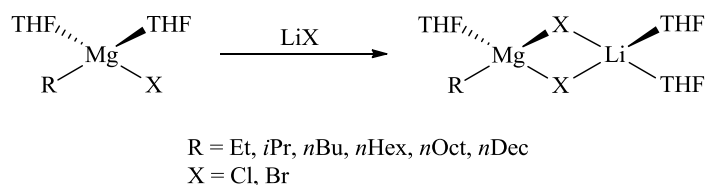


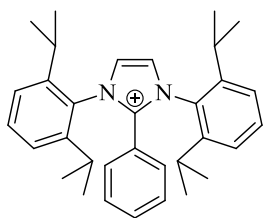
Figure 3-2: Disaggregation of polymeric alkali metal cyclopentadienides after solvation and the corresponding solution state structures in THF-*d*₈ proposed after investigation by ECC-DOSY.

While CpMs formed solely contact ion pairs (CIPs) in THF, which could also be underlined by the comparison of diffusion coefficients gathered from ¹H- and ⁷Li-DOSY experiments for CpLi, inDMSO and ammonia, where they seem to form solvent-separated ion pairs (SSIPs). Unfortunately, MW estimations did not result in reasonable structures; possibly due to dynamic exchange processes that average diffusion coefficients. However, through ⁷Li,¹H-HOESY and diffusion coefficient comparison the formation of SSIPs can at least for CpLi be confirmed. For the other CpMs a comparison of normalized diffusion coefficients showed the same behavior as observed for CpLi, therefore SSIPs are also most likely. Proceeding, it might be a good idea to take a closer look at the methylated derivatives, since it could already be shown that Cp^{*}Cs behaves differently to CpCs. Also, other solvent environments may present an interesting opportunity for investigation.

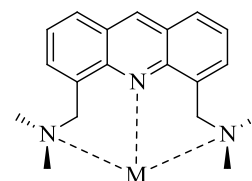
In the third and final chapter, NMR spectroscopy in general and diffusion-based approaches were used to solve ambiguities about solution state structures of different organometallic compounds or their precursors provided by collaborators (see Scheme 3-1).



**Alkyl *Grignard* reagents
as well as "turbo" analogues**

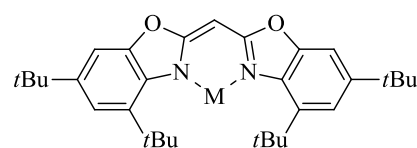


***N*-Heterocyclic carbene**



M = Zn²⁺, Cd²⁺

Acridine-based molecular sensor



M = Li⁺, K⁺, Mg²⁺

Heterocyclic substituted methanide

Scheme 3-1: Illustration of the different research areas discussed in the final part of this thesis.

Firstly, alkyl *Grignard* systems were shown to form monomers in THF solution, i.e. $[\text{RMgX}(\text{THF})_2]$ with R = Et, *i*Pr, *n*Bu, *n*Hex, *n*Oct and *n*Dec and X = Cl (for R = *n*Bu, X = Cl, Br). The clear preference of this solvation state could be shown through the establishment of further shape-optimized ECCs specialized for linear or rod-like molecules. Important to note is in this regard the ability to differentiate suitable model compounds by principle moment of inertia calculations. Furthermore, the influence of metal halides on these *Grignard* systems was elucidated exemplary for $[\text{nBuMgX} \cdot \text{LiX}]$ (X = Cl, Br). It can be concluded that the addition of LiX leads to the formation of *ate* complexes at least to some degree which *Knochel et al.* proposed previously.^[142] In the investigation of these conventional alkyl *Grignard* reagents, the importance of the combination of different analytical techniques could also be emphasized, e.g. by comparison of findings from NMR spectroscopy to ESI-MS (see Figure 3-3).



Figure 3-3: Frontispiece associated to “Association and Dissociation of Grignard Reagents $RMgCl$ and Their Turbo Variant $RMgCl \cdot LiCl$ ” published in *Chem. Eur. J.* **2016**, *22*, 7752-7762.^[3]

Additionally, solvent- and anion coordination were investigated for a multitude of different reagents: Ranging from an *N*-heterocyclic carbene that displayed interactions with a wide range of anions over an acridine-based fluorophore and its metal complexes which could be investigated *via* NMR and whose Zn^{2+} metal complex displayed an anion-solvent exchange equilibrium to an heterocyclic substituted methanide that not only showed concentration dependent solvent coordination, but also an aggregate that exceeded the recommended *MW* range and could therefore be used to rationalize the suitability of the ECCs for higher aggregates.

4 EXPERIMENTAL PART

4.1 Techniques and Experiments

4.1.1 Handling of Air- and Moisture-Sensitive Compounds

All experiments were performed either in an inert gas atmosphere of purified dry argon with standard *Schlenk* techniques^[9] or in an argon glove box. Glassware was dried at 130 °C, assembled hot and cooled down under vacuum. All solvents were dried over sodium-potassium alloy, sodium or potassium, distilled and degassed prior to use. Dicyclopentadiene was purchased from Fluka, thermally cracked and distilled directly before use at 170 °C and ambient pressure. The methylcyclopentadiene dimer was purchased from Sigma-Aldrich, also thermally cracked and distilled directly before use at 72 °C and ambient pressure. Other starting materials were either purchased commercially or synthesized according to known literature procedures and stored under inert atmosphere. *n*-Butyllithium was kindly donated by Rockwood Lithium and was filtered through Celite® before use, along with the determination of the concentration.^[155] Deuterated solvents for NMR measurements of organometallic compounds were kept in an argon glove box over 3 Å molecular sieves over a minimum of one week prior to use. THF-*d*₈ for alkyl *Grignard* measurements was dried over potassium and distilled prior to use.

4.1.2 NMR Techniques and Experiments

All NMR spectra were recorded either on a Bruker Avance III 400 MHz spectrometer with a BBFO (broadband-observe) probe, *z*-gradient (maximum gradient strength of 57 G/cm) and temperature unit or on a Bruker Ascend 400 MHz spectrometer with a BBI (broadband-inverse) probe, *z*-gradient (maximum gradient strength of 51 G/cm) and temperature unit. All samples were prepared using 5 mm NMR tubes made of borosilicate glass. NMR spectra were measured with diluted solutions (0.015 - 0.025 M) at ambient temperature, if not indicated otherwise. All relevant parameters regarding 1D and 2D experiments are given in Table 4-1.

Diffusion experiments (¹H- and ⁷Li-DOSY) were performed exclusively with the pulse program *dstebpgp3s*^[156] (double-stimulated echo sequence in combination with bipolar gradient pulses) employing a linear gradient ramp incremented from 2 to 98% of the maximum gradient strength, 16 dummy scans (ds) and 16 scans on 32K data points. This pulse program effectively reduces eddy-current distortions and dephasing due to convection which arises mostly at elevated temperatures due to heating that can lead to a temperature gradient along the main axis of the spectrometer. However, turbulent convection cannot be compensated by this pulse program. The relevant delays for ¹H-diffusion experiments were $\Delta = 0.1$ s and $\delta = 1.0 - 8.0$ ms, whereas for ⁷Li-DOSY measurements they were $\Delta = 0.06 - 0.08$ s and $\delta = 2.0 - 8.5$ ms. To achieve ideal signal attenuation, Δ or δ were adjusted and 1D spectra (*dstebpgp3s1d*) that only varied in their gradient

strength (either 5% or 95%) were recorded and compared. This was repeated until the signal attenuation was within a reasonable region. The delay for gradient recovery was 0.2 ms and the eddy-current delay 5 ms. Furthermore, all diffusion measurements were performed without sample spinning.

Table 4-1: Parameters of all conducted 1D and 2D NMR experiments.

Experiment	Pulse program	Number of scans	Acquisition time [s]
¹ H	zg30	8 – 16	4.9 - 5.1
¹³ C{ ¹ H}	zgdc30	256 – 1024	1.3 - 1.4
⁶ Li	zg30	128	1.1
⁷ Li	zg30	128	1.1
²³ Na	zg	16	19.3
¹³³ Cs	zg	64 – 256	0.1 – 3.2
¹ H, ¹ H-COSY	cosygppqf	1 (16 ds)	0.2
¹ H, ¹³ C-HSQC	hsqcedgpph	2 (16 ds)	0.2
¹ H, ¹³ C-HMBC	hmbcgplpndqf	2 (16 ds)	0.2
¹ H, ¹⁵ N-HMBC	hmbcgplpndqf	2 - 40 (16 ds)	0.1 - 0.2
¹ H, ¹¹³ Cd-HMBC	hmbcgplpndqf	2	0.2
¹ H, ⁷ Li-HOESY	hoesyph	16 - 32 (16 ds)	0.5 - 2.6 (mixing time 0.5 - 1.7 s)

All spectra were processed with Topspin 3.1, MestReNova 6.02 or MestReNova 10.1. Diffusion coefficients from DOSY experiments were calculated with the T1/T2 software of Topspin 3.1 utilizing *Gaussian* fits. Chemical shifts (δ) are given in ppm relative to TMS, either using the residual solvent signals^[157] or tabulated frequency ratios as internal standards. Coupling constants (J) are reported in Hz and standard abbreviations indicating multiplicity are used as follows: s = singlet, d = doublet, t = triplet, m = multiplet, br = broad. Combined abbreviations are derived from their components (e.g. dd = doublet of doublets).

4.1.3 DOSY Sample Preparation and Evaluation

Samples for DOSY NMR measurements were prepared by addition of equimolar amounts of one of the following internal references: 1,2,3,4-tetraphenylnaphthalene (TPhN), 2,2,3,3-tetramethylbutane (TMB) or adamantane (Adam). For all measurements, the diffusion coefficients of the analytes were normalized to the fixed diffusion coefficients of one of these references which are listed in Table 2-1 or given in the appendix.

4.1.4 Computation of Principal Moments of Inertia

Principal moments of inertia of different model compounds were calculated using PMIFST 16a.IT.2016^[122] (Principal Moments of Inertia From Molecular Structures) with force-field (MMFF94) optimized structures generated by Avogadro 1.0.3.

4.1.5 Programming in Java

An ECC-*MW* estimation software was programmed to make the methodology of ECC-DOSY more accessible (for more information see section 2.1.5). The software is available for download at:

<http://www.stalke.chemie.uni-goettingen.de/mwestimation/>

To achieve a maximum system interoperability, the software was implemented in Oracle's object-oriented programming language Java. Java uses a so-called Java virtual machine (JVM) which can run bytecode and needs to be installed on the computer that launches the application. The bytecode itself was created by compiling the Java code with the help of the Java compiler. With the combination of JVM and the system independent bytecode it is possible to run the software on a wide range of operating systems, including, but not limited to, Windows®, MacOS® and Linux. The source code of the program can be shared upon request.

4.2 Syntheses and Characterizations

4.2.1 Syntheses and Characterizations of CpMs (M = Li, Na, K, Rb, Cs)

4.2.1.1 Synthesis and Characterization of CpLi

Cyclopentadienyllithium (CpLi) was prepared following a preparation route similar to *Olbrich's*^[54] and *Wagner's*^[158]. It was synthesized by lithiation of freshly distilled CpH (0.45 mL, 5.50 mmol, 1.16 eq.; from dicyclopentadiene see 4.1.1) with *n*BuLi (4.74 M in hexane, 1.00 mL, 4.74 mmol, 1.00 eq.) at 0 °C in THF (50 mL). The colorless reaction mixture was stirred for 10 h and after evaporation of the solvent CpLi was received as a white powder (0.34 g, 4.72 mmol, 99%) and dried *in vacuo*. For NMR measurements in NH₃, gaseous NH₃ was introduced into the NMR tube for one minute at -78 °C; afterwards 0.1 mL of toluene-*d*₈ was added for referencing and after sealing the NMR tube spectra were recorded at 25 °C.

Sum formula: C₅H₅Li
Molecular weight: 72.04 g/mol



Dissolving the compound in different solvents (DMSO-*d*₆, THF-*d*₈, NH₃) resulted in different solution state structures and therefore different chemical shifts:

(THF-*d*₈):

Proposed aggregate: [C₅H₅Li(THF)₂]
Sum formula: C₁₃H₂₁O₂Li
Molecular weight: 216.25 g/mol

¹H NMR

(400.13 MHz, THF-*d*₈): δ = 5.69 (s, 5 H, 5 CH) ppm.

¹³C{¹H} NMR

(100.62 MHz, THF-*d*₈): δ = 103.4 (s, 5 C, 5 CH) ppm.

⁷Li NMR

(155.51 MHz, THF-*d*₈): δ = -7.75 (s) ppm.

(DMSO-*d*₆):

¹H NMR

(400.13 MHz, DMSO-*d*₆): $\delta = 5.33$ (s, 5 H, 5 CH) ppm.

¹³C{¹H} NMR

(100.62 MHz, DMSO-*d*₆): $\delta = 103.0$ (s, 5 C, 5 CH) ppm.

⁷Li NMR

(155.51 MHz, DMSO-*d*₆): $\delta = -1.07$ (s) ppm.

(NH₃):

¹H NMR

(400.13 MHz, NH₃): $\delta = 5.89$ (s, 5 H, 5 CH) ppm.

¹³C{¹H} NMR

(100.62 MHz, NH₃): $\delta = 104.1$ (s, 5 C, 5 CH) ppm.

⁷Li NMR

(155.51 MHz, NH₃): $\delta = -0.59$ (s) ppm.

4.2.1.2 Synthesis and Characterization of CpNa

Cyclopentadienylsodium (CpNa) was prepared following a preparation route similar to Olbrich's^[54]. It was synthesized by addition of freshly distilled CpH (0.90 mL, 10.80 mmol, 1.08 eq.; from dicyclopentadiene see 4.1.1) to a suspension of NaH (0.24 g, 10.00 mmol, 1.00 eq.) in Et₂O (50 mL) at ambient temperature. The reaction mixture was stirred for 24 h and turned light pink in the process. After filtration, cyclopentane (10 mL) and pentane (20 mL) were added to the filtrate and the product was crystallized at -28 °C. The white crystals (0.64 g, 7.27 mmol, 73%) were filtered, washed with cold pentane and dried *in vacuo*.

Sum formula: C₅H₅Na
Molecular weight: 88.08 g/mol



Dissolving the compound in different solvents (DMSO-*d*₆, THF-*d*₈) resulted in different solution state structures and therefore different chemical shifts:

(THF-*d*₈):

Proposed aggregate: [C₅H₅Na(THF)₃]

Sum formula: C₁₇H₂₉O₃Na

Molecular weight: 304.40 g/mol

¹H NMR

(400.13 MHz, THF-*d*₈): δ = 5.72 (s, 5 H, 5 CH) ppm.

¹³C{¹H} NMR

(100.62 MHz, THF-*d*₈): δ = 103.3 (s, 5 C, 5 CH) ppm.

²³Na NMR

(105.84 MHz, THF-*d*₈): δ = -28 to -31 (s_{br}) ppm.

(DMSO-*d*₆):

¹H NMR

(400.13 MHz, DMSO-*d*₆): δ = 5.35 (s, 5 H, 5 CH) ppm.

¹³C{¹H} NMR

(100.62 MHz, DMSO-*d*₆): δ = 103.0 (s, 5 C, 5 CH) ppm.

²³Na NMR

(105.84 MHz, DMSO-*d*₆): δ = -1 to -4 (s_{br}) ppm.

4.2.1.3 Synthesis and Characterization of CpK

Cyclopentadienylpotassium (CpK) was prepared by addition of freshly distilled CpH (0.96 g, 14.50 mmol, 1.00 eq.; from dicyclopentadiene see 4.1.1) to a solution of freshly cut potassium (2.3 g, 58.8 mmol, 4.1 eq.) in Et₂O (15 mL). After stirring the reaction mixture for 10 h and filtration of unreacted potassium, hexane (10 mL) was added. The product precipitated as a white solid (0.33 g, 3.17 mmol, 22%) and was filtered and dried *in vacuo*.

Sum formula: C₅H₅K
Molecular weight: 104.19 g/mol



Dissolving the compound in different solvents (DMSO-*d*₆, THF-*d*₈) resulted in different solution state structures and therefore different chemical shifts:

(THF-*d*₈):

Proposed aggregate: [C₅H₅K(THF)₃]
Sum formula: C₁₇H₂₉O₃K
Molecular weight: 320.51 g/mol

¹H NMR

(400.13 MHz, THF-*d*₈): δ = 5.63 (s, 5 H, 5 CH) ppm.

¹³C{¹H} NMR

(100.62 MHz, THF-*d*₈): Due to low solubility no resonance could be detected.

(DMSO-*d*₆):

¹H NMR

(400.13 MHz, DMSO-*d*₆): δ = 5.39 (s, 5 H, 5 CH) ppm.

¹³C{¹H} NMR

(100.62 MHz, DMSO-*d*₆): δ = 103.2 (s, 5 C, 5 CH) ppm.

4.2.1.4 Synthesis and Characterization of CpRb

Cyclopentadienylrubidium (CpRb) was prepared by addition of freshly distilled CpH (0.06 mL, 0.73 mmol, 1.06 eq.; from dicyclopentadiene see 4.1.1) to a stirred and cooled (0 °C) solution of RbHMDS (0.17 g, 0.69 mmol, 1.00 eq.) in THF (10 mL). After heating to ambient temperature and stirring for another hour, pentane (15 mL) was added. The product precipitated as a light brown solid (0.09 g, 0.6 mmol, 87%) and was filtered and dried *in vacuo*.

Sum formula: C_5H_5Rb
Molecular weight: 150.56 g/mol



Dissolving the compound in different solvents (DMSO- d_6 , THF- d_8) resulted in different solution state structures and therefore different chemical shifts:

(THF- d_8):

Proposed aggregate: $[C_5H_5Rb(THF)_2]$

Sum formula: $C_{13}H_{21}O_2Rb$

Molecular weight: 294.77 g/mol

1H NMR

(400.13 MHz, THF- d_8): $\delta = 5.61$ (s, 5 H, 5 CH) ppm.

$^{13}C\{^1H\}$ NMR

(100.62 MHz, THF- d_8): Due to low solubility no resonance could be detected.

(DMSO- d_6):

1H NMR

(400.13 MHz, DMSO- d_6): $\delta = 5.38$ (s, 5 H, 5 CH) ppm.

$^{13}C\{^1H\}$ NMR

(100.62 MHz, DMSO- d_6): $\delta = 103.3$ (s, 5 C, 5 CH) ppm.

4.2.1.5 Synthesis and Characterization of CpCs

Cyclopentadienylcaesium (CpCs) was prepared by addition of freshly distilled CpH (0.06 mL, 0.73 mmol, 1.06 eq.; from dicyclopentadiene see 4.1.1) to a stirred and cooled (0 °C) solution of CsHMDS (0.20 g, 0.69 mmol, 1.00 eq.) in THF (10 mL). After heating to ambient temperature and stirring for another hour, pentane (15 mL) was added. The product precipitated as a light brown solid (0.11 g, 0.56 mmol, 81%) and was filtered and dried *in vacuo*.

Sum formula: C_5H_5Cs
Molecular weight: 198.00 g/mol



Dissolving the compound in different solvents (DMSO- d_6 , THF- d_8) resulted in different solution state structures and therefore different chemical shifts:

(THF- d_8):

1H NMR

(400.13 MHz, THF- d_8): $\delta = 5.55$ (s, 5 H, 5 CH) ppm.

$^{13}C\{^1H\}$ NMR

(100.62 MHz, THF- d_8): $\delta = 107.0$ (s, 5 C, 5 CH) ppm.

^{133}Cs NMR

(52.48 MHz, THF- d_8): $\delta = -240.1$ (s) ppm.

(DMSO- d_6):

1H NMR

(400.13 MHz, DMSO- d_6): $\delta = 5.41$ (s, 5 H, 5 CH) ppm.

$^{13}C\{^1H\}$ NMR

(100.62 MHz, DMSO- d_6): $\delta = 103.9$ (s, 5 C, 5 CH) ppm.

^{133}Cs NMR

(52.48 MHz, DMSO- d_6): $\delta = -14.7$ (s) ppm.

4.2.2 Synthesis and Characterization of MeCpLi

4.2.2.1 Synthesis and Characterization of MeCpLi

Methylcyclopentadienyllithium (MeCpLi) was prepared by lithiation of freshly distilled methylcyclopentadiene (1.68 g, 21.00 mmol, 1.20 eq.; from methylcyclopentadiene dimer see 4.1.1) with *n*BuLi (4.74 M in hexane, 3.40 mL, 17.50 mmol, 1.00 eq.) at 0 °C in THF (50 mL). After heating to ambient temperature, hexane (10 mL) was added to the solution. The product precipitated as a white solid (1.63 g, 18.94 mmol, 90%) and was filtered and dried *in vacuo*. Carbon and hydrogen atoms are numbered according to IUPAC.

Sum formula: C_6H_8Li
Molecular weight: 86.06 g/mol



Proposed aggregate: $[C_6H_8Li(THF)_2]$
Sum formula: $C_{14}H_{23}O_2Li$
Molecular weight: 230.27 g/mol

1H NMR

(400.13 MHz, THF- d_6): $\delta = 5.51$ to 5.48 (m, 2 H, H-3, H-4), 5.47 to 5.44 (m, 2 H, H-2, H-5), 2.11 (s, 3 H, CH₃) ppm.

$^{13}C\{^1H\}$ NMR

(100.62 MHz, THF- d_6): $\delta = 113.8$ (C1), 103.8 (C2, C5), 102.4 (C3, C4), 15.6 (CH₃) ppm.

7Li NMR

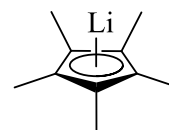
(155.51 MHz, THF- d_6): $\delta = -7.60$ (s) ppm.

4.2.3 Syntheses and Characterizations of Cp^{*}M (M = Li, K, Cs)

4.2.3.1 Synthesis of Cp^{*}Li

Pentamethylcyclopentadienyllithium (Cp^{*}Li) was prepared following a preparation route similar to Robbins^[159]. It was synthesized by lithiation of freshly distilled pentamethylcyclopentadiene (0.92 g, 6.80 mmol, 1.13 eq.) with *n*BuLi (5.1 M in hexane, 1.2 mL, 6.0 mmol, 1.0 eq.) at 0 °C in THF (15 mL). After heating to ambient temperature, pentane (10 mL) was added to the solution. The product precipitated as a white solid (0.53 g, 3.73 mmol, 62%) and was filtered and dried *in vacuo*.

Sum formula: C₁₀H₁₅Li
Molecular weight: 142.17 g/mol

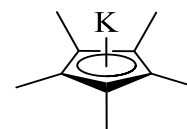


Cp^{*}Li was not soluble in THF-*d*₈. Therefore, no further structure elucidation was pursued.

4.2.3.2 Synthesis and Characterization of Cp^{*}K

Pentamethylcyclopentadienylpotassium (Cp^{*}K) was prepared by addition of freshly distilled pentamethylcyclopentadiene (1.31 g, 9.60 mmol, 1.20 eq.) to a solution of freshly cut potassium (0.32 g, 8.20 mmol, 1.0 eq.) in Et₂O (15 mL). After stirring the reaction mixture for 15 h, pentane (15 mL) was added. The product precipitated as a white solid (1.06 g, 6.10 mmol, 74%) and was filtered and dried *in vacuo*.

Sum formula: C₁₀H₁₅K
Molecular weight: 174.32 g/mol



Proposed aggregate: [C₁₀H₁₅K(THF)₃]
Sum formula: C₂₂H₃₉O₃K
Molecular weight: 390.64 g/mol

¹H NMR

(400.13 MHz, THF-*d*₈): δ = 1.95 (s, 15 H, 5 CH₃) ppm.

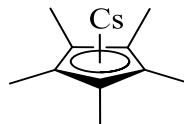
¹³C{¹H} NMR

(100.62 MHz, THF-*d*₈): δ = 104.8 (5 C_{tert}), 11.4 (5 CH₃) ppm.

4.2.3.3 Characterization of Cp*Cs

Pentamethylcyclopentadienylcaesium (Cp*Cs) was synthesized by *Neufeld* from our group and only further characterized in this work.

Sum formula: $C_{10}H_{15}Cs$
Molecular weight: 268.13 g/mol



Proposed aggregate: $[C_{10}H_{15}Cs(THF)_4]$
Sum formula: $C_{26}H_{47}O_4Cs$
Molecular weight: 556.55 g/mol

1H NMR

(400.13 MHz, THF- d_6): $\delta = 1.85$ (s, 15 H, 5 CH₃) ppm.

$^{13}C\{^1H\}$ NMR

(100.62 MHz, THF- d_6): $\delta = 108.0$ (5 C_{tert}), 11.1 (5 CH₃) ppm. (C_{tert} were observed via $^1H,^{13}C$ -HMBC experiments)

4.2.4 Characterizations of RMgCl (R = Et, *i*Pr, *n*Bu, *n*Hex, *n*Oct, *n*Dec)

Ethylmagnesium chloride (EtMgCl; in THF, 2 M) was purchased from Sigma-Aldrich and used as received for characterization. ***i*-Propyl-** (*i*PrMgCl), ***n*-butyl-** (*n*BuMgCl), ***n*-hexyl-** (*n*HexMgCl), ***n*-octyl-** (*n*OctMgCl) and ***n*-decylmagnesium chloride** (*n*DecMgCl) were synthesized by *Schnegelsberg* from the *Koszinowski* group and only further characterized in this work.^[3] Carbon and hydrogen atoms of the alkyl chains are numbered according to IUPAC.

4.2.4.1 Characterization of EtMgCl

Proposed aggregate: [C₂H₅MgCl(THF)₂]

Sum formula: C₁₀H₂₁O₂MgCl

Molecular weight: 233.03 g/mol

¹H NMR

(400.13 MHz, THF-*d*₈): δ = 1.12 (t, ³J_{HH} = 8.2 Hz, 3 H, H-2), -0.81 (q, ³J_{HH} = 8.2 Hz, 2 H, H-1) ppm.

¹³C{¹H} NMR

(100.62 MHz, THF-*d*₈): δ = 14.2 (C2), -2.3 (C1) ppm.

4.2.4.2 Characterization of *i*PrMgCl

Proposed aggregate: [C₃H₇MgCl(THF)₂]

Sum formula: C₁₁H₂₃O₂MgCl

Molecular weight: 247.06 g/mol

¹H NMR

(400.13 MHz, THF-*d*₈): δ = 1.26 (d, ³J_{HH} = 7.7 Hz, 6 H, H-2, H-2'), -0.31 to -0.47 (m, 1 H, H-1) ppm.

¹³C{¹H} NMR

(100.62 MHz, THF-*d*₈): δ = 26.2 (C2, C2'), 9.9 (C1) ppm.

4.2.4.3 Characterization of *n*BuMgCl

Proposed aggregate: $[\text{C}_4\text{H}_9\text{MgCl}(\text{THF})_2]$

Sum formula: $\text{C}_{12}\text{H}_{25}\text{O}_2\text{MgCl}$

Molecular weight: 261.08 g/mol

^1H NMR

(400.13 MHz, THF- d_8): $\delta = 1.58$ to 1.47 (m, 2 H, H-2), 1.31 to 1.19 (m, 2 H, H-3), 0.85 (t, $^3J_{\text{HH}} = 7.3$ Hz, 3 H, H-4), -0.57 to -0.65 (m, 2 H, H-1) ppm.

$^{13}\text{C}\{^1\text{H}\}$ NMR

(100.62 MHz, THF- d_8): $\delta = 33.9$ (C2), 32.5 (C3), 14.7 (C4), 7.9 (C1) ppm.

4.2.4.4 Characterization of *n*HexMgCl

Proposed aggregate: $[\text{C}_6\text{H}_{13}\text{MgCl}(\text{THF})_2]$

Sum formula: $\text{C}_{14}\text{H}_{29}\text{O}_2\text{MgCl}$

Molecular weight: 289.14 g/mol

^1H NMR

(400.13 MHz, THF- d_8): $\delta = 1.60$ to 1.49 (m, 2 H, H-2), 1.33 to 1.23 (m, 6 H, H-3, H-4, H-5), 0.91 to 0.85 (m, 3 H, H-6), -0.62 (t, $^3J_{\text{HH}} = 8.5$ Hz, 2 H, H-1) ppm.

$^{13}\text{C}\{^1\text{H}\}$ NMR

(100.62 MHz, THF- d_8): $\delta = 38.6$ (C3), 32.2 (C4), 30.2 (C2), 23.0 (C5), 13.8 (C6), 7.2 (C1) ppm.

4.2.4.5 Characterization of *n*OctMgCl

Proposed aggregate: $[\text{C}_8\text{H}_{17}\text{MgCl}(\text{THF})_2]$

Sum formula: $\text{C}_{16}\text{H}_{33}\text{O}_2\text{MgCl}$

Molecular weight: 317.19 g/mol

^1H NMR

(400.13 MHz, THF- d_8): $\delta = 1.60$ to 1.49 (m, 2 H, H-2), 1.36 to 1.16 (m, 10 H, H-3 to H-7), 0.90 to 0.87 (m, 3 H, H-8), -0.62 (t, $^3J_{\text{HH}} = 8.6$ Hz, 2 H, H-1) ppm.

$^{13}\text{C}\{^1\text{H}\}$ NMR

(100.62 MHz, THF- d_8): $\delta = 40.0$ (C3), 33.3 (C7), 31.3 (C5), 30.9 (C2), 30.8 (C4), 23.7 (C6), 14.8 (C8), 8.2 (C1) ppm.

4.2.4.6 Characterization of *n*DecMgCl

Proposed aggregate:	$[\text{C}_{10}\text{H}_{21}\text{MgCl}(\text{THF})_2]$
Sum formula:	$\text{C}_{18}\text{H}_{37}\text{O}_2\text{MgCl}$
Molecular weight:	317.19 g/mol

^1H NMR

(400.13 MHz, THF-d_8):	$\delta = 1.56$ to 1.39 (m, 2 H, H-2), 1.36 to 1.23 (m, 14 H, H-3 to H-9), 0.93 to 0.85 (m, 3 H, H-10), -0.59 to -0.67 (m, 2 H, H-1) ppm.
--	---

$^{13}\text{C}\{^1\text{H}\}$ NMR

(100.62 MHz, THF-d_8):	$\delta = 40.0$ (C3), 33.0 (C9), 31.3 (C2), 31.2 (C5 or C6 or C7), 30.9 (C5 or C6 or C7), 30.9 (C4), 30.5 (C5 or C6 or C7), 23.7 (C8), 14.5 (C10), 8.2 (C1) ppm.
--	--

4.2.5 Characterization of *n*BuMgBr

*n*Butylmagnesium bromide (*n*BuMgBr) was synthesized by Schnegelsberg from the Koszinowski group and only further characterized in this work.^[3] Carbon and hydrogen atoms of the alkyl chain are numbered according to IUPAC.

4.2.5.1 Characterization of *n*BuMgBr

Proposed aggregate:	$[\text{C}_4\text{H}_9\text{MgBr}(\text{THF})_2]$
Sum formula:	$\text{C}_{12}\text{H}_{25}\text{O}_2\text{MgBr}$
Molecular weight:	305.53 g/mol

^1H NMR

(400.13 MHz, THF-d_8):	$\delta = 1.57$ to 1.48 (m, 2 H, H-2), 1.26 (sextet, $^3J_{\text{HH}} = 7.4$ Hz, 2 H, H-3), 0.85 (t, $^3J_{\text{HH}} = 7.3$ Hz, 3 H, H-4), -0.59 (t, $^3J_{\text{HH}} = 8.2$ Hz, 2 H, H-1) ppm.
--	--

$^{13}\text{C}\{^1\text{H}\}$ NMR

(100.62 MHz, THF-d_8):	$\delta = 33.8$ (C2), 32.4 (C3), 14.7 (C4), 8.1 (C1) ppm.
--	---

4.2.6 Characterizations of [*n*BuMgX · LiX] (X = Cl, Br)

[*n*BuMgX · LiX] (X = Cl, Br) were prepared by addition of equimolar amounts of dry LiX in THF to solutions of *n*BuMgX. Carbon and hydrogen atoms of the alkyl chains are numbered according to IUPAC.

4.2.6.1 Characterization of [*n*BuMgCl · LiCl]

Proposed aggregate: [C₄H₉MgCl(THF)₂ · LiCl]
Sum formula: C₁₂H₂₅O₂MgLiCl₂
Molecular weight: 303.48 g/mol

¹H NMR

(400.13 MHz, THF-*d*₈): δ = 1.52 (quintet, ³J_{HH} = 7.4 Hz, 2 H, H-2), 1.25 (sextet, ³J_{HH} = 7.4 Hz, 2 H, H-3), 0.84 (t, ³J_{HH} = 7.4 Hz, 3 H, H-4), -0.59 (t, ³J_{HH} = 8.3 Hz, 2 H, H-1) ppm.

¹³C{¹H} NMR

(100.62 MHz, THF-*d*₈): δ = 33.8 (C2), 32.3 (C3), 14.7 (C4), 8.1 (C1) ppm.

⁷Li NMR

(155.51 MHz, THF-*d*₈): δ = 0.28 (s) ppm.

4.2.6.2 Characterization of [*n*BuMgBr · LiBr]

Proposed aggregate: [C₄H₉MgBr(THF)₂ · LiBr]
Sum formula: C₁₂H₂₅O₂MgLiBr₂
Molecular weight: 392.38 g/mol

¹H NMR

(400.13 MHz, THF-*d*₈): δ = 1.52 (quintet, ³J_{HH} = 8.0 Hz, 2 H, H-2), 1.25 (sextet, ³J_{HH} = 7.1 Hz, 2 H, H-3), 0.85 (t, ³J_{HH} = 7.1 Hz, 3 H, H-4), -0.59 (t, ³J_{HH} = 8.0 Hz, 2 H, H-1) ppm.

¹³C{¹H} NMR

(100.62 MHz, THF-*d*₈): δ = 33.7 (C2), 32.3 (C3), 14.6 (C4), 8.3 (C1) ppm.

⁷Li NMR

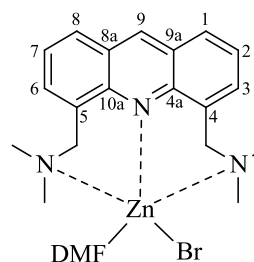
(155.51 MHz, THF-*d*₈): δ = 0.61 (s) ppm.

4.2.7 Characterizations of [MX₂{(Me₂NCH₂)₂Acr}] (MX₂ = ZnBr(DMF), CdBr₂)

[ZnBr(DMF){(Me₂NCH₂)₂Acr}] and [CdBr₂{(Me₂NCH₂)₂Acr}] were synthesized by *Visscher* from our group and only further characterized in this work.^[1,150]

4.2.7.1 Characterization of [ZnBr(DMF){(Me₂NCH₂)₂Acr}]

Sum formula: C₂₂H₃₀N₄OZnBr
Molecular weight: 511.78 g/mol



(DMF-*d*₇, 80 °C):

¹H NMR

(400.13 MHz, DMF-*d*₇): δ = 9.25 (s, 1 H, H-9), 8.22 (d, ³J_{HH} = 8.3 Hz, 2 H, H-1, H-8), 8.01 (d, ³J_{HH} = 7.1 Hz, 2 H, H-3, H-6), 7.69 (dd, ³J_{HH} = 8.3 Hz, 7.1 Hz, 2 H, H-2, H-7), 4.52 (s, 4 H, 2 CH₂), 2.26 (s, 12 H, 4 CH₃) ppm.

(DMF-*d*₇, -30 °C):

¹H NMR

(400.13 MHz, DMF-*d*₇): δ = 9.57 (s, 1 H, H-9), 8.39 (dd, ³J_{HH} = 8.0 Hz, ⁴J_{HH} = 1.6 Hz, 2 H, H-1, H-8), 8.11 (dd, ³J_{HH} = 6.1 Hz, ⁴J_{HH} = 1.3 Hz, 2 H, H-3, H-6), 7.76 (dd, ³J_{HH} = 8.4 Hz, 6.8 Hz, 2 H, H-2, H-7), 5.46 (d, ²J_{HH} = 11.9 Hz, 2 H, CH₂), 3.86 (d, ²J_{HH} = 11.9 Hz, 2 H, CH₂), 3.19 (s, 6 H, 2 CH₃), 2.38 (s, 6 H, 2 CH₃) ppm.

¹³C{¹H} NMR

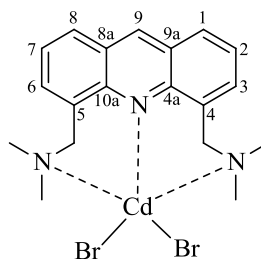
(100.62 MHz, DMF-*d*₇): δ = 148.7 (C4a, C10a) 142.0 (C9), 135.5 (C3, C6), 130.5 (C1, C8), 127.7 (C8a, C9a), 126.4 (C2, C7), 63.1 (2 CH₂), 48.9 (2 CH₃), 46.4 (2 CH₃) ppm.

¹⁵N NMR

(40.56 MHz, DMF-*d*₇): δ = -347 ppm. (Signal was observed via ¹H,¹⁵N-HMBC experiments)

4.2.7.2 Characterization of $[\text{CdBr}_2\{(\text{Me}_2\text{NCH}_2)_2\text{Acr}\}]$ Sum formula: $\text{C}_{19}\text{H}_{23}\text{N}_3\text{CdBr}_2$

Molecular weight: 565.63 g/mol

(DMF- d_7 , 80 °C): ^1H NMR

(400.13 MHz, DMF- d_7): $\delta = 9.32$ (s, 1 H, H-9), 8.28 (d, $^3J_{\text{HH}} = 8.5$ Hz, 2 H, H-1, H-8), 8.08 to 7.99 (m, 2 H, H-3, H-6), 7.71 (dd, $^3J_{\text{HH}} = 8.5$ Hz, 6.8 Hz, 2 H, H-2, H-7), 4.56 (s, 4 H, 2 CH_2), 2.74 (s, 12 H, 4 CH_3) ppm.

(DMF- d_7 , -30 °C): ^{113}Cd NMR

(88.80 MHz, DMF- d_7): $\delta = -345$ ppm. (Signal was observed via ^1H , ^{113}Cd -HMBC experiments)

5 APPENDIX

Table of Contents

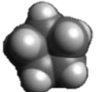
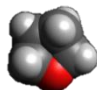



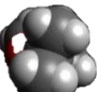
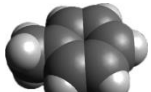
Categorization of Model Compounds	101
Principal Moments of Inertia of Model Compounds	104
Absolute Logarithmic Diffusion Coefficients of Model Compounds for Various Solvents	105
ECCs and Normalized Diffusion Coefficients of Model Compounds for Various Solvents	106
ECCs and Model Compounds for DMSO- <i>d</i> ₆	107
ECCs and Model Compounds for DMSO- <i>d</i> ₆ at Different Temperatures (Compact Spherical Molecules)	109
ECCs and Model Compounds for Cyclohexane- <i>d</i> ₁₂	110
ECCs and Model Compounds for CDCl ₃	112
ECCs and Model Compounds for CD ₂ Cl ₂	114
ECCs and Model Compounds for C ₆ D ₆	116
ECCs and Model Compounds for CD ₃ OD	118
ECCs and Model Compounds for CD ₃ CN	120
ECCs and Model Compounds for THF- <i>d</i> ₈ (Rod-Like and Brominated Rod-Like Molecules)	122
Theoretical Error Analysis of Model Compounds for Various Solvents	123
Molar <i>Van-Der-Waals</i> Densities (<i>MD</i>_w) of Model Compounds	125
ECC-<i>MW</i> Estimations of CpM Derivatives (M = Li, Na, K, Rb, Cs)	127
ECC- <i>MW</i> Estimation of CpLi in THF and DMSO	127
ECC- <i>MW</i> Estimation of CpNa in THF and DMSO	129
ECC- <i>MW</i> Estimation of CpK in THF and DMSO	130
ECC- <i>MW</i> Estimation of CpRb in THF and DMSO	131
ECC- <i>MW</i> Estimation of CpCs in THF and DMSO	131
ECC- <i>MW</i> Estimation of MeCpLi in THF	132
ECC- <i>MW</i> Estimation of Cp*K in THF	133
ECC- <i>MW</i> Estimation of Cp*Cs in THF	133
Molar <i>Van-Der-Waals</i> Densities (<i>MD</i> _w)	133
ECC-<i>MW</i> Estimations of RMgX (R = Et, <i>i</i>Pr, <i>n</i>Bu, <i>n</i>Hex, <i>n</i>Oct, <i>n</i>Dec; X = Cl, Br)	134
ECC- <i>MW</i> Estimation of EtMgCl in THF	134
ECC- <i>MW</i> Estimation of <i>i</i> PrMgCl in THF	134
ECC- <i>MW</i> Estimation of <i>n</i> BuMgCl in THF	134
ECC- <i>MW</i> Estimation of <i>n</i> HexMgCl in THF	135
ECC- <i>MW</i> Estimation of <i>n</i> OctMgCl in THF	135
ECC- <i>MW</i> Estimation of <i>n</i> DecMgCl in THF	135
ECC- <i>MW</i> Estimation of <i>n</i> BuMgBr in THF	136
Molar <i>Van-Der-Waals</i> Densities (<i>MD</i> _w)	136
ECC-<i>MW</i> Estimations of [<i>n</i>BuMgX · LiX] (X = Cl, Br)	137
ECC- <i>MW</i> Estimation of [<i>n</i> BuMgCl · LiCl] in THF	137
ECC- <i>MW</i> Estimation of [<i>n</i> BuMgBr · LiBr] in THF	137

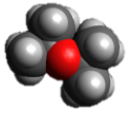

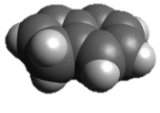
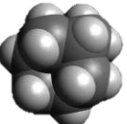
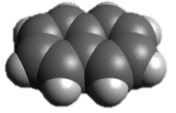
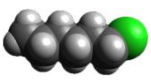
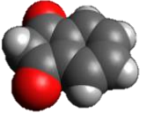
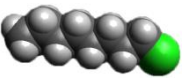
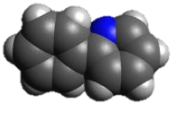
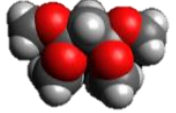
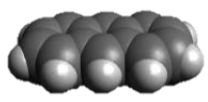

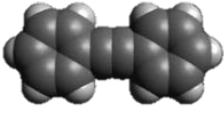
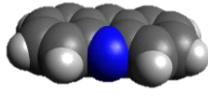
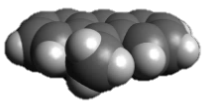
Molar <i>Van-Der-Waals</i> Densities (MD_w)	137
ECC-MW Estimations of (IPrPh)X (X = Br, I, OTf, BF₄, PF₆)	138
ECC-MW Estimation of (IPrPh)Br in Dichloromethane	138
ECC-MW Estimation of (IPrPh)I in Dichloromethane	138
ECC-MW Estimation of (IPrPh)OTf in Dichloromethane	138
ECC-MW Estimation of (IPrPh)BF ₄ in Dichloromethane	139
ECC-MW Estimation of (IPrPh)PF ₆ in Dichloromethane	139
Molar <i>Van-Der-Waals</i> Densities (MD_w)	139
ECC-MW Estimations of (4,6-<i>t</i>Bu-NCOC₆H₂)₂CH₂ and [M(4,6-<i>t</i>Bu-NCOC₆H₂)₂CH] (M = Li, K, Mg)	140
ECC-MW Estimation of the (4,6- <i>t</i> Bu-NCOC ₆ H ₂) ₂ CH ₂ Ligand in Benzene	140
ECC-MW Estimation of [Li(4,6- <i>t</i> Bu-NCOC ₆ H ₂) ₂ CH] in Benzene	140
ECC-MW Estimation of [K(4,6- <i>t</i> Bu-NCOC ₆ H ₂) ₂ CH] in Benzene	140
ECC-MW Estimation of [MgCl ₂ (4,6- <i>t</i> Bu-NCOC ₆ H ₂) ₂ CH] in Benzene	141
ECC-MW Estimation of [MgBr ₂ (4,6- <i>t</i> Bu-NCOC ₆ H ₂) ₂ CH] in Benzene	141
ECC-MW Estimation of [Mg((4,6- <i>t</i> Bu-NCOC ₆ H ₂) ₂ CH) ₂] in Benzene	141
Molar <i>Van-Der-Waals</i> Densities (MD_w)	142
NMR Spectra	143
¹ H-DOSY NMR Spectrum of CpLi in Ammonia	143
⁷ Li, ¹ H-HOESY NMR Spectrum of CpLi in DMSO	143

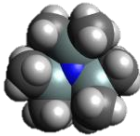
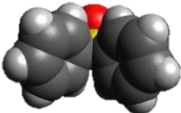
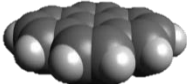
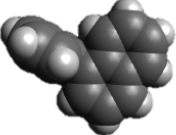
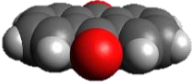
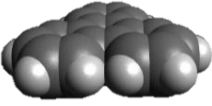
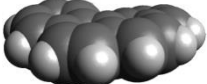
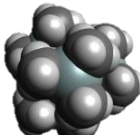
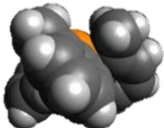

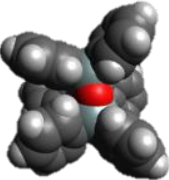
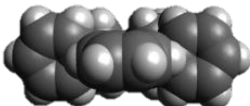

Categorization of Model Compounds

Three-dimensional models for reference molecules have been created using the program Avogadro 1.0.3. These can be associated to different molecular shapes (expanded discs (ED), dissipated spheres and ellipsoids (DSE), compact spheres (CS) or rod-like (RL) compounds). The transitions between these shapes are not sharp; still, there are clear systematic trends that can be rationalized. Compact spherical (CS) molecules have nearly the same radius in all dimensions with a highly filled space. Benzene (78 g/mol) was found to diffuse CS-like. Dissipated spheres and ellipsoids (DSE) have an elongated major axis and/or a less filled space. Small annelated aromatic compounds like toluene (92 g/mol), indene (116 g/mol) or naphthalene (128 g/mol) with MW s < 150 g/mol also diffuse DSE-like. Rod-like molecules have long alkyl chains which dominate the overall structure (brominated rod-like molecules have not been listed below). Lastly, enlarged discs are flat molecules, with two elongated major axes and MW s > 150 g/mol.

Table 5-1: Categorization of all model compounds depending to their molecular shapes. Note that in some cases this categorization may be empirical as described above.

	Compact spheres (CS)	Dissipated spheres and ellipsoids (DSE)	Expanded discs (ED)	Rod-like (RL) molecules
MW [g/mol]	(MW_{calc} [g/mol])	(MW_{calc} [g/mol])	(MW_{calc} [g/mol])	(MW_{calc} [g/mol])
70 - 80	 Cyclopentane (70)	 THF (72)		
	 Benzene (78)			
80 - 100	 Cyclohexane (84)			
	 TMS (88)			
	 MTBE (88)	 Toluene (92)		

	Compact spheres (CS)	Dissipated spheres and ellipsoids (DSE)	Expanded discs (ED)	Rod-like (RL) molecules
100+		 <i>iPr</i> ₂ O (102)		
	 TMB (114)	 Indene (116)		
	 Adam (136)	 Naphthalene (128)		 <i>n</i> HexCl (120)
		 1,3-Indanedione (146)		 <i>n</i> OctCl (148)
		 2-PhP (155)		
		 Tetramethoxypropane (164)	 Anthracene (178)	 <i>n</i> DecCl (176)
		 DPA (178)	 Acridine (179)	
			 9-MA (192)	

	Compact spheres (CS)	Dissipated spheres and ellipsoids (DSE)	Expanded discs (ED)	Rod-like (RL) molecules
200+	 N(SiMe ₃) ₃ (234)	 DPS (202)	 Pyrene (202)	
		 1-PhN (204)	 Anthrachinone (208)	
			 Triphenylene (228)	
			 DHBP (281)	
300+	 Si(SiMe ₃) ₄ (321)	 Tri(<i>o</i> tolyl)phosphine (304)		 Batylalcohol (345)
400+		 Hexaphenyltrisiloxane (595)	 TPhN (433)	
		 BINAP (623)		

Principal Moments of Inertia of Model Compounds

For a more theoretical approach towards categorization, principal moments of inertia of model compounds were calculated as described in section 2.1.2 (results and conclusion can also be found in section 2.1.2).

Table 5-2: Principal moments of inertia calculated with PMIPST^[122] for geometry optimized (MMFF94) structures of model compounds used in ECCs. The relative shape anisotropy κ^2 is also listed for each model compound.

Compound	I_{xx} [$\text{u}\text{\AA}^2$]	I_{yy} [$\text{u}\text{\AA}^2$]	I_{zz} [$\text{u}\text{\AA}^2$]	$\sim I_{xx} : I_{yy} : I_{zz}$	$\kappa^2 \cdot 100\%$
1,3-Indanedione	301	408	707	1 : 1 : 2	6.6
1-PhN	473	1354	1680	1 : 3 : 4	9.5
2-PhP	173	905	1053	1 : 5 : 6	14.7
9-MA	356	1133	1485	1 : 3 : 4	11.3
Acridine	227	1081	1304	1 : 5 : 6	14.2
Anthracene	230	1113	1343	1 : 5 : 6	14.4
Anthrachinone	450	1142	1592	1 : 3 : 4	9.8
Batylalcohol	274	20730	20911	1 : 76 : 76	24.0
Benzene	89	89	177	1 : 1 : 2	6.1
BINAP	6783	7518	9435	1 : 1 : 1	1.0
CHCl ₃	154	154	296	1 : 1 : 2	5.5
CH ₂ Cl ₂	16	150	163	1 : 9 : 10	18.4
CH ₃ CN	3	54	54	1 : 18 : 18	21.1
CH ₃ OH	4	20	21	1 : 5 : 5	13.5
nDecCl	70	3349	3387	1 : 48 : 48	23.5
DHBP	1146	1890	2716	1 : 2 : 2	5.6
Cyclohexane	117	117	205	1 : 1 : 2	4.0
Cyclopentane	76	76	132	1 : 1 : 3	3.9
DMSO	73	74	122	1 : 1 : 2	3.3
DPA	178	2020	2200	1 : 11 : 12	19.4
DPS	426	1217	1425	1 : 3 : 3	8.9
Hexaphenyltrisiloxane	6123	7683	8920	1 : 1 : 1	1.1
nHexCl	44	956	980	1 : 22 : 22	21.8
H ₂ O	0.6	1.2	1.8	1 : 2 : 3	4.0
Indene	135	313	444	1 : 2 : 3	9.1
iPr ₂ O	122	326	370	1 : 3 : 3	7.9
MTBE	115	187	187	1 : 2 : 2	2.2
Naphthalene	160	409	568	1 : 3 : 4	9.8
N(SiMe ₃) ₃	893	893	1311	1 : 1 : 1	1.8
nOctCl	57	1916	1948	1 : 34 : 34	22.9
Pyrene	490	904	1394	1 : 2 : 3	7.9
Si(OMe) ₄	345	412	494	1 : 1 : 1	1.1
Si(SiMe ₃) ₄	1914	1914	1914	1 : 1 : 1	0
Tetramethoxypropane	97	318	391	1 : 3 : 4	10.8
TPhN	2876	4349	6524	1 : 2 : 2	5.4
THF	70	72	126	1 : 1 : 2	4.2
TMB	219	510	515	1 : 2 : 2	5.6
TMS	162	162	162	1 : 1 : 1	0
Toluene	92	199	288	1 : 2 : 3	8.6
Tri(otolyl)phosphine	1790	1883	2840	1 : 1 : 2	2.4
Triphenylene	990	990	1980	1 : 1 : 2	6.3
Triphenylmethane	1372	1331	2271	1 : 1 : 2	3.4

Absolute Logarithmic Diffusion Coefficients of Model Compounds for Various Solvents

Table 5-3: Exemplary^a absolute logarithmic diffusion coefficients ($\log(D_x)$; not normalized) of model compounds and solvents (rod-like references used in ECC^{THF} are not listed) at 25 °C. Due to solubility problems not all references could be measured in all solvents (marked with *). There are also references not considered in calibration curves due to unknown aggregational behavior or elevated molar *van-der-Waals* densities (marked in red).

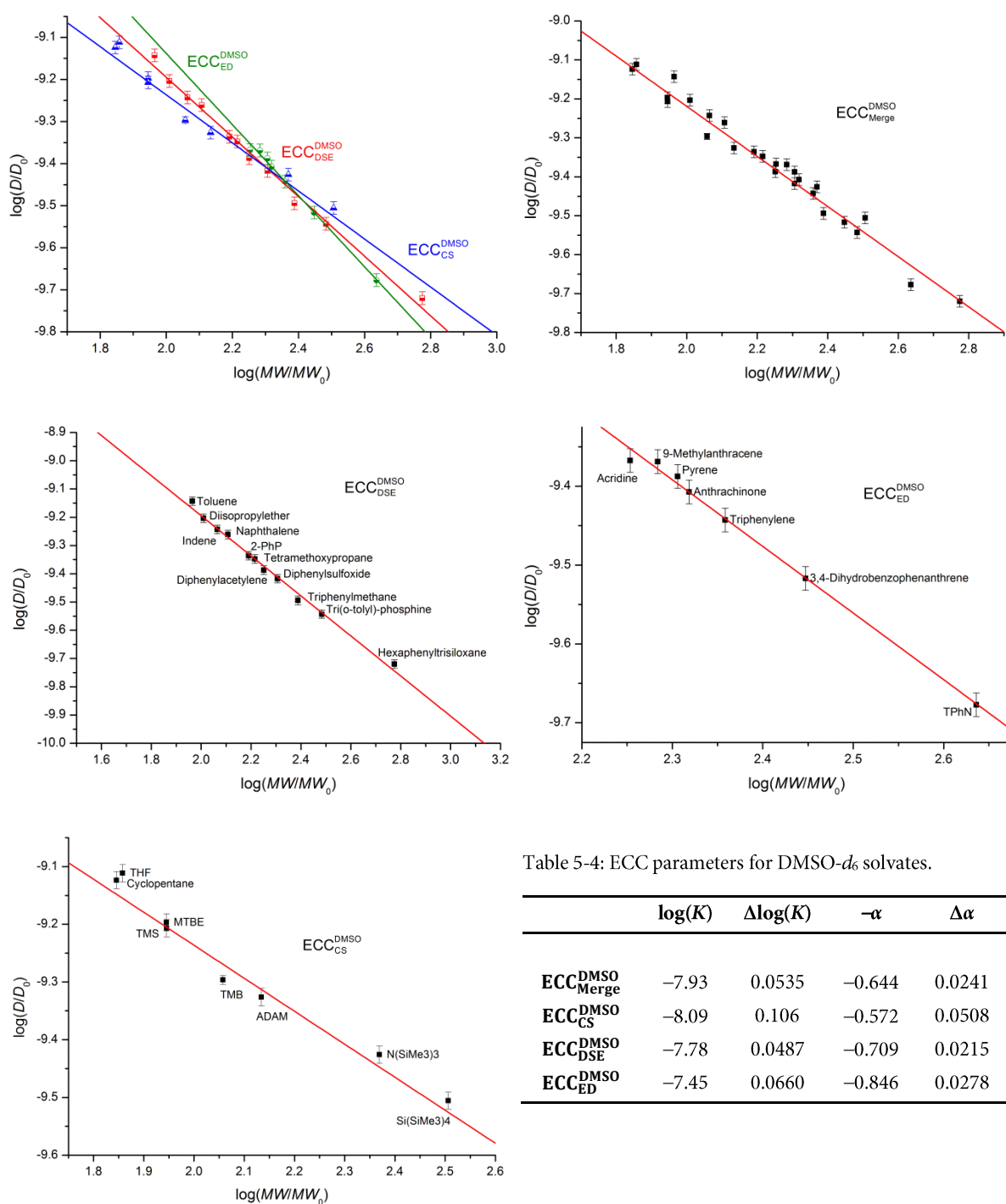
Solvent	DMSO	C ₆ D ₁₂	CDCl ₃	CD ₃ OD	C ₆ D ₆	CD ₂ Cl ₂	CD ₃ CN
Compound	$\log(D_x)$	$\log(D_x)$	$\log(D_x)$	$\log(D_x)$	$\log(D_x)$	$\log(D_x)$	$\log(D_x)$
1,3-Indanedione	*	-8.9258	-8.8558	-8.8496	-8.7970	-8.7172	-8.6146
1-PhN	*	-9.0487	-8.9019	-8.8757	-8.9027	-8.7908	-8.7908
2-PhP	-9.3307	-8.9081	-8.8359	-8.8606	-8.8189	-8.7126	-8.6121
9-MA	-9.3797	-8.9890	-8.8456	-8.8375	-8.8546	-8.7354	-8.6062
Acridine	-9.3672	-8.9643	-8.8644	-8.9049	-8.8449	-8.7363	-8.6248
Adam	-9.3590	-9.0204	-8.8155	-8.8005	-8.8077	-8.6997	-8.5603
Anthracene	*	-8.9240	-8.8043	-8.8047	-8.8432	-8.6929	-8.5502
Anthracinone	-9.4126	*	-8.8779	-8.8575	-8.8981	-8.7521	-8.6566
BINAP	*	-9.3629	-9.1735	*	-9.1941	-9.0582	*
C ₆ D ₆ ^b	-	-	-	-	-8.6882	-	-
CDCl ₃ ^b	-	-	-8.6519	-	-	-	-
CD ₂ Cl ₂ ^b	-	-	-	-	-	-8.4593	-
CD ₃ CN ^b	-	-	-	-	-	-	-8.3765
CD ₃ OD ^b	-	-	-	-8.6882	-	-	-
Cyclohexane- <i>d</i> ₁₂ ^b	-	-8.8821	-	-	-	-	-
Cyclopentane	-9.1184	-8.8119	-8.6459	-8.6216	-8.6192	-8.5411	-8.4043
DHBP	-9.5327	-9.1465	-8.9801	-8.9709	-8.9765	-8.8638	-8.7340
DPA	-9.3779	-8.9987	-8.8573	-8.8528	-8.8731	-8.7495	-8.6325
DPS	-9.4121	-9.0473	-8.9320	-8.9320	-8.8972	-8.7987	-8.6826
DMSO- <i>d</i> ₆ ^b	-9.1896	-	-	-	-	-	-
Hexaphenyltrisiloxane	-9.7354	-9.3500	-9.1586	-9.2094	-9.1963	-9.0484	-8.9409
Indene	-9.2499	-8.8743	-8.7479	-8.7439	-8.7649	-8.6424	-8.5318
<i>i</i> Pr ₂ O	-9.1983	-8.8708	-8.7747	-8.7655	-8.7087	-8.6505	-8.5143
MTBE	-9.2022	-8.8634	-8.6993	-8.7143	-8.7379	-8.6039	-8.4930
Naphthalene	-9.2642	-8.8531	-8.7086	-8.7351	-8.7566	-8.6336	-8.5261
N(SiMe ₃) ₃	-9.4419	-9.1007	-8.9212	-8.9136	-8.8993	-8.8179	-8.6749
Pyrene	-9.3946	-8.9644	-8.8427	-8.8806	-8.8814	-8.7349	-8.6437
Si(OMe) ₄	-9.3038	-8.9136	-8.8156	-8.7991	-8.7833	-8.7100	-8.5891
Si(SiMe ₃) ₄	-9.5361	-9.1894	-8.9590	-9.0094	-8.9731	-8.8697	-8.6910
Tetramethoxypropane	-9.3422	-8.9820	-8.9008	-8.8557	-8.8516	-8.7650	-8.6476
TPhN	-9.7006	-9.3511	-9.0567	-9.1041	-9.1406	-8.9472	-8.8724
THF	-9.1025	-8.7807	-8.6826	-8.6422	-8.6882	-8.5599	-8.4276
TMB	-9.2920	-8.9338	-8.7886	-8.7706	-8.7886	-8.6751	-8.5530
TMS	-9.2324	-8.8765	-8.7268	-8.7082	-8.7104	-8.6300	-8.4808
Toluene	-9.1525	-8.7901	-8.6849	-8.6611	-8.6842	-8.5885	-8.4654
Tri(<i>o</i> tolyl)phosphine	-9.5430	-9.2102	-9.0419	-9.0188	-9.0176	-8.9121	-8.7768
Triphenylene	-9.4481	-9.0358	-8.8916	-8.9003	-8.9361	-8.7605	-8.6642
Triphenylmethane	-9.5039	-9.1407	-8.9714	-8.9617	-8.9794	-8.8593	-8.7368
Water	-	-	-	-8.6893	-	-	-8.2326

^a For most model compounds, multiple diffusion coefficients have been recorded which varied to some degree before normalization (temperature or concentration effects).

^b Residual solvent signal.

ECCs and Normalized Diffusion Coefficients of Model Compounds for Various Solvents

ECCs were established using normalized diffusion coefficients ($\log(D_{x,\text{norm}})$) derived with the approaches and formulae discussed in chapter 2.1. The maximum deviation of $\log(D_{x,\text{norm}})$ was 0.0075. $\Delta\log(D_{x,\text{norm}})$ was defined as twice this deviation as represented by the error bars in the ECCs. For solvents and internal references (Adam, TMB) with more than 5 separate measurements the error bars represent standard deviations of their specific $\log(D_{x,\text{norm}})$. Normalized diffusion coefficients and estimated *MWs* may differ slightly from values given in literature:^[2-3] There have been on the one hand new insights into the ECC-DOSY methodology and on the other *MWs* were calculated using values in accordance with significance (for further information see sections 2.1.1 and 2.3.1).

ECCs and Model Compounds for DMSO- d_6 Table 5-4: ECC parameters for DMSO- d_6 solvates.

	$\log(K)$	$\Delta\log(K)$	$-\alpha$	$\Delta\alpha$
ECC_{Merge}^{DMSO}	-7.93	0.0535	-0.644	0.0241
ECC_{CS}^{DMSO}	-8.09	0.106	-0.572	0.0508
ECC_{DSE}^{DMSO}	-7.78	0.0487	-0.709	0.0215
ECC_{ED}^{DMSO}	-7.45	0.0660	-0.846	0.0278

Figure 5-1: Plots of $\log(D_{x,norm})$ vs. $\log(MW_{calc})$ of all used model compounds in DMSO- d_6 sorted by their molecular shape. There is also a merged ECC of all measured compounds for MW estimation, when the molecular shape of an analyte is unknown.

Table 5-5: Overview of all used model compounds for ECC^{DMSO} and their normalized diffusion coefficients $\log(D_{x,norm})$, the estimated MW_{det} and the deviation from the calculated molecular weight MW_{dif} . TMB was used as internal reference with $\log(D_{ref,fix})(TMB) = -9.2920$. All compounds have been measured as 15 mM solutions of analyte and TMB in an equimolar ratio.^a

<i>MW</i> [g/mol]	<i>D_{x,norm}</i> [m ² /s]	log (<i>D_{x,norm}</i>)	log (<i>MW_{det}</i>)	<i>MW_{det}</i> [g/mol]	<i>MW_{dif}</i> [%]
<i>Not assigned</i>					
78	DMSO ^b	6.6267E-10	-9.1787	-	-
152	Si(OMe) ₄ ^b	5.2977E-10	-9.2759	-	-
<i>Compact spheres, ECC_{CS}</i>					
70	Cyclopentane	7.5204E-10	-9.1238	1.81	64
72	THF	7.7359E-10	-9.1115	1.79	61
88	MTBE	6.3534E-10	-9.1970	1.94	86
88	TMS	6.2554E-10	-9.2037	1.95	89
114	TMB	5.0548E-10	-9.2963	2.11	129
136	Adam	4.7181E-10	-9.3262	2.16	145
234	N(SiMe ₃) ₃	3.7498E-09	-9.4260	2.34	217
321	Si(SiMe ₃) ₄	3.1204E-10	-9.5058	2.48	299
<i>Dissipated spheres & ellipsoids, ECC_{DSE}</i>					
92	Toluene	7.1967E-10	-9.1423	1.92	84
102	<i>i</i> Pr ₂ O	6.2574E-10	-9.2036	2.01	102
116	Indene	5.7155E-10	-9.2429	2.06	116
128	Naphthalene	5.4835E-10	-9.2609	2.09	123
155	2-PhP	4.6127E-10	-9.3360	2.19	157
164	Tetramethoxypropane	4.4923E-10	-9.3475	2.21	163
178	DPA	4.1031E-10	-9.3869	2.27	185
202	DPS	3.8249E-10	-9.4174	2.31	204
244	Triphenylmethane	3.2045E-10	-9.4942	2.42	262
304	Tri(<i>o</i> tolyl)phosphine	2.8624E-10	-9.5433	2.49	307
595	Hexaphenyltrisiloxane	1.9064E-10	-9.7198	2.74	544
<i>Expanded discs, ECC_{ED}</i>					
179	Acridine	4.2907E-10	-9.3675	2.27	185
192	9-MA	4.2782E-10	-9.3687	2.27	185
202	Pyrene	4.0960E-10	-9.3876	2.29	195
208	Anthrachinone	3.9145E-10	-9.4073	2.31	206
228	Triphenylene	3.6074E-10	-9.4428	2.36	227
281	DHBP	3.0426E-10	-9.5168	2.45	282
433	TPhN	2.1029E-10	-9.6772	2.63	429
				Ø	±4

^a When a compound had more than one resonance in the ¹H NMR spectrum, the average diffusion coefficient of all resonances was used.

^b DMSO and Si(OMe)₄ were excluded due to elevated molar *van-der-Waals* density (see Table 5-24).

ECCs and Model Compounds for DMSO- d_6 at Different Temperatures (Compact Spherical Molecules)

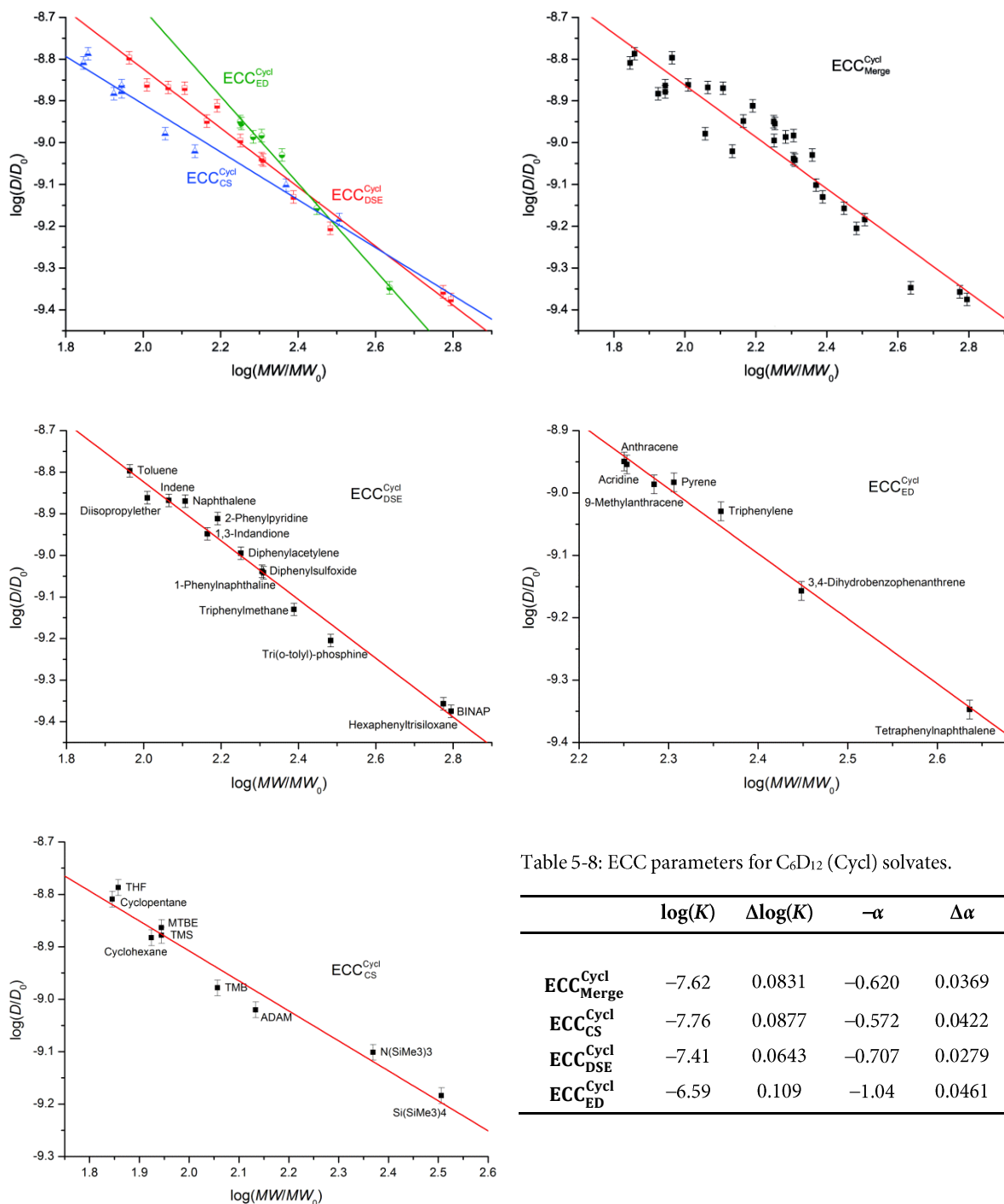
Table 5-6: Overview of compact spherical (CS) model compounds for ECC^{DMSO} and their normalized diffusion coefficients $\log(D_{x,norm})$ measured at different temperatures (25 °C to 60 °C). TMB was used as internal reference with $\log(D_{ref,fix})(TMB) = -9.2920$. All compounds have been measured as 15 mM solutions of analyte and TMB in an equimolar ratio.^a

<i>MW</i> [g/mol]		$\log(D_{x,norm})$	$\log(D_{x,norm})$	$\log(D_{x,norm})$	$\log(D_{x,norm})$	$\log(D_{x,norm})$
	Temperature	25 °C	30 °C	40 °C	50 °C	60 °C
70	Cyclopentane	-9.1238	-9.1324	-9.1321	-9.1492	-9.1430
72	THF	-9.1115	-9.1103	-9.1155	-9.1255	-9.1250
88	MTBE	-9.1970	-9.1999	-9.2021	-9.2030	-9.2094
88	TMS	-9.2037	-9.2146	-9.2163	-9.2225	-9.2271
136	Adam	-9.3262	-9.3261	-9.3221	-9.3430	-9.3283
234	N(SiMe ₃) ₃	-9.4260	-9.4227	-9.4250	-9.4249	-9.4160
321	Si(SiMe ₃) ₄	-9.5058	-9.4970	-9.4937	-9.4898	-9.5210

Table 5-7: ECC parameters for compact spherical solvates in DMSO- d_6 at different temperatures (plotted without TMB).

Temperature	$\log(K)$	$\Delta\log(K)$	$-\alpha$	$\Delta\alpha$	cor. R^2
25 °C	-8.06	0.0650	-0.580	0.0310	0.98
30 °C	-8.10	0.0745	-0.559	0.0355	0.98
40 °C	-8.12	0.0687	-0.553	0.0327	0.98
50 °C	-8.17	0.0807	-0.533	0.0384	0.97
60 °C	-8.12	0.0729	-0.558	0.0347	0.98

^a When a compound had more than one resonance in the ¹H NMR spectrum, the average diffusion coefficient of all resonances was used.

ECCs and Model Compounds for Cyclohexane- d_{12} Table 5-8: ECC parameters for C_6D_{12} (Cycl) solvates.

	$\log(K)$	$\Delta\log(K)$	$-\alpha$	$\Delta\alpha$
ECC_{Merge}^{Cycl}	-7.62	0.0831	-0.620	0.0369
ECC_{CS}^{Cycl}	-7.76	0.0877	-0.572	0.0422
ECC_{DSE}^{Cycl}	-7.41	0.0643	-0.707	0.0279
ECC_{ED}^{Cycl}	-6.59	0.109	-1.04	0.0461

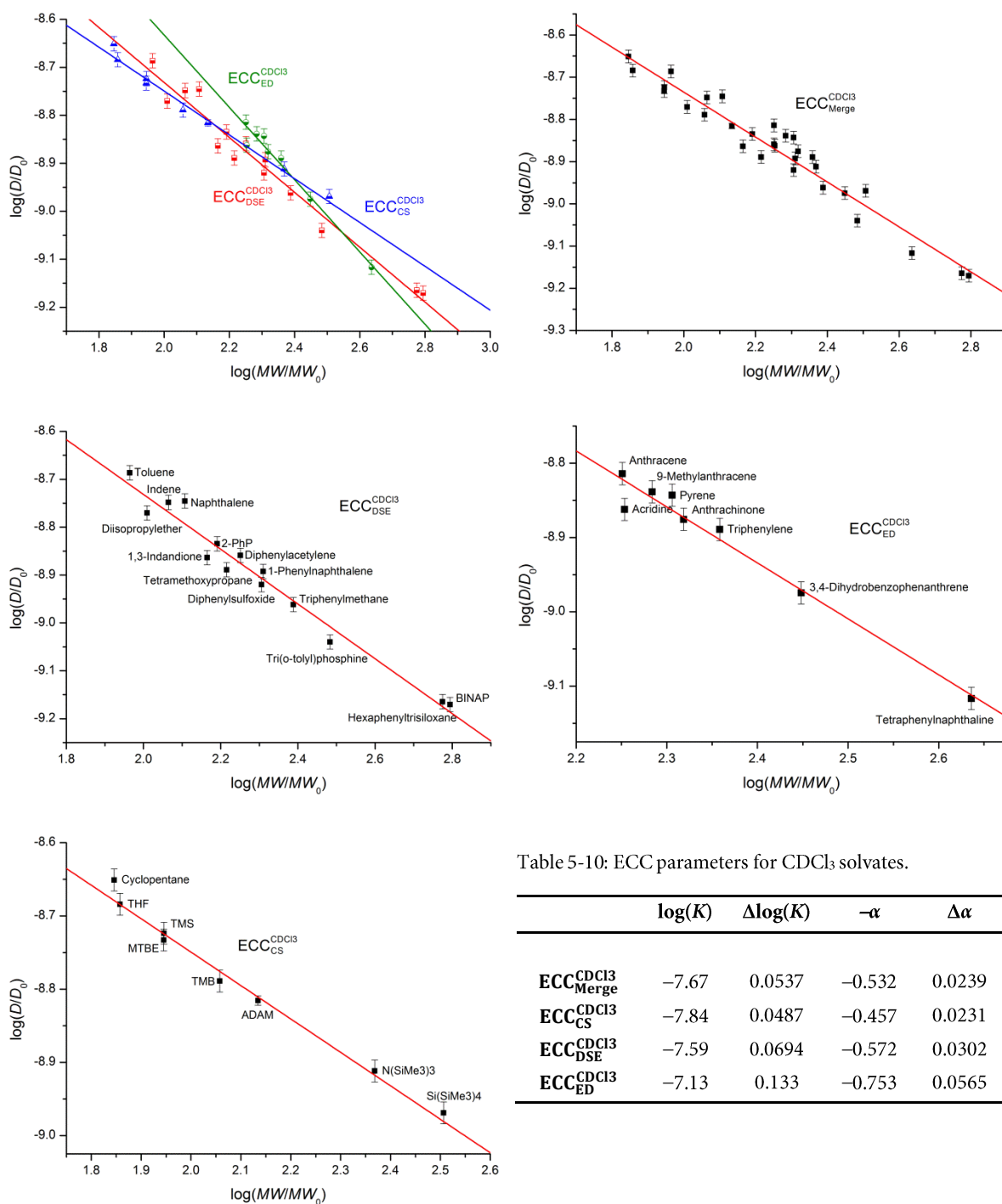
Figure 5-2: Plots of $\log(D_{x,norm})$ vs. $\log(MW_{calc})$ of all used model compounds in C_6D_{12} (Cycl) sorted by their molecular shape. There is also a merged ECC of all measured compounds for MW estimation, when the molecular shape of an analyte is unknown.

Table 5-9: Overview of all used model compounds for ECC^{Cycl} and their normalized diffusion coefficients $\log(D_{x,\text{norm}})$, the estimated MW_{det} and the deviation from the calculated molecular weight MW_{dif} . Adam was used as internal reference with $\log(D_{\text{ref,fix}})(\text{Adam}) = -9.0204$. All compounds have been measured as 15 mM solutions of analyte and Adam in an equimolar ratio.^a

<i>MW</i> [g/mol]		<i>D_{x, norm}</i> [m ² /s]	<i>log</i> (<i>D_{x, norm}</i>)	<i>log</i> (<i>MW_{det}</i>)	<i>MW_{det}</i> [g/mol]	<i>MW_{dif}</i> [%]
	<i>Not assigned</i>					
78	Si(OMe) ₄ ^b	1.2321E-10	-8.9093	-	-	-
	<i>Compact spheres, ECC_{CS}</i>					
70	Cyclopentane	1.5519E-09	-8.8091	1.83	68	3
72	THF	1.6324E-09	-8.7872	1.80	62	15
84	Cyclohexane	1.3101E-09	-8.8827	1.96	92	-8
88	MTBE	1.3695E-09	-8.8634	1.93	85	4
88	TMS	1.3240E-09	-8.8781	1.95	90	-2
114	TMB	1.0512E-09	-8.9783	2.13	135	-15
136	Adam	9.5422E-10	-9.0204	2.20	160	-15
234	N(SiMe ₃) ₃	7.9187E-10	-9.1013	2.35	221	6
321	Si(SiMe ₃) ₄	6.5485E-10	-9.1839	2.49	309	4
	<i>Dissipated spheres & ellipsoids, ECC_{DSE}</i>					
92	Toluene	1.5974E-09	-8.7966	1.96	91	1
102	<i>i</i> Pr ₂ O	1.3754E-09	-8.8616	2.05	113	-10
116	Indene	1.3555E-09	-8.8679	2.06	115	1
128	Naphthalene	1.3500E-09	-8.8697	2.06	116	10
146	1,3-Indanedione	1.1227E-09	-8.9484	2.18	150	-3
155	2-PhP	1.2257E-09	-8.9116	2.12	133	17
164	Tetramethoxypropane	1.0685E-09	-8.9712	2.21	162	2
178	DPA	1.0119E-09	-8.9949	2.24	174	2
202	DPS	9.1607E-10	-9.0381	2.30	201	1
204	1-PhN	9.0830E-10	-9.0418	2.31	203	0
244	Triphenylmethane	7.4143E-10	-9.1299	2.43	271	-10
304	Tri(<i>o</i> tolyl)phosphine	6.2356E-10	-9.2051	2.54	346	-12
595	Hexaphenyltrisiloxane	4.3976E-10	-9.3568	2.75	567	5
623	BINAP	4.2189E-10	-9.3749	2.78	601	4
	<i>Expanded discs, ECC_{ED}</i>					
178	Anthracene	1.1232E-09	-8.9495	2.27	186	-4
179	Acridine	1.1110E-09	-8.9543	2.27	188	-5
192	9-MA	1.0323E-09	-8.9862	2.30	201	-5
202	Pyrene	1.0399E-09	-8.9830	2.30	200	1
228	Triphenylene	9.3458E-10	-9.0294	2.35	222	3
281	DHBP	6.9666E-10	-9.1570	2.47	294	-4
433	TPhN	4.4971E-10	-9.3471	2.65	448	-3
					Ø	±5

^a When a compound had more than one resonance in the ¹H NMR spectrum, the average diffusion coefficient of all resonances was used.

^b Si(OMe)₄ was excluded due to elevated molar *van-der-Waals* density (see Table 5-24).

ECCs and Model Compounds for CDCl_3 Table 5-10: ECC parameters for CDCl_3 solvates.

	$\log(K)$	$\Delta\log(K)$	$-\alpha$	$\Delta\alpha$
ECC$^{\text{CDCl}_3}_{\text{Merge}}$	-7.67	0.0537	-0.532	0.0239
ECC$^{\text{CDCl}_3}_{\text{CS}}$	-7.84	0.0487	-0.457	0.0231
ECC$^{\text{CDCl}_3}_{\text{DSE}}$	-7.59	0.0694	-0.572	0.0302
ECC$^{\text{CDCl}_3}_{\text{ED}}$	-7.13	0.133	-0.753	0.0565

Figure 5-3: Plots of $\log(D_{x,\text{norm}})$ vs. $\log(MW_{\text{calc}})$ of all used model compounds in CDCl_3 sorted by their molecular shape. There is also a merged ECC of all measured compounds for MW estimation, when the molecular shape of an analyte is unknown.

Table 5-11: Overview of all used model compounds for ECC^{DCI3} and their normalized diffusion coefficients $\log(D_{x, \text{norm}})$, the estimated MW_{det} and the deviation from the calculated molecular weight MW_{dif} . Adam was used as internal reference with $\log(D_{\text{ref, fix}})(\text{Adam}) = -8.8155$. All compounds have been measured as 15 mM solutions of analyte and Adam in an equimolar ratio.^a

<i>MW</i> [g/mol]		<i>D_{x, norm}</i> [m ² /s]	<i>log</i> (<i>D_{x, norm}</i>)	<i>log</i> (<i>MW_{det}</i>)	<i>MW_{det}</i> [g/mol]	<i>MW_{dif}</i> [%]
	<i>Not assigned</i>					
78	CDCl ₃ ^b	2.1978E-09	-8.6580	-	-	-
152	Si(OMe) ₄ ^b	1.5337E-09	-8.8142	-	-	-
	<i>Compact spheres, ECC_{CS}</i>					
70	Cyclopentane	2.2338E-09	-8.6510	1.77	59	18
72	THF	2.0693E-09	-8.6842	1.85	70	2
88	MTBE	1.8497E-09	-8.7329	1.95	90	-2
88	TMS	1.8894E-09	-8.7237	1.93	86	3
114	TMB	1.6258E-09	-8.7889	2.08	119	-4
136	Adam	1.5292E-09	-8.8155	2.13	136	0
234	N(SiMe ₃) ₃	1.2253E-09	-8.9118	2.35	221	6
321	Si(SiMe ₃) ₄	1.0743E-09	-8.9689	2.47	295	9
	<i>Dissipated spheres & ellipsoids, ECC_{DSE}</i>					
92	Toluene	2.0587E-09	-8.6864	1.92	83	12
102	<i>i</i> Pr ₂ O	1.6968E-09	-8.7704	2.06	116	-12
116	Indene	1.7855E-09	-8.7482	2.02	106	9
128	Naphthalene	1.7976E-09	-8.7453	2.02	105	22
146	1,3-Indanedione	1.3693E-09	-8.8635	2.23	168	-13
155	2-PhP	1.4636E-09	-8.8346	2.18	150	4
164	Tetramethoxypropane	1.2914E-09	-8.8889	2.27	187	-12
178	DPA	1.3839E-09	-8.8589	2.22	165	8
202	DPS	1.2028E-09	-8.9198	2.32	211	-4
204	1-PhN	1.2810E-09	-8.8925	2.28	189	8
244	Triphenylmethane	1.0922E-09	-8.9617	2.40	250	-2
304	Tri(<i>o</i> tolyl)phosphine	9.1243E-10	-9.0398	2.53	342	-11
595	Hexaphenyltrisiloxane	6.8464E-10	-9.1645	2.75	566	5
623	BINAP	6.7551E-10	-9.1704	2.76	579	7
	<i>Expanded discs, ECC_{ED}</i>					
178	Anthracene	1.5341E-09	-8.8142	2.24	172	3
179	Acridine	1.3732E-09	-8.8623	2.30	200	-10
192	9-MA	1.4503E-09	-8.8385	2.27	186	3
202	Pyrene	1.4352E-09	-8.8431	2.28	188	7
208	Anthrachinone	1.3318E-09	-8.8756	2.32	208	0
228	Triphenylene	1.2905E-09	-8.8892	2.34	217	5
281	DHBP	1.0604E-09	-8.9745	2.45	282	0
433	TPhN	7.6453E-10	-9.1166	2.64	435	-1
					Ø	±7

^a When a compound had more than one resonance in the ¹H NMR spectrum, the average diffusion coefficient of all resonances was used.

^b CDCl₃ and Si(OMe)₄ were excluded due to elevated molar *van-der-Waals* density (see Table 5-24).

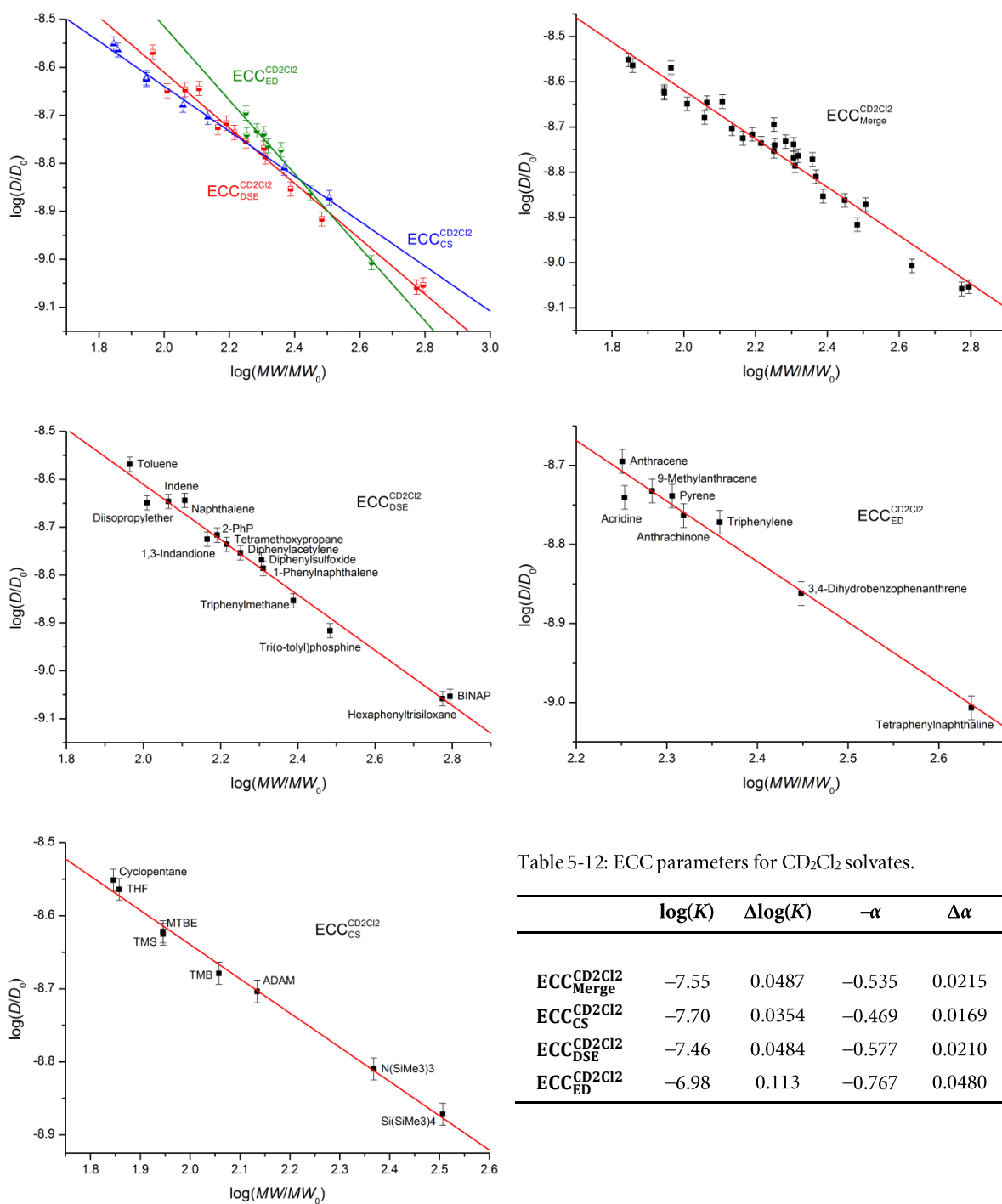
ECCs and Model Compounds for CD_2Cl_2 

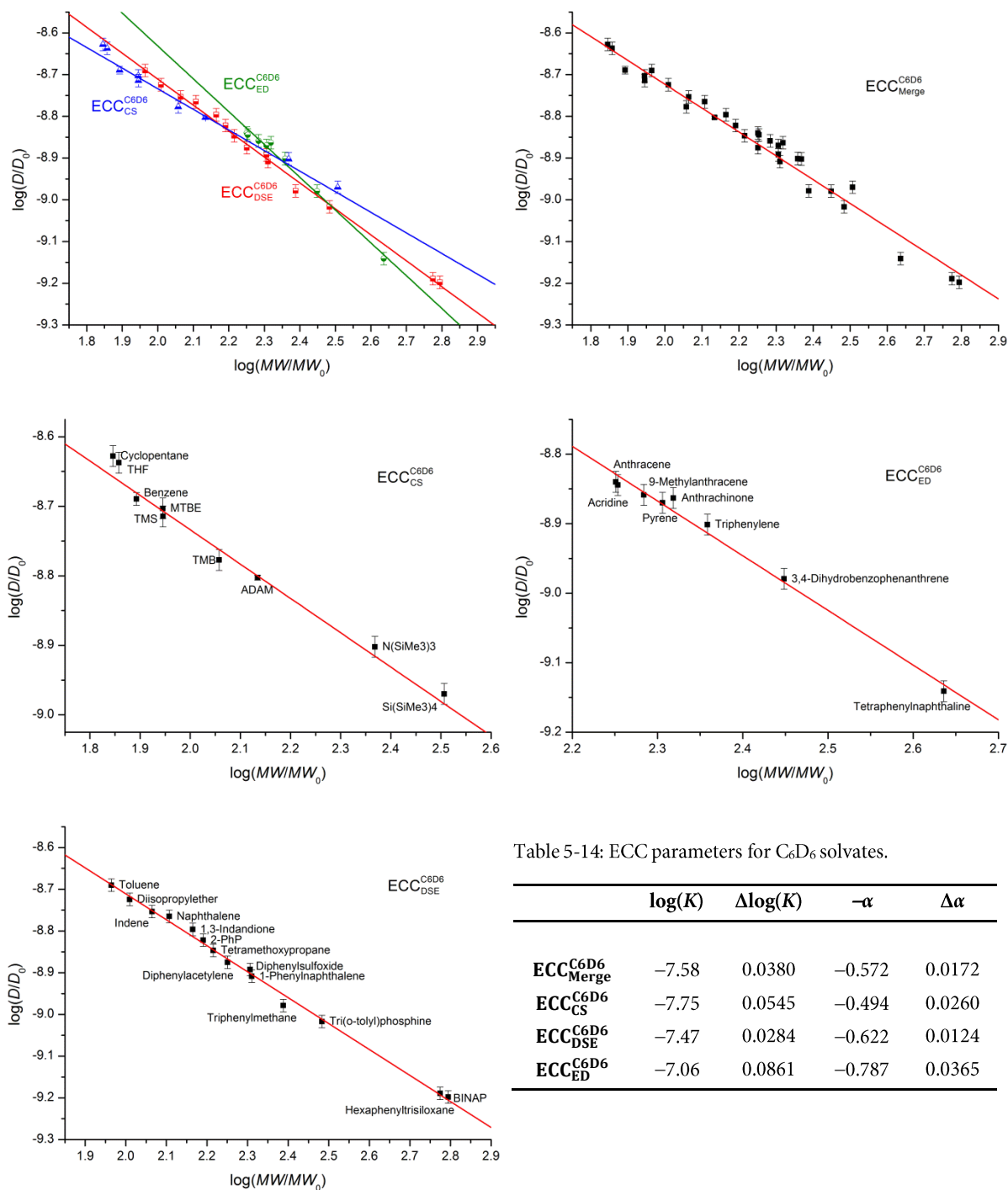
Figure 5-4: Plots of $\log(D_{x,norm})$ vs. $\log(MW_{cat})$ of all used model compounds in CD_2Cl_2 sorted by their molecular shape. There is also a merged ECC of all measured compounds for MW estimation, when the molecular shape of an analyte is unknown.

Table 5-13: Overview of all used model compounds for $ECC^{CD_2Cl_2}$ and their normalized diffusion coefficients $\log(D_{x,norm})$, the estimated MW_{det} and the deviation from the calculated molecular weight MW_{dif} . Adam was used as internal reference with $\log(D_{ref,fix})(Adam) = -8.7035$. All compounds have been measured as 15 mM solutions of analyte and Adam in an equimolar ratio.^a

<i>MW</i> [g/mol]		<i>D_{x,norm}</i> [m ² /s]	<i>log</i> (<i>D_{x,norm}</i>)	<i>log</i> (<i>MW_{det}</i>)	<i>MW_{det}</i> [g/mol]	<i>MW_{dif}</i> [%]
	<i>Not assigned</i>					
78	CD ₂ Cl ₂ ^b	3.1785E-09	-8.4982	-	-	-
152	Si(OMe) ₄ ^b	1.9330E-09	-8.7138	-	-	-
	<i>Compact spheres, ECC_{CS}</i>					
70	Cyclopentane	2.8292E-09	-8.5514	1.82	65	7
72	THF	2.7291E-09	-8.5640	1.84	70	4
88	MTBE	2.3889E-09	-8.6218	1.97	92	-4
88	TMS	2.3700E-09	-8.6252	1.97	94	-6
114	TMB	2.0947E-09	-8.6789	2.09	122	-7
136	Adam	1.9792E-09	-8.7035	2.14	138	-1
234	N(SiMe ₃) ₃	1.5498E-09	-8.8097	2.37	232	1
321	Si(SiMe ₃) ₄	1.3437E-09	-8.8717	2.50	315	2
	<i>Dissipated spheres & ellipsoids, ECC_{DSE}</i>					
92	Toluene	2.6994E-09	-8.5687	1.92	83	10
102	<i>i</i> Pr ₂ O	2.2436E-09	-8.6490	2.06	115	-11
116	Indene	2.2583E-09	-8.6462	2.06	114	2
128	Naphthalene	2.2702E-09	-8.6439	2.05	113	14
146	1,3-Indanedione	1.8832E-09	-8.7251	2.19	156	-6
155	2-PhP	1.9216E-09	-8.7163	2.18	150	3
164	Tetramethoxypropane	1.8372E-09	-8.7358	2.21	163	1
178	DPA	1.7638E-09	-8.7536	2.24	175	2
202	DPS	1.7061E-09	-8.7680	2.27	185	9
204	1-PhN	1.6370E-09	-8.7860	2.30	199	3
244	Triphenylmethane	1.4018E-09	-8.8533	2.41	260	-6
304	Tri(<i>o</i> tolyl)phosphine	1.2127E-09	-8.9162	2.52	334	-9
595	Hexaphenyltrisiloxane	8.7480E-10	-9.0581	2.77	588	1
623	BINAP	8.8427E-10	-9.0534	2.76	577	8
	<i>Expanded discs, ECC_{ED}</i>					
178	Anthracene	2.0189E-09	-8.6949	2.24	172	3
179	Acridine	1.8180E-09	-8.7404	2.30	197	-9
192	9-MA	1.8535E-09	-8.7322	2.28	192	0
202	Pyrene	1.8254E-09	-8.7386	2.29	196	3
208	Anthraquinone	1.7240E-09	-8.7635	2.33	211	-2
228	Triphenylene	1.6913E-09	-8.7718	2.34	217	5
281	DHBP	1.3730E-09	-8.8623	2.45	285	-1
433	TPhN	9.8418E-10	-9.0069	2.64	439	-2
					Ø	±4

^a When a compound had more than one resonance in the ¹H NMR spectrum, the average diffusion coefficient of all resonances was used.

^b CD₂Cl₂ and Si(OMe)₄ were excluded due to elevated molar *van-der-Waals* density (see Table 5-24).

ECCs and Model Compounds for C₆D₆Table 5-14: ECC parameters for C₆D₆ solvates.

	$\log(K)$	$\Delta\log(K)$	$-\alpha$	$\Delta\alpha$
ECC_{Merge}^{C₆D₆}	-7.58	0.0380	-0.572	0.0172
ECC_{CS}^{C₆D₆}	-7.75	0.0545	-0.494	0.0260
ECC_{DSE}^{C₆D₆}	-7.47	0.0284	-0.622	0.0124
ECC_{ED}^{C₆D₆}	-7.06	0.0861	-0.787	0.0365

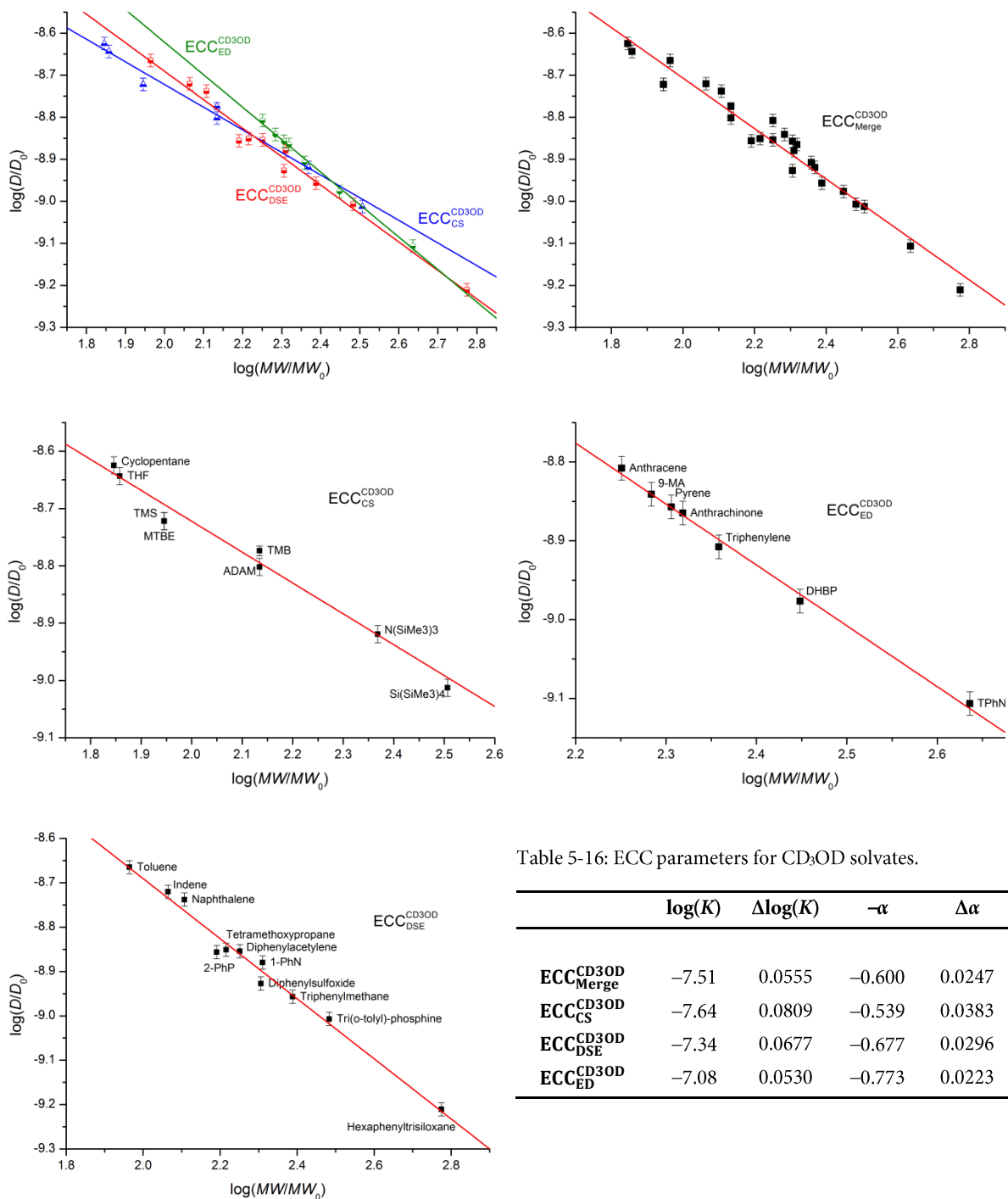
Figure 5-5: Plots of $\log(D_{x, \text{norm}})$ vs. $\log(MW_{\text{calc}})$ of all used model compounds in C₆D₆ sorted by their molecular shape. There is also a merged ECC of all measured compounds for MW estimation, when the molecular shape of an analyte is unknown.

Table 5-15: Overview of all used model compounds for ECC^{C6D6} and their normalized diffusion coefficients $\log(D_{x,\text{norm}})$, the estimated MW_{det} and the deviation from the calculated molecular weight MW_{dif} . Adam was used as internal reference with $\log(D_{\text{ref,fix}})(\text{Adam}) = -8.8025$. All compounds have been measured as 15 mM solutions of analyte and Adam in an equimolar ratio.^a

<i>MW</i> [g/mol]		<i>D_{x, norm}</i> [m ² /s]	<i>log</i> (<i>D_{x, norm}</i>)	<i>log</i> (<i>MW_{det}</i>)	<i>MW_{det}</i> [g/mol]	<i>MW_{dif}</i> [%]
	<i>Not assigned</i>					
152	Si(OMe) ₄ ^b	1.6358E-09	-8.7863	-	-	-
	<i>Compact spheres, ECC_{CS}</i>					
70	Cyclopentane	2.3723E-09	-8.6276	1.78	60	17
72	THF	2.3062E-09	-8.6371	1.80	62	15
78	C ₆ D ₆	2.0446E-09	-8.6894	1.90	80	-2
88	MTBE	1.9816E-09	-8.7030	1.93	85	4
88	TMS	1.9300E-09	-8.7144	1.95	90	-2
114	TMB	1.6708E-09	-8.7771	2.08	120	-5
136	Adam	1.5757E-09	-8.8025	2.13	135	1
234	N(SiMe ₃) ₃	1.2529E-09	-8.9021	2.33	215	9
321	Si(SiMe ₃) ₄	1.0720E-09	-8.9698	2.47	295	9
	<i>Dissipated spheres & ellipsoids, ECC_{DSE}</i>					
92	Toluene	2.0415E-09	-8.6900	1.96	92	1
102	<i>i</i> Pr ₂ O	1.8870E-09	-8.7242	2.02	104	-2
116	Indene	1.7647E-09	-8.7533	2.06	116	0
128	Naphthalene	1.7180E-09	-8.7650	2.08	121	6
146	1,3-Indanedione	1.5988E-09	-8.7962	2.13	136	8
155	2-PhP	1.5072E-09	-8.8218	2.17	149	4
164	Tetramethoxypropane	1.4242E-09	-8.8464	2.21	163	1
178	DPA	1.3338E-09	-8.8749	2.26	181	-2
202	DPS	1.2823E-09	-8.8920	2.29	193	5
204	1-PhN	1.2346E-09	-8.9085	2.31	205	-1
244	Triphenylmethane	1.0505E-09	-8.9786	2.43	266	-8
304	Tri(<i>o</i> tolyl)phosphine	9.6146E-10	-9.0171	2.49	307	-1
595	Hexaphenyltrisiloxane	6.4699E-10	-9.1891	2.76	581	2
623	BINAP	6.3374E-10	-9.1981	2.78	600	4
	<i>Expanded discs, ECC_{ED}</i>					
178	Anthracene	1.4455E-09	-8.8400	2.26	183	-3
179	Acridine	1.4309E-09	-8.8444	2.27	185	-3
192	9-MA	1.3831E-09	-8.8586	2.29	193	0
202	Pyrene	1.3494E-09	-8.8698	2.30	199	1
208	Anthraquinone	1.3704E-09	-8.8631	2.29	196	6
228	Triphenylene	1.2555E-09	-8.9012	2.34	219	4
281	DHBP	1.0487E-09	-8.9793	2.44	275	2
433	TPhN	7.2314E-10	-9.1408	2.64	440	-2
					Ø	±4

^a When a compound had more than one resonance in the ¹H NMR spectrum, the average diffusion coefficient of all resonances was used.

^b Si(OMe)₄ was excluded due to elevated molar *van-der-Waals* density (see Table 5-24).

ECCs and Model Compounds for CD₃ODTable 5-16: ECC parameters for CD₃OD solvates.

	$\log(K)$	$\Delta\log(K)$	$-\alpha$	$\Delta\alpha$
ECC^{CD3OD}_{Merge}	-7.51	0.0555	-0.600	0.0247
ECC^{CD3OD}_{CS}	-7.64	0.0809	-0.539	0.0383
ECC^{CD3OD}_{DSE}	-7.34	0.0677	-0.677	0.0296
ECC^{CD3OD}_{ED}	-7.08	0.0530	-0.773	0.0223

Figure 5-6: Plots of $\log(D_{x,norm})$ vs. $\log(MW_{calc})$ of all used model compounds in CD₃OD sorted by their molecular shape. There is also a merged ECC of all measured compounds for MW estimation, when the molecular shape of an analyte is unknown.

Table 5-17: Overview of all used model compounds for ECC^{CD3OD} and their normalized diffusion coefficients $\log(D_{x,\text{norm}})$, the estimated MW_{det} and the deviation from the calculated molecular weight MW_{dif} . TMB was used as internal reference with $\log(D_{\text{ref,fix}}(\text{TMB})) = -8.7737$. All compounds have been measured as 15 mM solutions of analyte and TMB in an equimolar ratio.^a

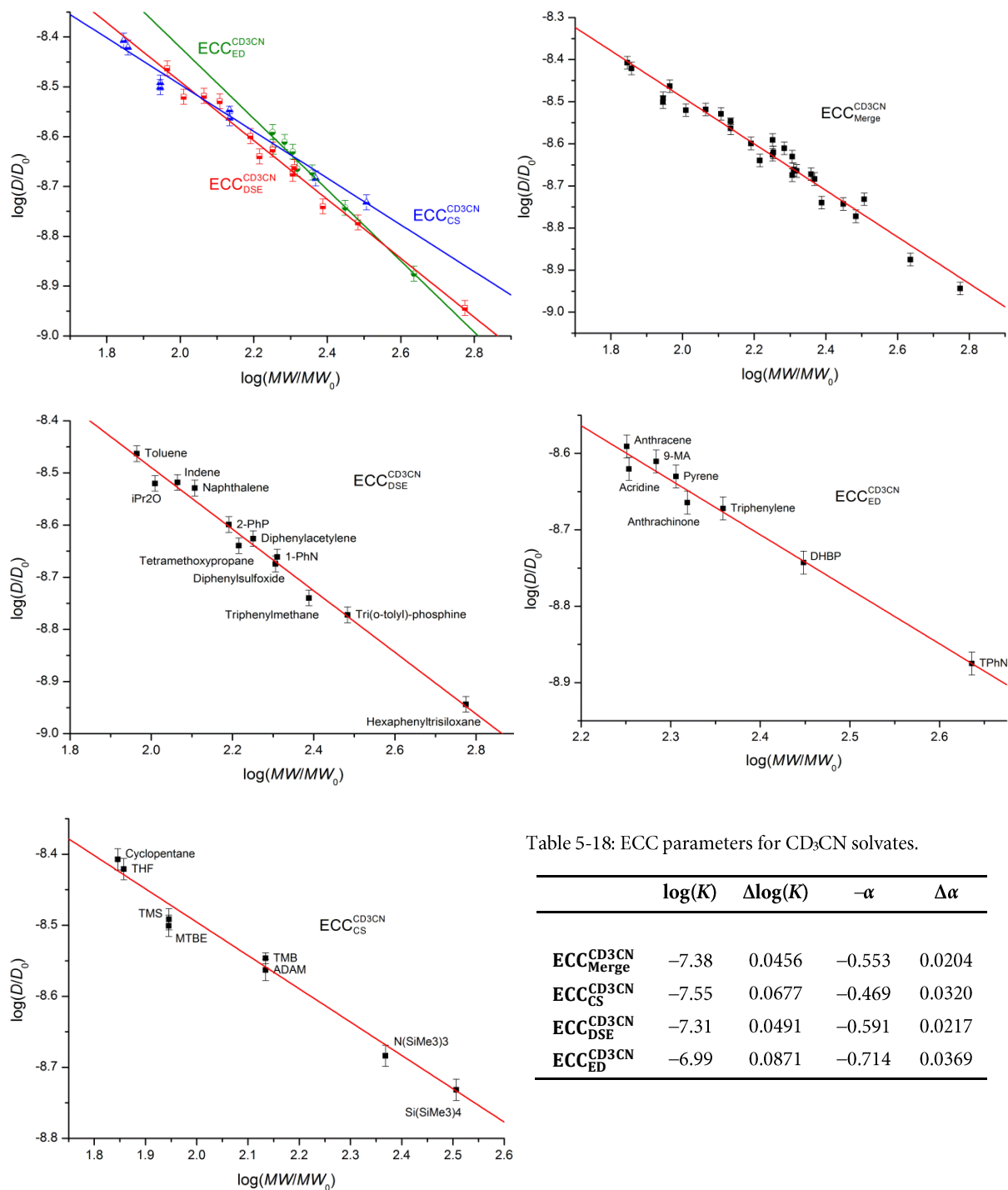
<i>MW</i> [g/mol]		<i>D_{x, norm}</i> [m ² /s]	<i>log</i> (<i>D_{x, norm}</i>)	<i>log</i> (<i>MW_{det}</i>)	<i>MW_{det}</i> [g/mol]	<i>MW_{dif}</i> [%]
	<i>Not assigned</i>					
18	H ₂ O ^b	2.0305E-10	-8.6924	-	-	-
32	CD ₃ OD ^b	2.0167E-10	-8.6926	-	-	-
102	<i>i</i> Pr ₂ O ^b	1.6967E-09	-8.7704	-	-	-
146	1,3-Indanedione ^c	1.4333E-09	-8.8437	-	-	-
152	Si(OMe) ₄ ^d	1.5757E-09	-8.8025	-	-	-
179	Acridine ^c	1.2788E-09	-8.8932	-	-	-
	<i>Compact spheres, ECC_{CS}</i>					
70	Cyclopentane	2.3729E-09	-8.6247	1.83	67	4
72	THF	2.2725E-09	-8.6435	1.86	73	-1
88	MTBE	1.9816E-09	-8.7030	1.97	94	-6
88	TMS	1.8959E-09	-8.7222	2.01	102	-13
114	TMB	1.6840E-09	-8.7737	2.10	127	-10
136	Adam	1.5757E-09	-8.8025	2.16	143	-5
234	N(SiMe ₃) ₃	1.2042E-09	-8.9193	2.37	236	-1
321	Si(SiMe ₃) ₄	9.7101E-10	-9.0128	2.55	352	-9
	<i>Dissipated spheres & ellipsoids, ECC_{DSE}</i>					
92	Toluene	2.1625E-09	-8.6650	1.96	91	2
116	Indene	1.9038E-09	-8.7204	2.04	109	6
128	Naphthalene	1.8273E-09	-8.7382	2.07	116	10
155	2-PhP	1.3923E-09	-8.8563	2.24	174	-11
164	Tetramethoxypropane	1.4242E-09	-8.8464	2.23	168	-2
178	DPA	1.3992E-09	-8.8541	2.24	172	3
202	DPS	1.1827E-09	-8.9271	2.34	221	-8
204	1-PhN	1.3196E-09	-8.8796	2.27	188	9
244	Triphenylmethane	1.1046E-09	-8.9568	2.39	244	0
304	Tri(<i>o</i> tolyl)phosphine	9.8373E-10	-9.0071	2.46	290	5
595	Hexaphenyltrisiloxane	6.1551E-10	-9.2108	2.76	580	3
	<i>Expanded discs, ECC_{ED}</i>					
178	Anthracene	1.5558E-09	-8.8080	2.24	172	3
192	9-MA	1.4425E-09	-8.8409	2.28	190	1
202	Pyrene	1.3897E-09	-8.8571	2.30	199	2
208	Anthrachinone	1.3649E-09	-8.8649	2.31	204	2
228	Triphenylene	1.2367E-09	-8.9078	2.36	231	-1
281	DHBP	1.0554E-09	-8.9766	2.45	284	-1
433	TPhN	7.8206E-10	-9.1068	2.62	419	3
					Ø	±4

^a When a compound had more than one resonance in the ¹H NMR spectrum, the average diffusion coefficient of all resonances was used.

^b CD₃OD, *i*Pr₂O and H₂O were excluded due to hydrogen-bonding. H₂O also has an elevated molar *van-der-Waals* density (see Table 5-24).

^c 1,3-Indanedione and Acridine were excluded due to unknown aggregational behavior.

^d Si(OMe)₄ was excluded due to elevated molar *van-der-Waals* density (see Table 5-24).

ECCs and Model Compounds for CD₃CNTable 5-18: ECC parameters for CD₃CN solvates.

	$\log(K)$	$\Delta\log(K)$	$-\alpha$	$\Delta\alpha$
$ECC^{CD_3CN}_{Merge}$	-7.38	0.0456	-0.553	0.0204
$ECC^{CD_3CN}_{CS}$	-7.55	0.0677	-0.469	0.0320
$ECC^{CD_3CN}_{DSE}$	-7.31	0.0491	-0.591	0.0217
$ECC^{CD_3CN}_{ED}$	-6.99	0.0871	-0.714	0.0369

Figure 5-7: Plots of $\log(D_{x,norm})$ vs. $\log(MW_{calc})$ of all used model compounds in CD₃CN sorted by their molecular shape. There is also a merged ECC of all measured compounds for MW estimation, when the molecular shape of an analyte is unknown.

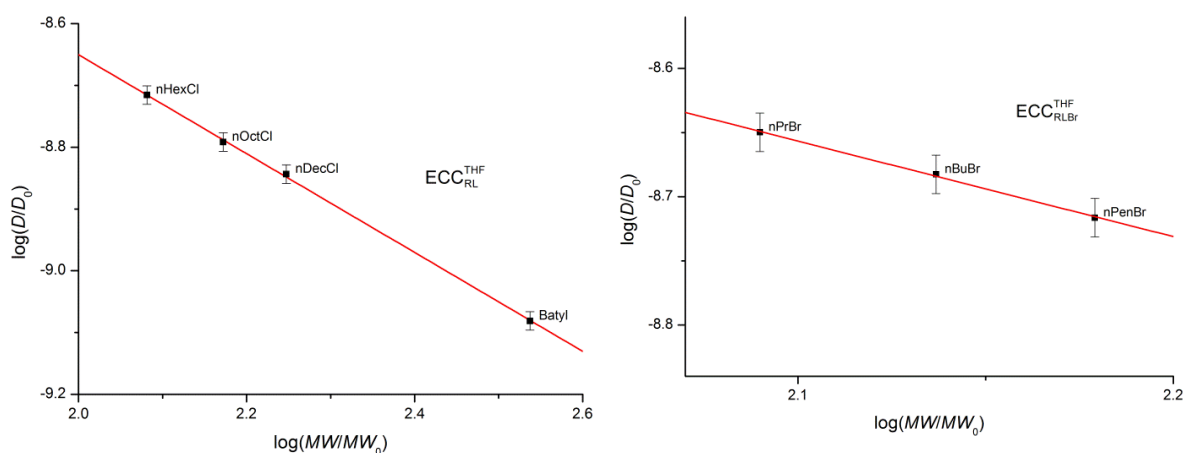
Table 5-19: Overview of all used model compounds for ECC^{CD₃CN} and their normalized diffusion coefficients $\log(D_{x,\text{norm}})$, the estimated MW_{det} and the deviation from the calculated molecular weight MW_{dif} . TMB was used as internal reference with $\log(D_{\text{ref,fix}}(\text{TMB})) = -8.5464$. All compounds have been measured as 15 mM solutions of analyte and TMB in an equimolar ratio.^a

<i>MW</i> [g/mol]		<i>D_{x, norm}</i> [m ² /s]	<i>log</i> (<i>D_{x, norm}</i>)	<i>log</i> (<i>MW_{det}</i>)	<i>MW_{det}</i> [g/mol]	<i>MW_{dif}</i> [%]
	<i>Not assigned</i>					
18	H ₂ O ^b	5.6678E-09	-8.2467	-	-	-
41	CD ₃ CN ^b	4.1844E-09	-8.3784	-	-	-
152	Si(OMe) ₄ ^c	2.5507E-09	-8.5933	-	-	-
	<i>Compact spheres, ECC_{CS}</i>					
70	Cyclopentane	3.9156E-09	-8.4072	1.83	67	4
72	THF	3.7932E-09	-8.4210	1.86	72	0
88	MTBE	3.1567E-09	-8.5007	2.03	106	-17
88	TMS	3.2243E-09	-8.4916	2.01	102	-13
114	TMB	2.8600E-09	-8.5464	2.12	133	-14
136	Adam	2.7352E-09	-8.5630	2.16	145	-6
234	N(SiMe ₃) ₃	2.0716E-09	-8.6837	2.42	261	-10
321	Si(SiMe ₃) ₄	1.8548E-09	-8.7317	2.52	331	-3
	<i>Dissipated spheres & ellipsoids, ECC_{DSE}</i>					
92	Toluene	3.4439E-09	-8.4630	1.95	89	3
102	<i>i</i> Pr ₂ O	3.0190E-09	-8.5201	2.05	112	-8
116	Indene	3.0319E-09	-8.5183	2.04	111	5
128	Naphthalene	2.9581E-09	-8.5290	2.06	116	11
146	1,3-Indanedione	2.3778E-09	-8.6238	2.22	167	-13
155	2-PhP	2.5179E-09	-8.5990	2.18	152	2
164	Tetramethoxypropane	2.2940E-09	-8.6394	2.25	178	-8
178	DPA	2.3667E-09	-8.6259	2.23	168	6
202	DPS	2.1164E-09	-8.6744	2.31	204	-1
204	1-PhN	2.1815E-09	-8.6612	2.29	193	6
244	Triphenylmethane	1.8203E-09	-8.7398	2.42	263	-7
304	Tri(<i>o</i> tolyl)phosphine	1.6895E-10	-8.7722	2.47	298	2
595	Hexaphenyltrisiloxane	1.1385E-09	-8.9437	2.76	581	2
	<i>Expanded discs, ECC_{ED}</i>					
178	Anthracene	2.5650E-09	-8.5909	2.24	175	2
179	Acridine	2.3974E-09	-8.6203	2.28	192	-7
192	9-MA	2.4517E-09	-8.6105	2.27	186	3
202	Pyrene	2.3429E-09	-8.6302	2.30	198	2
208	Anthrachinone	2.1660E-09	-8.6643	2.35	221	-6
228	Triphenylene	2.1282E-09	-8.6720	2.36	227	1
281	DHBP	1.8080E-09	-8.7428	2.45	285	-1
433	TPhN	1.3336E-09	-8.8750	2.64	437	-1
					Ø	±5

^a When a compound had more than one resonance in the ¹H NMR spectrum, the average diffusion coefficient of all resonances was used.

^b CD₃CN and H₂O were excluded due to unknown aggregational behavior. H₂O also has an elevated molar *van-der-Waals* density (see Table 5-24).

^c Si(OMe)₄ was excluded due to elevated molar *van-der-Waals* density (see Table 5-24).

ECCs and Model Compounds for THF- d_8 (Rod-Like and Brominated Rod-Like Molecules)Table 5-20: ECC parameters for THF- d_8 solvates.

	$\log(K)$	$\Delta\log(K)$	$-\alpha$	$\Delta\alpha$
ECC_{RL}^{THF}	-7.05	0.0277	-0.800	0.0122
ECC_{RLBr}^{THF}	-7.09	0.0625	-0.745	0.0293

Figure 5-8: Plots of $\log(D_{x,norm})$ vs. $\log(MW_{calc})$ of rod-like (RL) and brominated rod-like (RLBr) model compounds in THF.Table 5-21: Overview of rod-like model compounds for ECC^{THF} and their normalized diffusion coefficients $\log(D_{x,norm})$, the estimated MW_{det} and the deviation from the calculated molecular weight MW_{dif} . TPhN or THF were used as internal references with $\log(D_{ref,fix})(TPhN) = -9.1054$ or $\log(D_{ref,fix})(THF) = -8.6335$. All compounds have been measured as 25 mM solutions of analyte and reference in an equimolar ratio.^a

MW [g/mol]		$D_{x,norm}$ [m ² /s]	\log ($D_{x,norm}$)	\log (MW_{det})	MW_{det} [g/mol]	MW_{dif} [%] ^b
<i>Rod-like molecules, ECC_{RL}</i>						
121	<i>nHexCl</i>	1.9253E-09	-8.7155	2.08	121	0
149	<i>nOctCl</i>	1.6159E-09	-8.7916	2.18	150	-1
177	<i>nDecCl</i>	1.4338E-09	-8.8435	2.24	175	1
345	<i>Batyl</i>	8.2947E-09	-9.0812	2.54	346	0
<i>Rod-like brominated molecules, ECC_{RLBr}</i>						
123	<i>nPrBr</i>	2.2398E-09	-8.6498	2.09	124	-1
137	<i>nBuBr</i>	2.0773E-09	-8.6825	2.14	137	0
151	<i>nPenBr</i>	1.9218E-10	-8.7163	2.18	152	-1
						\emptyset
						± 1

^a When a compound had more than one resonance in the ¹H NMR spectrum, the average diffusion coefficient of all resonances was used.^b Due to the low reference count with very similar references, theoretical errors may be more feasible (see section 2.3.1).

Theoretical Error Analysis of Model Compounds for Various Solvents

Theoretical errors (ΔMW_{det}) have been calculated for model compounds utilizing the formulae discussed in section 2.1.3. ($\Delta MW_{\text{det,rel}}$ for rod-like molecules are listed in section 2.3.1.1, Table 2-14)

Table 5-22: Calculated relative theoretical errors ($\Delta MW_{\text{det,rel}}$) of model compounds and solvents in $\text{ECC}_{\text{merge}}$. Due to solubility problems, not all references could be measured in all solvents (marked with *).

Solvent	DMSO	C ₆ D ₁₂	CDCl ₃	CD ₃ OD	C ₆ D ₆	CD ₂ Cl ₂	CD ₃ CN	THF	Tol
Compound	ΔMW [%]	ΔMW [%]	ΔMW [%]	ΔMW [%]	ΔMW [%]	ΔMW [%]	ΔMW [%]	ΔMW [%]	ΔMW [%]
1,3-Indanedione	*	11	10	-	6	9	8	7	7
1-PhN	*	15	10	9	7	9	9	8	7
2-PhP	8	12	10	9	7	9	8	7	7
9-MA	8	14	10	9	7	9	8	7	7
Acridine	8	14	10	10	7	9	8	7	7
Adam	8	-	-	9	-	-	8	7	-
Anthracene	*	10	10	9	7	9	8	7	7
Anthraquinone	8	*	10	9	7	9	9	8	7
BINAP	*	15	13	*	9	11	*	9	8
C ₆ D ₆ ^a	-	-	-	-	6	-	-	-	-
CDCl ₃ ^a	-	-	8	-	-	-	-	-	-
CD ₂ Cl ₂ ^a	-	-	-	-	-	7	-	-	-
CD ₃ CN ^a	-	-	-	-	-	-	7	-	-
CD ₃ OD ^a	-	-	-	8	-	-	-	-	-
Cyclohexane- <i>d</i> ₁₂ ^a	-	12	-	-	-	-	-	-	-
Cyclopentane	7	12	8	8	6	8	7	6	6
DHBP	9	14	11	10	7	10	9	-	-
DPA	9	14	10	9	7	9	8	7	7
DPS	9	15	11	10	7	9	9	8	7
DMSO- <i>d</i> ₆ ^a	7	-	-	-	-	-	-	-	-
HexPhTSi ^b	11	16	13	12	9	11	11	9	8
Indene	8	13	9	8	6	8	8	7	6
<i>i</i> Pr ₂ O	7	13	9	9	6	8	8	7	6
MTBE	7	11	9	8	6	8	8	7	6
Naphthalene	8	10	9	9	6	8	8	7	6
N(SiMe ₃) ₃	9	14	11	10	7	10	9	8	7
Pyrene	9	11	10	9	7	9	8	7	7
Si(SiMe ₃) ₄	9	16	11	10	7	10	9	8	7
TMePr ^b	8	14	10	9	7	9	8	7	7
TPhN	10	17	12	11	8	11	10	9	8
THF	7	11	9	8	6	8	7	-	6
TMB	-	14	10	-	6	9	-	-	6
TMS	7	12	9	8	6	8	8	7	6
Toluene	7	11	9	8	6	8	7	6	-
TTolPh ^b	9	16	12	10	8	10	9	8	8
Triphenylene	9	14	10	10	7	9	9	8	7
TPhMe ^b	9	16	11	10	7	10	9	-	-
Water	-	-	-	8	-	-	6	-	-
Ø	8	13	10	9	7	9	8	7	7

Table 5-23: Calculated relative theoretical errors ($\Delta MW_{\text{det,rel}}$) of model compounds and solvents in their corresponding shape-optimized ECCs (ECC_{DSE} , ECC_{CS} , ECC_{ED}). References not fitting to any ECC and internal references are left out.

^a Residual solvent signal.

^b HexPhTSi = Hexamethyltrisiloxane; TMePr = Tetramethoxypropane; TTolPh = Tri(otolyl)phosphine; TPhMe = Triphenylmethane.

Due to solubility problems, not every reference could be measured in all solvents (marked with *). For average errors of the individual shape optimized ECCs see section 2.1.3.

Solvent	DMSO	C ₆ D ₁₂	CDCl ₃	CD ₃ OD	C ₆ D ₆	CD ₂ Cl ₂	CD ₃ CN	THF	Tol
Compound	ΔMW	ΔMW	ΔMW	ΔMW	ΔMW	ΔMW	ΔMW	ΔMW	ΔMW
	[%]	[%]	[%]	[%]	[%]	[%]	[%]	[%]	[%]
1,3-Indanedione	*	9	12	-	4	8	9	5	4
1-PhN	*	9	12	10	5	8	9	5	4
2-PhP	7	8	12	10	4	8	9	5	4
9-MA	8	10	17	7	11	14	12	6	9
Acridine	8	10	17	7	11	15	12	6	9
Adam	19	-	-	15	-	-	15	8	-
Anthracene	*	10	17	7	11	14	12	6	9
Anthraquinone	8	*	18	7	11	15	12	6	9
BINAP	*	11	15	*	6	10	*	6	5
C ₆ D ₆ ^a	-	-	-	-	10	-	-	-	-
Cyclohexane- <i>d</i> ₁₂ ^a	-	15	-	-	-	-	-	-	-
Cyclopentane	16	14	9	13	9	7	13	7	8
DHBP	8	11	19	7	11	16	13	-	-
DPA	7	9	12	10	5	8	9	5	4
DPS	7	9	12	10	5	8	9	5	4
HexPhTSi ^b	8	11	15	12	6	10	11	6	5
Indene	6	8	11	9	4	8	8	4	4
<i>i</i> Pr ₂ O	6	8	11	9	4	8	8	4	4
MTBE	17	14	10	14	10	7	14	7	9
Naphthalene	6	8	11	9	4	8	8	4	4
N(SiMe ₃) ₃	21	17	12	17	12	9	17	9	11
Pyrene	8	10	17	6	11	15	12	6	9
Si(SiMe ₃) ₄	22	18	13	18	13	9	17	10	11
TMePr ^b	7	9	12	10	4	8	9	5	4
TPhN	9	12	20	8	12	17	14	7	10
THF	16	13	9	13	10	7	13	-	8
TMB	-	16	11	-	11	8	-	-	9
TMS	17	15	10	14	10	7	14	7	9
Toluene	6	8	10	9	4	7	8	4	-
TTolPh ^b	8	10	14	11	5	9	10	5	4
Triphenylene	8	11	18	7	11	15	12	6	9
TPhMe ^b	7	10	13	11	5	9	9	-	-

^a Residual solvent signal.

^b HexPhTSi = Hexamethyltrisiloxane; TMePr = Tetramethoxypropane; TTolPh = Tri(*o*tolyl)phosphine; TPhMe = Triphenylmethane.

Molar *Van-Der-Waals* Densities (MD_W) of Model Compounds

Molar *van-der-Waals* densities (MD_W) for all model compounds and proposed solution state structures have been calculated as discussed in section 2.1.4. MD_W for proposed solution state structures are given in the following sections after the corresponding ECC- MW estimations. The ECC- MW estimation works best with molecules that have a molar *van-der-Waals* density between $MD_W = 4.30 \cdot 10^{29} \text{ g}/(\text{mol} \cdot \text{m}^3)$ and $MD_W = 5.92 \cdot 10^{29} \text{ g}/(\text{mol} \cdot \text{m}^3)$, if no correction factor is applied. If MD_W is bigger than $5.92 \cdot 10^{29} \text{ g}/(\text{mol} \cdot \text{m}^3)$, like e.g. for $\text{CHCl}_3/\text{CH}_2\text{Cl}_2$ (marked red) then the predicted MW would be underestimated.^[109a]

Table 5-24: MD_W for model compounds used for ECCs; except for rod-like molecules.

Model Compound	MW [g/mol]	C	H	O	N	S	Cl	P	Si	MD_W [g/(mol · m ³)]	ΣV_W [m ³]
1-PhN	204	16	12	0	0	0	0	0	0	5.16E+29	3.95E-28
1,3-Indanedione	146	9	6	2	0	0	0	0	0	5.89E+29	2.48E-28
2-PhP	155	11	9	0	1	0	0	0	0	5.31E+29	2.93E-28
2,2'-Methylenbisbenzothiazol	282	15	10	0	2	2	0	0	0	6.35E+29	4.44E-28
9-MA	192	15	12	0	0	0	0	0	0	5.12E+29	3.75E-28
Acridine	179	13	9	0	1	0	0	0	0	5.38E+29	3.33E-28
Adam	136	10	16	0	0	0	0	0	0	4.62E+29	2.94E-28
Anthracene	178	14	10	0	0	0	0	0	0	5.18E+29	3.44E-28
Anthracinone	208	14	8	2	0	0	0	0	0	5.75E+29	3.62E-28
BINAP	623	44	32	0	0	0	0	2	0	5.50E+29	1.13E-27
C ₆ H ₆	78	6	6	0	0	0	0	0	0	4.98E+29	1.57E-28
CHCl ₃	119	1	1	0	0	0	3	0	0	12.8E+29	9.30E-29
CH ₂ Cl ₂	85	1	2	0	0	0	2	0	0	11.1E+29	7.66E-29
CH ₃ CN	41	2	3	0	1	0	0	0	0	5.59E+29	7.33E-29
CH ₃ OH	32	1	4	1	0	0	0	0	0	5.56E+29	5.76E-29
Cyclohexane	84	6	12	0	0	0	0	0	0	4.42E+29	1.90E-28
Cyclopentane	70	5	10	0	0	0	0	0	0	4.42E+29	1.58E-28
DHBP	280	22	16	0	0	0	0	0	0	5.17E+29	5.42E-28
DPA	178	14	10	0	0	0	0	0	0	5.18E+29	3.44E-28
DPS	202	12	10	1	0	1	0	0	0	5.92E+29	3.41E-28
DMSO	78	2	6	1	0	1	0	0	0	6.87E+29	1.14E-28
Hexaphenyltrisiloxane	595	36	30	3	0	0	0	0	3	5.57E+29	1.07E-27
Indene	116	9	8	0	0	0	0	0	0	5.05E+29	2.30E-28
iPr ₂ O	102	6	14	1	0	0	0	0	0	4.73E+29	2.16E-28
MTBE	88	5	12	1	0	0	0	0	0	4.78E+29	1.84E-28
Naphthalene	128	10	8	0	0	0	0	0	0	5.12E+29	2.50E-28
N(SiMe ₃) ₃	234	9	27	0	1	0	0	0	3	4.99E+29	4.69E-28
Pyrene	202	16	10	0	0	0	0	0	0	5.25E+29	3.85E-28
Si(OMe) ₄	152	4	12	4	0	0	0	0	1	6.17E+29	2.46E-28
Si(SiMe ₃) ₄	321	12	36	0	0	0	0	0	5	5.00E+29	6.42E-28
Tetramethoxypropane	164	7	16	4	0	0	0	0	0	5.62E+29	2.92E-28
TPhN	433	34	24	0	0	0	0	0	0	5.19E+29	8.34E-28
THF	72	4	8	1	0	0	0	0	0	5.09E+29	1.41E-28
TMB	114	8	18	0	0	0	0	0	0	4.31E+29	2.65E-28
TMS	88	4	12	0	0	0	0	0	1	4.69E+29	1.88E-28
Toluene	92	7	8	0	0	0	0	0	0	4.88E+29	1.89E-28
Tri(otolyl)phosphine	304	21	21	0	0	0	0	1	0	5.31E+29	5.73E-28
Triphenylene	228	18	12	0	0	0	0	0	0	5.22E+29	4.37E-28
Triphenylmethane	244	19	16	0	0	0	0	0	0	5.09E+29	4.80E-28

Table 5-25: MD_W and $\log(D_{x,\text{norm}})$ for all reference compounds used by Wang and Pedersen *et al.* for their ^1H -DOSY ECC in CD_2Cl_2 .^[113]

Model Compound	MW [g/mol]	C	H	O	F	B	N	Cl	Si	S	MD_W [g/(mol · m ³)]	$\log(D_{x,\text{norm}})$
Et ₂ O	76	4	12	1	0	0	0	0	0	0	4.64E+29	-8.5724
BF ₃ · Et ₂ O	144	4	12	1	3	1	0	0	0	0	6.16E+29	-8.6364
A*	390	16	22	11	0	0	0	0	0	0	6.36E+29	-8.7342
B*	541	21	24	9	0	0	1	3	0	0	6.92E+29	-8.7578
C*	610	28	8	0	14	0	0	0	0	0	7.56E+29	-8.7759
D*	1226	76	88	5	0	0	0	0	4	1	5.31E+29	-8.8429

*Abbreviations according to Scheme 2-1.

ECC-MW Estimations of CpM Derivatives (M = Li, Na, K, Rb, Cs)

ECC-MW Estimation of CpLi in THF and DMSO

Table 5-26: ¹H- and ⁷Li-DOSY-ECC-MW estimation of CpLi in THF-*d*₈ (15 mM) at different temperatures. TPhN or TMB were used as internal references with $\log(D_{\text{ref,fix}}(\text{TPhN})) = -9.1054$ or $\log(D_{\text{ref,fix}}(\text{TMB})) = -8.7749$. The accuracy of the ECC^{THF} (DSE) is in the range of $MW_{\text{dif}} = \pm 8\%$. Hypothetical aggregates are $[\text{CpLi}(\text{THF})_x]$ and $[(\text{CpLi})_2(\text{THF})_x]$ with $x = 1-4$. A trend is visible towards higher MWs upon cooling, indicating the formation of a $[\text{Cp}_2\text{Li}]^-$ species proposed by Paquette *et al.*^[66]. Still, note that $[\text{CpLi}(\text{THF})]$ has a similar MW as $[\text{Cp}_2\text{Li}]^-$, $[\text{CpLi}(\text{THF})_2]$ as $[\text{Cp}_2\text{Li}(\text{THF})]^-$ and so on. For ECC^{THF} parameters and changes compared to literature^[109a] see section 2.1.1.

¹ H-DOSY			50 °C	
		Aggregate	MW _{calc} [g/mol]	MW _{dif} [%]
D_x [m ² /s]	2.175E-09	[CpLi(THF)]	144	-30
$\log(D_x)$	-8.6625	[CpLi(THF) ₂]	216	5
$\log(D_{x,\text{norm}})$	-8.8855	[CpLi(THF) ₃]	288	41
$D_{\text{ref}}(\text{TMB})$ [m ² /s]	2.806E-09	[CpLi(THF) ₄]	360	76
$\log(D_{\text{ref}})(\text{TMB})$	-8.5519	$[(\text{CpLi})_2(\text{THF})]$	216	5
MW _{det} [g/mol]	205	$[(\text{CpLi})_2(\text{THF})_2]$	288	41
ΔMW_{det} [g/mol] (%)	±10 (5)	$[(\text{CpLi})_2(\text{THF})_3]$	360	76
		$[(\text{CpLi})_2(\text{THF})_4]$	432	111
¹ H-DOSY			25 °C	
		Aggregate	MW _{calc} [g/mol]	MW _{dif} [%]
D_x [m ² /s]	1.407E-09	[CpLi(THF)]	144	-34
$\log(D_x)$	-8.8517	[CpLi(THF) ₂]	216	-1
$\log(D_{x,\text{norm}})$	-8.9012	[CpLi(THF) ₃]	288	32
$D_{\text{ref}}(\text{TPhN})$ [m ² /s]	8.791E-09	[CpLi(THF) ₄]	360	65
$\log(D_{\text{ref}})(\text{TPhN})$	-9.0559	$[(\text{CpLi})_2(\text{THF})]$	216	-1
MW _{det} [g/mol]	218	$[(\text{CpLi})_2(\text{THF})_2]$	288	32
ΔMW_{det} [g/mol] (%)	±11 (5)	$[(\text{CpLi})_2(\text{THF})_3]$	360	65
		$[(\text{CpLi})_2(\text{THF})_4]$	432	98
¹ H-DOSY			-50 °C	
		Aggregate	MW _{calc} [g/mol]	MW _{dif} [%]
D_x [m ² /s]	3.381E-10	[CpLi(THF)]	144	-35
$\log(D_x)$	-9.4710	[CpLi(THF) ₂]	216	-2
$\log(D_{x,\text{norm}})$	-8.9050	[CpLi(THF) ₃]	288	30
$D_{\text{ref}}(\text{TMB})$ [m ² /s]	4.562E-10	[CpLi(THF) ₄]	360	63
$\log(D_{\text{ref}})(\text{TMB})$	-9.3408	$[(\text{CpLi})_2(\text{THF})]$	216	-2
MW _{det} [g/mol]	222	$[(\text{CpLi})_2(\text{THF})_2]$	288	30
ΔMW_{det} [g/mol] (%)	±11 (5)	$[(\text{CpLi})_2(\text{THF})_3]$	360	63
		$[(\text{CpLi})_2(\text{THF})_4]$	432	95
¹ H-DOSY			-80 °C	
		Aggregate	MW _{calc} [g/mol]	MW _{dif} [%]
D_x [m ² /s]	1.144E-10	[CpLi(THF)]	144	-36
$\log(D_x)$	-9.9416	[CpLi(THF) ₂]	216	-4
$\log(D_{x,\text{norm}})$	-8.9090	[CpLi(THF) ₃]	288	28
$D_{\text{ref}}(\text{TMB})$ [m ² /s]	1.558E-10	[CpLi(THF) ₄]	360	60
$\log(D_{\text{ref}})(\text{TMB})$	-9.8074	$[(\text{CpLi})_2(\text{THF})]$	216	-4
MW _{det} [g/mol]	225	$[(\text{CpLi})_2(\text{THF})_2]$	288	28
ΔMW_{det} [g/mol] (%)	±11 (5)	$[(\text{CpLi})_2(\text{THF})_3]$	360	60
		$[(\text{CpLi})_2(\text{THF})_4]$	432	92
¹ H-DOSY			-100 °C	
No interpretable data				

⁷ Li-DOSY				50 °C
		Aggregate	MW _{calc} [g/mol]	MW _{dif} [%]
D_x [m ² /s]	2.085E-09	[CpLi(THF)]	144	-35
$\log(D_x)$	-8.6809	[CpLi(THF) ₂]	216	-2
$\log(D_{x,norm})$	-8.9039	[CpLi(THF) ₃]	288	31
D_{ref} (TMB) [m ² /s]	2.806E-09	[CpLi(THF) ₄]	360	63
$\log(D_{ref})$ (TMB)	-8.5519	[(CpLi) ₂ (THF)]	216	-2
MW _{det} [g/mol]	221	[(CpLi) ₂ (THF) ₂]	288	31
ΔMW_{det} [g/mol] (%)	±11 (5)	[(CpLi) ₂ (THF) ₃]	360	63
		[(CpLi) ₂ (THF) ₄]	432	96
⁷ Li-DOSY				25 °C
		Aggregate	MW _{calc} [g/mol]	MW _{dif} [%]
D_x [m ² /s]	1.519E-09	[CpLi(THF)]	144	-30
$\log(D_x)$	-8.8184	[CpLi(THF) ₂]	216	5
$\log(D_{x,norm})$	-8.8874	[CpLi(THF) ₃]	288	40
D_{ref} (TMB) [m ² /s]	1.968E-09	[CpLi(THF) ₄]	360	74
$\log(D_{ref})$ (TMB)	-8.7060	[(CpLi) ₂ (THF)]	216	5
MW _{det} [g/mol]	207	[(CpLi) ₂ (THF) ₂]	288	40
ΔMW_{det} [g/mol] (%)	±10 (5)	[(CpLi) ₂ (THF) ₃]	360	74
		[(CpLi) ₂ (THF) ₄]	432	109
⁷ Li-DOSY				-50 °C
		Aggregate	MW _{calc} [g/mol]	MW _{dif} [%]
D_x [m ² /s]	3.369E-10	[CpLi(THF)]	144	-35
$\log(D_x)$	-9.4724	[CpLi(THF) ₂]	216	-3
$\log(D_{x,norm})$	-8.9066	[CpLi(THF) ₃]	288	29
D_{ref} (TMB) [m ² /s]	4.562E-10	[CpLi(THF) ₄]	360	62
$\log(D_{ref})$ (TMB)	-9.3408	[(CpLi) ₂ (THF)]	216	-3
MW _{det} [g/mol]	223	[(CpLi) ₂ (THF) ₂]	288	29
ΔMW_{det} [g/mol] (%)	±11 (5)	[(CpLi) ₂ (THF) ₃]	360	62
		[(CpLi) ₂ (THF) ₄]	432	94
⁷ Li-DOSY				-80 °C & -100 °C
No interpretable data				

Table 5-27: ¹H- and ⁷Li-DOSY-ECC-MW estimation of CpLi in DMSO-*d*₆ (15 mM) at 25 °C. TMB was used as internal reference with $\log(D_{ref,fix})(TMB) = -9.2963$. The accuracy of the ECC^{DMSO} (merged) is in the range of $MW_{dif} = \pm 20\%$. Hypothetical, even though unlikely, aggregates are listed; other contributions are probably hindering diffusion. For the ⁷Li-DOSY only considering ECC-MW estimation leads to no viable structure. For ECC^{DMSO} parameters see Figure 5-1.

¹ H-DOSY				25 °C
		Aggregate	MW _{calc} [g/mol]	MW _{dif} [%]
D_x [m ² /s]	1.444E-10	[Cp] ⁻	65	-47
$\log(D_x)$	-9.8404	[CpLi]	72	-41
$\log(D_{x,norm})$	-9.2763	[CpLi(DMSO)]	150	23
D_{ref} (TMB) [m ² /s]	1.379E-10			
$\log(D_{ref})$ (TMB)	-9.8604			
MW _{det} [g/mol]	123			
ΔMW_{det} [g/mol] (%)	±10 (8)			

⁷ Li-DOSY			25 °C	
		Aggregate	MW _{calc} [g/mol]	MW _{dif} [%]
D_x [m ² /s]	2.853E-10	[CpLi]	72	67
$\log(D_x)$	-9.5447			
$\log(D_{x,norm})$	-8.9039			
D_{ref} (TMB) [m ² /s]	1.379E-10			
$\log(D_{ref})$ (TMB)	-9.8604			
MW _{det} [g/mol]	43			
ΔMW_{det} [g/mol] (%)	±3 (6)			

ECC-MW Estimation of CpNa in THF and DMSO

Table 5-28: ¹H-DOSY-ECC-MW estimation of CpNa in THF-*d*₈ (15 mM) at different temperatures. TPhN or TMB were used as internal references with $\log(D_{ref,fix})(TPhN) = -9.1054$ or $\log(D_{ref,fix})(TMB) = -8.7749$. The accuracy of the ECC^{THF} (DSE) is in the range of $MW_{dif} = \pm 8\%$.^[109a] Hypothetical aggregates are [CpNa(THF)_x] and [(CpNa)₂(THF)_x] with x = 1-4. For ECC^{THF} parameters and changes compared to literature^[109a] see section 2.1.1.

¹ H-DOSY			25 °C	
		Aggregate	MW _{calc} [g/mol]	MW _{dif} [%]
D_x [m ² /s]	1.120E-09	[CpNa(THF)]	160	-46
$\log(D_x)$	-8.9508	[CpNa(THF) ₂]	232	-21
$\log(D_{x,norm})$	-8.9778	[CpNa(THF) ₃]	304	3
D_{ref} (TPhN) [m ² /s]	8.348E-09	[CpNa(THF) ₄]	376	27
$\log(D_{ref})$ (TPhN)	-9.0784	[(CpNa) ₂ (THF)]	248	-16
MW _{det} [g/mol]	295	[(CpNa) ₂ (THF) ₂]	320	8
ΔMW_{det} [g/mol] (%)	±16 (5)	[(CpNa) ₂ (THF) ₃]	392	33
		[(CpNa) ₂ (THF) ₄]	464	57
¹ H-DOSY			-50 °C	
		Aggregate	MW _{calc} [g/mol]	MW _{dif} [%]
D_x [m ² /s]	2.817E-10	[CpNa(THF)]	160	-44
$\log(D_x)$	-9.5502	[CpNa(THF) ₂]	232	-19
$\log(D_{x,norm})$	-8.9705	[CpNa(THF) ₃]	304	6
D_{ref} (TMB) [m ² /s]	4.420E-10	[CpNa(THF) ₄]	376	31
$\log(D_{ref})$ (TMB)	-9.3546	[(CpNa) ₂ (THF)]	248	-14
MW _{det} [g/mol]	287	[(CpNa) ₂ (THF) ₂]	320	12
ΔMW_{det} [g/mol] (%)	±15 (5)	[(CpNa) ₂ (THF) ₃]	392	37
		[(CpNa) ₂ (THF) ₄]	464	62

Table 5-29: ¹H-DOSY-ECC-MW estimation of CpNa in DMSO-*d*₆ (15 mM) at different temperatures. TMB was used as internal reference with $\log(D_{ref,fix})(TMB) = -9.2963$. The accuracy of the ECC^{DMSO} (merged) is in the range of $MW_{dif} = \pm 20\%$. Hypothetical, even though unlikely, aggregates are listed; other factors are probably hindering diffusion. For ECC^{DMSO} parameters see Figure 5-1.

¹ H-DOSY			75 °C	
		Aggregate	MW _{calc} [g/mol]	MW _{dif} [%]
D_x [m ² /s]	1.396E-09	[Cp] ⁻	65	-51
$\log(D_x)$	-8.8551	[CpNa]	88	-34
$\log(D_{x,norm})$	-9.3003	[CpNa(DMSO)]	166	25
D_{ref} (TMB) [m ² /s]	1.409E-09			
$\log(D_{ref})$ (TMB)	-8.8511			
MW _{det} [g/mol]	134			
ΔMW_{det} [g/mol] (%)	±11 (8)			

¹ H-DOSY		50 °C		
		Aggregate	MW _{calc} [g/mol]	MW _{dif} [%]
D_x [m ² /s]	8.695E-10	[Cp] ⁻	65	-48
$\log(D_x)$	-9.0607	[CpNa]	88	-30
$\log(D_{x,norm})$	-9.2835	[CpNa(DMSO)]	166	32
D_{ref} (TMB) [m ² /s]	8.444E-10			
$\log(D_{ref})$ (TMB)	-9.0735			
MW _{det} [g/mol]	126			
ΔMW_{det} [g/mol] (%)	±10 (8)			
¹ H-DOSY		25 °C		
		Aggregate	MW _{calc} [g/mol]	MW _{dif} [%]
D_x [m ² /s]	5.171E-10	[Cp] ⁻	65	-47
$\log(D_x)$	-9.2864	[CpNa]	88	-28
$\log(D_{x,norm})$	-9.2733	[CpNa(DMSO)]	166	37
D_{ref} (TMB) [m ² /s]	4.905E-10			
$\log(D_{ref})$ (TMB)	-9.3094			
MW _{det} [g/mol]	122			
ΔMW_{det} [g/mol] (%)	±10 (8)			

ECC-MW Estimation of CpK in THF and DMSO

Table 5-30: ¹H-DOSY-ECC-MW estimation of CpK in THF-*d*₈ (15 mM) at 25 °C. TPhN was used as internal reference with $\log(D_{ref,fix})(TPhN) = -9.1054$. The accuracy of the ECC^{T^{HF}} (DSE) is in the range of $MW_{dif} = \pm 8\%$. Hypothetical aggregates are [CpK(THF)_x] and [(CpK)₂(THF)_x] with x = 1-4. For ECC^{T^{HF}} parameters and changes compared to literature^[109a] see section 2.1.1.

¹ H-DOSY		25 °C		
		Aggregate	MW _{calc} [g/mol]	MW _{dif} [%]
D_x [m ² /s]	1.136E-09	[CpK(THF)]	176	-47
$\log(D_x)$	-8.9446	[CpK(THF) ₂]	248	-26
$\log(D_{x,norm})$	-9.0098	[CpK(THF) ₃]	320	-4
D_{ref} (TPhN) [m ² /s]	9.116E-09	[CpK(THF) ₄]	392	17
$\log(D_{ref})$ (TPhN)	-9.0402	[(CpK) ₂ (THF)]	280	-16
MW _{det} [g/mol]	335	[(CpK) ₂ (THF) ₂]	353	5
ΔMW_{det} [g/mol] (%)	±18 (5)	[(CpK) ₂ (THF) ₃]	425	27
		[(CpK) ₂ (THF) ₄]	497	48

Table 5-31: ¹H-DOSY-ECC-MW estimation of CpK in DMSO-*d*₆ (15 mM) at 25 °C. TMB was used as internal reference with $\log(D_{ref,fix})(TMB) = -9.2963$. The accuracy of the ECC^{D^{MSO}} (merged) is in the range of $MW_{dif} = \pm 20\%$. Hypothetical, even though unlikely, aggregates are listed; other factors are probably hindering diffusion. For ECC^{D^{MSO}} parameters see Figure 5-1.

¹ H-DOSY		25 °C		
		Aggregate	MW _{calc} [g/mol]	MW _{dif} [%]
D_x [m ² /s]	5.304E-10	[Cp] ⁻	65	-46
$\log(D_x)$	-9.2754	[CpK]	104	-14
$\log(D_{x,norm})$	-9.2706	[CpK(DMSO)]	182	52
D_{ref} (TMB) [m ² /s]	4.999E-10			
$\log(D_{ref})$ (TMB)	-9.3011			
MW _{det} [g/mol]	121			
ΔMW_{det} [g/mol] (%)	±9 (8)			

ECC-MW Estimation of CpRb in THF and DMSO

Table 5-32: ¹H-DOSY-ECC-MW estimation of CpRb in THF-*d*₈ (15 mM) at 25 °C. TPhN was used as internal reference with $\log(D_{\text{ref,fix}})(\text{TPhN}) = -9.1054$. The accuracy of the ECC^{THF} (DSE) is in the range of $MW_{\text{dif}} = \pm 8\%$. Hypothetical aggregates are [CpRb(THF)_x] and [(CpRb)₂(THF)_x] with $x = 1-4$. For ECC^{THF} parameters and changes compared to literature^[109a] see section 2.1.1.

¹ H-DOSY		25 °C		
		Aggregate	MW_{calc} [g/mol]	MW_{dif} [%]
D_x [m ² /s]	1.272E-09	[CpRb(THF)]	223	-24
$\log(D_x)$	-8.8955	[CpRb(THF) ₂]	295	0
$\log(D_{x,\text{norm}})$	-8.9770	[CpRb(THF) ₃]	367	25
$D_{\text{ref}}(\text{TPhN})$ [m ² /s]	9.464E-09	[CpRb(THF) ₄]	439	49
$\log(D_{\text{ref}})(\text{TPhN})$	-9.0239	[(CpRb) ₂ (THF)]	373	27
MW_{det} [g/mol]	294	[(CpRb) ₂ (THF) ₂]	445	51
ΔMW_{det} [g/mol] (%)	±16 (5)	[(CpRb) ₂ (THF) ₃]	517	76
		[(CpRb) ₂ (THF) ₄]	589	100

Table 5-33: ¹H-DOSY-ECC-MW estimation of CpRb in DMSO-*d*₆ (15 mM) at 25 °C. TMB was used as internal reference with $\log(D_{\text{ref,fix}})(\text{TMB}) = -9.2963$. The accuracy of the ECC^{DMSO} (merged) is in the range of $MW_{\text{dif}} = \pm 20\%$. Hypothetical, even though unlikely, aggregates are listed; other contributions could be hindering diffusion. For ECC^{DMSO} parameters see Figure 5-1.

¹ H-DOSY		25 °C		
		Aggregate	MW_{calc} [g/mol]	MW_{dif} [%]
D_x [m ² /s]	5.282E-10	[Cp] ⁻	65	-45
$\log(D_x)$	-9.2772	[CpRb]	151	27
$\log(D_{x,\text{norm}})$	-9.2671	[CpRb(DMSO)]	229	93
$D_{\text{ref}}(\text{TMB})$ [m ² /s]	4.938E-10			
$\log(D_{\text{ref}})(\text{TMB})$	-9.3064			
MW_{det} [g/mol]	119			
ΔMW_{det} [g/mol] (%)	±9 (8)			

ECC-MW Estimation of CpCs in THF and DMSO

Table 5-34: ¹H-DOSY-ECC-MW estimation of CpCs in THF-*d*₈ (15 mM) at different temperatures. TPhN or TMB were used as internal references with $\log(D_{\text{ref,fix}})(\text{TPhN}) = -9.1054$ or $\log(D_{\text{ref,fix}})(\text{TMB}) = -8.7749$. The accuracy of the ECC^{THF} (merged) is in the range of $MW_{\text{dif}} = \pm 18\%$. Exemplary, hypothetical aggregates are [(CpCs)₅(THF)₁₀] or [(CpCs)₆(THF)₁₂], while other combinations may also be viable. For ECC^{THF} parameters and changes compared to literature^[109a] see section 2.1.1.

¹ H-DOSY		50 °C		
		Aggregate	MW_{calc} [g/mol]	MW_{dif} [%]
D_x [m ² /s]	6.201E-09	[(CpCs) ₅ (THF) ₁₀]	1710	-8
$\log(D_x)$	-9.2076	[(CpCs) ₆ (THF) ₁₂]	2053	10
$\log(D_{x,\text{norm}})$	-9.4085			
$D_{\text{ref}}(\text{TMB})$ [m ² /s]	2.667E-09			
$\log(D_{\text{ref}})(\text{TMB})$	-8.5740			
MW_{det} [g/mol]	1864			
ΔMW_{det} [g/mol] (%)	±199 (11)			

¹ H-DOSY			25 °C	
		Aggregate	MW _{calc} [g/mol]	MW _{dir} [%]
D_x [m ² /s]	4.595E-09	[(CpCs) ₅ (THF) ₁₀]	1710	-8
log(D_x)	-9.3377	[(CpCs) ₆ (THF) ₁₂]	2053	11
log($D_{x,norm}$)	-9.4072			
D_{ref} (TPhN) [m ² /s]	9.211E-09			
log(D_{ref})(TPhN)	-9.0359			
MW _{det} [g/mol]	1855			
ΔMW _{det} [g/mol] (%)	±198 (11)			

Table 5-35: ¹H-DOSY-ECC-MW estimation of CpCs in DMSO-*d*₆ (15 mM) at 25 °C. TMB was used as internal reference with log($D_{ref,fix}$)(TMB) = -9.2963. The accuracy of the ECC^{DMSO} (merged) is in the range of MW_{dir} = ±20%. Hypothetical, even though unlikely, aggregates are listed; other contributions are probably hindering diffusion. For ECC^{DMSO} parameters see Figure 5-1.

¹ H-DOSY			25 °C	
		Aggregate	MW _{calc} [g/mol]	MW _{dir} [%]
D_x [m ² /s]	4.747E-10	[Cp] ⁻	65	-62
log(D_x)	-9.3236	[CpCs]	151	-12
log($D_{x,norm}$)	-9.3699	[CpCs(DMSO)]	276	62
D_{ref} (TMB) [m ² /s]	5.624E-10			
log(D_{ref})(TMB)	-9.2500			
MW _{det} [g/mol]	172			
ΔMW _{det} [g/mol] (%)	±15 (8)			

ECC-MW Estimation of MeCpLi in THF

Table 5-36: ¹H-DOSY-ECC-MW estimation of MeCpLi in THF-*d*₈ (15 mM) at 25 °C. Adam was used as internal reference with log($D_{ref,fix}$)(Adam) = -8.8078. The accuracy of the ECC^{THF} (DSE) is in the range of MW_{dir} = ±8%. Hypothetical aggregates are [MeCpLi(THF)_x] and [(MeCpLi)₂(THF)_x] with x = 1-4. For ECC^{THF} parameters and changes compared to literature^[109a] see section 2.1.1.

¹ H-DOSY			25 °C	
		Aggregate	MW _{calc} [g/mol]	MW _{dir} [%]
D_x [m ² /s]	3.427E-10	[MeCpLi(THF)]	157	-34
log(D_x)	-9.4650	[MeCpLi(THF) ₂]	229	-3
log($D_{x,norm}$)	-8.9218	[MeCpLi(THF) ₃]	301	27
D_{ref} (Adam) [m ² /s]	4.432E-10	[MeCpLi(THF) ₄]	373	57
log(D_{ref})(Adam)	-9.3534	[(MeCpLi) ₂ (THF)]	242	2
MW _{det} [g/mol]	237	[(MeCpLi) ₂ (THF) ₂]	314	32
ΔMW _{det} [g/mol] (%)	±12 (5)	[(MeCpLi) ₂ (THF) ₃]	386	63
		[(MeCpLi) ₂ (THF) ₄]	458	93

ECC-MW Estimation of Cp*K in THF

Table 5-37: ¹H-DOSY-ECC-MW estimation of Cp*K in THF-*d*₈ (15 mm) at 25 °C. TPhN was used as internal reference with $\log(D_{\text{ref,fix}}(\text{TPhN})) = -9.1054$. The accuracy of the ECC^{THF} (DSE) is in the range of $MW_{\text{dif}} = \pm 8\%$. Hypothetical aggregates are $[\text{Cp}^*\text{K}(\text{THF})_x]$ and $[(\text{Cp}^*\text{K})_2(\text{THF})_x]$ with $x = 1-4$. For ECC^{THF} parameters and changes compared to literature^[109a] see section 2.1.1.

¹ H-DOSY		25 °C		
		Aggregate	MW_{calc} [g/mol]	MW_{dif} [%]
D_x [m ² /s]	1.096E-09	[Cp*K(THF)]	246	-35
$\log(D_x)$	-8.9602	[Cp*K(THF) ₂]	318	-16
$\log(D_{x,\text{norm}})$	-9.0393	[Cp*K(THF) ₃]	391	4
$D_{\text{ref}}(\text{TPhN})$ [m ² /s]	9.414E-09	[Cp*K(THF) ₄]	463	23
$\log(D_{\text{ref}}(\text{TPhN}))$	-9.0262	[(Cp*K) ₂ (THF)]	421	12
MW_{det} [g/mol]	377	[(Cp*K) ₂ (THF) ₂]	493	31
ΔMW_{det} [g/mol] (%)	± 21 (5)	[(Cp*K) ₂ (THF) ₃]	565	50
		[(Cp*K) ₂ (THF) ₄]	637	69

ECC-MW Estimation of Cp*Cs in THF

Table 5-38: ¹H-DOSY-ECC-MW estimation of Cp*Cs in THF-*d*₈ (15 mm) at 25 °C. TPhN was used as internal reference with $\log(D_{\text{ref,fix}}(\text{TPhN})) = -9.1054$. The accuracy of the ECC^{THF} (DSE) is in the range of $MW_{\text{dif}} = \pm 8\%$. Hypothetical aggregates are $[\text{Cp}^*\text{Cs}(\text{THF})_x]$ and $[(\text{Cp}^*\text{Cs})_2(\text{THF})_x]$ with $x = 1-4$. For ECC^{THF} parameters and changes compared to literature^[109a] see section 2.1.1.

¹ H-DOSY		25 °C		
		Aggregate	MW_{calc} [g/mol]	MW_{dif} [%]
D_x [m ² /s]	9.218E-10	[Cp*Cs(THF)]	340	-40
$\log(D_x)$	-9.0354	[Cp*Cs(THF) ₂]	412	-27
$\log(D_{x,\text{norm}})$	-9.1411	[Cp*Cs(THF) ₃]	484	-14
$D_{\text{ref}}(\text{TPhN})$ [m ² /s]	1.001E-09	[Cp*Cs(THF) ₄]	556	-1
$\log(D_{\text{ref}}(\text{TPhN}))$	-8.9996	[(Cp*Cs) ₂ (THF)]	608	8
MW_{det} [g/mol]	564	[(Cp*Cs) ₂ (THF) ₂]	680	21
ΔMW_{det} [g/mol] (%)	± 33 (6)	[(Cp*Cs) ₂ (THF) ₃]	752	33
		[(Cp*Cs) ₂ (THF) ₄]	825	46

Molar Van-Der-Waals Densities (MD_W)

Table 5-39: MD_W for most likely solution state structures of CpM derivatives.

Aggregate	MW [g/mol]	C	H	O	M ^a	MD_W [g/(mol · m ³)]	ΣV_W [m ³]
[CpLi(THF) ₂]	216	13	21	2	1	4.92E+29	4.39E-28
[CpNa(THF) ₃]	304	17	29	3	1	5.03E+29	6.05E-28
[CpK(THF) ₃]	321	17	29	3	1	4.99E+29	6.43E-28
[CpRb(THF) ₂]	295	13	21	3	1	5.56E+29	5.31E-28
[(CpCs) ₅ (THF) ₁₀]	1711	65	105	10	5	5.87E+29	2.92E-27
[MeCpLi(THF) ₂]	230	14	23	2	1	4.89E+29	4.71E-28
[Cp*K(THF) ₃]	391	22	39	3	1	4.87E+29	8.01E-28
[Cp*Cs(THF) ₄]	557	26	47	4	1	5.43E+29	1.02E-27

^a Always the corresponding alkali metal: M = Li, Na, K, Rb or Cs

ECC-MW Estimations of RMgX (R = Et, *i*Pr, *n*Bu, *n*Hex, *n*Oct, *n*Dec; X = Cl, Br)

ECC-MW Estimation of EtMgCl in THF

Table 5-40: ¹H-DOSY-ECC-MW estimation of EtMgCl in THF-*d*₈ (25 mM) at 25 °C. TPhN was used as internal reference with $\log(D_{\text{ref,fix}})(\text{TPhN}) = -9.1054$. The accuracy of the ECC^{THF} (RL) is in the range of $MW_{\text{dir}} = \pm 8\%$ (see section 2.3.1.1). Hypothetical aggregates are [EtMgCl(THF)₂] and [EtMgCl(THF)]₂. For ECC^{THF} parameters see Figure 5-8.

¹ H-DOSY		25 °C		
		Aggregate	MW _{calc} [g/mol]	MW _{dir} [%]
D_x [m ² /s]	1.299E-09	[EtMgCl(THF) ₂]	233	2
$\log(D_x)$	-8.8864	[EtMgCl(THF)] ₂	322	41
$\log(D_{x,\text{norm}})$	-8.9360			
$D_{\text{ref}}(\text{TPhN})$ [m ² /s]	8.794E-10			
$\log(D_{\text{ref}})(\text{TPhN})$	-9.0558			
MW _{det} [g/mol]	228			
ΔMW_{det} [g/mol] (%)	±8 (4)			

ECC-MW Estimation of *i*PrMgCl in THF

Table 5-41: ¹H-DOSY-ECC-MW estimation of *i*PrMgCl in THF-*d*₈ (25 mM) at 25 °C. TPhN was used as internal reference with $\log(D_{\text{ref,fix}})(\text{TPhN}) = -9.1054$. The accuracy of the ECC^{THF} (DSE) is in the range of $MW_{\text{dir}} = \pm 8\%$. Hypothetical aggregates are [*i*PrMgCl(THF)₂] and [*i*PrMgCl(THF)]₂. For ECC^{THF} parameters and changes compared to literature^[109a] see section 2.1.1.

¹ H-DOSY		25 °C		
		Aggregate	MW _{calc} [g/mol]	MW _{dir} [%]
D_x [m ² /s]	1.243E-09	[<i>i</i> PrMgCl(THF) ₂]	247	-2
$\log(D_x)$	-8.9055	[<i>i</i> PrMgCl(THF)] ₂	350	39
$\log(D_{x,\text{norm}})$	-8.9371			
$D_{\text{ref}}(\text{TPhN})$ [m ² /s]	8.436E-10			
$\log(D_{\text{ref}})(\text{TPhN})$	-9.0739			
MW _{det} [g/mol]	251			
ΔMW_{det} [g/mol] (%)	±13 (5)			

ECC-MW Estimation of *n*BuMgCl in THF

Table 5-42: ¹H-DOSY-ECC-MW estimation of *n*BuMgCl in THF-*d*₈ (25 mM) at 25 °C. TPhN was used as internal reference with $\log(D_{\text{ref,fix}})(\text{TPhN}) = -9.1054$. The accuracy of the ECC^{THF} (RL) is in the range of $MW_{\text{dir}} = \pm 8\%$ (see section 2.3.1.1). Hypothetical aggregates are [*n*BuMgCl(THF)₂] and [*n*BuMgCl(THF)]₂. For ECC^{THF} parameters see Figure 5-8.

¹ H-DOSY		25 °C		
		Aggregate	MW _{calc} [g/mol]	MW _{dir} [%]
D_x [m ² /s]	1.234E-09	[<i>n</i> BuMgCl(THF) ₂]	261	2
$\log(D_x)$	-8.9088	[<i>n</i> BuMgCl(THF)] ₂	378	48
$\log(D_{x,\text{norm}})$	-8.9750			
$D_{\text{ref}}(\text{TPhN})$ [m ² /s]	9.137E-10			
$\log(D_{\text{ref}})(\text{TPhN})$	-9.0392			
MW _{det} [g/mol]	255			
ΔMW_{det} [g/mol] (%)	±9 (4)			

ECC-MW Estimation of *n*HexMgCl in THF

Table 5-43: ¹H-DOSY-ECC-MW estimation of *n*HexMgCl in THF-*d*₈ (25 mM) at 25 °C. TPhN was used as internal reference with $\log(D_{\text{ref,fix}}(\text{TPhN})) = -9.1054$. The accuracy of the ECC^{THF} (RL) is in the range of $MW_{\text{dif}} = \pm 8\%$ (see section 2.3.1.1). Hypothetical aggregates are $[n\text{HexMgCl}(\text{THF})_2]$ and $[n\text{HexMgCl}(\text{THF})]_2$. For ECC^{THF} parameters see Figure 5-8.

¹ H-DOSY		25 °C		
		Aggregate	MW_{calc} [g/mol]	MW_{dif} [%]
D_x [m ² /s]	1.100E-09	$[n\text{HexMgCl}(\text{THF})_2]$	289	0
$\log(D_x)$	-8.9586	$[n\text{HexMgCl}(\text{THF})]_2$	434	51
$\log(D_{x,\text{norm}})$	-9.0173			
$D_{\text{ref}}(\text{TPhN})$ [m ² /s]	8.980E-10			
$\log(D_{\text{ref}}(\text{TPhN}))$	-9.0467			
MW_{det} [g/mol]	288			
ΔMW_{det} [g/mol] (%)	±11 (4)			

ECC-MW Estimation of *n*OctMgCl in THF

Table 5-44: ¹H-DOSY-ECC-MW estimation of *n*OctMgCl in THF-*d*₈ (25 mM) at 25 °C. TPhN was used as internal reference with $\log(D_{\text{ref,fix}}(\text{TPhN})) = -9.1054$. The accuracy of the ECC^{THF} (RL) is in the range of $MW_{\text{dif}} = \pm 8\%$ (see section 2.3.1.1). Hypothetical aggregates are $[n\text{OctMgCl}(\text{THF})_2]$ and $[n\text{OctMgCl}(\text{THF})]_2$. For ECC^{THF} parameters see Figure 5-8.

¹ H-DOSY		25 °C		
		Aggregate	MW_{calc} [g/mol]	MW_{dif} [%]
D_x [m ² /s]	1.029E-09	$[n\text{OctMgCl}(\text{THF})_2]$	317	0
$\log(D_x)$	-8.9875	$[n\text{OctMgCl}(\text{THF})]_2$	490	55
$\log(D_{x,\text{norm}})$	-9.0509			
$D_{\text{ref}}(\text{TPhN})$ [m ² /s]	9.079E-10			
$\log(D_{\text{ref}}(\text{TPhN}))$	-9.0420			
MW_{det} [g/mol]	317			
ΔMW_{det} [g/mol] (%)	±12 (4)			

ECC-MW Estimation of *n*DecMgCl in THF

Table 5-45: ¹H-DOSY-ECC-MW estimation of *n*DecMgCl in THF-*d*₈ (25 mM) at 25 °C. TPhN was used as internal reference with $\log(D_{\text{ref,fix}}(\text{TPhN})) = -9.1054$. The accuracy of the ECC^{THF} (RL) is in the range of $MW_{\text{dif}} = \pm 8\%$ (see section 2.3.1.1). Hypothetical aggregates are $[n\text{DecMgCl}(\text{THF})_2]$ and $[n\text{DecMgCl}(\text{THF})]_2$. For ECC^{THF} parameters see Figure 5-8.

¹ H-DOSY		25 °C		
		Aggregate	MW_{calc} [g/mol]	MW_{dif} [%]
D_x [m ² /s]	9.055E-10	$[n\text{DecMgCl}(\text{THF})_2]$	345	-1
$\log(D_x)$	-9.0431	$[n\text{DecMgCl}(\text{THF})]_2$	546	57
$\log(D_{x,\text{norm}})$	-9.0837			
$D_{\text{ref}}(\text{TPhN})$ [m ² /s]	8.613E-10			
$\log(D_{\text{ref}}(\text{TPhN}))$	-9.0648			
MW_{det} [g/mol]	348			
ΔMW_{det} [g/mol] (%)	±14 (4)			

ECC-MW Estimation of *n*BuMgBr in THF

Table 5-46: ¹H-DOSY-ECC-MW estimation of *n*BuMgBr in THF-*d*₈ (25 mM) at 25 °C. TPhN was used as internal reference with $\log(D_{\text{ref,fix}}(\text{TPhN})) = -9.1054$. The accuracy of the ECC^{THF} (RLBr) is in the range of $\Delta MW = \pm 9\%$ (theoretical; see section 2.3.1.1). Hypothetical aggregates are $[\textit{nBuMgBr}(\text{THF})_2]$ and $[\textit{nBuMgBr}(\text{THF})]_2$. For ECC^{THF} parameters see Figure 5-8.

¹ H-DOSY		25 °C		
		Aggregate	MW _{calc} [g/mol]	MW _{dif} [%]
D_x [m ² /s]	1.222E-09	$[\textit{nBuMgBr}(\text{THF})_2]$	305	-8
$\log(D_x)$	-8.9129	$[\textit{nBuMgBr}(\text{THF})]_2$	466	41
$\log(D_{x,\text{norm}})$	-8.9660			
$D_{\text{ref}}(\text{TPhN})$ [m ² /s]	8.865E-10			
$\log(D_{\text{ref}})(\text{TPhN})$	-9.0523			
MW _{det} [g/mol]	330			
ΔMW_{det} [g/mol] (%)	±33 (10)			

Molar Van-Der-Waals Densities (MD_W)

Table 5-47: MD_W for most likely solution state structures of RMgX (R = Et, *i*Pr, *n*Bu, *n*Hex, *n*Oct, *n*Dec; X = Cl, Br).

Aggregate	MW [g/mol]	C	H	O	Mg	Cl	Br	MD_W [g/(mol · m ³)]	ΣV_W [m ³]
$[\text{EtMgCl}(\text{THF})_2]$	233	10	21	2	1	1	0	5.88E+29	3.96E-28
$[\textit{iPrMgCl}(\text{THF})_2]$	247	11	23	2	1	1	0	5.77E+29	4.28E-28
$[\textit{nBuMgCl}(\text{THF})_2]$	261	12	25	2	1	1	0	5.68E+29	4.60E-28
$[\textit{nHexMgCl}(\text{THF})_2]$	289	14	29	2	1	1	0	5.52E+29	5.23E-28
$[\textit{nOctMgCl}(\text{THF})_2]$	317	16	33	2	1	1	0	5.41E+29	5.87E-28
$[\textit{nDecMgCl}(\text{THF})_2]$	345	18	37	2	1	1	0	5.31E+29	6.50E-28
$[\textit{nBuMgBr}(\text{THF})_2]$	306	12	25	2	1	0	1	6.59E+29	4.64E-28

ECC-MW Estimations of $[n\text{BuMgX} \cdot \text{LiX}]$ (X = Cl, Br)

ECC-MW Estimation of $[n\text{BuMgCl} \cdot \text{LiCl}]$ in THF

Table 5-48: ^1H -DOSY-ECC-MW estimation of $[n\text{BuMgCl} \cdot \text{LiCl}]$ in THF- d_8 (25 mM) at 25 °C. TPhN was used as internal reference with $\log(D_{\text{ref,fix}})(\text{TPhN}) = -9.1054$. The accuracy of the ECC^{THF} (DSE) is in the range of $MW_{\text{dif}} = \pm 8\%$. Hypothetical aggregates are $[n\text{BuMgCl}(\text{THF})_x \cdot \text{LiCl}]$ with $x = 2-3$ and $[n\text{BuMgCl}(\text{THF}) \cdot \text{LiCl}]_2$. For ECC^{THF} parameters and changes compared to literature^[109a] see section 2.1.1.

^1H -DOSY			25 °C	
		Aggregate	MW_{calc} [g/mol]	MW_{dif} [%]
D_x [m^2/s]	9.9193E-10	$[n\text{BuMgCl}(\text{THF})_2 \cdot \text{LiCl}]$	303	-16
$\log(D_x)$	-9.0035	$[n\text{BuMgCl}(\text{THF})_3 \cdot \text{LiCl}]$	376	4
$\log(D_{x,\text{norm}})$	-9.0293	$[n\text{BuMgCl}(\text{THF}) \cdot \text{LiCl}]_2$	463	28
$D_{\text{ref}}(\text{TPhN})$ [m^2/s]	8.325E-10			
$\log(D_{\text{ref}})(\text{TPhN})$	-9.0796			
MW_{det} [g/mol]	362			
ΔMW_{det} [g/mol] (%)	± 20 (6)			

ECC-MW Estimation of $[n\text{BuMgBr} \cdot \text{LiBr}]$ in THF

Table 5-49: ^1H -DOSY-ECC-MW estimation of $[n\text{BuMgBr} \cdot \text{LiBr}]$ in THF- d_8 (25 mM) at 25 °C. TPhN was used as internal reference with $\log(D_{\text{ref,fix}})(\text{TPhN}) = -9.1054$. The accuracy of the ECC^{THF} (Br₂) is in the range of $MW_{\text{dif}} = \pm 18\%$. Hypothetical aggregates are $[n\text{BuMgBr}(\text{THF})_x \cdot \text{LiBr}]$ with $x = 2-3$ and $[n\text{BuMgBr}(\text{THF}) \cdot \text{LiBr}]_2$. For ECC^{THF} parameters see reference^[124].

^1H -DOSY			25 °C	
		Aggregate	MW_{calc} [g/mol]	MW_{dif} [%]
D_x [m^2/s]	1.136E-09	$[n\text{BuMgBr}(\text{THF})_2 \cdot \text{LiBr}]$	392	-5
$\log(D_x)$	-8.9447	$[n\text{BuMgBr}(\text{THF})_3 \cdot \text{LiBr}]$	465	12
$\log(D_{x,\text{norm}})$	-8.9816	$[n\text{BuMgBr}(\text{THF}) \cdot \text{LiBr}]_2$	641	55
$D_{\text{ref}}(\text{TPhN})$ [m^2/s]	8.541E-10			
$\log(D_{\text{ref}})(\text{TPhN})$	-9.0685			
MW_{det} [g/mol]	413			
ΔMW_{det} [g/mol] (%)	± 96 (23)			

Molar Van-Der-Waals Densities (MD_W)

Table 5-50: MD_W for most likely solution state structures of $[n\text{BuMgX} \cdot \text{LiX}]$ (X = Cl, Br).

Aggregate	MW [g/mol]	C	H	O	Li	Mg	Cl	Br	MD_W [g/(mol · m ³)]	ΣV_W [m ³]
$[n\text{BuMgCl}(\text{THF})_3 \cdot \text{LiCl}]$	376	16	33	3	1	1	2	0	5.79E+29	6.49E-28
$[n\text{BuMgBr}(\text{THF})_3 \cdot \text{LiBr}]$	465	16	33	3	1	1	0	2	7.61E+29	6.58E-28

ECC-MW Estimations of (IPrPh)X (X = Br, I, OTf, BF₄, PF₆)^a**ECC-MW Estimation of (IPrPh)Br in Dichloromethane**

Table 5-51: ¹H-DOSY-ECC-MW estimation of (IPrPh)Br in CD₂Cl₂ at 25 °C. Adam was used as internal reference with $\log(D_{\text{ref,fix}})(\text{Adam}) = -8.7035$. The accuracy of the ECC^{CD₂Cl₂} (DSE) is in the range of $MW_{\text{dif}} = \pm 14\%$. Hypothetical aggregates are (IPrPh)⁺ and (IPrPh)Br. For ECC^{CD₂Cl₂}-parameters see Figure 5-4.

¹ H-DOSY		25 °C		
		Aggregate	MW _{calc} [g/mol]	MW _{dif} [%]
D_x [m ² /s]	8.735E-10	(IPrPh) ⁺	466	-21
$\log(D_x)$	-9.0587	(IPrPh)Br	546	-8
$\log(D_{x,\text{norm}})$	-9.0589			
$D_{\text{ref}}(\text{Adam})$ [m ² /s]	1.980E-09			
$\log(D_{\text{ref}})(\text{Adam})$	-8.7033			
MW _{det} [g/mol]	590			
ΔMW_{det} [g/mol] (%)	±60 (10)			

ECC-MW Estimation of (IPrPh)I in Dichloromethane

Table 5-52: ¹H-DOSY-ECC-MW estimation of (IPrPh)I in CD₂Cl₂ at 25 °C. Adam was used as internal reference with $\log(D_{\text{ref,fix}})(\text{Adam}) = -8.7035$. The accuracy of the ECC^{CD₂Cl₂} (DSE) is in the range of $MW_{\text{dif}} = \pm 14\%$. Hypothetical aggregates are (IPrPh)⁺ and (IPrPh)I. For ECC^{CD₂Cl₂}-parameters see Figure 5-4.

¹ H-DOSY		25 °C		
		Aggregate	MW _{calc} [g/mol]	MW _{dif} [%]
D_x [m ² /s]	9.610E-10	(IPrPh) ⁺	466	-15
$\log(D_x)$	-9.0173	(IPrPh)I	593	8
$\log(D_{x,\text{norm}})$	-9.0416			
$D_{\text{ref}}(\text{Adam})$ [m ² /s]	2.093E-09			
$\log(D_{\text{ref}})(\text{Adam})$	-8.6792			
MW _{det} [g/mol]	551			
ΔMW_{det} [g/mol] (%)	±55 (10)			

ECC-MW Estimation of (IPrPh)OTf in Dichloromethane

Table 5-53: ¹H-DOSY-ECC-MW estimation of (IPrPh)OTf in CD₂Cl₂ at 25 °C. Adam was used as internal reference with $\log(D_{\text{ref,fix}})(\text{Adam}) = -8.7035$. The accuracy of the ECC^{CD₂Cl₂} (DSE) is in the range of $MW_{\text{dif}} = \pm 14\%$. Hypothetical aggregates are (IPrPh)⁺ and (IPrPh)OTf. For ECC^{CD₂Cl₂}-parameters see Figure 5-4.

¹ H-DOSY		25 °C		
		Aggregate	MW _{calc} [g/mol]	MW _{dif} [%]
D_x [m ² /s]	8.894E-10	(IPrPh) ⁺	466	-17
$\log(D_x)$	-9.0509	(IPrPh)OTf	615	9
$\log(D_{x,\text{norm}})$	-9.0474			
$D_{\text{ref}}(\text{Adam})$ [m ² /s]	1.964E-09			
$\log(D_{\text{ref}})(\text{Adam})$	-8.7070			
MW _{det} [g/mol]	564			
ΔMW_{det} [g/mol] (%)	±57 (10)			

^a For further information, see section 2.3.2.1.

ECC-MW Estimation of (IPrPh)BF₄ in Dichloromethane

Table 5-54: ¹H-DOSY-ECC-MW estimation of (IPrPh)BF₄ in CD₂Cl₂ at 25 °C. Adam was used as internal reference with $\log(D_{\text{ref,fix}})(\text{Adam}) = -8.7035$. The accuracy of the ECC^{CD₂Cl₂} (DSE) is in the range of $MW_{\text{dif}} = \pm 14\%$. Hypothetical aggregates are (IPrPh)⁺ and (IPrPh)BF₄. For ECC^{CD₂Cl₂}-parameters see Figure 5-4.

¹ H-DOSY		25 °C		
		Aggregate	MW _{calc} [g/mol]	MW _{dif} [%]
D_x [m ² /s]	8.506E-10	(IPrPh) ⁺	466	-19
$\log(D_x)$	-9.0703	(IPrPh)BF ₄	553	-4
$\log(D_{x,\text{norm}})$	-9.0515			
$D_{\text{ref}}(\text{Adam})$ [m ² /s]	1.896E-09			
$\log(D_{\text{ref}})(\text{Adam})$	-8.7223			
MW _{det} [g/mol]	573			
ΔMW_{det} [g/mol] (%)	±58 (10)			

ECC-MW Estimation of (IPrPh)PF₆ in Dichloromethane

Table 5-55: ¹H-DOSY-ECC-MW estimation of (IPrPh)PF₆ in CD₂Cl₂ at 25 °C. Adam was used as internal reference with $\log(D_{\text{ref,fix}})(\text{Adam}) = -8.7035$. The accuracy of the ECC^{CD₂Cl₂} (DSE) is in the range of $MW_{\text{dif}} = \pm 14\%$. Hypothetical aggregates are (IPrPh)⁺ and (IPrPh)PF₆. For ECC^{CD₂Cl₂}-parameters see Figure 5-4.

¹ H-DOSY		25 °C		
		Aggregate	MW _{calc} [g/mol]	MW _{dif} [%]
D_x [m ² /s]	8.510E-10	(IPrPh) ⁺	466	-18
$\log(D_x)$	-9.0701	(IPrPh)PF ₆	611	8
$\log(D_{x,\text{norm}})$	-9.0480			
$D_{\text{ref}}(\text{Adam})$ [m ² /s]	1.881E-09			
$\log(D_{\text{ref}})(\text{Adam})$	-8.7256			
MW _{det} [g/mol]	565			
ΔMW_{det} [g/mol] (%)	±57 (10)			

Molar Van-Der-Waals Densities (MD_w)

Table 5-56: MD_w for all hypothetical solution state structures of Table 5-51 to Table 5-55.

Aggregate	MW [g/mol]	C	H	N	O	F	B	Br	I	S	P	MD _w [g/(mol · m ³)]
(IPrPh) ⁺	466	33	41	2	0	0	0	0	0	0	0	4.96E+29
(IPrPh)Br	546	33	41	2	0	0	0	1	0	0	0	5.65E+29
(IPrPh)I	593	33	41	2	0	0	0	0	1	0	0	6.10E+29
(IPrPh)OTf	615	34	41	2	3	3	0	0	0	1	0	5.76E+29
(IPrPh)BF ₄	553	33	41	2	0	4	1	0	0	0	0	5.41E+29
(IPrPh)PF ₆	611	33	41	2	0	6	0	0	0	0	1	5.85E+29

ECC-MW Estimations of (4,6-*t*Bu-NCOC₆H₂)₂CH₂ and [M(4,6-*t*Bu-NCOC₆H₂)₂CH] (M = Li, K, Mg)^a**ECC-MW Estimation of the (4,6-*t*Bu-NCOC₆H₂)₂CH₂ Ligand in Benzene**

Table 5-57: ¹H-DOSY-ECC-MW estimation of the (4,6-*t*Bu-NCOC₆H₂)₂CH₂ ligand in C₆D₆ at 25 °C. TMB was used as internal reference with log(*D*_{ref,fix})(TMB) = -8.7771. The accuracy of the ECC^{C₆D₆} (ED) is in the range of *MW*_{dif} = ±6%. Hypothetical aggregate is (4,6-*t*Bu-NCOC₆H₂)₂CH₂. For ECC^{C₆D₆}-parameters see Figure 5-4.

¹ H-DOSY		25 °C		
		Aggregate	<i>MW</i> _{calc} [g/mol]	<i>MW</i> _{dif} [%]
<i>D</i> _x [m ² /s]	6.851E-10	(4,6- <i>t</i> Bu-NCOC ₆ H ₂) ₂ CH ₂	475	-2
log(<i>D</i> _x)	-9.1642			
log(<i>D</i> _{x,norm})	-9.1720			
<i>D</i> _{ref} (TMB) [m ² /s]	1.701E-10			
log(<i>D</i> _{ref})(TMB)	-8.7693			
<i>MW</i> _{det} [g/mol]	483			
Δ <i>MW</i> _{det} [g/mol] (%)	±61 (13)			

ECC-MW Estimation of [Li(4,6-*t*Bu-NCOC₆H₂)₂CH] in Benzene

Table 5-58: ¹H-DOSY-ECC-MW estimation of [Li(4,6-*t*Bu-NCOC₆H₂)₂CH] in C₆D₆ at 25 °C. TMB was used as internal reference with log(*D*_{ref,fix})(TMB) = -8.7771. The accuracy of the ECC^{C₆D₆} (DSE) is in the range of *MW*_{dif} = ±8%. Hypothetical aggregates are [Li(4,6-*t*Bu-NCOC₆H₂)₂CH(THF)_x] with x = 0-2. For ECC^{C₆D₆}-parameters see Figure 5-4. Coordinated THF originates from synthesis.

¹ H-DOSY		25 °C		
		Aggregate	<i>MW</i> _{calc} [g/mol]	<i>MW</i> _{dif} [%]
<i>D</i> _x [m ² /s]	6.357E-10	[Li(4,6- <i>t</i> Bu-NCOC ₆ H ₂) ₂ CH]	481	-16
log(<i>D</i> _x)	-9.1967	[Li(4,6- <i>t</i> Bu-NCOC ₆ H ₂) ₂ CH(THF)]	553	-4
log(<i>D</i> _{x,norm})	-9.1863	[Li(4,6- <i>t</i> Bu-NCOC ₆ H ₂) ₂ CH(THF) ₂]	625	9
<i>D</i> _{ref} (TMB) [m ² /s]	1.631E-10			
log(<i>D</i> _{ref})(TMB)	-8.7875			
<i>MW</i> _{det} [g/mol]	575			
Δ <i>MW</i> _{det} [g/mol] (%)	±32 (6)			

ECC-MW Estimation of [K(4,6-*t*Bu-NCOC₆H₂)₂CH] in Benzene

Table 5-59: ¹H-DOSY-ECC-MW estimation of [K(4,6-*t*Bu-NCOC₆H₂)₂CH] in C₆D₆ at 25 °C. TMB was used as internal reference with log(*D*_{ref,fix})(TMB) = -8.7771. The accuracy of the ECC^{C₆D₆} (DSE) is in the range of *MW*_{dif} = ±8%. Hypothetical aggregates are [K(4,6-*t*Bu-NCOC₆H₂)₂CH(THF)_x] with x = 0-2. For ECC^{C₆D₆}-parameters see Figure 5-4. Coordinated THF originates from synthesis.

¹ H-DOSY		25 °C		
		Aggregate	<i>MW</i> _{calc} [g/mol]	<i>MW</i> _{dif} [%]
<i>D</i> _x [m ² /s]	7.050E-10	[K(4,6- <i>t</i> Bu-NCOC ₆ H ₂) ₂ CH]	513	-8
log(<i>D</i> _x)	-9.1518	[K(4,6- <i>t</i> Bu-NCOC ₆ H ₂) ₂ CH(THF)]	585	5
log(<i>D</i> _{x,norm})	-9.1774	[K(4,6- <i>t</i> Bu-NCOC ₆ H ₂) ₂ CH(THF) ₂]	657	18
<i>D</i> _{ref} (TMB) [m ² /s]	1.772E-10			
log(<i>D</i> _{ref})(TMB)	-8.7515			
<i>MW</i> _{det} [g/mol]	556			
Δ <i>MW</i> _{det} [g/mol] (%)	±31 (6)			

^a As this is an ongoing investigation, synthetic and other structural information is not given. For further information, see section 2.3.2.3.

ECC-MW Estimation of [MgCl₂(4,6-*t*Bu-NCOC₆H₂)₂CH] in Benzene

Table 5-60: ¹H-DOSY-ECC-MW estimation of [MgCl₂(4,6-*t*Bu-NCOC₆H₂)₂CH] in C₆D₆ at 25 °C. TMB was used as internal reference with log(*D*_{ref,fix})(TMB) = -8.7771. The accuracy of the ECC^{C6D6} (DSE) is in the range of *MW*_{dif} = ±8%. Hypothetical aggregates are [MgCl_{2-x}(4,6-*t*Bu-NCOC₆H₂)₂CH(THF)_x] with x = 0-2. For ECC^{C6D6}-parameters see Figure 5-4. Coordinated THF originates from synthesis.

¹ H-DOSY		25 °C		
		Aggregate	<i>MW</i> _{calc} [g/mol]	<i>MW</i> _{dif} [%]
<i>D</i> _x [m ² /s]	5.845E-10	[MgCl ₂ (4,6- <i>t</i> Bu-NCOC ₆ H ₂) ₂ CH]	569	-7
log(<i>D</i> _x)	-9.2332	[MgCl(4,6- <i>t</i> Bu-NCOC ₆ H ₂) ₂ CH(THF)]	606	-1
log(<i>D</i> _{x,norm})	-9.2020	[Mg(4,6- <i>t</i> Bu-NCOC ₆ H ₂) ₂ CH(THF) ₂]	642	5
<i>D</i> _{ref} (TMB) [m ² /s]	1.555E-09			
log(<i>D</i> _{ref})(TMB)	-8.8083			
<i>MW</i> _{det} [g/mol]	609			
Δ <i>MW</i> _{det} [g/mol] (%)	±34 (6)			

ECC-MW Estimation of [MgBr₂(4,6-*t*Bu-NCOC₆H₂)₂CH] in Benzene

Table 5-61: ¹H-DOSY-ECC-MW estimation of [MgBr₂(4,6-*t*Bu-NCOC₆H₂)₂CH] in C₆D₆ at 25 °C. TMB was used as internal reference with log(*D*_{ref,fix})(TMB) = -8.7771. The accuracy of the ECC^{C6D6} (DSE) is in the range of *MW*_{dif} = ±8%. Hypothetical aggregates are [MgBr_{2-x}(4,6-*t*Bu-NCOC₆H₂)₂CH(THF)_x] with x = 0-2. For ECC^{C6D6}-parameters see Figure 5-4. Coordinated THF originates from synthesis.

¹ H-DOSY		25 °C		
		Aggregate	<i>MW</i> _{calc} [g/mol]	<i>MW</i> _{dif} [%]
<i>D</i> _x [m ² /s]	5.476E-10	[MgBr ₂ (4,6- <i>t</i> Bu-NCOC ₆ H ₂) ₂ CH]	658	4
log(<i>D</i> _x)	-9.2616	[MgBr(4,6- <i>t</i> Bu-NCOC ₆ H ₂) ₂ CH(THF)]	650	3
log(<i>D</i> _{x,norm})	-9.2127	[Mg(4,6- <i>t</i> Bu-NCOC ₆ H ₂) ₂ CH(THF) ₂]	642	1
<i>D</i> _{ref} (TMB) [m ² /s]	1.493E-09			
log(<i>D</i> _{ref})(TMB)	-8.8259			
<i>MW</i> _{det} [g/mol]	634			
Δ <i>MW</i> _{det} [g/mol] (%)	±36 (6)			

ECC-MW Estimation of [Mg((4,6-*t*Bu-NCOC₆H₂)₂CH)₂] in Benzene

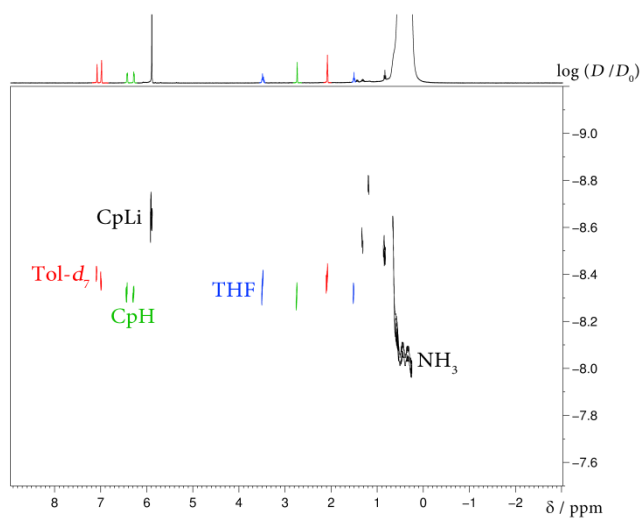
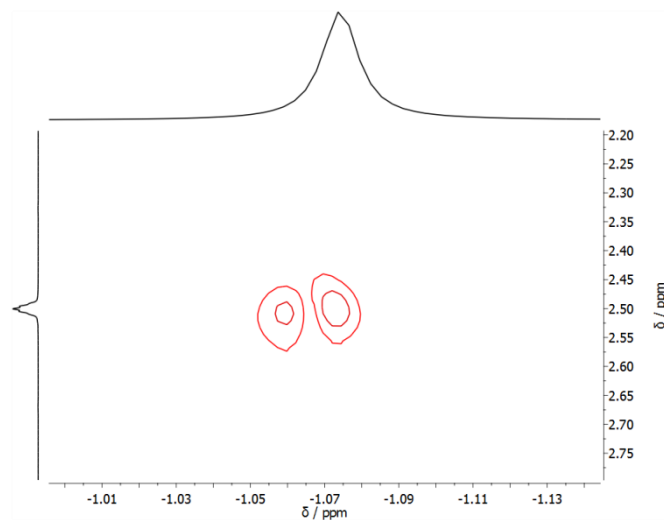
Table 5-62: ¹H-DOSY-ECC-MW estimation of [Mg((4,6-*t*Bu-NCOC₆H₂)₂CH)₂] in C₆D₆ at 25 °C. TMB was used as internal reference with log(*D*_{ref,fix})(TMB) = -8.7771. The accuracy of the ECC^{C6D6} (merged) is in the range of *MW*_{dif} = ±19%. Hypothetical aggregate is [Mg((4,6-*t*Bu-NCOC₆H₂)₂CH)₂]. For ECC^{C6D6}-parameters see Figure 5-4.

¹ H-DOSY		25 °C		
		Aggregate	<i>MW</i> _{calc} [g/mol]	<i>MW</i> _{dif} [%]
<i>D</i> _x [m ² /s]	4.548E-10	[Mg((4,6- <i>t</i> Bu-NCOC ₆ H ₂) ₂ CH) ₂]	972	-2
log(<i>D</i> _x)	-9.3422			
log(<i>D</i> _{x,norm})	-9.2942			
<i>D</i> _{ref} (TMB) [m ² /s]	1.496E-09			
log(<i>D</i> _{ref})(TMB)	-8.8251			
<i>MW</i> _{det} [g/mol]	993			
Δ <i>MW</i> _{det} [g/mol] (%)	±90 (9)			

Molar Van-Der-Waals Densities (MD_w)Table 5-63: MD_w for all hypothetical solution state structures of Table 5-57 to Table 5-62.

Aggregate	MW [g/mol]	C	H	N	O	Li	K	Mg	Cl	Br	MD_w [g/(mol · m ³)]
(4,6- <i>t</i> Bu-NCOC ₆ H ₂) ₂ CH ₂	475	31	42	2	2	0	0	0	0	0	5.09E+29
[Li(4,6- <i>t</i> Bu-NCOC ₆ H ₂) ₂ CH]	481	31	41	2	2	1	0	0	0	0	5.05E+29
[Li(4,6- <i>t</i> Bu-NCOC ₆ H ₂) ₂ CH(THF)]	553	35	49	2	3	1	0	0	0	0	5.05E+29
[Li(4,6- <i>t</i> Bu-NCOC ₆ H ₂) ₂ CH(THF) ₂]	625	39	57	2	4	1	0	0	0	0	5.06E+29
[K(4,6- <i>t</i> Bu-NCOC ₆ H ₂) ₂ CH]	513	31	41	2	2	0	1	0	0	0	5.06E+29
[K(4,6- <i>t</i> Bu-NCOC ₆ H ₂) ₂ CH(THF)]	585	35	49	2	3	0	1	0	0	0	5.06E+29
[K(4,6- <i>t</i> Bu-NCOC ₆ H ₂) ₂ CH(THF) ₂]	657	39	57	2	4	0	1	0	0	0	5.06E+29
[MgCl ₂ (4,6- <i>t</i> Bu-NCOC ₆ H ₂) ₂ CH]	569	31	41	2	2	0	0	1	2	0	5.72E+29
[MgCl(4,6- <i>t</i> Bu-NCOC ₆ H ₂) ₂ CH(THF)]	606	35	49	2	3	0	0	1	1	0	5.44E+29
[MgBr ₂ (4,6- <i>t</i> Bu-NCOC ₆ H ₂) ₂ CH]	658	31	41	2	2	0	0	1	0	2	6.57E+29
[MgBr(4,6- <i>t</i> Bu-NCOC ₆ H ₂) ₂ CH(THF)]	650	35	49	2	3	0	0	1	0	1	5.82E+29
[Mg(4,6- <i>t</i> Bu-NCOC ₆ H ₂) ₂ CH(THF) ₂]	642	39	57	2	4	0	0	1	0	0	5.21E+29
[Mg((4,6- <i>t</i> Bu-NCOC ₆ H ₂) ₂ CH) ₂]	972	62	82	4	4	0	0	1	0	0	5.18E+29

NMR Spectra

 ^1H -DOSY NMR Spectrum of CpLi in AmmoniaFigure 5-9: ^1H -DOSY NMR spectrum of CpLi in ammonia at 25 °C. ^7Li , ^1H -HOESY NMR Spectrum of CpLi in DMSOFigure 5-10: ^7Li , ^1H -HOESY NMR spectrum of CpLi in DMSO- d_6 at 25 °C.

6 REFERENCES

- [1] A. Visscher, S. Bachmann, C. Schnegelsberg, T. Teuteberg, R. A. Mata, D. Stalke, *Dalton Trans.* **2016**, 45, 5689-5699.
- [2] S. Bachmann, R. Neufeld, M. Dzemski, D. Stalke, *Chem. Eur. J.* **2016**, 22, 8462-8465.
- [3] C. Schnegelsberg, S. Bachmann, M. Kolter, T. Auth, M. John, D. Stalke, K. Koszinowski, *Chem. Eur. J.* **2016**, 22, 7752-7762.
- [4] S. Bachmann, B. Gernert, D. Stalke, *Chem. Commun.* **2016**, 52, 12861-12864.
- [5] A. Kreyenschmidt, S. Bachmann, T. Niklas, D. Stalke, in preparation.
- [6] S. Bachmann, T. Niklas, M. John, D. Stalke, in preparation.
- [7] a) S. J. Blundell, F. L. Pratt, *J. Phys.: Condens. Matter* **2004**, 16, R771; b) C. Elschenbroich, *Organometallchemie, Vol. 6*, Vieweg+Teubner Verlag, Wiesbaden, **2008**.
- [8] a) P. Beak, A. Basu, D. J. Gallagher, Y. S. Park, S. Thayumanavan, *Acc. Chem. Res.* **1996**, 29, 552-560; b) M. Schlosser, *Organoalkali Chemistry*, 2nd ed., John Wiley & Sons Ltd., Chichester, **2004**.
- [9] W. Schlenk, J. Holtz, *Ber. d. chem. Ges.* **1917**, 50, 262-274.
- [10] a) B. J. Wakefield, in *The Chemistry of Organolithium Compounds*, Pergamon Press, Oxford, New York, **1974**; b) J. Clayden, *Organolithiums: Selectivity for Synthesis, Vol. 23*, Elsevier Science (Pergamon), Oxford, **2002**; c) G. Wu, M. Huang, *Chem. Rev.* **2006**, 106, 2596-2616.
- [11] H. Dietrich, *Acta Crystallogr. Sect. E: Struct. Rep.* **1963**, 16, 681-689.
- [12] T. Kottke, D. Stalke, *Angew. Chem.* **1993**, 105, 619-621; *Angew. Chem. Int. Ed.* **1993**, 32, 580-582.
- [13] U. Siemeling, T. Redecker, B. Neumann, H.-G. Stammler, *J. Am. Chem. Soc.* **1994**, 116, 5507-5508.
- [14] E. Weiss, G. Hencken, *J. Organomet. Chem.* **1970**, 21, 265-268.
- [15] M. A. Nichols, P. G. Williard, *J. Am. Chem. Soc.* **1993**, 115, 1568-1572.
- [16] U. Schümann, J. Kopf, E. Weiss, *Angew. Chem.* **1985**, 97, 222-223; *Angew. Chem. Int. Ed.* **1985**, 24, 215-216.
- [17] a) T. Stey, D. Stalke, in *The chemistry of organolithium compounds* (Eds.: Z. Rappoport, I. Marek), John Wiley & Sons, Chichester, **2004**; b) E. Carl, D. Stalke, in *Lithium Compounds in Organic Synthesis - From Fundamentals to Applications* (Eds.: R. Luisi, V. Capriati), Wiley-VCH, Weinheim, **2014**, 1-13.
- [18] A. C. Jones, A. W. Sanders, M. J. Bevan, H. J. Reich, *J. Am. Chem. Soc.* **2007**, 129, 3492-3493.
- [19] J. F. McGarrity, J. Prodolliet, T. Smyth, *Org. Magn. Res.* **1981**, 17, 59-65.
- [20] J. F. McGarrity, C. A. Ogle, Z. Brich, H. R. Loosli, *J. Am. Chem. Soc.* **1985**, 107, 1810-1815.

- [21] C. A. Ogle, H. C. Johnson, X. L. Wang, F. H. Strickler, D. Bucca, B. Gordon, III, *Macromolecules* **1995**, *28*, 5184-5191.
- [22] R. O. Ebewele, *Polymer Science and Technology*, CRC Press, Boca Raton - New York, **2000**.
- [23] P. Zhao, D. B. Collum, *J. Am. Chem. Soc.* **2003**, *125*, 4008-4009.
- [24] D. B. Collum, *Acc. Chem. Res.* **1992**, *25*, 448-454.
- [25] B. O. T. Kammermeier, G. W. Klumpp, K. Kolthof, M. Vos, *Tetrahedron Lett.* **1991**, *32*, 3111-3114.
- [26] a) G. Wittig, F. J. Meyer, G. Lange, *Liebigs Ann. Chem.* **1951**, *571*, 167-201; b) G. Wittig, *Angew. Chem.* **1958**, *70*, 65-71; c) G. Wittig, *Chem. Soc. Rev.* **1966**, *20*, 191-210.
- [27] a) A. C. Jones, A. W. Sanders, W. H. Sikorski, K. L. Jansen, H. J. Reich, *J. Am. Chem. Soc.* **2008**, *130*, 6060-6061; b) H. J. Reich, W. H. Sikorski, A. W. Sanders, A. C. Jones, K. N. Plessel, *J. Org. Chem.* **2009**, *74*, 719-729.
- [28] C. Eaborn, P. B. Hitchcock, J. D. Smith, A. C. Sullivan, *Chem. Commun.* **1983**, *0*, 827-828.
- [29] a) M. M. Olmstead, P. P. Power, *J. Am. Chem. Soc.* **1985**, *107*, 2174-2175; b) A. D. Pajerski, M. Parvez, H. G. Richey, *J. Am. Chem. Soc.* **1988**, *110*, 2660-2662; c) S. Buchholz, K. Harms, M. Marsch, W. Massa, G. Boche, *Angew. Chem.* **1989**, *101*, 57-58; *Angew. Chem. Int. Ed.* **1989**, *28*, 72-73; d) B. Becker, V. Enkelmann, K. Müllen, *Angew. Chem.* **1989**, *101*, 501-503; *Angew. Chem. Int. Ed.* **1989**, *28*, 458-460; e) H. Gornitzka, D. Stalke, *Organometallics* **1994**, *13*, 4398-4405; f) F. Zaegel, J. C. Gallucci, P. Meunier, B. Gautheron, M. R. Sivik, L. A. Paquette, *J. Am. Chem. Soc.* **1994**, *116*, 6466-6467; g) H. Bock, A. John, C. Arad, C. Näther, Z. Havlas, *Angew. Chem.* **1994**, *106*, 931-934; *Angew. Chem. Int. Ed.* **1994**, *33*, 931-933; h) H. Viebrock, U. Behrens, E. Weiss, *Angew. Chem.* **1994**, *106*, 1364-1365; *Angew. Chem. Int. Ed.* **1994**, *33*, 1257-1259; i) H. Viebrock, D. Abeln, E. Weiss, *Z. Naturforsch., B Chem. Sci.* **1994**, *49*, 89-99; j) R. Haag, B. Ohlhorst, M. Noltemeyer, R. Fleischer, D. Stalke, A. Schuster, D. Kuck, A. de Meijere, *J. Am. Chem. Soc.* **1995**, *117*, 10474-10485; k) W. A. Herrmann, O. Runte, G. Artus, *J. Organomet. Chem.* **1995**, *501*, C1-C4; l) C. Näther, H. Bock, Z. Havlas, T. Hauck, *Organometallics* **1998**, *17*, 4707-4715; m) J. S. Alexander, K. Ruhlandt-Senge, *Angew. Chem.* **2001**, *113*, 2732-2734; *Angew. Chem. Int. Ed.* **2001**, *40*, 2658-2660; n) S. Harder, F. Feil, T. Repo, *Chem. Eur. J.* **2002**, *8*, 1991-1999; o) R. Michel, R. Herbst-Irmer, D. Stalke, *Organometallics* **2010**, *29*, 6169-6171; p) R. Michel, T. Nack, R. Neufeld, J. M. Dieterich, R. A. Mata, D. Stalke, *Angew. Chem.* **2013**, *125*, 762-766; *Angew. Chem. Int. Ed.* **2013**, *52*, 734-738; q) A.-C. Pöppler, M. Granitzka, R. Herbst-Irmer, Y.-S. Chen, B. B. Iversen, M. John, R. A. Mata, D. Stalke, *Angew. Chem.* **2014**, *126*, 13498-13503; *Angew. Chem. Int. Ed.* **2014**, *53*, 13282-13287.
- [30] a) J. Smid, *Angew. Chem.* **1972**, *84*, 127-144; *Angew. Chem. Int. Ed.* **1972**, *11*, 112-127; b) A. Streitwieser, *Acc. Chem. Res.* **1984**, *17*, 353-357.
- [31] a) A. I. Vogel, A. R. Tachtell, B. S. Furnis, A. J. Hannaford, P. W. G. Smith, *Vogel's Textbook of Practical Organic Chemistry, Vol. 5*, Prentice Hall, **1989**; b) D. R. Lide, *CRC Handbook of Chemistry and Physics, Vol. 87*, CRC Press, Boca Raton, **2006**.
- [32] a) A. V. Yakimansky, A. H. E. Muller, M. Van Beylen, *Macromolecules* **2000**, *33*, 5686-5692; b) M. Granitzka, *Aggregation Study on Lithiated Five-Membered Heterocycles - Towards The Pentuple Ion*, Ph.D. thesis, Göttingen, **2013**; c) A.-C. Pöppler, *Advanced NMR Methodology for the Investigation of Organometallic Compounds in Solution*, Ph.D. thesis, Göttingen, **2013**.
- [33] a) P. Jutzi, in *Adv. Organomet. Chem., Vol. 26* (Eds.: F. G. A. Stone, W. Robert), Academic Press, **1986**, 217-295; b) P. Jutzi, *J. Organomet. Chem.* **1990**, *400*, 1-17; c) E. Weiss, *Angew. Chem.* **1993**, *105*, 1565-

- 1587; *Angew. Chem. Int. Ed.* **1993**, 32, 1501-1523; d) D. Stalke, *Angew. Chem.* **1994**, 106, 2256-2259; *Angew. Chem. Int. Ed.* **1994**, 33, 2168-2171; e) S. Harder, *Coord. Chem. Rev.* **1998**, 176, 17-66.
- [34] a) T. J. Kealy, P. L. Pauson, *Nature* **1951**, 168, 1039-1040; b) G. Wilkinson, R. B. Woodward, *J. Am. Chem. Soc.* **1952**, 74, 2125.
- [35] J. Thiele, *Ber. d. chem. Ges.* **1900**, 33, 666-673.
- [36] J. Thiele, *Ber. d. chem. Ges.* **1901**, 34, 68-71.
- [37] a) H. E. Roscoe, *Liebigs Ann. Chem.* **1886**, 232, 348-352; b) G. Kraemer, A. Spilker, *Ber. Dtsch. Chem. Ges.* **1896**, 29, 552.
- [38] a) E. O. Fischer, R. Jira, K. Hafner, *Z. Naturforsch., B: Chem. Sci.* **1953**, 8, 327; b) E. O. Fischer, W. Hafner, H. O. Stahl, *Z. Anorg. Allg. Chem.* **1955**, 282, 47-62.
- [39] K. Ziegler, H. Froitzheim-Kühlhorn, K. Hafner, *Chem. Ber.* **1956**, 89, 434-443.
- [40] N. J. Long, *Metallocenes: An Introduction to Sandwich Complexes*, Wiley-Blackwell, **1997**.
- [41] J. E. Huheey, E. A. Keiter, R. L. Keiter, *Anorganische Chemie - Prinzipien von Struktur und Reaktivität*, Vol. 3, Walter de Gruyter, Berlin, **2003**.
- [42] H. Sinn, W. Kaminsky, H.-J. Vollmer, R. Woldt, *Angew. Chem.* **1980**, 92, 396-402; *Angew. Chem. Int. Ed.* **1980**, 19, 390-392.
- [43] a) W. Kaminsky, M. Miri, H. Sinn, R. Woldt, *Macromol. Rapid Commun.* **1983**, 4, 417-421; b) J. Herwig, W. Kaminsky, *Polym. Bull.* **1983**, 9, 464-469; c) W. Kaminsky, *Dalton Trans.* **1998**, 1413-1418.
- [44] B. Ye, N. Cramer, *Angew. Chem.* **2014**, 126, 8030-8033; *Angew. Chem. Int. Ed.* **2014**, 53, 7896-7899.
- [45] M. Sawamura, Y. Kuninobu, M. Toganoh, Y. Matsuo, M. Yamanaka, E. Nakamura, *J. Am. Chem. Soc.* **2002**, 124, 9354-9355.
- [46] B. Ye, N. Cramer, *Science* **2012**, 338, 504-506.
- [47] L. Y. Kuo, M. G. Kanatzidis, M. Sabat, A. L. Tipton, T. J. Marks, *J. Am. Chem. Soc.* **1991**, 113, 9027-9045.
- [48] P. Jutzi, N. Burford, *Chem. Rev.* **1999**, 99, 969-990.
- [49] a) H. P. Fritz, R. Schneider, *Chem. Ber.* **1960**, 93, 1171-1183; b) H. P. Fritz, L. Schäfer, *Chem. Ber.* **1964**, 97, 1829-1833.
- [50] a) W. T. Ford, *J. Organomet. Chem.* **1971**, 32, 27-33; b) R. H. Cox, H. W. Terry, L. W. Harrison, *J. Am. Chem. Soc.* **1971**, 93, 3297-3298; c) P. Fischer, J. Stadelhofer, J. Weidlein, *J. Organomet. Chem.* **1976**, 116, 65-73.
- [51] V. M. Rayón, G. Frenking, *Chem. Eur. J.* **2002**, 8, 4693-4707.
- [52] a) T. Aoyagi, H. M. M. Shearer, K. Wade, G. Whitehead, *Chem. Commun.* **1976**, 164-165; b) T. Aoyagi, H. M. M. Shearer, K. Wade, G. Whitehead, *J. Organomet. Chem.* **1979**, 175, 21-31.

- [53] a) V. Jordan, U. Behrens, F. Olbrich, E. Weiss, *J. Organomet. Chem.* **1996**, *517*, 81-88; b) M. L. Cole, C. Jones, P. C. Junk, *Dalton Trans.* **2002**, 896-905; c) W. J. Evans, D. G. Giarikos, J. W. Ziller, *J. Organomet. Chem.* **2003**, *688*, 200-205.
- [54] R. E. Dinnebier, U. Behrens, F. Olbrich, *Organometallics* **1997**, *16*, 3855-3858.
- [55] a) R. E. Dinnebier, F. Olbrich, S. VanSmaalen, P. W. Stephens, *Acta Crystallogr., Sect. B: Struct. Sci.* **1997**, *53*, 153-158; b) R. E. Dinnebier, F. Olbrich, G. M. Bendele, *Acta Crystallogr., Sect. C: Cryst. Struct. Commun.* **1997**, *53*, 699-701.
- [56] a) P. Jutzi, W. Leffers, B. Hampel, S. Pohl, W. Saak, *Angew. Chem.* **1987**, *99*, 563-564; *Angew. Chem. Int. Ed.* **1987**, *26*, 583-584; b) W. J. Evans, T. J. Boyle, J. W. Ziller, *Organometallics* **1992**, *11*, 3903-3907; c) R. E. Dinnebier, M. Schneider, S. van Smaalen, F. Olbrich, U. Behrens, *Acta Crystallogr., Sect. B: Struct. Sci.* **1999**, *55*, 35-44; d) C. Tedesco, R. E. Dinnebier, F. Olbrich, S. van Smaalen, *Acta Crystallogr., Sect. B: Struct. Sci.* **2001**, *57*, 673-679; e) S. Kheradmandan, H. W. Schmalle, H. Jacobsen, O. Blacque, T. Fox, H. Berke, M. Gross, S. Decurtins, *Chem. Eur. J.* **2002**, *8*, 2526-2533; f) G. Bai, H. W. Roesky, P. Müller, *Bull. Pol. Acad. Sci. Chem.* **2002**, *50*, 1; g) U. Behrens, R. E. Dinnebier, S. Neander, F. Olbrich, *Organometallics* **2008**, *27*, 5398-5400.
- [57] P. Jutzi, E. Schlüter, C. Krüger, S. Pohl, *Angew. Chem.* **1983**, *95*, 1015-1016; *Angew. Chem. Int. Ed.* **1983**, *22*, 994.
- [58] a) M. F. Lappert, A. Singh, L. M. Engelhardt, A. H. White, *J. Organomet. Chem.* **1984**, *262*, 271-278; b) P. Jutzi, E. Schlüter, S. Pohl, W. Saak, *Chem. Ber.* **1985**, *118*, 1959-1967.
- [59] a) P. Jutzi, W. Leffers, S. Pohl, W. Saak, *Chem. Ber.* **1989**, *122*, 1449-1456; b) A. Hammel, W. Schwarz, J. Weidlein, *Acta Crystallogr. C* **1990**, *46*, 2337-2339; c) G. Rabe, H. W. Roesky, D. Stalke, F. Pauer, G. M. Sheldrick, *J. Organomet. Chem.* **1991**, *403*, 11-19; d) H. Chen, P. Jutzi, W. Leffers, M. M. Olmstead, P. P. Power, *Organometallics* **1991**, *10*, 1282-1286; e) J. Hiermeier, F. H. Koehler, G. Mueller, *Organometallics* **1991**, *10*, 1787-1793; f) A. Sekiguchi, Y. Sugai, K. Ebata, C. Kabuto, H. Sakurai, *J. Am. Chem. Soc.* **1993**, *115*, 1144-1146; g) M. A. Edelman, P. B. Hitchcock, M. F. Lappert, D.-S. Liu, S. Tian, *J. Organomet. Chem.* **1998**, *550*, 397-408; h) S. Neander, F. E. Tio, R. Buschmann, U. Behrens, F. Olbrich, *J. Organomet. Chem.* **1999**, *582*, 58-65; i) S. Neander, U. Behrens, F. Olbrich, *J. Organomet. Chem.* **2000**, *604*, 59-67; j) T. Kähler, U. Behrens, S. Neander, F. Olbrich, *J. Organomet. Chem.* **2002**, *649*, 50-54; k) W. J. Evans, J. C. Brady, C. H. Fujimoto, D. G. Giarikos, J. W. Ziller, *J. Organomet. Chem.* **2002**, *649*, 252-257; l) H. Schumann, M. R. Keitsch, S. H. Mühle, *Z. Anorg. Allg. Chem.* **2002**, *628*, 1311-1318; m) C. M. Widdifield, J. A. Tang, C. L. B. Macdonald, R. W. Schurko, *Magn. Reson. Chem.* **2007**, *45*, S116-S128; n) R. Michel, R. Herbst-Irmer, D. Stalke, *Organometallics* **2011**, *30*, 4379-4386; o) J. Hey, D. M. Andrada, R. Michel, R. A. Mata, D. Stalke, *Angew. Chem.* **2013**, *125*, 10555-10559; *Angew. Chem. Int. Ed.* **2013**, *52*, 10365-10369; p) J. Hey, *From X-ray diffraction data annealing to comprehensive charge density analysis*, Ph. D. thesis, Göttingen, **2013**; q) C. B. Benda, M. Waibel, T. F. Fässler, *Angew. Chem.* **2015**, *127*, 532-536; *Angew. Chem. Int. Ed.*, **2015**, *54*, 522-526; r) F. Ortu, J. M. Fowler, M. Burton, A. Formanuk, D. P. Mills, *New J. Chem.* **2015**, *39*, 7633-7639.
- [60] a) G. Lin, W.-T. Wong, *Polyhedron* **1994**, *13*, 3027-3030; b) C. Dohmeier, E. Baum, A. Ecker, R. Köppe, H. Schnöckel, *Organometallics* **1996**, *15*, 4702-4706.
- [61] A. A. Fyfe, A. R. Kennedy, J. Klett, R. E. Mulvey, *Angew. Chem.* **2011**, *123*, 7922-7926; *Angew. Chem. Int. Ed.* **2011**, *50*, 7776-7780.
- [62] S. Harder, M. H. Prosenc, *Angew. Chem.* **1994**, *106*, 1830-1832; *Angew. Chem. Int. Ed.* **1994**, *33*, 1744-1746.

- [63] J. Wessel, E. Lork, R. Mews, *Angew. Chem.* **1995**, *107*, 2565-2567; *Angew. Chem. Int. Ed.*, **1995**, *34*, 2376-2378.
- [64] S. Harder, M. H. Prosenc, U. Rief, *Organometallics* **1996**, *15*, 118-122.
- [65] M. Westerhausen, S. Schneiderbauer, N. Makropoulos, M. Warchhold, H. Nöth, H. Piotrowski, K. Karaghiosoff, *Organometallics* **2002**, *21*, 4335-4341.
- [66] L. A. Paquette, W. Bauer, M. R. Sivik, M. Buehl, M. Feigel, P. v. R. Schleyer, *J. Am. Chem. Soc.* **1990**, *112*, 8776-8789.
- [67] R. den Besten, S. Harder, L. Brandsma, *J. Organomet. Chem.* **1990**, *385*, 153-159.
- [68] a) S. D. Stults, R. A. Andersen, A. Zalkin, *J. Am. Chem. Soc.* **1989**, *111*, 4507-4508; b) J.-C. Berthet, C. Villiers, J.-F. Le Maréchal, B. Delavaux-Nicot, M. Lance, M. Nierlich, J. Vigner, M. Ephritikhine, *J. Organomet. Chem.* **1992**, *440*, 53-65; c) W. J. Evans, M. S. Sollberger, J. L. Shreeve, J. M. Olofson, J. H. Hain, J. W. Ziller, *Inorg. Chem.* **1992**, *31*, 2492-2501.
- [69] S. Harder, M. H. Prosenc, *Angew. Chem.* **1996**, *108*, 101-103; *Angew. Chem. Int. Ed.* **1996**, *35*, 97-99.
- [70] a) D. Seebach, R. Amstutz, T. Laube, W. B. Schweizer, J. D. Dunitz, *J. Am. Chem. Soc.* **1985**, *107*, 5403-5409; b) H. Hope, *Acta Crystallogr., Sect. B: Struct. Sci.* **1988**, *44*, 22-26; c) R. Boese, D. Blaser, *J. Appl. Crystallogr.* **1989**, *22*, 394-395; d) T. Kottke, D. Stalke, *J. Appl. Crystallogr.* **1993**, *26*, 615-619; e) A. E. H. Wheatley, *Chem. Soc. Rev.* **2001**, *30*, 265-273.
- [71] a) T. Niklas, D. Stalke, M. John, *Chem. Commun.* **2015**, *51*, 1275-1277; b) T. Niklas, C. Steinmetzger, W. Liu, D. Zell, D. Stalke, L. Ackermann, M. John, *Eur. J. Org. Chem.* **2015**, *2015*, 6801-6805.
- [72] a) J. Heinzer, J. F. M. Oth, D. Seebach, *Helv. Chim. Acta* **1985**, *68*, 1848-1862; b) T. Claridge, *High-Resolution NMR Techniques in Organic Chemistry, Vol. 27*, Elsevier, **2009**; c) J. Keeler, *Understanding NMR Spectroscopy*, 2nd ed., John Wiley & Sons, **2010**; d) H. Friebolin, *Basic One- and Two-Dimensional NMR Spectroscopy*, 5th ed., WILEY-VCH Verlag, Weinheim, **2011**.
- [73] C. Yu, G. C. Levy, *J. Am. Chem. Soc.* **1983**, *105*, 6994-6996.
- [74] P. L. Rinaldi, *J. Am. Chem. Soc.* **1983**, *105*, 5167-5168.
- [75] W. Bauer, G. Müller, R. Pi, P. von Ragué Schleyer, *Angew. Chem.* **1986**, *98*, 1130-1132; *Angew. Chem. Int. Ed.* **1986**, *25*, 1103-1104.
- [76] M. Granitzka, A.-C. Pöppler, E. K. Schwarze, D. Stern, T. Schulz, M. John, R. Herbst-Irmer, S. K. Pandey, D. Stalke, *J. Am. Chem. Soc.* **2011**, *134*, 1344-1351.
- [77] F. T. Edelmann, F. Knösel, F. Pauer, D. Stalke, W. Bauer, *J. Organomet. Chem.* **1992**, *438*, 1-10.
- [78] Bruker, *Almanac 2014*, 1st ed., **2014**.
- [79] a) W. Bauer, *Magn. Reson. Chem.* **1991**, *29*, 494-499; b) D. Hoffmann, W. Bauer, P. v. R. Schleyer, U. Pieper, D. Stalke, *Organometallics* **1993**, *12*, 1193-1200.
- [80] a) P. Stilbs, *Prog. Nucl. Magn. Res. Spectr.* **1987**, *19*, 1-45; b) C. S. Johnson Jr, *Prog. Nucl. Magn. Res. Spectr.* **1999**, *34*, 203-256; c) Y. Cohen, L. Avram, L. Frish, *Angew. Chem.* **2005**, *117*, 524-560; *Angew. Chem. Int. Ed.* **2005**, *44*, 520-554; d) A. Macchioni, G. Ciancaleoni, C. Zuccaccia, D. Zuccaccia, *Chem.*

- Soc. Rev.* **2008**, *37*, 479-489; e) T. D. W. Claridge, *High-Resolution NMR Techniques in Organic Chemistry*, Vol. 27, Elsevier, **2009**; f) L. Avram, Y. Cohen, *Chem. Soc. Rev.* **2015**, *44*, 586-602.
- [81] E. O. Stejskal, J. E. Tanner, *J. Chem. Phys.* **1965**, *42*, 288-292.
- [82] E. L. Hahn, *Phys. Rev.* **1950**, *80*, 580-594.
- [83] J. E. Tanner, *J. Chem. Phys.* **1970**, *52*, 2523-2526.
- [84] a) S. J. Gibbs, C. S. Johnson, *J. Magn. Reson.* **1991**, *93*, 395-402; b) D. H. Wu, A. D. Chen, C. S. Johnson, *J. Magn. Reson., Ser. A* **1995**, *115*, 260-264.
- [85] A. Jerschow, N. Müller, *J. Magn. Reson.* **1996**, *123*, 222-225.
- [86] a) K. Zangger, H. Sterk, *J. Magn. Reson.* **1997**, *124*, 486-489; b) J. A. Aguilar, S. Faulkner, M. Nilsson, G. A. Morris, *Angew. Chem.* **2010**, *122*, 3993-3995; *Angew. Chem. Int. Ed.* **2010**, *49*, 3901-3903; c) R. W. Adams, L. Byrne, P. Kiraly, M. Foroozandeh, L. Paudel, M. Nilsson, J. Clayden, G. A. Morris, *Chem. Commun.* **2014**, *50*, 2512-2514.
- [87] G. Hamdoun, M. Sebban, E. Cossoul, A. Harrison-Marchand, J. Maddaluno, H. Oulyadi, *Chem. Commun.* **2014**, *50*, 4073-4075.
- [88] K. F. Morris, C. S. Johnson, *J. Am. Chem. Soc.* **1992**, *114*, 3139-3141.
- [89] J. S. Gounarides, A. Chen, M. J. Shapiro, *J. Chromatogr. B.* **1999**, *725*, 79-90.
- [90] a) S. Beck, A. Geyer, H.-H. Brintzinger, *Chem. Commun.* **1999**, 2477-2478; b) M. Valentini, P. S. Pregosin, H. Rüegger, *Organometallics* **2000**, *19*, 2551-2555; c) A. Pichota, P. S. Pregosin, M. Valentini, M. Würle, D. Seebach, *Angew. Chem.* **2000**, *112*, 157-160; *Angew. Chem. Int. Ed.* **2000**, *39*, 153-156.
- [91] I. Keresztes, P. G. Williard, *J. Am. Chem. Soc.* **2000**, *122*, 10228-10229.
- [92] a) M. Nilsson, A. M. Gil, I. Delgadillo, G. A. Morris, *Chem. Commun.* **2005**, 1737-1739; b) B. Vitorge, D. Jeanneat, *Anal. Chem.* **2006**, *78*, 5601-5606.
- [93] M. D. Pluth, K. N. Raymond, *Chem. Soc. Rev.* **2007**, *36*, 161-171.
- [94] J. T. Edward, *J. Chem. Educ.* **1970**, *47*, 261.
- [95] A. Gierer, K. Wirtz, *Z. Naturforsch., A: Phys. Sci.* **1953**, *8*, 532.
- [96] H. C. Chen, S. H. Chen, *J. Phys. Chem.* **1984**, *88*, 5118-5121.
- [97] F. Perrin, *J. Phys. Radium* **1936**, *7*, 1-11.
- [98] R. Evans, Z. Deng, A. K. Rogerson, A. S. McLachlan, J. J. Richards, M. Nilsson, G. A. Morris, *Angew. Chem.* **2013**, *125*, 3281-3284; *Angew. Chem. Int. Ed.* **2013**, *52*, 3199-3202.
- [99] S. Augé, P.-O. Schmit, C. A. Crutchfield, M. T. Islam, D. J. Harris, E. Durand, M. Clemancey, A.-A. Quoineaude, J.-M. Lancelin, Y. Prigent, F. Taulelle, M.-A. Delsuc, *J. Phys. Chem. B* **2009**, *113*, 1914-1918.
- [100] P. Flory, *Principles of Polymer Chemistry*, Cornell University Press, Ithaca, New York, **1953**.

- [101]a) A. Chen, D. Wu, C. S. Johnson, *J. Am. Chem. Soc.* **1995**, *117*, 7965-7970; b) K. Chari, B. Antalek, J. Minter, *Phys. Rev. Lett.* **1995**, *74*, 3624-3627.
- [102]S. Floquet, S. Brun, J.-F. Lemonnier, M. Henry, M.-A. Delsuc, Y. Prigent, E. Cadot, F. Taulelle, *J. Am. Chem. Soc.* **2009**, *131*, 17254-17259.
- [103]a) D. K. Wilkins, S. B. Grimshaw, V. Receveur, C. M. Dobson, J. A. Jones, L. J. Smith, *Biochemistry* **1999**, *38*, 16424-16431; b) S. Viel, D. Capitani, L. Mannina, A. Segre, *Biomacromolecules* **2003**, *4*, 1843-1847.
- [104]C. A. Crutchfield, D. J. Harris, *J. Magn. Reson.* **2007**, *185*, 179-182.
- [105]a) J. A. Jones, D. K. Wilkins, L. J. Smith, C. M. Dobson, *J. Biomol. NMR* **1997**, *10*, 199-203; b) E. J. Cabrita, S. Berger, *Magn. Reson. Chem.* **2001**, *39*, S142-S148.
- [106]a) D. Li, I. Keresztes, R. Hopson, P. G. Williard, *Acc. Chem. Res.* **2009**, *42*, 270-280; b) D. Li, G. Kagan, R. Hopson, P. G. Williard, *J. Am. Chem. Soc.* **2009**, *131*, 5627-5634.
- [107]a) D. Li, C. Sun, P. G. Williard, *J. Am. Chem. Soc.* **2008**, *130*, 11726-11736; b) A. M. Socha, G. Kagan, W. Li, R. Hopson, J. K. Sello, P. G. Williard, *Energy Fuels* **2010**, *24*, 4518-4521; c) D. R. Armstrong, P. García-Álvarez, A. R. Kennedy, R. E. Mulvey, S. D. Robertson, *Chem. Eur. J.* **2011**, *17*, 6725-6730; d) P. García-Álvarez, R. E. Mulvey, J. A. Parkinson, *Angew. Chem.* **2011**, *123*, 9842-9845; *Angew. Chem. Int. Ed.* **2011**, *50*, 9668-9671; e) C. Su, R. Hopson, P. G. Williard, *J. Am. Chem. Soc.* **2013**, *135*, 12400-12406; f) C. Su, R. Hopson, P. G. Williard, *Eur. J. Inorg. Chem.* **2013**, *2013*, 4136-4141; g) C. Su, R. Hopson, P. G. Williard, *J. Am. Chem. Soc.* **2013**, *135*, 14367-14379; h) D. R. Armstrong, A. R. Kennedy, R. E. Mulvey, S. D. Robertson, *Dalton Trans.* **2013**, *42*, 3704-3711; i) A. J. Martínez-Martínez, D. R. Armstrong, B. Conway, B. J. Fleming, J. Klett, A. R. Kennedy, R. E. Mulvey, S. D. Robertson, C. T. O'Hara, *Chem. Sci.* **2014**, *5*, 771-781; j) S. C. Hunter, S.-J. Chen, C. A. Steren, M. G. Richmond, Z.-L. Xue, *Organometallics* **2015**, *34*, 5687-5696.
- [108]a) D. Li, R. Hopson, W. Li, J. Liu, P. G. Williard, *Org. Lett.* **2008**, *10*, 909-911; b) G. Kagan, W. Li, R. Hopson, P. G. Williard, *Org. Lett.* **2009**, *11*, 4818-4821; c) J. Guang, R. Hopson, P. G. Williard, *J. Org. Chem.* **2015**, *80*, 9102-9107.
- [109]a) R. Neufeld, D. Stalke, *Chem. Sci.* **2015**, *6*, 3354-3364; b) R. Neufeld, *DOSY External Calibration Curve Molecular Weight Determination as a Valuable Methodology in Characterizing Reactive Intermediates in Solution*, Ph. D. thesis, Göttingen, **2016**.
- [110]R. Neufeld, M. John, D. Stalke, *Angew. Chem.* **2015**, *127*, 7100-7104; *Angew. Chem. Int. Ed.* **2015**, *54*, 6994-6998.
- [111]a) R. Neufeld, D. Stalke, *Chem. Eur. J.* **2016**, *22*, 12624-12628; b) R. Neufeld, T. L. Teuteberg, R. Herbst-Irmer, R. A. Mata, D. Stalke, *J. Am. Chem. Soc.* **2016**, *138*, 4796-4806.
- [112]M. Á. Fuentes, A. Zabala, A. R. Kennedy, R. E. Mulvey, *Chem. Eur. J.* **2016**, *22*, 14968-14978.
- [113]Y. Qiao, W. Ge, L. Jia, X. Hou, Y. Wang, C. M. Pedersen, *Chem. Commun.* **2016**, *52*, 11418-11421.
- [114]A. I. Ojeda-Amador, A. J. Martínez-Martínez, A. R. Kennedy, C. T. O'Hara, *Inorg. Chem.* **2016**, *55*, 5719-5728.
- [115]R. Neufeld, R. Michel, R. Herbst-Irmer, R. Schöne, D. Stalke, *Chem. Eur. J.* **2016**, *22*, 12340-12346.

- [116] J. Wang, T. Hou, *J. Comput. Chem.* **2011**, 32, 3505-3519.
- [117] W. M. Haynes, D. R. Lide, *CRC Handbook of Chemistry and Physics, Vol. 92*, Taylor & Francis, Boca Raton, **2011**.
- [118] J. Goubeau, J. Jiménez-Barberá, *Z. Anorg. Allg. Chem.* **1960**, 303, 217-342.
- [119] <http://macro.lsu.edu/HowTo/solvents/>, accessed on 22.10.2016, provided by Louisiana State University.
- [120] L. Mak, S. Grandison, R. J. Morris, *J. Mol. Graphics Modell.* **2008**, 26, 1035-1045.
- [121] H. Lee, J. R. Baker, R. G. Larson, *J. Phys. Chem. B* **2006**, 110, 4014-4019.
- [122] 16a.IT.2016 ed., Institute of Physics, Polish Academy of Sciences, Al. Lotnikow 32/46, Warszawa, Poland, **2016**.
- [123] a) A. Bondi, *J. Phys. Chem.* **1964**, 68, 441-451; b) R. S. Rowland, R. Taylor, *J. Phys. Chem.* **1996**, 100, 7384-7391; c) M. Mantina, A. C. Chamberlin, R. Valero, C. J. Cramer, D. G. Truhlar, *J. Phys. Chem. A* **2009**, 113, 5806-5812.
- [124] A. Kreyenschmidt, *Externe Kalibrierungskurven zur Bestimmung des Molekulargewichtes von Verbindungen mit Schweratomen*, Master thesis, Göttingen, **2016**.
- [125] a) R. H. Cox, H. W. Terry Jr, *J. Magn. Reson.* **1974**, 14, 317-322; b) E. Herdtweck, F. H. Köhler, R. Mölle, *Eur. J. Inorg. Chem.* **2005**, 2005, 952-958; c) D. Johnels, A. Boman, U. Edlund, *Magn. Reson. Chem.* **1998**, 36, S151-S156.
- [126] J. Mason, *Multinuclear NMR*, Plenum Press, New York, **1987**.
- [127] U. Behrens, F. Olbrich, *Private Communication*, CCDC 687263 **2008**.
- [128] M. Kaupp, P. v. R. Schleyer, *J. Phys. Chem.* **1992**, 96, 7316-7323.
- [129] U. Pieper, D. Stalke, *Organometallics* **1993**, 12, 1201-1206.
- [130] S. Harvey, C. L. Raston, B. W. Skelton, A. H. White, M. F. Lappert, G. Srivastava, *J. Organomet. Chem.* **1987**, 328, C1-C6.
- [131] O. T. Beachley, R. Blom, M. R. Churchill, K. Faegri, J. C. Fettinger, J. C. Pazik, L. Victoriano, *Organometallics* **1989**, 8, 346-356.
- [132] A. I. Popov, *Pure Appl. Chem.* **1975**, 41, 275.
- [133] W. J. DeWitte, L. Liu, E. Mei, J. L. Dye, A. I. Popov, *J. Solution Chem.* **1977**, 6, 337-348.
- [134] J. W. Strauch, J.-L. Fauré, S. Bredeau, C. Wang, G. Kehr, R. Fröhlich, H. Luftmann, G. Erker, *J. Am. Chem. Soc.* **2004**, 126, 2089-2104.
- [135] V. Grignard, *Comptes Rendus Hebdomadaires de la Seances de l' Academie des Sciences* **1900**, 130, 1322-1324.
- [136] a) K. Ziegler, *Angew. Chem.* **1957**, 69, 657-657; b) E. C. Ashby, *Chem. Soc. Rev.* **1967**, 21, 259-285; c) M. Tamura, J. K. Kochi, *J. Am. Chem. Soc.* **1971**, 93, 1487-1489; d) G. Fouquet, M. Schlosser, W. Malisch, M. Kuhn, *Angew. Chem.* **1974**, 86, 50-51; *Angew. Chem. Int. Ed.* **1974**, 13, 82-83; e) P. Knochel, W.

- Dohle, N. Gommermann, F. F. Kneisel, F. Kopp, T. Korn, I. Sapountzis, V. A. Vu, *Angew. Chem.* **2003**, *115*, 4438-4456; *Angew. Chem. Int. Ed.* **2003**, *42*, 4302-4320; f) D. Martin, S. Kehrli, M. d'Augustin, H. Clavier, M. Mauduit, A. Alexakis, *J. Am. Chem. Soc.* **2006**, *128*, 8416-8417; g) S. R. Harutyunyan, T. den Hartog, K. Geurts, A. J. Minnaard, B. L. Feringa, *Chem. Rev.* **2008**, *108*, 2824-2852; h) D. Seyferth, *Organometallics* **2009**, *28*, 1598-1605.
- [137] K. C. Nicolaou, M. Takayanagi, N. F. Jain, S. Natarajan, A. E. Koumbis, T. Bando, J. M. Ramanjulu, *Angew. Chem.* **1998**, *110*, 2881-2883; *Angew. Chem. Int. Ed.* **1998**, *37*, 2717-2719.
- [138] H. G. Richey, *Grignard reagents: new developments*, Wiley, **2000**.
- [139] W. Schlenk, W. Schlenk, *Ber. d. chem. Ges.* **1929**, *62*, 920-924.
- [140] a) R. M. Salinger, H. S. Mosher, *J. Am. Chem. Soc.* **1964**, *86*, 1782-1786; b) M. B. Smith, W. E. Becker, *Tetrahedron* **1967**, *23*, 4215-4227; c) F. W. Walker, E. C. Ashby, *J. Am. Chem. Soc.* **1969**, *91*, 3845-3850; d) T. Holm, *Acta Chem. Scand.* **1969**, *23*, 579-586; e) E. C. Ashby, G. E. Parris, *J. Am. Chem. Soc.* **1971**, *93*, 1206-1213; f) E. C. Ashby, *Pure Appl. Chem.* **1980**, *52*, 545-569; g) R. Benn, H. Lehmkuhl, K. Mehler, A. Ruffinska, *Angew. Chem.* **1984**, *96*, 521-523; *Angew. Chem. Int. Ed.* **1984**, *23*, 534-535; h) T. S. Ertel, H. Bertagnolli, *Polyhedron* **1993**, *12*, 2175-2184.
- [141] a) E. C. Ashby, W. E. Becker, *J. Am. Chem. Soc.* **1963**, *85*, 118-119; b) F. Blasberg, M. Bolte, M. Wagner, H.-W. Lerner, *Organometallics* **2012**, *31*, 1001-1005; c) S. Sakamoto, T. Imamoto, K. Yamaguchi, *Org. Lett.* **2001**, *3*, 1793-1795; d) J. Toney, G. D. Stucky, *J. Organomet. Chem.* **1971**, *28*, 5-20.
- [142] a) A. Krasovskiy, P. Knochel, *Angew. Chem.* **2004**, *116*, 3396-3399; *Angew. Chem. Int. Ed.* **2004**, *43*, 3333-3336; b) F. Kopp, A. Krasovskiy, P. Knochel, *Chem. Commun.* **2004**, 2288-2289; c) H. Ren, A. Krasovskiy, P. Knochel, *Org. Lett.* **2004**, *6*, 4215-4217; d) C. B. Rauhut, V. A. Vu, F. F. Fleming, P. Knochel, *Org. Lett.* **2008**, *10*, 1187-1189.
- [143] a) D. Hauk, S. Lang, A. Murso, *Org. Process Res. Dev.* **2006**, *10*, 733-738; b) F. M. Piller, P. Appukkuttan, A. Gavryushin, M. Helm, P. Knochel, *Angew. Chem.* **2008**, *120*, 6907-6911; *Angew. Chem. Int. Ed.* **2008**, *47*, 6802-6806; c) F. M. Piller, A. Metzger, M. A. Schade, B. A. Haag, A. Gavryushin, P. Knochel, *Chem. Eur. J.* **2009**, *15*, 7192-7202; Chemistry; d) R. Li-Yuan Bao, R. Zhao, L. Shi, *Chem. Commun.* **2015**, *51*, 6884-6900.
- [144] A. Krasovskiy, B. F. Straub, P. Knochel, *Angew. Chem.* **2006**, *118*, 165-189; *Angew. Chem. Int. Ed.* **2006**, *45*, 159-162.
- [145] S. O. Reichmann, *Unconventional Carbene-Donor Ligands for the Development of New Catalysts*, Ph. D. thesis, Göttingen, **2016**.
- [146] A. J. Arduengo, R. L. Harlow, M. Kline, *J. Am. Chem. Soc.* **1991**, *113*, 361-363.
- [147] G. C. Vougioukalakis, R. H. Grubbs, *Chem. Rev.* **2010**, *110*, 1746-1787.
- [148] a) O. Schuster, L. Yang, H. G. Raubenheimer, M. Albrecht, *Chem. Rev.* **2009**, *109*, 3445-3478; b) E. Aldeco-Perez, A. J. Rosenthal, B. Donnadiou, P. Parameswaran, G. Frenking, G. Bertrand, *Science* **2009**, *326*, 556-559; c) G. Ung, G. Bertrand, *Chem. Eur. J.* **2011**, *17*, 8269-8272.
- [149] a) N. Wellinghausen, M. Martin, L. Rink, *Eur. J. Immunol.* **1997**, *27*, 2529-2535; b) M. J. Salgueiro, M. Zubillaga, A. Lysionek, M. I. Sarabia, R. Caro, T. De Paoli, A. Hager, R. Weill, J. Boccio, *Nutr. Res.* **2000**, *20*, 737-755; c) K. Nogawa, A. Ishizaki, E. Kobayashi, *Environ. Res.* **1979**, *18*, 397-409; d) C. Tohyama, Z. A. Shaikh, K. Nogawa, E. Kobayashi, R. Honda, *Arch. Toxicol.* **1982**, *50*, 159-166.

- [150] A. Visscher, *Fluorescence Studies of Amine-Substituted Azaanthracene Metal Complexes*, Ph.D thesis, Göttingen, **2016**.
- [151] M. Karplus, *J. Am. Chem. Soc.* **1963**, *85*, 2870-2871.
- [152] a) H. Gornitzka, D. Stalke, *Eur. J. Inorg. Chem.* **1998**, *1998*, 311-317; b) T. E. Wood, B. Berno, C. S. Beshara, A. Thompson, *J. Org. Chem.* **2006**, *71*, 2964-2971.
- [153] a) D.-R. Dauer, D. Stalke, *Dalton Trans.* **2014**, *43*, 14432-14439; b) D.-R. Dauer, M. Flügge, R. Herbst-Irmer, D. Stalke, *Dalton Trans.* **2016**, *45*, 6149-6158; c) D.-R. Dauer, M. Flügge, R. Herbst-Irmer, D. Stalke, *Dalton Trans.* **2016**, *45*, 6136-6148.
- [154] F. M. Arrabal-Campos, P. Ona-Burgos, I. Fernandez, *Polym. Chem.* **2016**, *7*, 4326-4329.
- [155] W. G. Kofron, L. M. Baclawski, *J. Org. Chem.* **1976**, *41*, 1879-1880.
- [156] A. Jerschow, N. Müller, *J. Magn. Reson.* **1997**, 372-375.
- [157] G. R. Fulmer, A. J. M. Miller, N. H. Sherden, H. E. Gottlieb, A. Nudelman, B. M. Stoltz, J. E. Bercaw, K. I. Goldberg, *Organometallics* **2010**, *29*, 2176-2179.
- [158] B. O. Wagner, H. F. Ebel, *Tetrahedron* **1970**, *26*, 5155-5167.
- [159] J. L. Robbins, N. M. Edelstein, S. R. Cooper, J. C. Smart, *J. Am. Chem. Soc.* **1979**, *101*, 3853-3857.

DANKSAGUNG

Es gibt viele Menschen, ohne die diese Arbeit nicht oder zumindest nicht in dieser Form zustande gekommen wäre und für all die Mühe und Unterstützung in den vergangenen 3 Jahren möchte ich mich an dieser Stelle bedanken:

Mein besonderer Dank gilt meinem Doktorvater Prof. Dr. Dietmar Stalke, der es mir nicht nur ermöglichte, diese Arbeit in seinem Arbeitskreis zu schreiben, sondern es mir auch sehr leicht gemacht hat, durch das frei wählbare Thema und die vielen Kooperationsmöglichkeiten im und um den Arbeitskreis, diese Arbeit mit Leben zu füllen. Auch für die Möglichkeiten, Chemie auf mehreren Tagungen einmal in einem internationalen Umfeld zu erleben, möchte ich mich bedanken.

Außerdem möchte ich mich bei meinem Betreuer Dr. Michael John bedanken, der mir bei NMR-spektroskopischen Fragestellungen aller Art und vor allem auch an den Maschinen immer mit Rat und Tat zur Seite stand.

Ich danke Prof. Dr. Konrad Koszinowski für die Übernahme des Korreferats und der gesamten Prüfungskommission für die Mühe des Lesens dieser Arbeit.

Ein weiterer Dank gilt auch allen Korrekturlesern dieser Arbeit: Thomas Niklas, Jochen Jung, Alexander Paesch, Anne Kreyenschmidt, Johannes Kretsch und Vivian Bachmann.

Nun folgen die Menschen, durch die der „Arbeitsalltag“ insgesamt immer sehr angenehm war: Zuerst muss ich dabei Roman Neufeld und Thomas Niklas danken, sowohl für die super Atmosphäre durch die ganze Promotion hinweg als auch für das Diskutieren, welches sich nicht nur auf NMR-spektroskopische Fragen beschränkte. Ich erinnere mich immer noch gern an die gemeinsame Zeit auf der Euromar in Prag. Zudem danke ich der gesamten Kickertruppe für die intensiv gefüllten „Denkpausen“ zwischen Messungen und Schreibaarbeiten. Ich könnte an dieser Stelle noch viele weitere Namen aus dem Arbeitskreis aufzählen, die die ganze Promotion sehr kurzweilig haben werden lassen, aber um niemanden zu vergessen, möchte ich mich einfach bei allen aus dem Arbeitskreis bedanken: Ihr seid großartig!

Ein weiterer Dank gilt all meinen Kooperationspartnern, insbesondere Christoph „Kroko“ Schnegelsberg, Arne Visscher, Sven Ole Reichmann und Ingo Köhne.

Ein großer Teil der Promotion fand vor den NMR-Geräten statt und die gesamte NMR-Abteilung, insbesondere Christiane Siebert, Martin Weitemeyer und Ralf Schöne, half, dass ich immer besonders gerne meine Zeit vor den Geräten verbracht habe. Zudem möchte ich auch noch Martin Schlote danken für die ganzen Chemikalien und Geräte, die man doch hin und wieder, selbst bei einem NMR-spektroskopischen Thema, benötigte.

Darüber hinaus möchte ich mich auch bei Ann-Christin Pöppler bedanken, nicht nur für das Korrekturlesen von Arbeiten und Papern, sondern auch dafür, dass ich durch sie den ersten Einblick in die NMR-Spektroskopie bekommen habe, an der ich bis heute gerne arbeite. Auch Anne Kreyenschmidt soll erwähnt werden, die in ihrer Masterarbeit und hoffentlich auch in Zukunft die NMR-Spektroskopie im AK Stalke würdig fortsetzt.

In diesem Sinn möchte ich mich auch bei meinem ACF Praktikanten Kris Bielefeld bedanken für die Synthese so mancher Cp Verbindung.

Meiner Familie und meinen Freunden danke ich für die Zeiten, in denen sie mir durch das gesamte Studium hindurch geholfen und zur Seite gestanden haben.

Zu guter Letzt danke ich meiner Frau Vivian: Ohne dich wäre all das in dieser Arbeit Zusammengetragene nur halb so schön und auch jede neue Erkenntnis für mich ganz persönlich ziemlich bedeutungslos. Danke, dass du es die ganzen Jahre in Kauf genommen hast, dass meine Zeit doch ziemlich begrenzt gewesen ist. Ich bin mir nicht sicher, wie erfolgreich ich diesen Weg ohne deine fortwährende Unterstützung hätte gehen können.

Ich danke allen von Herzen und hoffe, dass sich auch diejenigen mit Dank versehen fühlen, die ich in dieser kurzen Zusammenfassung nicht namentlich nennen konnte!

CURRICULUM VITAE

Sebastian Bachmann

Richard-Koch-Str. 2
38685 Langelsheim
mobil: +49 (0)151 – 55573622
mail: sbachmann@chemie.uni-goettingen.de

*02.09.1987 in Goslar
Married



Scientific Career

10/13 – today	Ph.D. thesis „ <i>Estimating Molecular Weights of Organometallics in Solution with Diffusion NMR Techniques</i> “ with Prof. Dr. D. Stalke and Dr. M. John at the Institute of Inorganic Chemistry at Georg-August-University Göttingen within the Georg-August University School of Science (GAUSS).
10/11 – 09/13	Master of Science at Georg-August-University Göttingen passed with grade 2.2 („gut“)
03/13 - 09/13	Master thesis under the supervision of Prof. Dr. Stalke „ <i>Kinetische Untersuchungen von Aggregaten des Trimethylsilyl-methylithiums mittels NMR-Spektroskopie</i> “ passed with grade 1.7 („gut“)
10/08 - 09/11	Bachelor of Science at Georg-August-University Göttingen passed with grade 1.9 („gut“)
03/11 - 06/11	Bachelor thesis under the supervision of Prof. Dr. Stalke „ <i>NMR-spektroskopische Untersuchungen von Amminboran und seinen Derivaten</i> “ passed with grade 1.3 („sehr gut“)
08/00 – 06/07	A-level at Ratsgymnasium Goslar (grade 2.3 („gut“))

Experience in University and Abroad

10/13 - today	Scientific researcher with Prof. Dr. D. Stalke
10/13 - today	Supervision of practical and theoretical labwork of main subject chemistry students
10/13 - today	Lecturer and organizer of the associated seminar and lab course for the first and second year chemistry students as part of their bachelor of science

Memberships and awards

Sozialdemokratische Partei Deutschlands (SPD)
Gesellschaft Deutscher Chemiker (GdCh)
Student's choice award for „Beste nicht-selbstständige Lehre IAC“ (SS15)

Personal skills

Languages	German (mother tongue) English, fluent (ZESS Göttingen, Scientific English I, C1) Japanese, good (ZESS Göttingen, B1) Spanish, basic (ZESS Göttingen, A1)
Computer applications	Microsoft Office Scientific data processing (ChemDraw, Origin, Topspin, MestreNova, PMFIST, Avogadro) Video and image data processing (Photoshop CS2, Magix Video Deluxe Pro) Administrative (Admin) work in the group of Prof. Dr. D. Stalke since 04/15 Basic Programming (Java, Delphi, HTML)
Expertise	According to §5 Chemikalienverbotsverordnung

Conference participations

- Niedersächsisches Katalyse Symposium (NiKaS), 21.-22.10.2010 in Göttingen (Poster)
Title: „NMR-spectroscopic studies of ammonia borane and its derivatives“
- Center of Materials Crystallography (CMC) workshop, 09.-10.10.2014 in Aarhus (Talk)
Title: „Understanding Grignard Aggregation by DOSY NMR“
- Jungchemikerforum (JCF), 15.-20.04.2015 in Göttingen (Poster)
- European congress on magnetic resonance (Euromar), 05.-09.07.2015 in Prague (Poster; travel grant)
Title: „ECCs for DOSY NMR as valuable tool in understanding aggregation of Grignard compounds and alkali cyclopentadienes“
- 18. Norddeutsches Doktorandenkolloquium (NDDK), 07.-08.09.2015 in Goslar (Poster)
- Center of Materials Crystallography (CMC) meeting, 29.01.2016 in Göttingen (Talk)
Title: „Update on Molecular Weight Determination by ECC-DOSY NMR“
- Practical Applications of NMR in Industry Conference (PANIC), 15.-18.02.2016 in Houston, TX, USA (Talk; travel grant)
Title: „ECC-DOSY: A powerful tool to determine molecular weights of small molecule aggregates“

Scientific Publications in Print

1. A. Visscher, S. Bachmann, C. Schnegelsberg, T. Teuteberg, R. A. Mata, D. Stalke, „Highly selective and sensitive fluorescence detection of Zn^{2+} and Cd^{2+} ions by using an acridine sensor“, *Dalton Trans.* **2016**, 45, 5689-5699.
2. S. Bachmann, R. Neufeld, M. Dzemski, D. Stalke, „New External Calibration Curves (ECCs) for the Estimation of Molecular Weights in Various Common NMR Solvents“, *Chem. Eur. J.* **2016**, 22, 8462-8465.
3. C. Schnegelsberg, S. Bachmann, M. Kolter, T. Auth, M. John, D. Stalke, K. Koszinowski, „Association and Dissociation of Grignard Reagents $RMgCl$ and Their Turbo Variant $RMgCl \cdot LiCl$ “, *Chem. Eur. J.* **2016**, 22, 7752-7762.
4. S. Bachmann, B. Gernert, D. Stalke, „Solution structures of alkali metal cyclopentadienides in THF estimated by ECC-DOSY NMR-spectroscopy (incl. software)“, *Chem. Commun.* **2016**, 52, 12861-12864.